NATIONAL TECHNICAL UNIVERSITY OF ATHENS
SCHOOL OF CIVIL ENGINEERING

Stochastic Analysis and Optimum Design of Structures Subjected to Fracture

Manolis Georgioudakis

A Thesis submitted for the Degree of
Doctor of Engineering

Athens, July 2014

PhD THESIS

NATIONAL TECHNICAL UNIVERSITY OF ATHENS
SCHOOL OF CIVIL ENGINEERING

Stochastic Analysis and Optimum Design of Structures Subjected to Fracture

Manolis Georgioudakis

A Thesis submitted for the Degree of
Doctor of Engineering

Athens, July 2014

Stochastic Analysis and Optimum Design of Structures Subjected to Fracture

Manolis Georgioudakis

Submitted to the School of Civil Engineering
in Partial Fulfillment of the Requirements for the Degree of
Doctor of Engineering
at the
National Technical University of Athens (NTUA)

August, 2014

Supervisor: Prof. Manolis Papadrakakis

NATIONAL TECHNICAL UNIVERSITY OF ATHENS (NTUA)
SCHOOL OF CIVIL ENGINEERING
P.O. Box 15780 Zografou Campus, Athens

This page intentionally left blank

I certify that I have read this dissertation and that, in my opinion, it is fully adequate in scope and quality as a dissertation for the degree of Doctor of Philosophy.

Manolis Papadrakakis
Professor
(Principal Advisor)
School of Civil Engineering
National Technical University of Athens

I certify that I have read this dissertation and that, in my opinion, it is fully adequate in scope and quality as a dissertation for the degree of Doctor of Philosophy.

Michael Kavvadas
Associate Professor
(Member of advisory committee)
School of Civil Engineering
National Technical University of Athens

I certify that I have read this dissertation and that, in my opinion, it is fully adequate in scope and quality as a dissertation for the degree of Doctor of Philosophy.

Nikos D. Lagaros
Assistant Professor
(Member of advisory committee)
School of Civil Engineering
National Technical University of Athens

This page intentionally left blank

I certify that I have read this dissertation and that, in my opinion, it is fully adequate in scope and quality as a dissertation for the degree of Doctor of Philosophy.

Charis Gantes
Professor
School of Civil Engineering
National Technical University of Athens

I certify that I have read this dissertation and that, in my opinion, it is fully adequate in scope and quality as a dissertation for the degree of Doctor of Philosophy.

Ioannis Vagias
Professor
School of Civil Engineering
National Technical University of Athens

I certify that I have read this dissertation and that, in my opinion, it is fully adequate in scope and quality as a dissertation for the degree of Doctor of Philosophy.

Efstathios Theotokoglou
Professor
School of Applied Sciences
National Technical University of Athens

I certify that I have read this dissertation and that, in my opinion, it is fully adequate in scope and quality as a dissertation for the degree of Doctor of Philosophy.

Konstantinos Spiliopoulos
Associate Professor
School of Civil Engineering
National Technical University of Athens

Manolis Georgioudakis
Institute of Structural Analysis & Antiseismic Research
School of Civil Engineering
National Technical University of Athens (NTUA)
Zografou Campus, 15780 Athens, Greece

PhD Thesis

Author e-mail: geoem@mail.ntua.gr

Dedicated to my parents

"Everything existing in the Universe
is the fruit of chance and necessity".
Democritus

This page intentionally left blank

Abstract

The present thesis deals with a unified framework for stochastic analysis and optimum design of structures subjected to fracture developed in the ambit of modern numerical techniques for crack growth simulation mainly based on enriched finite elements methods. This has been done within the context of the stochastic finite element method as well as within a modern optimization environment implementing metaheuristic search algorithms.

In the first part of this thesis, the stochastic finite element method is presented within the framework of the sequentially linear analysis (SLA) scheme, providing solutions to stochastic nonlinear static problems for structures made with softening materials whose properties are randomly distributed in the structure, but also giving specific information on the probability of failure. The uncertainty characterizing the material properties, is quantified by using the theory of stochastic functions (processes/fields). The response variability of the structures is computed by means of the direct Monte Carlo simulation. Furthermore, the influence of the variation of each random parameter, the probability distribution, coefficient of variation and correlation length of the stochastic fields are examined. The analysis of two benchmark structures has shown that the load-displacement curves and the probability of failure are strongly affected by the statistical characteristics of the stochastic fields. This extension of SLA to the stochastic framework offers an efficient means to perform parametric investigations of the fracture behavior of structures in the case of variable material properties.

In the second part of this thesis, the extended finite element method which consists an appropriate framework for the simulation of the fracture process in structural members caused by fatigue, is incorporated into a shape optimization environment. A reliability analysis combined with a structural shape design optimization formulation is proposed where probabilistic constraints are considered in the formulation of the design optimization problem. Shape design optimization problems are formulated aiming at investigating the relation between structural geometry and service life in the design process. Randomness on the crack initialization along with the uncertainty on the material properties are also examined. A sensitivity analysis of four optimization algorithms based on evolution process is conducted in order to identify the best algorithm for solving the structural shape optimization problem. The applicability and potential of the formulations presented are demonstrated with two characteristic numerical examples. It is shown that with proper shape changes, the service life of structural members subjected to fatigue loads can be enhanced significantly. Comparisons with optimized shapes found for targeted service life are also addressed, while the choice of initial imperfection position and orientation was found to have a significant effect on the optimal shapes.

Keywords: fracture, crack propagation, finite elements, xfem, sequentially linear analysis, stochastic analysis, optimization, computational mechanics.

This page intentionally left blank

Περίληψη

Η παρούσα διατριβή ασχολείται με τη στοχαστική ανάλυση και το βέλτιστο σχεδιασμό κατασκευών που υπόκεινται σε θραύση, σε ένα ενοποιημένο πλαίσιο βασισμένο στις σύγχρονες αριθμητικές τεχνικές προσομοίωσης των φαινομένων θραύσης που προφέρουν τα εμπλουτισμένα πεπερασμένα στοιχεία. Η διαμόρφωση του πλαισίου αυτού, γίνεται εφικτή αφενός στη βάση της μεθόδου των στοχαστικών πεπερασμένων στοιχείων, αφετέρου εντός ενός σύγχρονου περιβάλλοντος βελτιστοποίησης με τη χρήση μεταευρετικών αλγορίθμων αναζήτησης (metaheuristic search algorithms).

Στο πρώτο μέρος της διατριβής, προτείνεται η σύζευξη της μεθόδου των στοχαστικών πεπερασμένων στοιχείων και της διαδοχικής γραμμικής ανάλυσης (sequentially linear analysis), παρέχοντας λύσεις στα μη-γραμμικά στατικά προβλήματα κατασκευών από υλικά που χαρακτηρίζονται από χαλάρωση, των οποίων οι ιδιότητες είναι τυχαία κατανεμημένες εντός της δομής τους. Η αβεβαιότητα που χαρακτηρίζει τις ιδιότητες του υλικού, ποσοτικοποιείται με τη χρήση της θεωρίας των στοχαστικών συναρτήσεων (διαδικασίες/πεδία) και η μεταβλητότητα στην απόκριση των κατασκευών υπολογίζεται με τη μέθοδο της άμεσης προσομοίωσης Monte Carlo. Επιπλέον, εξετάζονται η επίδραση της μεταβολής της κάθε τυχαίας παραμέτρου, η κατανομή της συνάρτησης πιθανότητας, ο συντελεστής διακύμανσης καθώς και το μήκος συσχέτισης των στοχαστικών πεδίων. Η ανάλυση δύο κατασκευών αναφοράς έδειξε ότι οι καμπύλες φορτίου-μετατόπισης και η πιθανότητα αστοχίας επηρεάζονται έντονα από τα στατιστικά χαρακτηριστικά των στοχαστικών πεδίων.

Στο δεύτερο μέρος της διατριβής, η μέθοδος των εκτεταμένων πεπερασμένων στοιχείων (extended finite element method) συνιστά ένα κατάλληλο πλαίσιο για την προσομοίωση της διαδικασίας θραύσης σε κατασκευές υποκείμενες σε κόπωση. Προτείνεται μια ανάλυση αξιοπιστίας με στόχο την διερεύνηση της σχέσης μεταξύ των γεωμετρικών χαρακτηριστικών των κατασκευών και της διάρκειας ζωής αυτών. Κατά τη διαδικασία βέλτιστου σχεδιασμού λαμβάνονται υπόψη, η τυχαιότητα στη θέση της αρχικής ατέλειας και η αβεβαιότητα στις ιδιότητες του υλικού των κατασκευών με την εισαγωγή συγκεκριμένων πιθανοτικών περιορισμών στην διατύπωση των προβλημάτων βελτιστοποίησης. Προκειμένου να επιλεχθεί ο κατάλληλος μεταευρετικός αλγόριθμος για την επίλυση των προβλημάτων βελτιστοποίησης, διεξήχθη ανάλυση ευαισθησίας τεσσάρων αλγορίθμων βασισμένων στη εξελικτική διαδικασία (evolutionary algorithms). Το πεδίο εφαρμογής των προτεινόμενων διατυπώσεων διερευνάται με δύο χαρακτηριστικά αριθμητικά παραδείγματα. Αποδεικνύεται ότι με τις κατάλληλες αλλαγές στη γεωμετρία των κατασκευών, η διάρκεια ζωής τους μπορεί να ενισχυθεί σημαντικά και ακολουθεί σύγκριση των βέλτιστων γεωμετρικών μορφών που προκύπτουν για τα επιθυμητά επίπεδα διάρκειας ζωής. Η επιλογή ως προς την θέση της αρχικής ατέλειας και ο προσανατολισμός αυτής βρέθηκαν επίσης να έχουν σημαντική επίδραση στις βέλτιστες γεωμετρικές μορφές.

Λέξεις κλειδιά: διάδοση ρωγμών, θραυστομηχανική, εμπλουτισμένα πεπερασμένα στοιχεία, βελτιστοποίηση, στοχαστική ανάλυση.

This page intentionally left blank

Εκτενής Περίληψη

0.1 Εισαγωγή

Μία από τις πιο ευέλικτες αριθμητικές μεθόδους που έχουν αποκτήσει μεγάλη δημοτικότητα τις τελευταίες δεκαετίες στην ανάλυση των φυσικών διεργασιών αποτελεί αναμφίβολα η μέθοδος των πεπερασμένων στοιχείων (finite element method - FEM). Η FEM εφαρμόζεται κατά κύριο λόγο σε προβλήματα για τα οποία δεν υπάρχουν αναλυτικές λύσεις, που χαρακτηρίζονται από πολύπλοκη γεωμετρία, φόρτιση και συμπεριφορά του υλικού, παρέχοντας έτσι προσεγγιστικές λύσεις σε αυτά. Η FEM έχει εφαρμοστεί με επιτυχία σε πολλούς τομείς της επιστήμης του μηχανικού, μεταξύ άλλων στην αεροναυτική, στην αεροδιαστημική μηχανική, στην αυτοκινητοβιομηχανία, στην εμβιομηχανική, στην επιστήμη των υλικών, κλπ. Στον τομέα της δομικής μηχανικής η FEM έχει εφαρμοστεί στη μελέτη, στην προσομοίωση και στην πρόβλεψη της συμπεριφοράς των κατασκευών, επιτρέποντας τον υπολογισμό κρίσιμων μεγεθών, όπως της παραμόρφωσης, της εντατικής κατάστασης καθώς και του φορτίου κατάρρευσης των κατασκευών.

Έτσι, η ανάπτυξη προηγμένων μεθόδων πεπερασμένων στοιχείων συνοδεύεται από εκτενή έρευνα στο πεδίο της προσομοίωσης των υλικών. Τα αντίστοιχα μαθηματικά προσομοιώματα είναι ικανά να περιγράψουν τη μη-γραμμική συμπεριφορά των υλικών υπό διαφορετικά σενάρια φόρτισης και προσφέρουν αυξημένες δυνατότητες στη FEM. Ως εκ τούτου, τα πεπερασμένα στοιχεία διαρκώς βελτιώνονται με στόχο την πιο ρεαλιστική περιγραφή της συμπεριφοράς του υλικού.

Ανάμεσα στα πιο ενδιαφέροντα φαινόμενα στην επιστήμη των υλικών αποτελεί η διαδικασία θραύσης αυτών η οποία προκαλείται από διαφορετικούς μηχανισμούς. Η προσομοίωση των διαδικασιών θραύσης παίζει σημαντικό ρόλο στην ανάπτυξη νέων υλικών για τη βιομηχανία όσο και στη κατανόηση της αντοχής τους. Η υπολογιστική μηχανική των θραύσεων έχει προσελκύσει μεγάλο ενδιαφέρον της επιστημονικής κοινότητας, αφού η προσομοίωση μαζί με την αντικειμενική και αποτελεσματική μαθηματική περιγραφή των φαινομένων αυτών, παραμένει ένα δύσκολο πρόβλημα στο πεδίο της μηχανικής, παρά τις προόδους που έχουν σημειωθεί στην ανάπτυξη της ΜΠΣ.

0.1.1 Προσομοίωση της θραύσης των κατασκευών

0.1.1.1 Συμπεριφορά του υλικού

Η επιστήμη των υλικών έχει μελετηθεί σε πολλαπλές κλίμακες (βλ. Σχ. 1) (Willam, 2002) και έχουν διατυπωθεί πολλές θεωρίες σε αυτές για την προσομοίωση του προβλήματος έναρξης και διάδοσης των ρωγμών. Η παρούσα διατριβή εστιάζει στη συμπεριφορά του υλικού σε μακροσκοπικό επίπεδο για την προσομοίωση των διαδικασιών θραύσης στις κατασκευές. Η συμπεριφορά του υλικού σε μακροσκοπικό επιπέδο, περιγράφεται από το φαινόμενο του εντοπισμού της ανηγμένης παραμόρφωσης (strain localization). Το φαι-

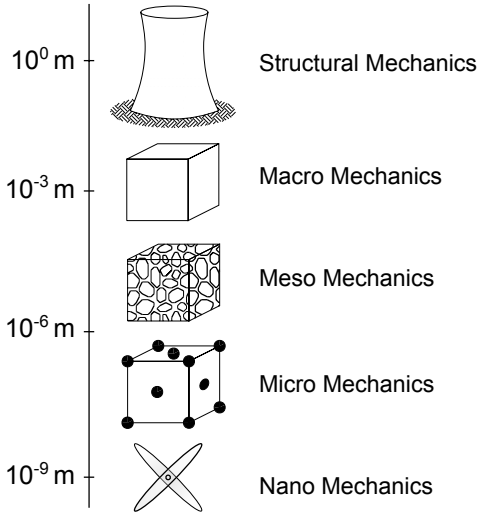

Σχήμα 1: Περιγραφή υλικού σε πολλαπλές κλίμακες.

νόμενο αυτό εμφανίζεται με πολλές μορφές σε διάφορα υλικά, όπως π.χ. στα μέταλλα (ζώνες διάτμησης) (βλ. Σχήμα 2α′), στα εδάφη (γραμμές ολίσθησης) (βλ. Σχήμα 2β′) ή ακόμα και σε βραχώδη υλικά.

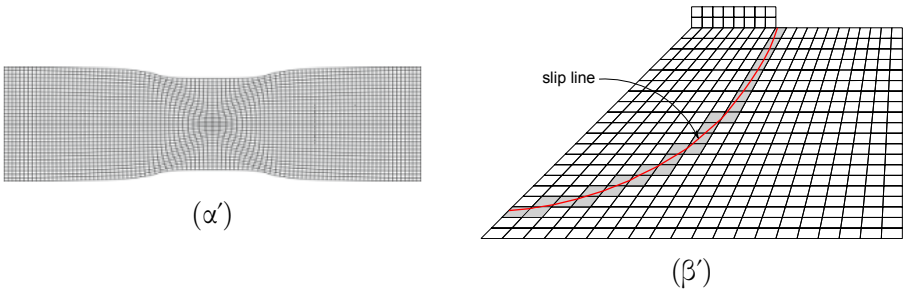

Σχήμα 2: (α′) Ζώνες διάτμησης στα μέταλλα και (β′) γραμμές ολίσθησης στα εδάφη.

Αν και ο εντοπισμός των ανηγμένων παραμορφώσεων έχει τις ρίζες του σε μικροσκοπικό επίπεδο, που προκαλείται από την παρουσία των κενών, μικρορωγμών ή άλλων φαινομένων, ωστόσο ζώνες διάτμησης και γραμμές ολίσθησης παρατηρούνται και σε μακροσκοπικό επίπεδο. Ο εντοπισμός των παραμορφώσεων χαρακτηρίζεται από τη συγκέντρωση των ανελαστικών ανηγμένων παραμορφώσεων σε μια στενή διακριτή ζώνη, ενώ το περιβάλλον υλικό αποφορτίζεται, γεγονός που προκαλεί τις αριθμητικές αστάθειες στη διαδικασία επίλυσης των κατασκευών.

0.1.1.2 Θεωρίες περιγραφής του υλικού

Για την προσομοίωση του φαινομένου της θραύσης σε μακροσκοπικό επίπεδο, τα αποδεκτά πλαισία περιγραφής είναι: η Θραυστομηχανική (Fracture Mechanics) και η Μηχανική του Συνεχούς Μέσου (Continuum Mechanics). Τα δύο αυτά πλαίσια ωστόσο περιγράφουν διαφορετικές κατηγορίες προβλημάτων θραύσης. Ενώ η θεωρία της πλαστικότητας και της μηχανικής των βλαβών (Damage Mechanics) έχουν σχεδιαστεί για προβλήματα όπου το πεδίο των μετατοπίσεων και των ανηγμένων παραμόρφωσεων παραμένουν συνεχή (συνεχή προβλήματα), η μηχανική των θραύσεων σχεδιάστηκε για να περιγράψει προβλήματα ισχυ-

ρών ασυνεχειών (ρωγμές), όπου τόσο το πεδίο των μετατοπίσεων όσο και το πεδίο των ανηγμένων παραμορφώσεων είναι ασυνεχές κατά το μήκος (ή την επιφάνεια) της ρωγμής (βλέπε Σχήμα 3).

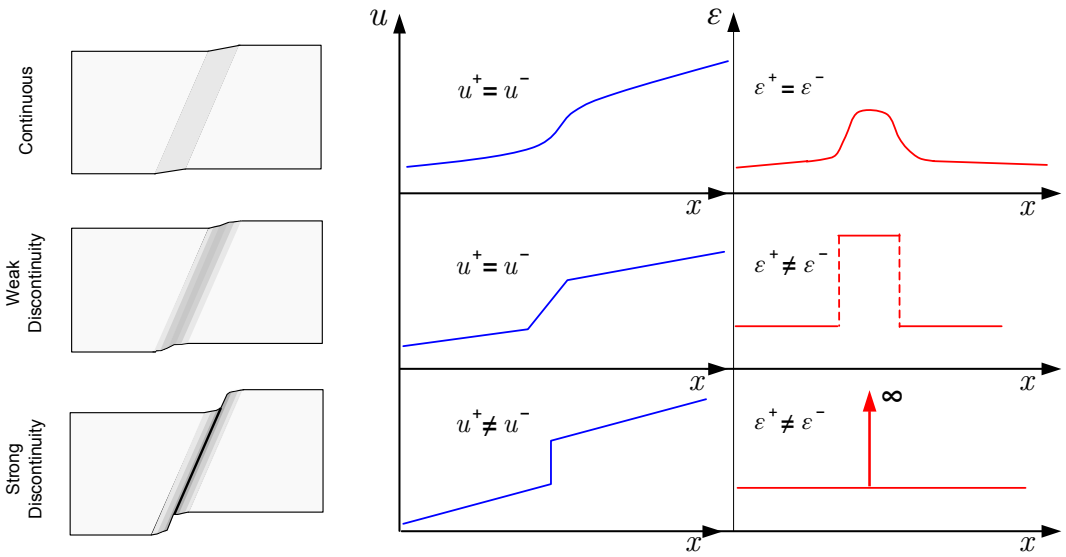

Σχήμα 3: Ασθενείς - ισχυρές ασυνέχειες και τα αντίστοιχα πεδία μετατόπισης και ανηγμένης παραμόρφωσης.

Προκειμένου να υπολογιστεί όχι μόνο το φορτίο αστοχίας, αλλά και η συμπεριφορά μιας κατασκευής πέραν αυτού του φορτίου, απαιτούνται εύρωστοι και σταθεροί υπολογιστικοί αλγόριθμοι ικανοί επιλύσουν τα σύνθετα μη-γραμμικά προβλήματα που διέπουν τα φαινόμενα θραύσης. Έτσι, εντός των προαναφερθέντων πλαισίων περιγραφής των φαινομένων θραύσης έχουν αναπτυχθεί αναλυτικές, ημι-αριθμητικές και αριθμητικές θεωρίες ανάλυσης κάθε μια με τα αντίστοιχα πλεονεκτήματα και μειονεκτήματα για την προσομοίωση των φαινομένων αυτών.

Οι κυριότερες αναλυτικές θεωρήσεις αποτελούν οι: α) γραμμική ελαστική θραυστομηχανική (linear elastic fracture mechanics - LEFM), β) θεώρηση διακριτής ρωγμής (discrete crack approach), γ) θεώρηση κατανεμημένης ρωγμής (smeared crack approach), δ) ενδοστοιχειακή ρωγμή (intra-element crack), ε) ενισχυμένες συνεχείς θεωρήσεις (συνεχές Cosserat, μη-τοπικά προσομοιώματα (non-local models), κλπ.

Οι κυριότερες αριθμητικές θεωρήσεις αποτελούν οι: α) η θεώρηση της ισχυρής ασυνέχειας (strong discrontinuity approach - SDA), β) η μέθοδος των εκτεταμένων πεπερασμένων στοιχείων (extended finite element method - XFEM), γ) η μέθοδος της γραμμικής διαδοχικής προσέγγισης (sequentially linear analysis - SLA) κλπ.

0.1.2 Αντικείμενο και στόχοι της διατριβής

Η παρούσα διατριβή ασχολείται με τη στοχαστική ανάλυση και το βέλτιστο σχεδιασμό κατασκευών που υπόκεινται σε θραύση, σε ένα ενοποιημένο πλαίσιο βασισμένο στις σύγχρονες αριθμητικές τεχνικές προσομοίωσης των φαινομένων θραύσης που προφέρουν τα εμπλουτισμένα πεπερασμένα στοιχεία. Η διαμόρφωση αυτού του πλαισίου, γίνεται εφικτή αφενός στη βάση της μεθόδου των στοχαστικών πεπερασμένων στοιχείων, αφετέρου εντός ενός σύγχρονου περιβάλλοντος βελτιστοποίησης με τη χρήση μετευρετικών αλγορίθμων αναζήτησης (metaheuristic search algorithms).

Οι κύριοι στόχοι της παρούσας διατριβής είναι:

- να γεφυρώσει διαφορετικά πεδία έρευνας που σχετίζονται με την προσομοίωση ανάπτυξης και διάδοσης ρωγμών, τη στοχαστική ανάλυση και το βέλτιστο σχεδιασμό σε ένα σύγχρονο περιβάλλον σχεδιασμού των κατασκευών,
- να διερευνήσει την επίδραση της αβεβαιότητας στη θραύση των κατασκευών όταν οι ιδιότητες των υλικών τους μεταβάλλονται χωρικά και να προτείνει μια αποτελεσματική σύζευξη που να επιτρέπει τη στοχαστική ανάλυση διάδοσης των ρωγμών, τονίζοντας παράλληλα την ανάγκη της μέσω της ποσοτικοποίησης της στοχαστικής αυτής συμπεριφοράς,
- να αναπτύξει και να εφαρμόσει ένα πλαίσιο σχεδιασμού βελτιστοποίησης σχήματος, ικανό να διερεύνησει τη σχέση μεταξύ της γεωμετρίας και της διάρκειας ζωής κατά το σχεδιασμό των κατασκευών με ρωγμές, χρησιμοποιώντας τις υπάρχουσες τεχνικές βελτιστοποίησης (μεταευρετικοί αλγόριθμοι αναζήτησης),
- να αποδείξει τη σκοπιμότητα και τη χρησιμότητα των προαναφερθέντων θεωρήσεων σε σύνθετα προβλήματα σχετικά με βιομηχανικές εφαρμογές.

0.2 Στοχαστική ανάλυση κατασκευών με υλικά χαρακτηριζόμενα από χαλάρωση

Στο πρώτο μέρος της διατριβής, προτείνεται η σύζευξη της μεθόδου των στοχαστικών πεπερασμένων στοιχείων και της διαδοχικής γραμμικής ανάλυσης (sequentially linear analysis), παρέχοντας λύσεις στα μη-γραμμικά στατικά προβλήματα κατασκευών από υλικά που χαρακτηρίζονται από χαλάρωση, των οποίων οι ιδιότητες είναι τυχαία κατανεμημένες εντός της δομής τους. Η αβεβαιότητα που χαρακτηρίζει τις ιδιότητες του υλικού, ποσοτικοποιείται με τη χρήση της θεωρίας των στοχαστικών συναρτήσεων (διαδικασίες/πεδία) και η μεταβλητότητα στην απόκριση των κατασκευών υπολογίζεται με τη μέθοδο της άμεσης προσομοίωσης Monte Carlo. Επιπλέον, εξετάζονται η επίδραση της μεταβολής της κάθε τυχαίας παραμέτρου, η κατανομή της συνάρτησης πιθανότητας, ο συντελεστής διακύμανσης καθώς και το μήκος συσχέτισης των στοχαστικών πεδίων. Η ανάλυση δύο κατασκευών αναφοράς έδειξε ότι οι καμπύλες φορτίου-μετατόπισης και η πιθανότητα αστοχίας επηρεάζονται έντονα από τα στατιστικά χαρακτηριστικά των στοχαστικών πεδίων.

0.2.1 Η μέθοδος της διαδοχικής γραμμικής ανάλυσης

Στη μηχανική των αστοχιών, η χαλάρωση των υλικών (material softening) είναι συχνά υπεύθυνη για την ασταθή συμπεριφορά των κατασκευών (Bažant & Cedolin, 2010). Αυτή η αστάθεια μπορεί να οδηγήσει σε δευτερεύουσες καταστάσεις ισορροπίας ή την διακλάδωση του δρόμου ισορροπίας, οι οποίες απαιτούν προηγμένες τεχνικές στην επαυξητική/επαναληπτική διαδικασία επίλυσης (de Borst *et al.*, 2012). Αυτό έχει ως συνέπεια να επηρεάζεται έντονα η ευρωστία της αριθμητικής διαδικασίας που χρησιμοποιείται στην επίλυση του μη-γραμμικού προβλήματος. Προκειμένου να ξεπεραστούν αυτά τα προβλήματα, μια εναλλακτική μέθοδος, που ονομάζεται διαδοχική γραμμική ανάλυση (sequentially linear analysis - SLA), εισήχθει από τον Rots (2001).

Η SLA είναι μια στρατηγική βασισμένη στη τέμνουσα διαδικασία δυσκαμψίας που δεν απαιτεί επαναλήψεις και αντικαθιστά την επαυξητική μη-γραμμική ανάλυση με πεπερασμένα στοιχεία από μια σειρά διαδοχικών γραμμικών αναλύσεων και τη μη-γραμμική καμπύλη

τάσης-παραμόρφωσης του υλικού από μια καμπύλη πριονωτής μορφής. Το πλεονέκτημα αυτής της αντικατάστασης είναι ότι η τέμνουσα γραμμική (πριονωτή) δυσκαμψία είναι πάντα θετική και η ανάλυση συγκλίνει πάντα. Η μέθοδος εφαρμόζεται γενικά σε υλικά με μη-γραμμική συμπεριφορά χαλάρωσης, και είναι ιδιαίτερα επωφελής κατά την ανάλυση προβλημάτων ψαθυρής θραύσης στα οποία εμφανίζονται ζητήματα σύγκλισης εντός του πλαισίου εφαρμογής της θεώρησης κατανεμημένης ρωγμής. Η SLA έχει εφαρμοστεί σε προβλήματα ανάλυσης τοιχοποιίας (DeJong *et al.*, 2009; Rots, 2001; Rots *et al.*, 2008, 2009; van De Graaf *et al.*, 2009), σε δοκούς από οπλισμένο σκυρόδεμα (Graça-e Costa & Alfaiate, 2006), σε δοκούς από σύνθετα υλικά (Billington, 2009), σε κατασκευές από εξαιρετικά εύθραυστα υλικά (π.χ. γυαλί) (Invernizzi et al., 2011; van De Graaf *et al.*, 2009) και γενικά σε κατασκευές από σκυρόδεμα, παρέχοντας ικανοποιητικά αποτελέσματα σε προβλήματα που είναι δύσκολο να επιλυθούν λόγω των προαναφερθέντων ζητημάτων σύγκλισης. Βελτιώσεις της μεθόδου SLA για την περίπτωση της μη αναλογικής φόρτισης έχουν επίσης προταθεί από τους Eliáš *et al.* (2010); Graça-e Costa *et al.* (2012) και Graça-e Costa *et al.* (2013), καθώς και για δοκούς με διατμητική αστοχία από τους Slobbe *et al.* (2012).

Στη παρούσα διατριβή η SLA υιοθετείται ως μια αποδεκτή μέθοδος ανάλυσης αστοχίας εντός ενός στοχαστικού πλαισίου στην διατύπωση των προβλημάτων θραύσης. Η προτεινόμενη σύξευξη αποτελεί μια αποτελεσματική διαδικασία για τη διερεύνηση της επίδρασης της χωρικής αβεβαιότητας των ιδιοτήτων του υλικού στην συμπεριφορά θραύσης των κατασκευών με υλικά από χαλάρωση.

0.2.1.1 Ο αλγόριθμος της SLA

Ο γενικός αλγόριθμος της SLA ακολουθεί την κλασική πορεία ανάλυσης της μεθόδου των πεπερασμένων στοιχείων. Έτσι, ένα δομικό σύστημα διακριτοποιείται, με τη χρήση των συμβατικών πεπερασμένων στοιχείων στα οποία προσάπτονται και οι εκάστοτε ιδιότητες του υλικού (μέτρο ελαστικότητας Young, ο λόγος Poisson και η αρχική αντοχή). Στη συνέχεια, πραγματοποιούνται διαδοχικά τα ακόλουθα βήματα, χωρίς την ανάγκη αλλαγής του αρχικού δικτύου πεπερασμένων στοιχείων:

- Εκτέλεση μιας γραμμικής-ελαστικής ανάλυσης πεπερασμένων στοιχείων με μοναδιαία εξωτερική φόρτιση και υπολογισμός των κυρίων τάσεων,
- Επαναληπτικός βρόχος σε όλα τα σημεία ολοκλήρωσης για όλα τα στοιχεία προκειμένου να βρεθεί το κρίσιμο στοιχείο για το οποίο ο λόγος της τάσης του με την τρέχουσα εφελκυστική αντοχή του είναι η μεγαλύτερη σε ολόκληρη την κατασκευή,
- Υπολογισμός του πολλαπλασιαστικού φορτικού συντελεστή, που ανήκει στο κρίσιμο σημείο ολοκλήρωσης,
- Αναλογική κλιμάκωση του φορτίου αναφοράς σύμφωνα με τον κρίσιμο πολλαπλασιαστικό φορτικό συντελεστή,
- Αύξηση της στάθμης βλάβης στο κρίσιμο σημείο ολοκλήρωσης μέσω της μείωσης της δυσκαμψίας E και της εφελκυστικής αντοχής f_f, σύμφωνα με το πριονωτό διάγραμμα τάσης-ανηγμένης παραμόρφωσης (βλέπε Ενότητα 0.2.1.2),
- Διαρκής επανάληψη του προηγούμενου κύκλου βημάτων έως ότου η βλάβη έχει εξαπλωθεί επαρκώς εντός της κατασκευής.

Πιο αναλυτικά ο αλγόριθμος της SLA περιγράφεται στον πίνακα που ακολουθεί: Αρχικά, πραγματοποιείται μια γραμμική ελαστική ανάλυση με ένα φορτίο αναφοράς $\mathbf{P}$ (γραμμή 2) (όπου $\mathbf{K}_N$ είναι το συνολικό μητρώο δυσκαμψίας της κατασκευής και $\mathbf{d}_N$ το διάνυσμα

των άγνωστων μετατοπίσεων στο βήμα N). Μετά τον υπολογισμό των μέγιστων κύριων τάσεων εφελκυσμού ($\sigma_{t_{pr}}$), μέσα από την γραμμική ελαστική ανάλυση, ακολουθεί μια επαναληπτική διαδικασία σε όλα τα σημεία ολοκλήρωσης για όλα τα στοιχεία προκειμένου να βρεθεί το κρίσιμο στοιχείο για το οποίο η τρέχουσα $f_{t_i}^{+}$ διαιρεμένη με τη μέγιστη κύρια εφελκυστική τάση είναι η μέγιστη σε ολόκληρη την κατασκευή (γραμμές 3-7). Στη συνέχεια (γραμμή 8), το φορτίο αναφοράς $\mathbf{P}$ (καθώς και οι μετακινήσεις και οι τάσεις αντίστοιχα) κλιμακώνεται αναλογικά κατά τον κρίσιμο πολλαπλασιαστικό φορτικό συντελεστή λ_{cr_N} που ανήκει στο κρίσιμο σημείο ολοκλήρωσης. Τέλος (γραμμές 9-13), αυξάνεται η βλάβη στο κρίσιμο σημείο ολοκλήρωσης μέσω της αντίστοιχης μείωσης της δυσκαμψίας E και της εφελκυστικής αντοχής f_t, σύμφωνα με το πριονωτό διάγραμμα τάσης-ανηγμένης παραμόρφωσης (βλ. Ενότητα 0.2.1.2). Η εν λόγω διαδικασία επαναλαμβάνεται διαδοχικά, μέχρις ότου η βλάβη έχει εξαπλωθεί επαρκώς εντός της κατασκευής.

Αλγόριθμος Διαδοχικής Γραμμικής Ανάλυσης

1: **repeat**
2: $\quad\mathbf{K}_N\mathbf{d}_N = \mathbf{P} \rightarrow \sigma_{t_{pr}}$
3: $\quad$**for** $element = 1, ..., TotalElements$ **do**
4: $\quad\quad$**for** $GaussPoint = 1, ..., TotalGPperElement$ **do**
5: $\quad\quad\quad$Υπολογισμός $\frac{f_{t_i}^{+}}{\sigma_{t_{pr}}}$ και εύρεση $\lambda_{cr_N} = max\{\frac{f_{t_i}^{+}}{\sigma_{t_{pr}}}\}$
6: $\quad\quad$**end for**
7: $\quad$**end for**
8: $\quad$Αναλογική κλιμάκωση των μετατοπίσεων και των τάσεων $(\mathbf{d}_N, \sigma_N)$ κατά λ_{cr_N}
9: $\quad$**for** $element = 1, ..., TotalElements$ **do**
10: $\quad\quad$**for** $GaussPoint = 1, ..., TotalGPperElement$ **do**
11: $\quad\quad\quad$Εύρεση νέων $f_{t_{i+1}}^{+}, E_{i+1}$
12: $\quad\quad$**end for**
13: $\quad$**end for**
14: $\quad$Ανανέωση ολικού μητρώου δυσκαμψίας $\mathbf{K}_{N+1} \leftarrow \mathbf{K}_N$
15: **until** η βλάβη έχει εξαπλωθεί επαρκώς στην κατασκευή

Με τον τρόπο αυτό, η μη-γραμμική απόκριση της κατασκευής προκύπτει συνδέοντας διαδοχικά τα σημεία του δρόμου ισορροπίας από κάθε βήμα της ανάλυσης. Η ομαλότητα της καμπύλης P-δ εξαρτάται από τον αριθμό N_t των 'δοντιών' του πριονωτού προσωμοιώματος (βλ. Ενότητα 0.2.1.2). Κατά την διαδικασία της SLA μόνο ένα σημείο ολοκλήρωσης επιτρέπεται κάθε φορά να αλλάξει την κατάστασή του από την ελαστική στην κατάσταση χαλάρωσης, σε αντίθεση με την συμβατική μη-γραμμική ανάλυση πεπερασμένων στοιχείων, όπου η χρήση του επαυξητικού φορτίου έχει ως συνέπεια πολλαπλά σημεία ολοκλήρωσης να διαρρεύσουν ταυτόχρονα με αποτέλεσμα η τοπική δυσκαμψία σε αυτά τα σημεία να μεταβεί από θετική σε αρνητική.

0.2.1.2 Το 'πριονωτό' καταστατικό προσομοίωμα

Κατά τη διαδικασία της SLA, η ενημέρωση της τέμνουσας δυσκαμψίας οδηγεί σε ένα πριωνοτής μορφής διαγράμμα τάσης-ανηγμένης παραμόρφωσης (βλ. Σχήμα 4) και απαιτεί την κανονικοποίηση του δικτύου (mesh regularization) προκειμένου να αποφευχθούν αποκλίσεις από την ενέργεια που διαχέεται στη ρωγμή. Στη παρούσα διατριβή, υιοθετήθηκε

το γενικευμένο προσομοίωμα (προσομοίωμα C) (Rots *et al.*, 2008), το οποίο δεν απαιτεί ειδικές τεχνικές διαχείρισης ως προς την αντικειμενικότητα του μεγέθους του δικτύου (mesh size objectivity), προκειμένου τα αποτελέσματα να είναι αντικειμενικά σε σχέση με το δίκτυο. Ο τρόπος με τον οποίο μειώνονται προοδευτικά η δυσκαμψία και η αντοχή των κρίσιμων στοιχείων σε κάθε βήμα ανάλυσης, παρουσιάζεται στο Σχήμα 4 όπου η καμπύλη χαλάρωσης (με αρνητική κλίση) στο καταστατικό προσομοίωμα έχει αντικατασταθεί από ένα διακριτοποιημένο πριονωτό διάγραμμα με θετικές κλίσεις το οποίο παρέχει τη σωστή διάχυση ενέργειας. Έτσι, η γραμμική εφελκυστική καμπύλη χαλάρωσης τάσης-ανηγμένης παραμόρφωσης ορίζεται από το μέτρο ελαστικότητας Young E, την εφελκυστική αντοχή f_t και το εμβαδό κάτω από το πριονωτό διάγραμμα. Το εμβαδό αυτό (βλ. Σχήμα 4) είναι πάντοτε ίσο με την ενέργεια θραύσης G_f, η οποία θεωρείται εδώ ως ιδιότητα του υλικού, διαιρούμενη με το εύρος ζώνης της ρωγμής h, η οποία συνδέεται με το μέγεθος, τον προσανατολισμό και τον κανόνα ολοκλήρωσης του πεπερασμένου στοιχείου.

Στη περίπτωση της γραμμικής χαλάρωσης, η τελική ανηγμένη παραμόρφωση ϵ_u δίνεται από την σχέση:

$$\epsilon_u = \frac{2G_f}{f_t h}$$

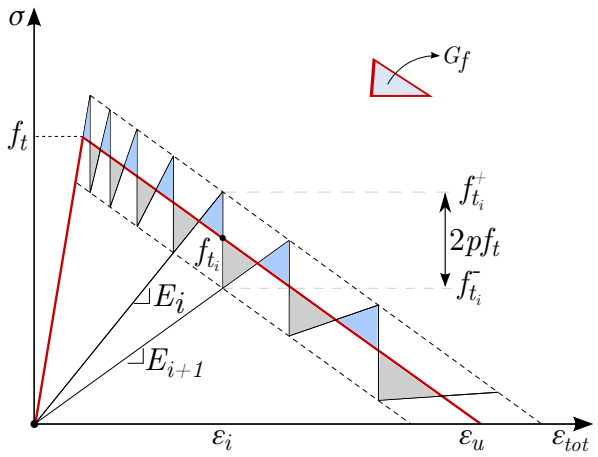

Σχήμα 4: Καμπύλη τάσεως-ανηγμένης παραμόρφωσης ($\sigma - \epsilon$) για τη περίπτωση της γραμμικής χαλάρωσης.

Τόσο το μέτρο ελαστικότητας Young E όσο και η εφελκυστική αντοχή f_t μπορούν να απομειωθούν κατά την ίδια χρονική στιγμή (στο ίδιο βήμα επίλυσης) κατά την διαδικασία της SLA κατά έναν παράγοντα a, έτσι ώστε:

$$E_i = \frac{E_{i-1}}{a}, \quad for \quad i = 1, 2, ..., N$$

όπου i και $i-1$ δηλώνουν το τρέχον και το προηγούμενο βήμα ανάλυσης αντίστοιχα στο πριονωτό διάγραμμα. Για την εύρεση του νόμου απομείωσης του μέτρου ελαστικότητας Young E, όπως και της εφελκυστικής αντοχής f_t, κατά τον παράγοντα a στο βήμα i, σύμφωνα με το Σχήμα 5, ισχύει:

$$f_{ti}^- = f_{ti}^+ - 2pf_t$$

$$E_{i+1} = \frac{f_{ti}^-}{\epsilon_i}$$

$$a_{i+1} = \frac{E_i}{f_{ti}^-}\epsilon_i = \frac{f_{ti}^+}{f_{ti}^-} = \frac{f_{ti}^+}{f_{ti}^+ - 2pf_t}$$

Έτσι για την περίπτωση της γραμμικής χαλάρωσης (βλ. Σχήμα 4) η τιμή της εφελκυστικής αντοχής f_{ti}^+ μπορεί εύκολα να οριστεί ως:

$$f_{ti}^+ = \epsilon_u^+ E_i \frac{D}{E_i + D}$$

όπου,

$$\epsilon_u^+ = \epsilon_u + p\frac{f_t}{D}$$

και D είναι η εφαπτομένη στην εφελκυστική καμπύλη χαλάρωσης τάσης-ανηγμένης παραμόρφωσης. Το πλήθος N_t των 'δοντιών' υπολογίζεται αυτόματα και εξαρτάται από την παράμετρο p που δίνεται από τον χρήστη. Για μικρές τιμές της παραμέτρου p, απαιτούνται περισσότερα δόντια N_t προκειμένου να καλύψουν τον κλάδο χαλάρωσης, κατά συνέπεια και σε περισσότερο ακριβή αποτελέσματα. Η διαδικασία τερματίζει, σε σχέση με το αντίστοιχο σημείο ολοκλήρωσης Gauss, όταν όταν η διαφορά μεταξύ του αθροίσματος των θετικών τριγώνων πάνω από την πραγματική καμπύλη και το άθροισμα των αρνητικών τριγώνων κάτω από την πραγματική καμπύλη μηδενίζεται, όπως φαίνεται στο Σχήμα 4.

0.2.2 Η μέθοδος των στοχαστικών πεπερασμένων στοιχείων

Η μέθοδος των στοχαστικών πεπερασμένων στοιχείων, που προέκυψε ως γενίκευση της μεθόδου των προσδιοριστικών πεπερασμένων στοιχείων για την αντιμετώπιση στοχαστικών προβλημάτων, έχει εφαρμοστεί με επιτυχία σε πολλές κατηγορίες προβλημάτων (δομική μηχανική, ρευστομηχανική, ακουστική, ηλεκτρομαγνητισμός, μεταφορά θερμότητας). Στις επόμενες παραγράφους επιχειρείται μία σύντομη παρουσίαση της μεθόδου των στοχαστικών πεπερασμένων στοιχείων από τη σκοπιά των προβλημάτων της δομικής μηχανικής. Αρχικά γενικεύεται η προσδιοριστική αρχή των δυνατών έργων που αποτελεί το θεωρητικό υπόβαθρο της κλασσικής μεθόδου των πεπερασμένων στοιχείων, λαμβάνοντας υπόψη τυχαίες διακυμάνσεις των ιδιοτήτων του υλικού και ακολουθεί αδρή περιγραφή των τριών θεμελιωδών βημάτων της μεθόδου: 1) υπολογισμός στοχαστικού μητρώου δυσκαμψίας, 2) διακριτοποίηση των στοχαστικών πεδίων, 3) υπολογισμός απόκρισης της κατασκευής.

0.2.2.1 Στοχαστική αρχή των δυνατών έργων

Η κλασσική θεωρία των πεπερασμένων στοιχείων θεμελιώνεται στη προσδιοριστικά καθορισμένη αρχή των δυνατών έργων και βασίζεται στη διακριτοποίηση του συνεχούς μέσου σ' έναν αριθμό κόμβων και στοιχείων. Με τη χρήση των συναρτήσεων σχήματος N, το πεδίο των μετατοπίσεων $\boldsymbol{u}$ στο εσωτερικό του κάθε στοιχείου εκφράζεται συναρτήσει των επικόμβιων μετατοπίσεών του $\boldsymbol{d}$ ως εξής:

$$\boldsymbol{u} = \boldsymbol{N}\boldsymbol{d}$$

Το πεδίο των μετατοπίσεων εκλέγεται έτσι ώστε να ικανοποιείται το συμβιβαστό των παραμορφώσεων σε κάθε στοιχείο (κινηματική συμβιβαστότητα). Αυτό που δεν εξασφαλίζεται στην παραπάνω εξίσωση είναι οι συνθήκες ισορροπίας. Αυτές μπορούν να ικανοποιηθούν με την εφαρμογή της αρχής των δυνατών έργων:

$$\delta W = W^{ext} - W^{int} = 0$$

όπου W^{ext} είναι το έργο των εξωτερικών δυνάμεων και W^{ext} το έργο των εσωτερικών δυνάμεων. Οι παραμορφώσεις στους κόμβους ενός στοιχείου δίνονται από τη σχέση:

$$\boldsymbol{\epsilon} = \boldsymbol{B}\boldsymbol{d}$$

όπου B είναι το μητρώο των παραγώγων των συναρτήσεων σχήματος. Χωρίς να ληφθεί υπόψη η επίδραση των θερμοκρασιακών διαφορών, οι τάσεις μπορούν να εκφραστούν ως εξής:

$$\boldsymbol{\sigma} = \mathbb{C}\boldsymbol{B}\boldsymbol{d}$$

όπου $\mathbb{C}$ το μητρώο που περιγράφει τις ιδιότητες του υλικού.

Όταν οι ιδιότητες του υλικού εμπεριέχουν τυχαιότητα (randomness), τότε αυτές διακυμαίνονται χωρικά και η διακύμανσή τους μπορεί να περιγραφεί, στην γενικότερη περίπτωση, από ένα $nD - mV$ στοχαστικό πεδίο. Το καταστατικό μητρώο $\mathbb{C}$ γράφεται ως εξής:

$$\mathbb{C} = \mathbb{C}_0[1 + f(\boldsymbol{x})]$$

όπου $f(x, y, z)$ είναι ένα ομογενές στοχαστικό πεδίο μηδενικής μέσης τιμής και συνάρτησης αυτοσυσχέτισης R_{ff}. Η μέση τιμή του μητρώου $\mathbb{C}$ είναι $\mathbb{C}_0$. Επιβάλλοντας στο στοιχείο (e) ένα δυνατό πεδίο μετατοπίσεων $\widetilde{\boldsymbol{u}}^{(e)}$:

$$\widetilde{\boldsymbol{u}}^{(e)} = \boldsymbol{N}^{(e)}\widetilde{\boldsymbol{d}}^{(e)}$$

και εισάγοντας το διάνυσμα των γενικευμένων επικομβίων δράσεων $\boldsymbol{f}^{ext}$, από την εφαρμογή της αρχής των δυνατών έργων προκύπτει η σχέση:

$$\widetilde{\boldsymbol{d}}^{(e)^T}\boldsymbol{f}^{ext} = \int\limits_{V^{(e)}} \widetilde{\boldsymbol{\epsilon}}^{(e)^T}\boldsymbol{\sigma}^{(e)}dV^{(e)}$$

Μετά από πράξεις καταλήγουμε στην έκφραση:

$$\begin{aligned}\widetilde{\boldsymbol{d}}^{(e)^T}\boldsymbol{f}^{ext} &= \widetilde{\boldsymbol{d}}^{(e)^T}\left[\int\limits_{V^{(e)}} \boldsymbol{B}^{(e)^T}\mathbb{C}^{(\boldsymbol{e})}\boldsymbol{B}^{(e)}dV^{(e)}\right]\boldsymbol{d}^{(e)} \\ &= \widetilde{\boldsymbol{d}}^{(e)^T}\left[\int\limits_{V^{(e)}} \boldsymbol{B}^{(e)^T}\mathbb{C}_{\boldsymbol{0}}^{(\boldsymbol{e})}\boldsymbol{B}^{(e)}dV^{(e)} + \int\limits_{V^{(e)}} \boldsymbol{B}^{(e)^T}\mathbb{C}_{\boldsymbol{0}}^{(\boldsymbol{e})}\boldsymbol{B}^{(e)}f^{(e)}(\boldsymbol{x})dV^{(e)}\right]\boldsymbol{d}^{(e)}\end{aligned}$$

απ' όπου προκύπτει το στοχαστικό μητρώο στιβαρότητας του στοιχείου (e):

$$\mathbb{k}^{(e)} = \underbrace{\int\limits_{V^{(e)}} \boldsymbol{B}^{(e)} \mathbb{C}_0^{(e)} \boldsymbol{B}^{(e)} dV^{(e)}}_{\mathbb{k}_0^{(e)}} + \underbrace{\int\limits_{V^{(e)}} \boldsymbol{B}^{(e)T} \mathbb{C}_0^{(e)} \boldsymbol{B}^{(e)} f^{(e)}(\boldsymbol{x}) dV^{(e)}}_{\Delta\mathbb{k}^{(e)}}$$

Τα $\mathbb{k}_0^{(e)}$ και $\Delta\mathbb{k}^{(e)}$ αποτελούν το σταθερό και το διακυμαινόμενο μέρος του στοχαστικού μητρώου στιβαρότητας αντίστοιχα, $B^{(e)}$ είναι το σταθερό μητρώο παραμορφωσιμότητας, $\mathbb{C}_0^{(e)}$ είναι η μέση τιμή του καταστατικού μητρώου και $V^{(e)}$ είναι ο όγκος του πεπερασμένου στοιχείου. Το καθολικό μητρώο στιβαρότητας μπορεί να εκφραστεί με τον ίδιο τρόπο αθροίζοντας τα επιμέρους τοπικά μητρώα δυσκαμψίας ως εξής:

$$\mathbb{K} = \sum_{e=1}^{N_e} \mathbb{k}^{(e)} = \mathbb{K}_0 + \Delta\mathbb{K}$$

όπου N_e ο συνολικός αριθμός των στοιχείων.

Η στοχαστική ανάλυση των κατασκευών με πεπερασμένα στοιχεία ανάγεται τελικά στην επίλυση του παρακάτω προβλήματος:

$$(\mathbb{K}_0 + \Delta\mathbb{K})\boldsymbol{u} = \boldsymbol{f}^{ext}$$

όπου $\boldsymbol{f}^{ext}$ και $\boldsymbol{u}$ τα διανύσματα των εξωτερικών δράσεων και επικομβίων μετατοπίσεων του φορέα αντίστοιχα. Στην περίπτωση των προβλημάτων μεγάλης κλίμακας, η επίλυσή τους είναι υπολογιστικά δαπανηρή και ως εκ τούτου αποτελεί το κρίσιμο σημείο της εφαρμογής και της αποτελεσματικότητας της μεθόδου των στοχαστικών πεπερασμένων στοιχείων.

0.2.2.2 Διακριτοποίηση στοχαστικών πεδίων

Όπως φαίνεται ο υπολογισμός του στοχαστικού μητρώου στιβαρότητας $\mathbb{k}^{(e)}$ απαιτεί διακριτοποίηση του στοχαστικού πεδίου $f(x, y, z)$. Με τον όρο διακριτοποίηση (discretization) εννοούμε την προσέγγιση (αντικατάσταση) ενός συνεχούς στοχαστικού πεδίου $f(x)$ από ένα πεπερασμένο σύνολο τυχαίων μεταβλητών f_i που αποτελούν ένα τυχαίο διάνυσμα:

$$f(\boldsymbol{x}) \Rightarrow \text{discretization} \Rightarrow \widetilde{f}(\boldsymbol{x}) = \{f_i\}, \quad i = \{1, 2, \ldots, n\}$$

Οι μέθοδοι διακριτοποίησης υποδιαιρούνται σε δύο βασικές κατηγορίες: α) στις μεθόδους σημειακής διακριτοποίησης όπου οι τυχαίες μεταβλητές $\{f_i\}$ είναι επιλεγμένες τιμές του πεδίου σε δεδομένα σημεία x_i, β) στις μεθόδους διακριτοποίησης τύπου «μέσου όρου» όπου οι τυχαίες μεταβλητές $\{f_i\}$ είναι σταθμισμένα ολοκληρώματα του πεδίου στο χωρίο Ω_e (π.χ. στο χωρίο ενός πεπερασμένου στοιχείου). Στη παρούσα διατριβή υιοθετείται η μέθοδος της σημειακής διακριτοποίησης και συγκεκριμένα η μέθοδος του κεντρικού σημείου (midpoint method).

Η μέθοδος του κεντρικού σημείου είναι μία από τις ευρύτερα διαδεδομένες μεθόδους σημειακής διακριτοποίησης (der Kiureghian, 1988) και συνίσταται στην προσέγγιση του στοχαστικού πεδίου σε κάθε πεπερασμένο στοιχείο (e) από μία τυχαία μεταβλητή που ορίζεται ως η τιμή του πεδίου στο «κεντρικό» σημείο του στοιχείου. Οι συντεταγμένες

του κεντροειδούς δίνονται συναρτήσει των συντεταγμένων των κόμβων x_j του στοιχείου (e) σύμφωνα με τη σχέση:

$$x_e^* = \frac{1}{q}\sum_{j=1}^{q} x_j^{(e)}$$

όπου q είναι ο αριθμός των κόμβων του στοιχείου. Έχει αποδειχθεί ότι η μέθοδος αυτή τείνει να υπερβάλλει τη διακύμανση του στοχαστικού πεδίου μέσα σε κάθε στοιχείο (der Kiureghian, 1988).

0.2.2.3 Υπολογισμός απόκρισης κατασκευής

Η προσομοίωση Monte Carlo είναι η απλούστερη μέθοδος που μπορεί να χρησιμοποιηθεί για τον υπολογισμό της διακύμανσης της απόκρισης μίας κατασκευής. Η προσομοίωση Monte Carlo (Gentle, 2003; Rubinstein, 2007) αποτελεί μία μέθοδο αριθμητικής επίλυσης προβλημάτων στα Μαθηματικά, τη Φυσική, τη Μηχανική και άλλες επιστήμες μέσω της πραγματοποίησης πειραμάτων δειγματοληψίας (sampling experiments). Η αξία της μεθόδου είναι μεγάλη ιδιαίτερα στις περιπτώσεις όπου είναι αδύνατο ή εξαιρετικά δύσκολο να υπολογιστεί η αναλυτική λύση ενός προβλήματος. Στην παρούσα διατριβή η προσομοίωση Monte Carlo χρησιμοποιείται για τον προσδιορισμό της διακύμανσης της απόκρισης κατασκευών με τυχαίες παραμέτρους.

Στη μέθοδο αυτή, δημιουργούνται με χρήση μίας γεννήτριας τυχαίων αριθμών N_{sim} δείγματα του στοχαστικού μητρώου στιβαρότητας και το πρόβλημα επιλύεται τόσες φορές όσες και ο αριθμός των δειγμάτων, παράγοντας έτσι έναν πληθυσμό για το διάνυσμα των μετατοπίσεων. Μία τελική στατιστική επεξεργασία στον πληθυσμό αυτόν παρέχει τη διακύμανση της απόκρισης του εξεταζόμενου συστήματος. Αν είναι u_i η μετατόπιση του βαθμού ελευθερίας i, τότε οι αμερόληπτες εκτιμήτριες (unbiased estimates) της μέσης τιμής και της διασποράς του πληθυσμού της μετατόπισης δίνονται από τις γνωστές σχέσεις:

$$E(u_i) = \frac{1}{N_{sim}}\sum_{n=1}^{N_{sim}} u_i(n)$$

$$\sigma^2(u_i) = \frac{1}{N_{sim}-1}\Big[\sum_{n=1}^{N_{sim}} u_i^2(n) - N_{sim}\cdot E^2(u_i)\Big]$$

Με βάση τις προηγούμενες σχέσεις, είναι φανερό ότι: α) η ποιότητα της εκτίμησης εξαρτάται από τον αριθμό N_{sim} των δειγμάτων, και β) η εκτιμήτρια της τυπικής απόκλισης σ είναι αντιστρόφως ανάλογη προς τη $\sqrt{N_{sim}}$. Ένας μικρός αριθμός δειγμάτων, π.χ. $N_{sim} \geq 50$, επιτρέπει μία αδρή προσέγγιση της μέσης τιμής και της διασποράς της απόκρισης. Αν ο αριθμός των δειγμάτων αυξηθεί π.χ. σε $N_{sim} \geq 500$, είναι δυνατή η εκτίμηση της συνάρτησης κατανομής της απόκρισης (κανονική, λογαριθμοκανονική, βήτα, κλπ.) (Schuëller, 2006).

Η προσομοίωση Monte Carlo που περιγράφηκε στην ενότητα αυτή αποτελεί την απλούστερη εκδοχή της μεθόδου και ονομάζεται άμεση προσομοίωση Monte Carlo (direct MCS). Μέχρι πριν λίγα χρόνια, η εφαρμογή της μεθόδου σε ρεαλιστικά προβλήματα καθίστατο σχεδόν αδύνατη λόγω του υπερβολικά μεγάλου υπολογιστικού κόστους που τη

χαρακτήριζε. Η χρήση όμως των προηγμένων τεχνικών επίλυσης γραμμικών εξισώσεων που αναπτύχθηκαν πρόσφατα, η αλματώδης ανάπτυξη της τεχνολογίας των H/Υ και η δυνατότητα εφαρμογής της μεθόδου σε περιβάλλον παράλληλης επεξεργασίας (parallel processing), αίρουν τον περιορισμό αυτό σε ένα μεγάλο βαθμό. Έτσι, η προσομοίωση Monte Carlo σε συνδυασμό με οικονομικές μεθόδους διακριτοποίησης του στοχαστικού πεδίου, αποτελεί σήμερα το ισχυρότερο εργαλείο για τη στοχαστική ανάλυση κατασκευών με πεπερασμένα στοιχεία. Όχι μόνο κάνει εφικτή την αντιμετώπιση ρεαλιστικών και πολύπλοκων προβλημάτων, αλλά αποτελεί και τη μέθοδο που χρησιμοποιείται για τον έλεγχο της ποιότητας των αποτελεσμάτων όλων των άλλων μεθόδων.

0.2.3 Αριθμητικές εφαρμογές

Για τα αριθμητικά παραδείγματα, στο πρώτο αυτό μέρος της παρούσας διατριβής, η μέθοδος των στοχαστικών πεπερασμένων στοιχείων (SFEM) (βλ. Ενότητα 0.2.2) σε συνδυασμό με την μέθοδο SLA, παρέχει λύσεις στα μη-γραμμικά στατικά προβλήματα κατασκευών από υλικά με χαλάρωση όταν οι ιδιότητες τους μεταβάλλονται χωρικά (Georgioudakis et al., 2014c). Το μέτρο ελαστικότητας Young E, η εφελκυστική αντοχή f_t και η ενέργεια θραύσης G_f του υλικού περιγράφονται από διδιαστάτα (2D-1V) ομογενή στοχαστικά πεδία. Η διακύμανση του E περιγράφεται ως εξής:

$$E(x, y) = E_0[1 + f(x, y)]$$

όπου E_0 είναι η μέση τιμή του μέτρου ελαστικότητας και $f(x, y)$ είναι ομογενές στοχαστικό πεδίο μηδενικής μέσης τιμής. Τα διακριτοποιημένα στοχαστικά πεδία χρησιμοποιούνται για τη διαμόρφωση του στοχαστικού μητρώου δυσκαμψίας $\mathbb{k}^{(e)}$ του κάθε στοιχείου (e). Οι δυο άλλες ιδιότητες του υλικού (f_t και G_f) μεταβάλλονται κατά παρόμοιο τρόπο. Το ολικό στοχαστικό μητρώο δυσκαμψίας του φορέα υπολογίζεται χρησιμοποιώντας τη μέθοδο του μέσου σημείου (βλέπε Ενότητα 0.2.2.2), δηλαδή ένα σημείο ολοκλήρωσης στο κέντρο βάρους του κάθε πεπερασμένου στοιχείου. Αυτή η προσέγγιση δίνει ακριβή αποτελέσματα για σχετικά αραιά δίκτυα κρατώντας το υπολογιστικό κόστος σε λογικά επίπεδα (Stefanou, 2009).

Για την περιγραφή των αβέβαιων ιδιοτήτων του υλικού χρησιμοποιήθηκαν, τόσο Γκαουσιανά, όσο και μη-Γκαουσιανά στοχαστικά πεδία. Για τον υπολογισμό της απόκρισης της κατασκευής χρησιμοποιήθηκε ένας μεγάλος αριθμός N_{sim} δειγματοσυναρτήσεων (sample functions) οι οποίες κατ' επέκταση οδηγούν στη παραγωγή ενός αντίστοιχου συνόλου από στοχαστικά μητρώα δυσκαμψίας. Ακολούθησε επίλυση του κάθε προβλήματος N_{sim} φορές και η τελική απόκριση υπολογίστηκε από τη στατιστική επεξεργασία των N_{sim} πλήθος προσομοιώσεων.

0.2.3.1 Παράδειγμα 1ο: Καμπτική δοκός τεσσάρων σημείων

Στο αριθμητικό αυτό παράδειγμα αναλύθηκε μια συμμετρική δοκός με εγκοπή (Rots & Invernizzi, 2004). Στο Σχήμα 5 φαίνεται η γεωμετρία της, η φόρτιση και οι συνοριακές συνθήκες. Το πάχος της δοκού είναι 50 mm και το βάθος της εγκοπής είναι 10 mm. Στην επίλυση χρησιμοποιήθηκαν 4κομβικά – 4πλευρικά ισοπαραμετρικά πεπερασμένα στοιχεία σε συνθήκες επίπεδης έντασης με κανόνα ολοκλήρωσης Gauss 2x2. Οι αβέβαιες παράμετροι του προβλήματος είναι το μέτρο ελαστικότητας Young E, η εφελκυστική αντοχή f_t

και η ενέργεια θραύσης G_f του υλικού όπου οι μέσες τιμές τους είναι ίσες με 38 GPa, 3 MPa και 0.06 N/mm, αντίστοιχα. Η προς παρακολούθηση μετατόπιση αποτελεί η κατακόρυφη συνιστώσα της μετατόπισης στο σημείο όπου εφαρμόζεται το φορτίο.

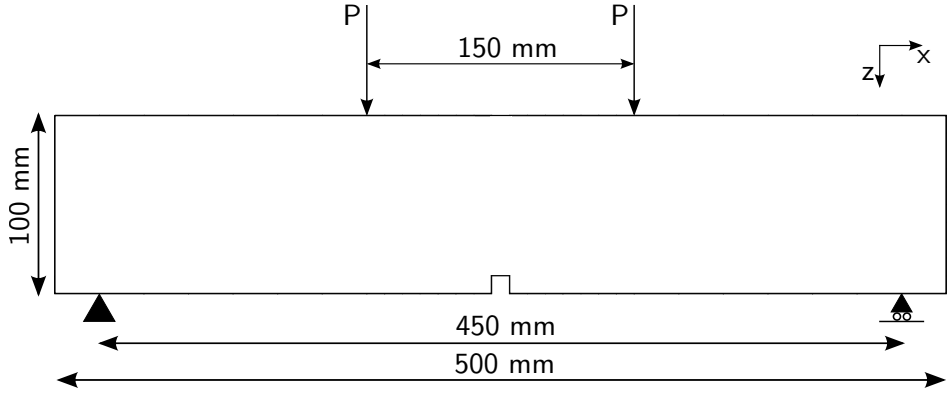

Σχήμα 5: Καμπτική δοκός τεσσάρων σημείων: γεωμετρία, φόρτιση και συνθήκες στήριξης.

Η χωρική διακύμανση των αβέβαιων παραμέτρων περιγράφεται από διαδιάστατα (2D-1V) ομογενή Γκαουσιανά στοχαστικά πεδία καθώς και λογαριθμοκανονικής κατανομής μη-Γκαουσιανά στοχαστικά πεδία μεταφοράς. Γίνεται χρήση τριών διαφορετικών τιμών ($b = 1, 10, 100$) της παραμέτρου b ($= b_1 = b_2$) του μήκους συσχέτισης, που αντιστοιχούν σε στοχαστικό πεδίο ασθενούς, μέτριας και ισχυρής συσχέτισης (όλες οι τιμές του b είναι σε mm). Με βάση την υπόθεση των Yang & Xu (2008); Papadopoulos *et al.* (2009), λαμβάνεται η ίδια τιμή του μήκους συσχέτισης τόσο για το υποκείμενο Γκαουσιανό, όσο και για το μη-Γκαουσιανό πεδίο μεταφοράς με την εύλογη ακρίβεια. Ο αριθμός των όρων N_j που χρησιμοποιούνται στην σειρά της μεθόδου της φασματικής απεικόνισης είναι ίσος με 20 και οι κυματικοί αριθμοί αποκοπής $\kappa_{ju}, j = 1, 2$ είναι ίσοι 2π, 0.2π και 0.02π για b ίσο με 1, 10 και 100, αντίστοιχα.

Αρχικά πραγματοποιήθηκε μια παραμετρική διερεύνηση σύγκλισης προκειμένου να καθοριστεί το κατάλληλο δίκτυο πεπερασμένων στοιχείων που συνδυάζει την ακρίβεια και την υπολογιστική αποδοτικότητα. Η κατανομή των τάσεων για τα δίκτυα που χρησιμοποιήθηκαν φαίνονται στο Σχήμα 6 για μια τυχαία επιλεγμένη πραγματοποίηση του πεδίου απεικονίζοντας παράλληλα την σύγκλιση των αποτελεσμάτων. Ως αποτέλεσμα αυτής της παραμετρικής διερεύνησης επιλέχθηκε για τις αναλύσεις το δίκτυο μεσαίας πυκνότητας που αποτελείται συνολικά από 1237 κόμβους και 1156 στοιχεία.

Η μεταβλητότητα της απόκρισης υπολογίζεται χρησιμοποιώντας την μέθοδο MCS (βλ. Ενότητα 0.2.2.3) με μέγεθος δείγματος ίσο με 500. Η στατιστική σύγκλιση επιτυγχάνεται εντός αυτού του αριθμού των δειγμάτων και απεικονίζεται στο Σχήμα 7, όπου η μέση τιμή και η τυπική απόκλιση του φορτίου αιχμής απεικονίζονται ως συνάρτηση του αριθμού των προσομοιώσεων Monte Carlo.

Οι καμπύλες φορτίου-μετατόπισης που αντιστοιχούν σε τυπική απόκλιση 10% για τα E, G_f με $b = 1$ φαίνονται στο Σχήμα 8 για την περίπτωση των μη-Γκαουσιανών πεδίων. Επιπλέον, οι καμπύλες φορτίου-μετατόπισης που αντιστοιχούν σε τυπική απόκλιση 20% για τα E, G_f με $b = 100$ παρουσιάζονται στο Σχήμα 8 και Σχήμα 10 για Γκαουσιανά και μη-Γκαουσιανά στοχαστικά πεδία, αντίστοιχα.

Όπως φαίνεται στα Σχήματα 8α′-10α′ η διακύμανση του E επηρεάζει τη δυσκαμψία της κατασκευής. Η περίπτωση της Γκαουσιανής υπόθεσης οδηγεί σε μια σημαντική, μη-

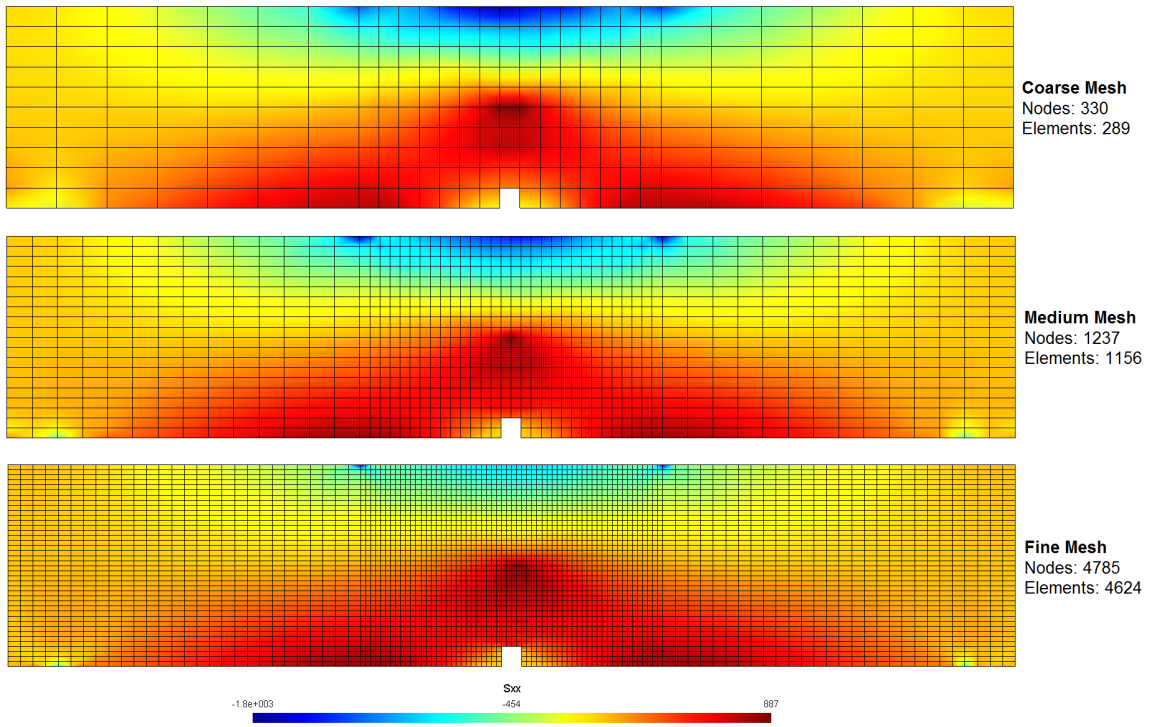

Σχήμα 6: Παραμετρική διερεύνηση σύγκλισης: κατανομή ορθής τάσης (σ_{xx}) στο βήμα ανάλυσης μετά το φορτίο αιχμής για μια τυχαία πραγματοποίηση του πεδίου σε κάθε δίκτυο.

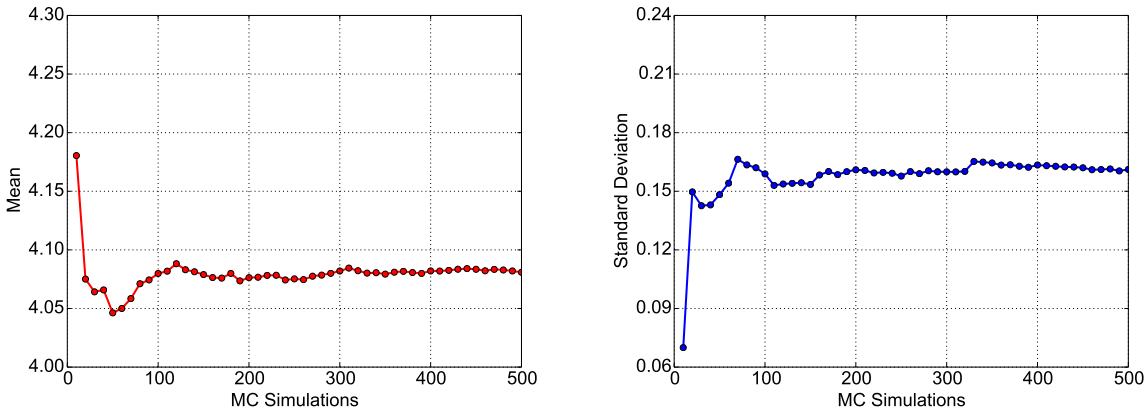

(α′) (β′)

Σχήμα 7: Στατιστική σύγκλιση για (α′) τη μέση τιμή και (β′) τη τυπική απόκλιση του φορτίου αιχμής (στοχαστικό G_f με $\sigma = 20\%$ και $b = 100$, για μη-Γκαουσιανό πεδίο Lognormal.

ρεαλιστική απομείωση της δυσκαμψίας σε ορισμένες περιπτώσεις (βλ. Σχήμα 9α′). Επίσης μεγαλύτερες τιμές του συντελεστή μεταβλητότητας καθώς και του μήκους συσχέτισης των στοχαστικών πεδίων οδηγεί σε μεγαλύτερη μεταβλητότητα στις καμπύλες φορτίου-μετατόπισης, όπως αναμενόταν άλλωστε (Σχήματα 9-10). Στην περίπτωση που οριστεί ως πιθανότητα αστοχίας p_f της δοκού ως η πιθανότητα όπου το φορτίο αιχμής να μην υπερβαίνει το φορτίο αιχμής της ντετερμινιστικής λύσης (το οποίο σημαίνει ότι η κατασκευή αστοχεί σε ένα μικρότερο φορτίο), τότε η p_f είναι ίση με 16% και 31% για τις περιπτώσεις

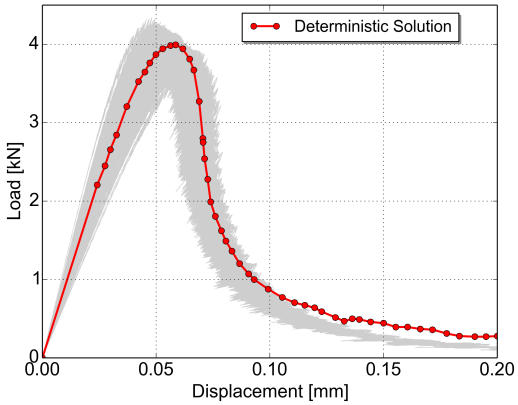

(α′) Στοχαστικό E

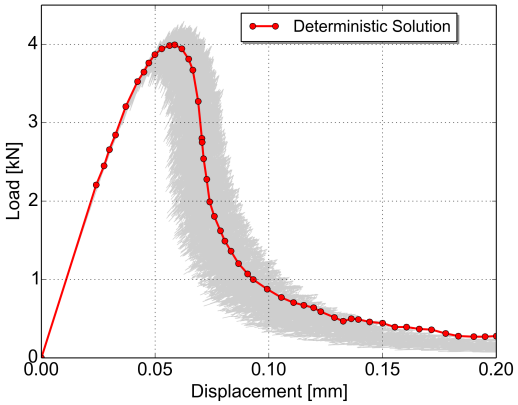

(β′) Στοχαστικό G_f

Σχήμα 8: Καμπύλες φορτίου-μετατόπισης για στοχαστικές παραμέτρους E και G_f με $\sigma = 10\%$ και $b = 1$ (για μη-Γκαουσιανό πεδίο, Lognormal).

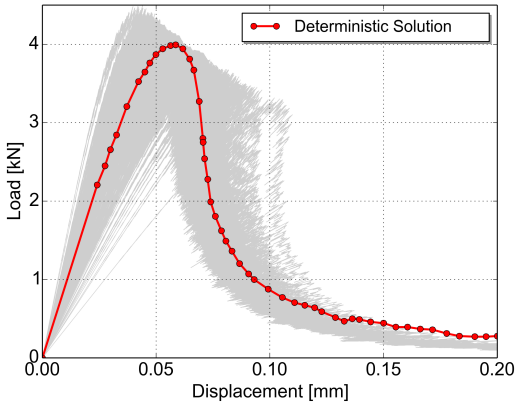

(α′) Στοχαστικό E

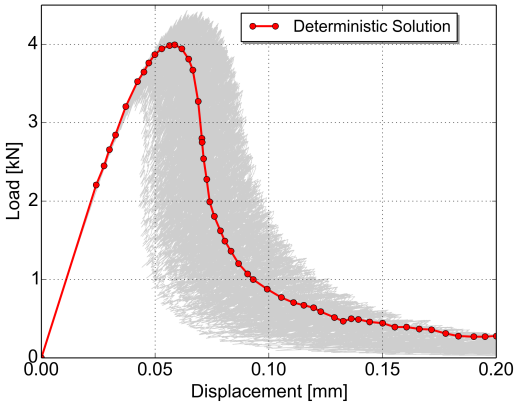

(β′) Στοχαστικό G_f

Σχήμα 9: Καμπύλες φορτίου-μετατόπισης για στοχαστικές παραμέτρους E και G_f με $\sigma = 20\%$ και $b = 100$ (για Γκαουσιανό πεδίο).

που περιγράφονται στο Σχήμα 8β′ και Σχήμα 10β′ αντίστοιχα.

0.2.3.2 Παράδειγμα 2ο: Δοκίμιο διπλής εγκοπής

Ως δεύτερο παράδειγμα, αναλύθηκε ένα δοκίμιο διπλής εγκοπής σε εφελκυσμό (Nguyen, 2008; Shi *et al.*, 2000) το οποίο φαίνεται στο Σχήμα 11. Οι κόμβοι της κάτω πλευράς του δοκιμίου είναι δεσμευμένοι ως προς τις δυο διευθύνσεις στο επίπεδο, καθώς και οι κόμβοι της πάνω πλευράς ως προς την οριζόντια διεύθυνση. Οι αριθμητικές αναλύσεις πραγματοποιήθηκαν χρησιμοποιώντας 4κομβικά – 4πλευρικά ισοπαραμετρικά πεπερασμένα στοιχεία. Οι αβέβαιες παράμετροι του προβλήματος είναι το μέτρο ελαστικότητας Young E, η εφελκυστική αντοχή f_t και η ενέργεια θραύσης G_f του υλικού όπου οι μέσες τιμές τους είναι ίσες με 24 GPa, 2.4 MPa και 0.059 N/mm, αντίστοιχα.

Η χωρική διακύμανση των αβέβαιων παραμέτρων περιγράφεται από διαδιάστατα (2D-1V) ομογενή λογαριθμοκανονικής κατανομής μη-Γκαουσιανά στοχαστικά πεδία μεταφοράς. Ε-

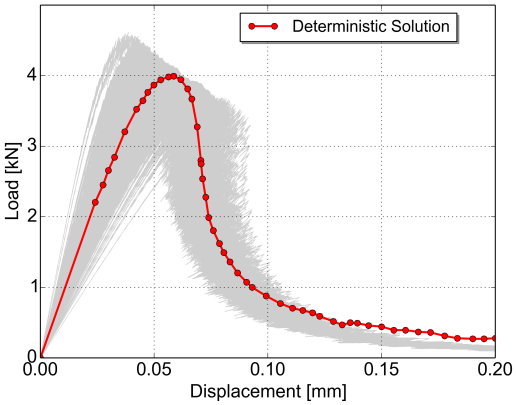

(α′) Στοχαστικό E

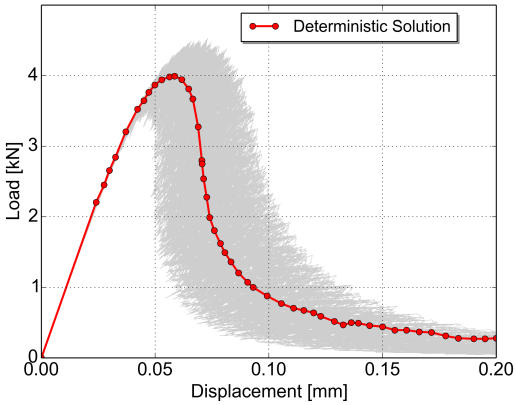

(β′) Στοχαστικό G_f

Σχήμα 10: Καμπύλες φορτίου-μετατόπισης για στοχαστικές παραμέτρους E και G_f με $\sigma = 20\%$ και $b = 100$ (για μη-Γκαουσιανό πεδίο, Lognormal).

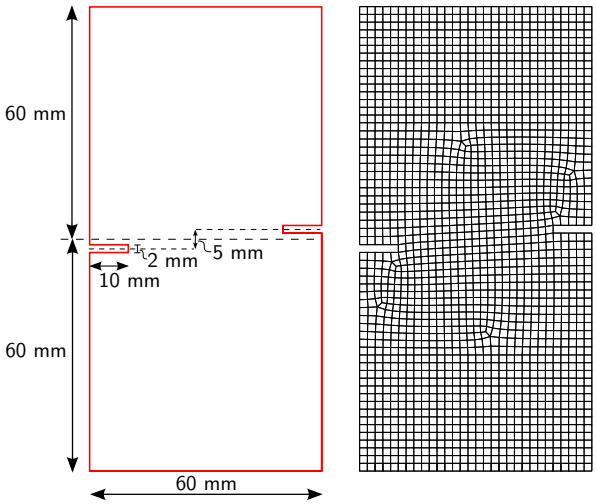

Σχήμα 11: Δοκίμιο διπλής εγκοπής (γεωμετρία και δίκτυο: 1950 κόμβοι και 1850 στοιχεία).

πιλέχθηκαν τρεις διαφορετικές τιμές ($b = 1.2, 12, 120$) της παραμέτρου b ($= b_1 = b_2$) του μήκους συσχέτισης, που αντιστοιχούν σε στοχαστικό πεδίο ασθενούς, μέτριας και ισχυρής συσχέτισης. Ο αριθμός των όρων N_j που χρησιμοποιήθηκαν στην σειρά της μεθόδου της φασματικής απεικόνισης είναι ίδιος με αυτόν του Παραδείγματος 1. Στα Σχήματα 12α′, 12β′ φαίνονται τρεις τυχαίες πραγματοποιήσεις του λογαριθμοκανονικού πεδίου για $\sigma = 20\%$ και $b = 1.2$, $b = 120$ αντίστοιχα.

Θεωρήθηκε επίσης η περίπτωση της ανισότροπης συσχέτισης ($b_1 \neq b_2$) για να εξεταστεί η επιρροή της στη μεταβλητότητα απόκρισης της κατασκευής. Η τελευταία υπολογίζεται χρησιμοποιώντας την άμεση μέθοδο Monte Carlo για ένα δείγμα μεγέθους ίσο με 500. Η στατιστική σύγκλιση επιτυγχάνεται μέσα σε αυτόν τον αριθμό των δειγμάτων και στο Σχήμα 13 η μέση τιμή και την τυπική απόκλιση της φορτίου αιχμής απεικονίζεται ως συνάρτηση του αριθμού των προσομοιώσεων Monte Carlo.

Στα Σχήματα 14, 15 φαίνονται οι καμπύλες φορτίου-μετατόπισης που προέρχονται από διαφορετικές στοχαστικές προσομοιώσεις με στοχαστικές μεταβλητές το E και τη G_f

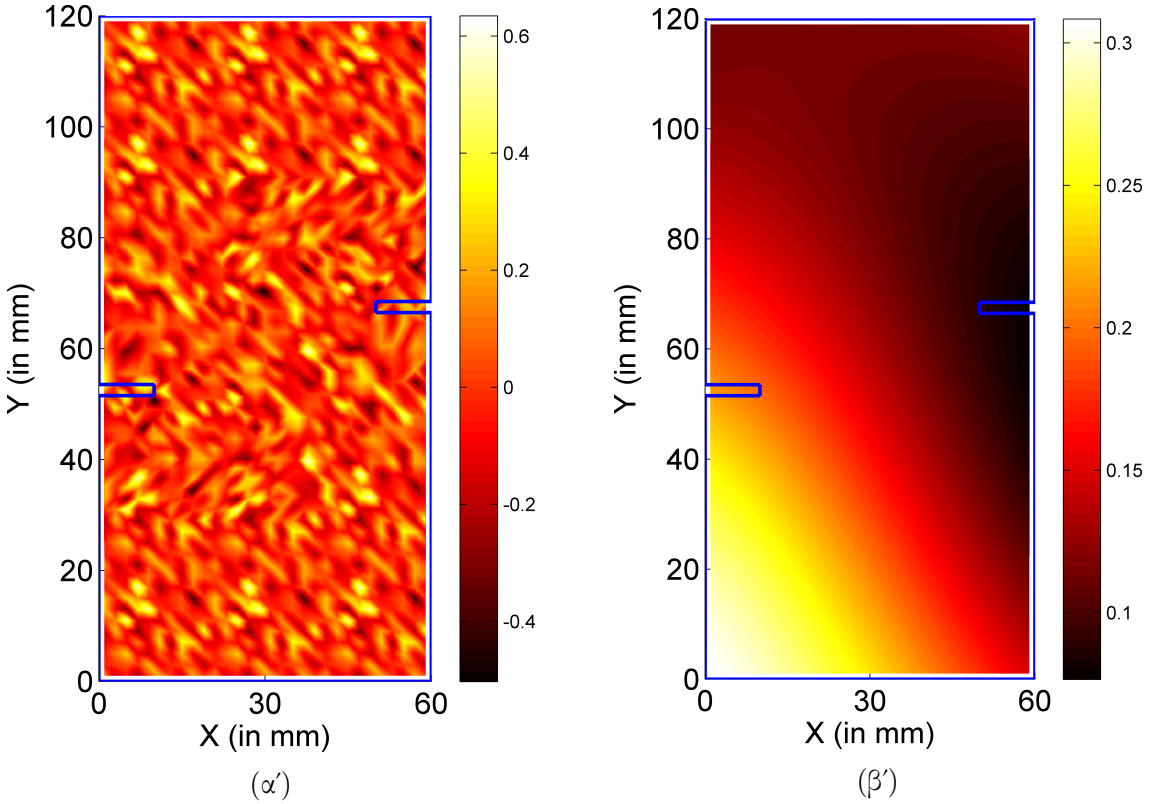

Σχήμα 12: Πραγματοποιήσεις του λογαριθμοκανονικού πεδίου για $\sigma = 20\%$ και (α′) $b = 1.2$, (β′) $b = 120$.

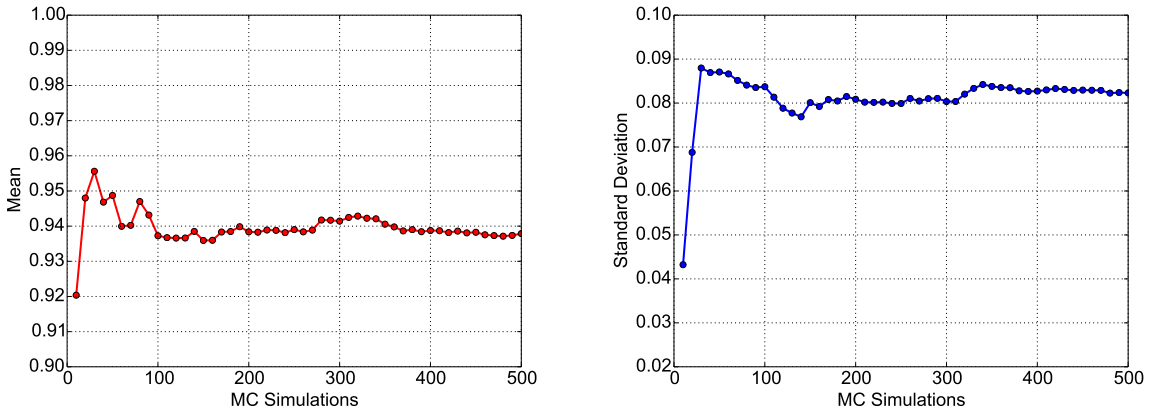

Σχήμα 13: Στατιστική σύγκλιση για (α′) την μέση τιμή και (β′) την τυπική απόκλιση του φορτίου αιχμής (όταν E, f_t, G_f είναι πλήρως συσχετισμένα με $\sigma = 10\%$ και $b = 120$, (μη-Γκαουσιανό πεδίο, Lognormal).

καθώς και συγκρίσεις με την ντετερμινιστική μη-γραμμική λύση του προβλήματος (Nguyen, 2008). Τα αποτελέσματα που ελήφθησαν με την υπόθεση της ανισότροπης συσχέτισης ήταν παρόμοια και, ως εκ τούτου σε όλες τις προσομοιώσεις υιοθετήθηκε η ισοτροπική συσχέτιση ($b = b_1 = b_2$).

Επιπρόσθετα, θεωρήθηκαν δύο περιπτώσεις συνδυασμένων παραλλαγών των E, f_t και G_f. Στη πρώτη περίπτωση, τα λογαριθμοκανονικά στοχαστικά πεδία που εκπροσωπούν τις τρεις παραμέτρους ήταν πλήρως συσχετισμένα, ενώ στη δεύτερη περίπτωση δεν υπήρχε συσχέτιση μεταξύ τους. Οι αντίστοιχες καμπύλες φορτίου-μετατόπισης που φαίνονται

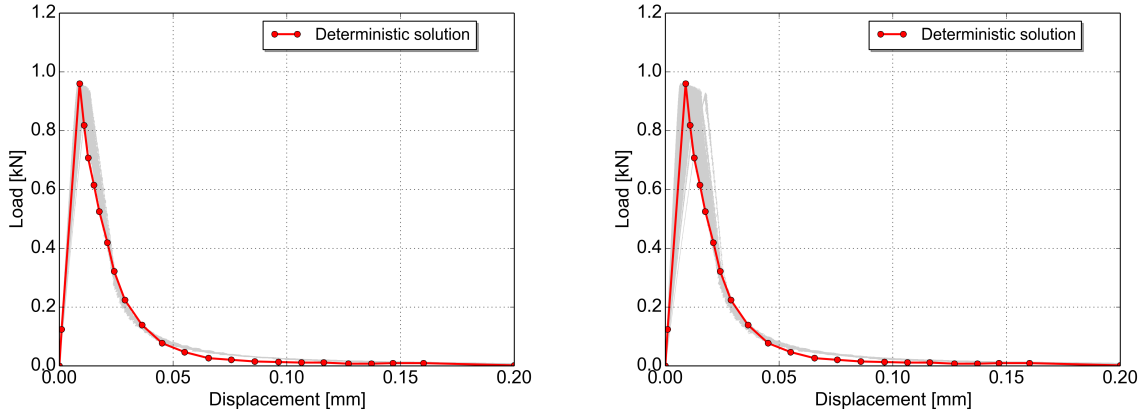

(α′) (β′)

Σχήμα 14: Καμπύλες φορτίου-μετατόπισης για στοχαστική παράμετρο E με (α′) $\sigma = 10\%$ και (β′) $\sigma = 20\%$ (μη-Γκαουσιανό πεδίο, Lognormal, $\beta = 120$).

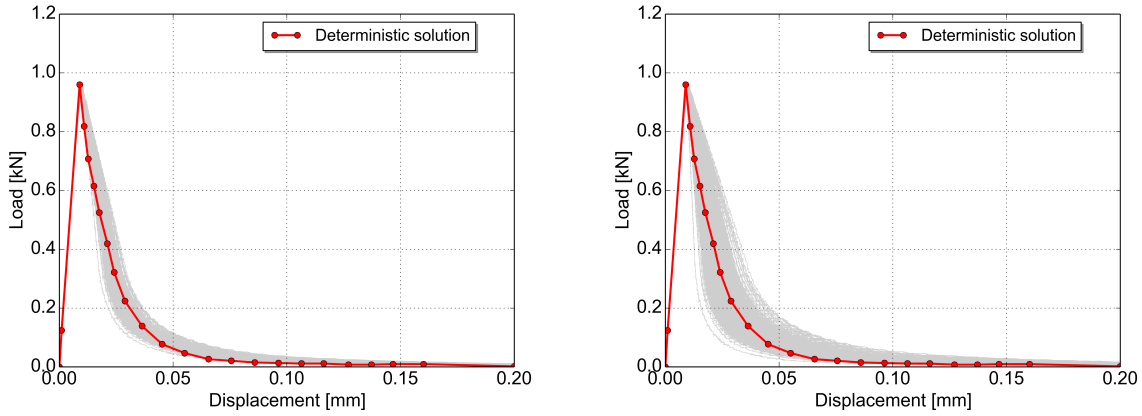

(α′) (β′)

Σχήμα 15: Καμπύλες φορτίου-μετατόπισης για στοχαστική παράμετρο G_f με (α′) $\sigma = 10\%$ και (β′) $\sigma = 20\%$ (μη-Γκαουσιανό πεδίο, Lognormal, $\beta = 120$).

στο Σχήμα 16 παρουσιάζουν μεγάλη μεταβλητότητα με αποτέλεσμα να οδηγούν σε μία μεγάλη πιθανότητα αστοχίας της κατασκευής. Για $b = 1.2$, το φορτίο αιχμής από όλες τις πραγματοποιήσεις του πεδίου είναι μικρότερο από το αντίστοιχο ντετερμινιστικό, ενώ η πιθανότητα αστοχίας p_f είναι ίση με 87% και 61% για τις περιπτώσεις όπου $b = 12$ και 120, αντίστοιχα (περίπτωση πλήρως συσχετισμένων ιδιοτήτων).

Τέλος, στο Σχήμα 17 απεικονίζονται οι διαδρομές των ρωγμών για μια τυχαία επιλεγμένη πραγματοποίηση των πεδίων και για διαφορετικές τιμές της παραμέτρου b του μήκους συσχέτισης. (Οι διαδρομές αυτές σχηματίζονται εμμέσως από τα στοιχεία με μηδενική δυσκαμψία στο τέλος της κάθε ανάλυσης SLA). Η μη-ρεαλιστική διαδρομή που ελήφθη στη περίπτωση όπου $b = 1.2$ οφείλεται στη μεγάλη μεταβλητότητα του μέτρου ελαστικότητας E η οποία οδηγεί κατ' επέκταση και σε μεγάλες διαφορές στις τιμές του E στα όμορα στοιχεία.

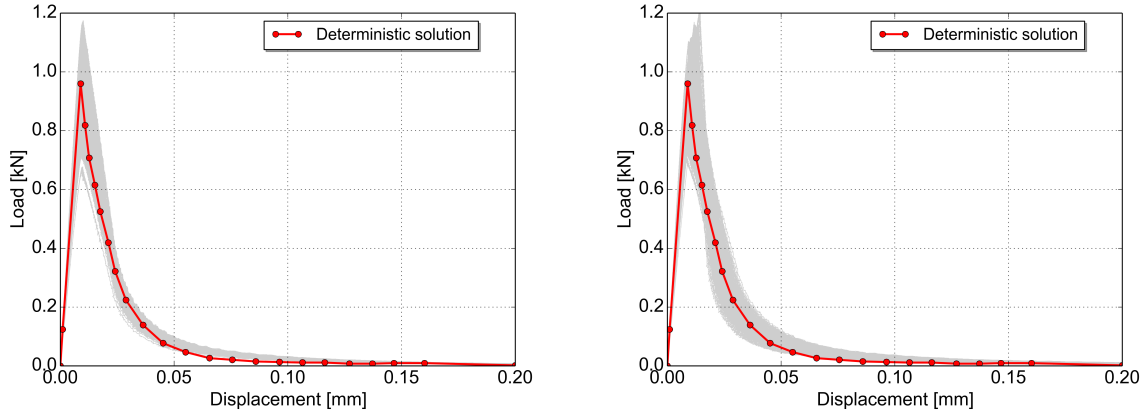

(α′) (β′)

Σχήμα 16: Καμπύλες φορτίου-μετατόπισης της συνδυασμένης περίπτωσης των τριων παραμέτρων για $\sigma = 10\%$ (μη-Γκαουσιανό πεδίο, Lognormal, $\beta = 120$): (α′) E, f_t, G_f πλήρως συσχετισμένες, (β′) E, f_t, G_f ασυσχέτιστες.

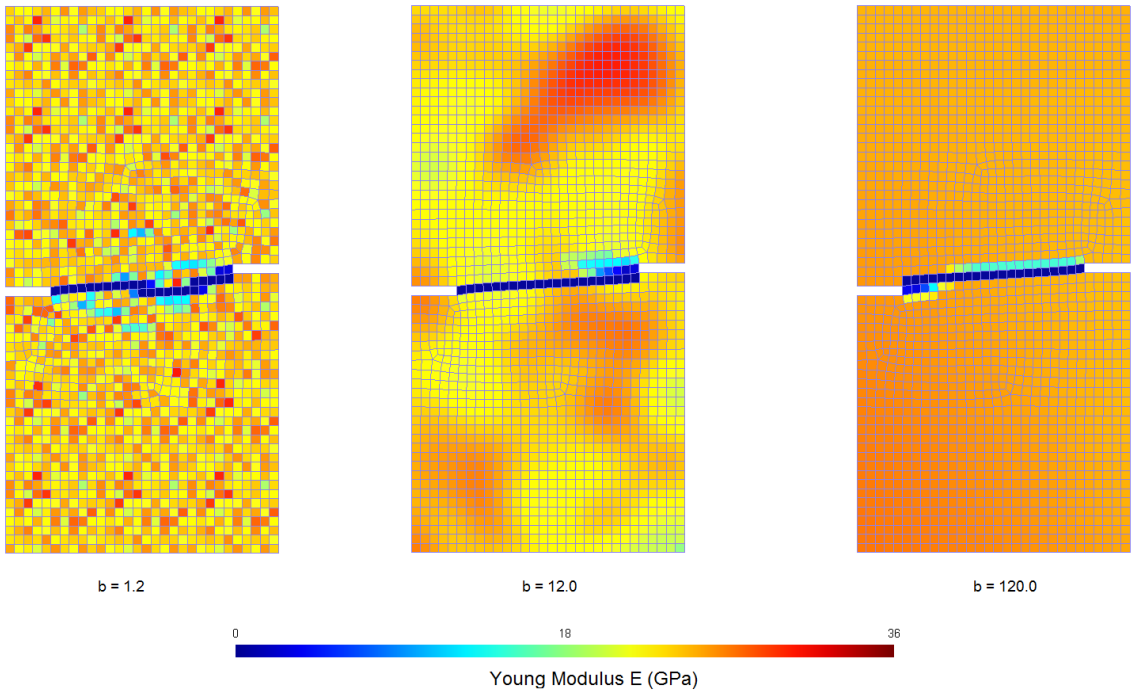

Σχήμα 17: Διαδρομές ρωγμής για τυχαίες επιλεγμένες πραγματοποιήσεις του πεδίου και για διαφορετικές τιμές της παραμέτρου b (E, f_t, G_f περίπτωση πλήρους συσχέτισης).

0.3 Βέλτιστος σχεδιασμός κατασκευών υποκείμενων σε κόπωση

Στο δεύτερο μέρος της διατριβής, η μέθοδος των εκτεταμένων πεπερασμένων στοιχείων (extended finite element method - XFEM) συνιστά ένα κατάλληλο πλαίσιο για την προσομοίωση της διαδικασίας θραύσης σε κατασκευές υποκείμενες σε κόπωση. Προτείνεται μια ανάλυση αξιοπιστίας με στόχο την διερεύνηση της σχέσης μεταξύ των γεωμετρικών χαρακτηριστικών των κατασκευών και της διάρκειας ζωής αυτών. Κατά τη διαδικασία βέλτιστου σχεδιασμού λαμβάνονται υπόψη, η τυχαιότητα στη θέση της αρχικής ατέλειας

και η αβεβαιότητα στις ιδιότητες του υλικού των κατασκευών με την εισαγωγή συγκεκριμένων πιθανοτικών περιορισμών στην διατύπωση των προβλημάτων βελτιστοποίησης. Προκειμένου να επιλεχθεί ο κατάλληλος μεταευρετικός αλγόριθμος για την επίλυση των προβλημάτων βελτιστοποίησης, διεξάγεται ανάλυση ευαισθησίας τεσσάρων αλγορίθμων βασισμένων στη εξελικτική διαδικασία (evolutionary algorithms). Το πεδίο εφαρμογής των προτεινόμενων διατυπώσεων διερευνάται με χαρακτηριστικά αριθμητικά παραδείγματα. Αποδεικνύεται ότι με τις κατάλληλες αλλαγές στη γεωμετρία των κατασκευών, η διάρκεια ζωής τους μπορεί να ενισχυθεί σημαντικά και ακολουθεί σύγκριση των βέλτιστων γεωμετρικών μορφών που προκύπτουν για τα επιθυμητά επίπεδα διάρκειας ζωής. Η επιλογή ως προς την θέση της αρχικής ατέλειας και ο προσανατολισμός αυτής βρέθηκαν επίσης να έχουν σημαντική επίδραση στις βέλτιστες γεωμετρικές μορφές.

0.3.1 Η μέθοδος των εκτεταμένων πεπερασμένων στοιχείων

Βασική ιδέα της μεθόδου XFEM αποτελεί ο εμπλουτισμός του χώρου προσέγγισης έτσι ώστε να καταστεί ικανός να αναπαράγει τις ασυνέχειες (ρωγμές ή διεπιφάνειες). Η μέθοδος XFEM στηρίζεται στη κλασική μέθοδο των πεπερασμένων στοιχείων, προσομοιώνοντας τυχαίες ασθενείς και ισχυρές ασυνέχειες. Κατά την διαδικασία της XFEM, αρχικά, παράγεται ένα δίκτυο πεπερασμένων στοιχείων και στη συνέχεια λαμβάνοντας υπόψη τη θέση των ασυνεχειών, γίνεται εμπλουτισμός επιλεγμένων κόμβων των κλασικών πεπερασμένων στοιχείων με επιπλέον βαθμούς ελευθερίας, κοντά στις ασυνέχειες και στα άκρα της ρωγμής προκειμένου να παρέχουν ένα υψηλότερο επίπεδο ακρίβειας.

0.3.1.1 Εμπλουτισμένες προσεγγίσεις

Οι εμπλουτισμένες προσεγγίσεις έχουν αποτελέσει το αντικείμενο πολλών υπολογιστικών μελετών των δυο τελευταίων δεκαετιών. Οι περισσότερες από αυτές αναπτύχθηκαν στο πλαίσιο της μεθόδου (partition of unity - PU) (Melenk & Babuška, 1996). Η βασική ιδέα στην XFEM είναι η προσθήκη ασυνεχών συναρτήσεων στις κλασικές προσεγγίσεις των πεπερασμένων στοιχείων βάσει της μεθόδου PU. Έτσι, για τον υπολογισμό της μετατόπισης στο σημείο $\boldsymbol{x}$ εντός του χωρίου που περιλαμβάνει τις ασυνέχειες, χρησιμοποιείται η ακόλουθη προσέγγιση (Belytschko & Black, 1999):

$$u(\boldsymbol{x}) = \boldsymbol{u}^{\text{std}} + \boldsymbol{u}^{\text{enr}} = \sum_{j=1}^{n} N_j(\boldsymbol{x})\boldsymbol{u}_j + \sum_{k=1}^{m} N_k(\boldsymbol{x})\psi(\boldsymbol{x})\boldsymbol{a}_k$$

όπου $\boldsymbol{u}_j$ είναι το διάνυσμα των επικόμβιων βαθμών ελευθερίας, $\boldsymbol{a}_k$ είναι το σύνολο των βαθμών ελευθερίας που προστίθεται στο κλασικό προσομοίωμα πεπερασμένων στοιχείων και $\psi(\boldsymbol{x})$ είναι το σύνολο των τεχνητών βαθμών ελευθερίας εμπλουτισμού που ορίζονται στο σύνολο των κόμβων που περιλαμβάνονται στην περιοχή επιρροής (υποστήριξης) της ασυνέχειας. Ο πρώτος όρος στη δεξιά πλευρά της εξίσωσης αποτελεί τις κλασικές προσεγγίσεις των πεπερασμένων στοιχείων για τον προσδιορισμό του πεδίου της μετατόπισης, ενώ ο δεύτερος όρος αποτελεί τις εμπλουτισμένες προσεγγίσεις που λαμβάνουν υπόψη την ύπαρξη ασυνεχειών.

0.3.1.2 Προσομοίωση της ρωγμής

Για τη προσομοίωση των ρωγμών στη μέθοδο XFEM, χρησιμοποιούνται δύο τύποι συναρτήσεων εμπλουτισμού: (α) η 'βηματική' συνάρτηση Heaviside και (β) οι ασυμπτωτικές συναρτήσεις άκρου-ρωγμής από την κλασική θεωρία θραυστομηχανικής. Έτσι το προσεγγιστικό πεδίο μετατοπίσεων μπορεί να εκφραστεί σε όρους ενός κλασικού πεδίου μετατοπίσεων u^{std}, ενός πεδίου μετατοπίσεων που τέμνεται από τη ρωγμή u^{H}, καθώς και ενός πεδίου μετατοπίσεων στα άκρα της ρωγμής u^{tip} ως εξής:

$$u(\boldsymbol{x}) = \boldsymbol{u}^{\text{std}} + \boldsymbol{u}^{\text{H}} + \boldsymbol{u}^{\text{tip}}$$

ή πιο ρητά:

$$u(\boldsymbol{x}) = \sum_{j=1}^{n} N_j(\boldsymbol{x})\boldsymbol{u}_j + \sum_{h=1}^{mh} N_h(\boldsymbol{x})H(\boldsymbol{x})\boldsymbol{a}_h + \sum_{k=1}^{mt} N_k(\boldsymbol{x})\Big(\sum_{l=1}^{mf} F_l(\boldsymbol{x})\boldsymbol{b}_k^l\Big)$$

όπου n είναι ο αριθμός των κόμβων του κάθε πεπερασμένου στοιχείου με τους κλασικούς βαθμούς ελευθερίας $\boldsymbol{u}_j$ και τις συναρτήσεις σχήματος $N_j(\boldsymbol{x})$, mh είναι ο αριθμός των κόμβων των στοιχείων που περιέχουν την ρωγμή (αλλά όχι το άκρο της), $\boldsymbol{a}_h$ είναι το διάνυσμα των πρόσθετων επικόμβιων βαθμών ελευθερίας για την προσομοίωση της ρωγμής (όχι των άκρων της) με τη συνάρτηση Heaviside $H(\boldsymbol{x})$, m_t είναι ο αριθμός των κόμβων σχετικοί με το άκρο της ρωγμής στο πεδίο επιρροής της, $\boldsymbol{b}_k^l$ είναι το διάνυσμα των πρόσθετων επικόμβιων βαθμών ελευθερίας για την προσομοίωση των άκρων της ρωγμής και $F_l(\boldsymbol{x})$ είναι οι συναρτήσεις εμπλουτισμού άκρου-ρωγμής.

Συνάρτηση **Heaviside** Τα στοιχεία τα οποία τέμνονται ολόκληρα από τη ρωγμή, και διαχωρίζονται σε δύο τμήματα, εμπλουτίζονται με την 'βηματική' συνάρτηση Heaviside. Η συνάρτηση Heaviside είναι ασυνεχής κατά μήκος της ρωγμής και σταθερή εκατέρωθεν της ρωγμής. Ο διαχωρισμός του στοιχείου από τη ρωγμή προκαλεί ένα άλμα στο πεδίο της μετατόπισης και η συνάρτηση Heaviside δίνει την επιθυμητή συμπεριφορά προκειμένου να προσεγγίσει το πραγματικό πεδίο. Μαθηματικά, η συνάρτηση ορίζεται ως εξής:

$$H = \begin{cases} +1, & \text{for } (\boldsymbol{x} - \boldsymbol{x}^*) \cdot \boldsymbol{n} > 0 \\ -1, & \text{for } (\boldsymbol{x} - \boldsymbol{x}^*) \cdot \boldsymbol{n} < 0 \end{cases}$$

όπου $\boldsymbol{x}$ είναι το σημείο ενδιαφέροντος, $\boldsymbol{x}^*$ είναι το πλησιέστερο σημείο στο τμήμα Γ της ρωγμής και $\boldsymbol{n}$ είναι το μοναδιαίο κάθετο διάνυσμα στο $\boldsymbol{x}^*$. Με άλλα λόγια, η συνάρτηση Heaviside καθορίζει εάν το σημείο $\boldsymbol{x}^*$ βρίσκεται πάνω ή κάτω από το τμήμα της ρωγμής. Αυτό μπορεί να καθοριστεί επίσης από τον υπολογισμό της ελάχιστης προσημασμένης απόστασης signed distance από τη γεωμετρία της ρωγμής. Η συνάρτηση θα έχει θετική τιμή εάν το εσωτερικό γινόμενο των δύο διανυσμάτων έχει θετική τιμή και αρνητική σε διαφορετική περίπτωση. Αν δεν ορίζεται μοναδικό κάθετο διάνυσμα τότε η συνάρτηση θα έχει θετική τιμή αν $(x - x^*)$ ανήκουν στον κώνο των καθέτων (βλ. Σχήμα 18).

Συνάρτηση άκρου ρωγμής Στην περίπτωση όπου το στοιχείο περιέχει το άκρο ρωγμής,

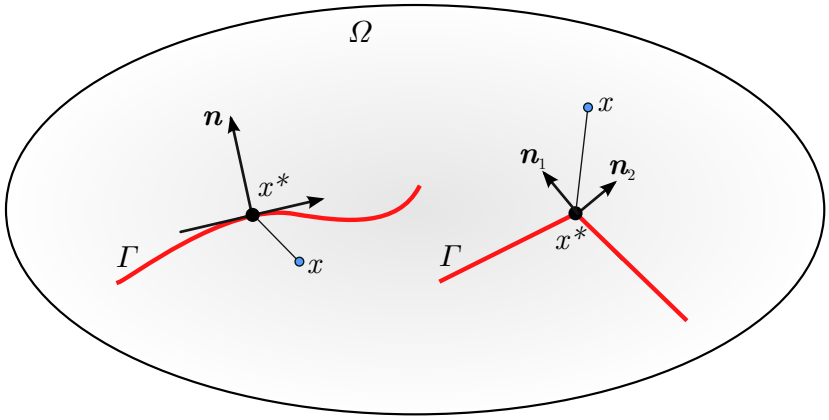

Σχήμα 18: Υπολογισμός της συνάρτησης Heaviside για τις περιπτώσεις της λείας και γωνιακής ρωγμής.

τότε ένα μέρος του στοιχείου τέμνεται από τη ρωγμή. Ως εκ τούτου, σε τέτοιες περιπτώσεις, η συνάρτηση Heaviside δεν μπορεί να χρησιμοποιηθεί για τον εμπλουτισμό του στοιχείου αυτού. Από την κλασική θεωρία της θραυστομηχανικής η ακριβής λύση του πεδίου της μετατόπισης γύρω από το άκρο ρωγμής δίνεται από τις εξής σχέσεις:

$$u_x = \frac{K_I}{2\mu}\sqrt{\frac{r}{2\pi}}cos\frac{\theta}{2}(\kappa - 1 + 2sin^2\frac{\theta}{2}) + \frac{K_{II}}{2\mu}\sqrt{\frac{r}{2\pi}}sin\frac{\theta}{2}(\kappa + 1 + 2cos^2\frac{\theta}{2})$$
$$u_y = \frac{K_I}{2\mu}\sqrt{\frac{r}{2\pi}}cos\frac{\theta}{2}(\kappa + 1 - 2cos^2\frac{\theta}{2}) - \frac{K_I}{2\mu}\sqrt{\frac{r}{2\pi}}cos\frac{\theta}{2}(\kappa - 1 - 2sin^2\frac{\theta}{2})$$

όπου K_I, K_{II} είναι οι συντελεστές εντατικής κατάστασης (stress intensity factors - SIFs) για τις περιπτώσεις θραύσης τύπου I και II αντίστοιχα, (r, θ) είναι ένα πολικό σύστημα συντεταγμένων με αρχή στην άκρη της ρωγμής και κ η σταθερά Kolosov. Τα παραπάνω πεδία μετατόπισης περιέχονται εντός του πεδίου των ακόλουθων τεσσάρων συναρτήσεων, οι οποίες σχηματίζουν τη βάση του ασυμπτωτικού πεδίου γύρω από το άκρο ρωγμής (Fleming, 1997):

$$\{F_l(r,\theta)\}_{l=1}^4 = \left\{\sqrt{r}\sin(\frac{\theta}{2}); \sqrt{r}\cos(\frac{\theta}{2}); \sqrt{r}\sin(\frac{\theta}{2})\sin(\theta); \sqrt{r}\cos(\frac{\theta}{2})\sin(\theta)\right\}$$

Εκτός από τους κλασικούς βαθμούς ελευθερίας, οι παραπάνω συναρτήσεις προκαλούν αύξηση κατά τέσσερις επιπλέον βαθμούς ελευθερίας σε κάθε κατεύθυνση για κάθε κόμβο και χρησιμοποιούνται για τον εμπλουτισμό του πεδίου των μετατοπίσεων κοντά στο άκρο ρωγμής. Η πρώτη συνάρτηση (βλ. Σχήμα 19α′) είναι ασυνεχής κατά μήκος της ρωγμής και αντιπροσωπεύει την ασυνέχεια κοντά στο άκρο της ρωγμής, ενώ οι υπόλοιπες τρεις συναρτήσεις (βλ. Σχήματα 19β′-19δ′) προστίθενται για μεγαλύτερη ακρίβεια στα αποτελέσματα για σχετικά αραιά δίκτυα. Ο όρος $\sqrt{r}$ στις συναρτήσεις εμπλουτισμού προσδίδει τη μοναδικότητα στο τασικό πεδίο. Επιπλέον, οι συναρτήσεις εμπλουτισμού είναι ασυνεχείς κατά μήκος της ακτίνας $\theta = \pm\pi$.

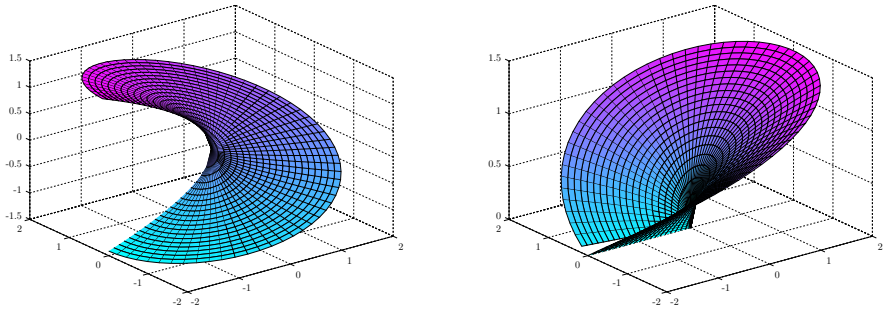

$(\alpha')\ \sqrt{r}\sin(\frac{\theta}{2})$ $(\beta')\ \sqrt{r}\cos(\frac{\theta}{2})$

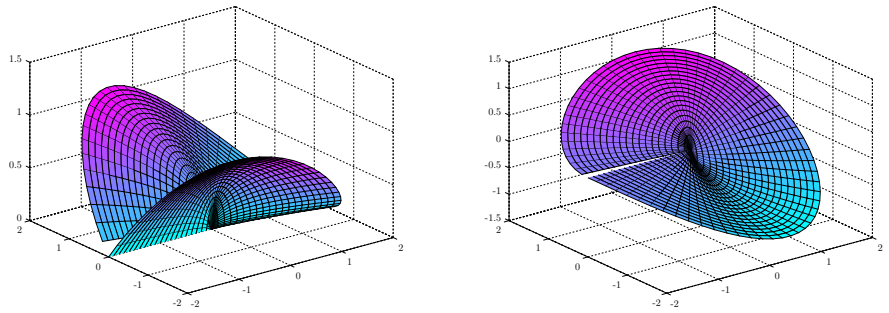

$(\gamma')\ \sqrt{r}\sin(\frac{\theta}{2})\sin(\theta)$ $(\delta')\ \sqrt{r}\cos(\frac{\theta}{2})\sin(\theta)$

Σχήμα 19: Συναρτήσεις εμπλουτισμού άκρου-ρωγμής.

0.3.1.3 Κυβερνώσες εξισώσεις

Θεωρούμε ένα σώμα σε κατάσταση ισορροπίας με τις συνοριακές συνθήκες όπως στο Σχήμα 20. Η ισχυρή μορφή της εξίσωσης ισορροπίας γράφεται ως εξής:

$$\nabla \cdot \sigma + \boldsymbol{f}^b = 0 \quad \text{στο } \Omega$$

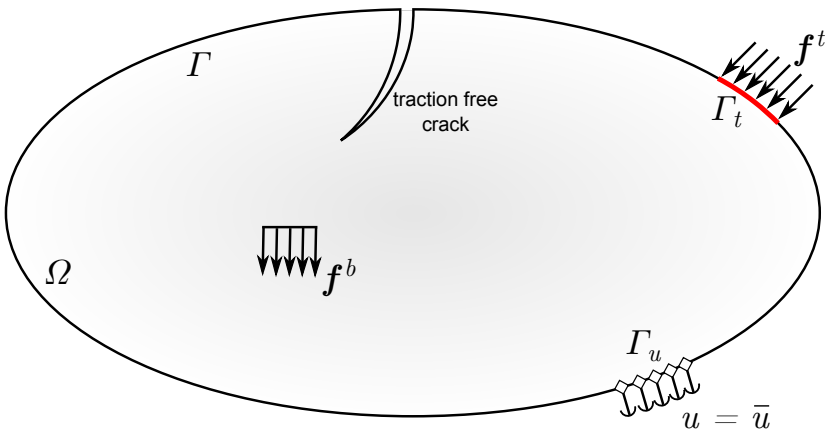

Σχήμα 20: Ένα σώμα σε κατάσταση ισορροπίας.

με τις ακόλουθες συνοριακές συνθήκες:

$$\begin{cases} \boldsymbol{\sigma} \cdot \boldsymbol{n} = \boldsymbol{f}^t, & \text{στο } \Gamma_t\text{: εξωτερικός ελκυστής} \\ \boldsymbol{u} = \overline{\boldsymbol{u}}, & \text{στο } \Gamma_u\text{: προκαθορισμένη μετατόπιση} \\ \boldsymbol{\sigma} \cdot \boldsymbol{n} = 0, & \text{στο } \Gamma_c\text{: ρωγμή ελεύθερη ελκυστών} \end{cases}$$

όπου Γ_t, Γ_u και Γ_c είναι τα σύνορα που αφορούν τους ελκυστές, τις μετατοπίσεις και τη ρωγμή, αντίστοιχα, $\boldsymbol{\sigma}$ είναι ο τανυστής της τάσης και $\boldsymbol{f}^b$, $\boldsymbol{f}^t$ είναι τα διανύσματα του ίδιου βάρους και των εξωτερικών ελκυστών αντίστοιχα.

Έτσι, η μεταβολική διατύπωση του προβλήματος συνοριακών τιμών (boundary value problem - BVP) λαμβάνει την εξής μορφή:

$$W^{int} = W^{ext}$$

ή

$$\int_\Omega \boldsymbol{\sigma} \cdot \delta\boldsymbol{\epsilon} d\Omega = \int_\Omega \boldsymbol{f}^b \cdot \delta\boldsymbol{u} d\Omega + \int_{\Gamma_t} \boldsymbol{f}^t \cdot \delta\boldsymbol{u} d\Gamma$$

0.3.1.4 Διακριτή μορφή της εξίσωσης ισορροπίας

Κατά τη διακριτοποίηση της τελευταίας εξίσωσης κάνοντας χρήση των προσεγγιστικών συναρτήσεων που παρουσιάστηκαν στην Ενότητα 0.3.1.2, προκύπτει το ακόλουθο διακριτό σύστημα γραμμικών εξισώσεων ισορροπίας:

$$\boldsymbol{K}\boldsymbol{u}^h = \boldsymbol{f}$$

όπου $\boldsymbol{K}$ είναι το ολικό μητρώο δυσκαμψίας, $\boldsymbol{u}^h$ είναι το διάνυσμα των επικόμβιων βαθμών ελευθερίας (κλασικοί και εμπλουτισμένοι) και $\boldsymbol{f}$ είναι το διάνυσμα τις εξωτερικής φόρτισης. Το ολικό μητρώο και τα διανύσματα υπολογίζονται με τη προσθήκη της συνεισφοράς του κάθε στοιχείου σε αυτά. Το μητρώο δυσκαμψίας $\boldsymbol{K}^e$ του στοιχείου και το διάνυσμα της εξωτερικής φόρτισης $\boldsymbol{f}^e$ ορίζονται ως εξής:

$$\boldsymbol{K}_{ij}^e = \begin{bmatrix} \boldsymbol{K}_{ij}^{\boldsymbol{uu}} & \boldsymbol{K}_{ij}^{\boldsymbol{ua}} & \boldsymbol{K}_{ij}^{\boldsymbol{ub}} \\ \boldsymbol{K}_{ij}^{\boldsymbol{au}} & \boldsymbol{K}_{ij}^{\boldsymbol{aa}} & \boldsymbol{K}_{ij}^{\boldsymbol{ab}} \\ \boldsymbol{K}_{ij}^{\boldsymbol{bu}} & \boldsymbol{K}_{ij}^{\boldsymbol{ba}} & \boldsymbol{K}_{ij}^{\boldsymbol{bb}} \end{bmatrix}$$
$$f_i^e = \{\boldsymbol{f}_i^u \ \boldsymbol{f}_i^{\boldsymbol{a}} \ \boldsymbol{f}_i^{\boldsymbol{b}1} \ \boldsymbol{f}_i^{\boldsymbol{b}2} \ \boldsymbol{f}_i^{\boldsymbol{b}3} \ \boldsymbol{f}_i^{\boldsymbol{b}4}\}^T$$

και $\boldsymbol{u}^h$ είναι το διάυνυσμα των επικόμβιων μετατοπίσεων:

$$\boldsymbol{u}^h = \{\boldsymbol{u} \ \boldsymbol{a} \ \boldsymbol{b}_1 \ \boldsymbol{b}_2 \ \boldsymbol{b}_3 \ \boldsymbol{b}_4\}^T$$

με

$$\boldsymbol{K}_{ij}^{rs} = \int_{\Omega_e} (\boldsymbol{B}_i^r)^T \mathbb{C} \boldsymbol{B}_j^s d\Omega \quad \{r,s\} = \{\boldsymbol{u}, \boldsymbol{a}, \boldsymbol{b}\}$$

και

$$
\begin{aligned}
f_i^{\boldsymbol{u}} &= \int_{\Gamma_t} N_i \boldsymbol{f}^t d\Gamma + \int_{\Omega^e} N_i \boldsymbol{f}^b d\Omega \\
f_i^{\boldsymbol{a}} &= \int_{\Gamma_t} N_i H \boldsymbol{f}^t d\Gamma + \int_{\Omega^e} N_i H \boldsymbol{f}^b d\Omega \\
f_i^{\boldsymbol{b}\alpha} &= \int_{\Gamma_t} N_i F_\alpha \boldsymbol{f}^t d\Gamma + \int_{\Omega^e} N_i F_\alpha \boldsymbol{f}^b d\Omega \quad (\alpha = 1,2,3,4)
\end{aligned}
$$

όπου $\boldsymbol{B}$ είναι το μητρώο παραμορφωσιμότητας, που περιλαμβάνει τις παραγώγους των συναρτήσεων σχήματος:

$$
\begin{aligned}
\boldsymbol{B}_i^{\boldsymbol{u}} &= \begin{bmatrix} N_{i,x} & 0 \\ 0 & N_{i,y} \\ N_{i,y} & N_{i,x} \end{bmatrix} \\
\boldsymbol{B}_i^{\boldsymbol{a}} &= \begin{bmatrix} (N_i H(\phi))_{,x} & 0 \\ 0 & (N_i H(\phi))_{,y} \\ (N_i H(\phi))_{,y} & (N_i H(\phi))_{,x} \end{bmatrix} \\
\boldsymbol{B}_i^{\boldsymbol{b}} &= \begin{bmatrix} \boldsymbol{B}_i^{\boldsymbol{b}1} & \boldsymbol{B}_i^{\boldsymbol{b}2} & \boldsymbol{B}_i^{\boldsymbol{b}3} & \boldsymbol{B}_i^{\boldsymbol{b}4} \end{bmatrix} \\
\boldsymbol{B}_i^{\alpha} &= \begin{bmatrix} (N_i F_\alpha)_{,x} & 0 \\ 0 & (N_i F_\alpha)_{,y} \\ (N_i F_\alpha)_{,y} & (N_i F_\alpha)_{,x} \end{bmatrix} \quad (\alpha = 1,2,3,4)
\end{aligned}
$$

Τα μητρώα παραμορφωσιμότητας για τους πρόσθετους βαθμούς ελευθερίας μπορούν να γραφούν και ως εξής:

$$
\begin{aligned}
\boldsymbol{B}_i^{\boldsymbol{a}} &= \begin{bmatrix} (N_i[H(\phi) - H(\phi_i)])_{,x} & 0 \\ 0 & (N_i[H(\phi) - H(\phi_i)])_{,y} \\ (N_i[H(\phi) - H(\phi_i)])_{,y} & (N_i[H(\phi) - H(\phi_i)])_{,x} \end{bmatrix} \\
\boldsymbol{B}_i^{\alpha} &= \begin{bmatrix} (N_i[F_\alpha - F_{\alpha i}])_{,x} & 0 \\ 0 & (N_i[F_\alpha - F_{\alpha i}])_{,y} \\ (N_i[F_\alpha - F_{\alpha i}])_{,y} & (N_i[F_\alpha - F_{\alpha i}])_{,x} \end{bmatrix} \quad (\alpha = 1,2,3,4)
\end{aligned}
$$

και επιπρόσθετα τα διάνυσματα εξωτερικής φόρτισης μετατρέπονται ως ακολούθως:

$$
\begin{aligned}
f_i^{\boldsymbol{a}} &= \int_{\Gamma_t} N_i[H(\phi) - H(\phi_i)] \boldsymbol{f}^t d\Gamma + \int_{\Omega^e} N_i[H(\phi) - H(\phi_i)] \boldsymbol{f}^b d\Omega \\
f_i^{\boldsymbol{b}\alpha} &= \int_{\Gamma_t} N_i[F_\alpha - F_{\alpha i}] \boldsymbol{f}^t d\Gamma + \int_{\Omega^e} N_i[F_\alpha - F_{\alpha i}] \boldsymbol{f}^b d\Omega \quad (\alpha = 1,2,3,4)
\end{aligned}
$$

0.3.1.5 Έναρξη και διάδοση ρωγμής

Η ακρίβεια και η αξιοπιστία της ανάλυσης ενός φορέα υπό θραύση εξαρτάται κατά κύριο λόγο από τον ακριβή προσδιορισμό και τη συνέχεια της διαδρομής της ρωγμής. Ως εκ τούτου, το κριτήριο έναρξης και διάδοσης της ρωγμής παίζει σημαντικό ρόλο. Μερικά από τα ευρέως χρησιμοποιούμενα κριτήρια διάδοσης ρωγμών είναι τα εξής:

- ελάχιστης πυκνότητας ανηγμένης παραμόρφωσης (minimum strain energy density) (Sih, 1974),
- μέγιστου ρυθμού απελευθέρωσης ενέργειας (maximum energy release rate) (Nuismer, 1975),
- μέγιστης περιφερειακής τάσης (maximum hoop stress) (Erdogan & Sih, 1963),
- καθολικός αλγόριθμος εντοπισμού (global tracking algorithm) (Oliver & Huespe, 2004).

Στην παρούσα διατριβή υιοθετήθηκε το κριτήριο της μέγιστης περιφερειακής τάσης. Το κριτήριο αυτό βασίζεται στην αξιολόγηση των συντελεστών εντατικής κατάστασης K_I και K_{II}. Σύμφωνα με αυτό: (α) η έναρξη της ρωγμής συντελείται όταν η μέγιστη περιφερειακή τάση ξεπεράσει μία κρίσιμη τιμή, (β) η ρωγμή διαδίδεται σε κατεύθυνση θ_{cr} κατά την οποία η περιφερειακή τάση $\sigma_{\theta\theta}$ είναι μέγιστη.

Η γωνία θ_{cr} υπολογίζεται από τους συντελεστές K_I και K_{II} γύρω από το άκρο ρωγμής αν υποτεθεί ότι οι επιφάνειες της ρωγμής είναι ελεύθερες ελκυστών. Η περιφερειακή τάση στην κατεύθυνση διάδοσης της ρωγμής αποτελεί κύρια τάση, και έτσι η κατεύθυνση διαδόσεως της ρωγμής προσδιορίζεται θέτοντας την διατμητική τάση ίση με το μηδέν, δηλαδή:

$$\sigma_{r\theta} = \frac{1}{2\pi r} cos\frac{\theta}{2}\Big(\frac{1}{2}K_I sin\theta + \frac{1}{2}K_{II}(3cos\theta - 1\Big) = 0$$

Η τελευταία σχέση οδηγεί στον υπολογισμό της κρίσιμης γωνίας διάδοσης θ_{cr} της ρωγμής στο τοπικό σύστημα συντεταγμένων της:

$$\theta_{cr} = 2atan\frac{1}{4}\Big(\frac{K_I}{K_{II}} \pm \sqrt{\frac{K_I^2}{K_{II}} + 8}\Big)$$

Αξίζει να σημειωθεί ότι σύμφωνα με αυτό το κριτήριο η μέγιστη γωνία διάδοσης είναι ίση με $70.5°$ για την περίπτωση της θραύσης τύπου II. Μια πιο αποδοτική έκφραση της κρίσιμης γωνίας διάδοσης για τους αριθμητικούς υπολογισμούς έχει προταθεί από τους Liang *et al.*, 2003 και δίνεται από την σχέση:

$$\theta_{cr} = 2atan\frac{-2\frac{K_{II}}{K_I}}{1 + \sqrt{1 + 8(\frac{K_{II}}{K_I})^2}}$$

0.3.1.6 Αντοχή σε θραύση

Όπως και στη κλασική θεωρία της αντοχής των υλικών, όπου η υπάρχουσα τάση συγκρίνεται με την επιτρεπόμενη τάση του υλικού, στη θραυστομηχανική η κατάσταση ασταθούς αστοχίας ορίζεται όταν ο συντελεστής εντατικής κατάστασης K υπερβεί μια κρίσιμη τιμή K_c, η οποία ονομάζεται αντοχή σε θραύση (fracture toughness) και αντιπροσωπεύει

την ικανότητα ενός υλικού να αντέχει ένα δεδομένο επίπεδο τάσης στο άκρο μιας ρωγμής και να αντιστέκεται σε εφελκυσμό κατά τη προοδευτική επέκταση αυτής. Με άλλα λόγια ο συντελεστής K_c συμπεριφέρεται ως μια οριακή τιμή των συντελεστών εντατικής κατάστασης για κάθε τύπο θραύσης.

0.3.1.7 Διάδοση ρωγμής υπό κόπωση

Η έννοια των συντελεστών εντατικής κατάστασης χρησιμεύει επίσης στον υπολογισμό των χαρακτηριστικών ενός δομικού μέλους που υπόκεινται θραύση υπό κόπωση. Η ανάπτυξη της ρωγμής λόγω κόπωσης εκτιμάται από τον νόμο του Paris, (Paris *et al.*, 1961), ο οποίος προτάθηκε αρχικά για θραύσεις τύπου I συσχετίζοντας τον ρυθμό ανοίγματος ρωγμής υπό φορτίο κόπωσης με τους συντελεστές εντατικής κατάστασης. Για μικτού τύπου θραύση, ο τροποποιημένος νόμος του Paris εκφράζεται χρησιμοποιώντας το ενεργό εύρος των συντελεστών εντατικής κατάστασης $\Delta K_{\text{eff}} = K_{max} - K_{min}$. Έτσι, για ένα δεδομένο φορτίο κόπωσης και για άνοιγμα ρωγμής ίσο με Δa σε ΔN κύκλους φόρτισης, σύμφωνα με το νόμο του Paris ισχύει ότι:

$$\frac{\Delta a}{\Delta N} \approx \frac{da}{dN} = C(\Delta K_{\text{eff}})^m$$

όπου C και m είναι εμπειρικές σταθερές του υλικού. Η σταθερά m κυμαίνεται συνήθως μεταξύ 3 - 4 για τους δομικούς χάλυβες και τα κράματα αλουμινίου. Η τελευταία εξίσωση αντιπροσωπεύει μια γραμμική σχέση μεταξύ της ποσότητας $log(\Delta K_{\text{eff}})$ και της ποσότητας $log(\frac{da}{dN})$ οι οποίες χρησιμοποιούνται για να περιγράψουν τη συμπεριφορά διάδοσης ρωγμής υπό κόπωση στην περιοχή II (βλ. Σχήμα 21).

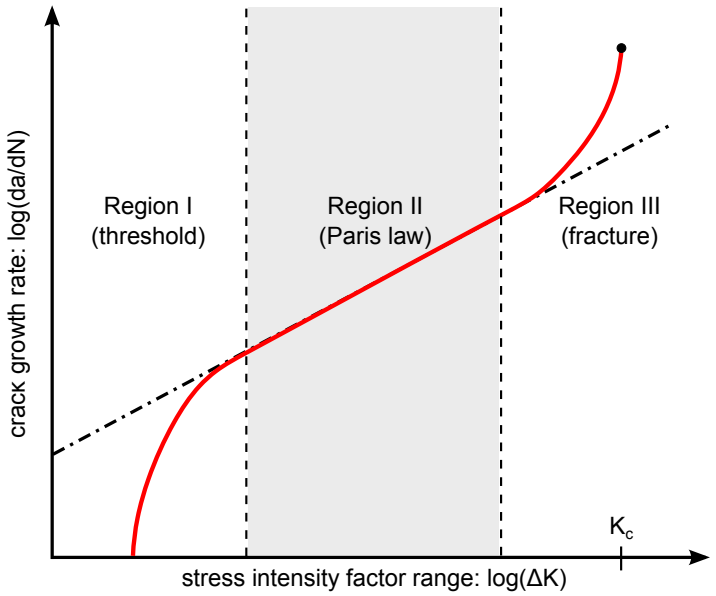

Σχήμα 21: Λογαριθμικός νόμος διάδοσης ρωγμής και ενεργή περιοχή του νόμου Paris.

Για τον υπολογισμό του ενεργού συντελεστή εντατικής κατάστασης K_{eff}, έχουν προταθεί διάφορα κριτήρια στη διεθνή βιβλιογραφία. Στη παρούσα εργασία ωστόσο, υιοθετήθηκε το προσομοίωμα του ρυθμού απελευθέρωσης ενέργειας που οδηγεί στην ακόλουθη έκφρα-

ση του ενεργού συντελεστή:

$$\Delta K_{\text{eff}} = \sqrt{\Delta K_I^2 + \Delta K_{II}^2}$$

μέσω της οποίας υπολογίζεται ο αντίστοιχος αριθμός κύκλων κόπωσης ως εξής (Anderson, 2004):

$$\Delta N = \frac{\Delta a}{C(\Delta K_{\text{eff}})^m}$$

0.3.2 Βέλτιστος σχεδιασμός κατασκευών με ρωγμές

Στη παρούσα διατριβή προτείνονται δυο διατυπώσεις προβλημάτων σύζευξης της μεθόδου XFEM στο πλαίσιο ενός περιβάλλοντος βέλτιστου σχεδιασμού των κατασκευών με ρωγμές: μια ντετερμινιστική και μια πιθανοτική (Georgioudakis *et al.*, 2014a, 2014b). Σύμφωνα με τη ντετερμινιστική διατύπωση, στόχος είναι η ελαχιστοποίηση του απαιτούμενου όγκου υλικού της κατασκευής υπό τον περιορισμό μιας ελάχιστης διάρκειας ζωής που εκφράζεται από την βέλτιστη γεωμετρία. Η διάρκεια ζωής υπολογίζεται μέσω των κύκλων κόπωσης, όπως περιγράφεται στην Ενότητα 0.3.1.7.

0.3.2.1 Ντετερμινιστική διατύπωση

Το ντετερμινιστικό πρόβλημα σχεδιασμού (DET) ορίζεται ως εξής:

$$\begin{aligned} \text{ελαχιστοποίηση} \quad & V(\boldsymbol{s}) \\ \text{υπό:} \quad & N(\boldsymbol{s}) \geq N_{min} \\ & s_i^{low} \leq s_i \leq s_i^{up}, \quad i = 1, 2, \ldots, n \end{aligned}$$

όπου V είναι ο όγκος του δομικού μέλους, s_i είναι οι μεταβλητές σχεδιασμού σχετικές με τη γεωμετρία του μέλους με άνω και κάτω όρια s_i^{low} και s_i^{up}, αντίστοιχα και N είναι η διάρκεια ζωής σε κύκλους κόπωσης με κάτω όριο την τιμή N_{min}.

0.3.2.2 Πιθανοτική διατύπωση

Κατ' επέκταση το πιθανοτικό πρόβλημα σχεδιασμού (PROB) ορίζεται ως εξής:

$$\begin{aligned} \text{ελαχιστοποίηση:} \quad & V(\boldsymbol{s}) \\ \text{υπό:} \quad & \bar{N}(\boldsymbol{s}, \boldsymbol{x}) \geq N_{min} \\ & s_i^{low} \leq s_i \leq s_i^{up}, \quad i = 1, 2, \ldots, n \\ & x_j \sim N(\mu_x, \sigma_x^2) \quad j = 1, 2, \ldots, nr \end{aligned}$$

όπου $\boldsymbol{s}$ και $\boldsymbol{x}$ είναι τα διανύσματα των μεταβλητών σχεδιασμού και των τυχαίων μεταβλητών, αντίστοιχα, και $\bar{N}$ είναι η μέση τιμή των κύκλων κόπωσης.

Η πιθανοτική ποσότητα x_j της τελευταίας εξίσωσης υπολογίζεται με τη βοήθεια της τεχνικής δειγματοληψίας (latin hybercube sampling - LHS) (βλ. Παράρτημα A). Η τεχνική LHS εισήχθη από τον McKay (2000) σε μια προσπάθεια να μειωθεί το απαιτούμενο υπολογιστικό κόστος των καθαρά τυχαίων μεθοδολογιών δειγματοληψίας. Η δειγματοληπτική μέθοδος δημιουργεί ένα μεταβλητό αριθμό δειγμάτων ομοιόμορφα κατανεμημένο

σε ολόκληρο το φάσμα ενδιαφέροντος. Ένα δείγμα υπερκύβου δημιουργείται με τη διαίρεση αυτού του φάσματος της κάθε μιας εκ των nr αβέβαιων μεταβλητών σε M μη-επικαλυπτόμενα τμήματα ίσης οριακής πιθανότητας. Έτσι, το σύνολο του χώρου, που αποτελείται από M παραμέτρους, διαχωρίζεται σε M^{nr} κελιά και ακολουθεί επιλογή μιας τυχαίας μοναδικής τιμής από κάθε διάστημα, παράγοντας M τιμές δείγματος για κάθε μεταβλητή εισόδου.

0.3.2 Επίλυση του προβλήματος βελτιστοποίησης

Η επίλυση των προβλημάτων βελτιστοποίησης που διατυπώθηκαν στην Ενότητα 0.3.2, γίνεται με τη χρήση μεταευρετικών αλγορίθμων αναζήτησης καθολικού βέλτιστου, βασισμένες στην εξελικτική διαδικασία. Προκειμένου να επιλεχθεί ο κατάλληλος μεταευρετικός διεξήχθη ανάλυση ευαισθησίας τεσσάρων εξελικτικών αλγορίθμων (evolution strategies, covariance matrix adaptation, elitist covariance matrix adaptation, differential evolution) σε περιβάλλον συγκριτικής αξιολόγησης με πολλαπλά τοπικά βέλτιστα. Από την ανάλυση αυτή προέκυψε ότι ο αλγόριθμος της differential evolution (DE) είχε την καλύτερη συμπεριφορά.

Η DE αποτελεί μια στοχαστική μέθοδο βασισμένη στον πληθυσμό για την επίλυση προβλημάτων καθολικού βέλτιστου σε συνεχείς χώρους που εισήχθη από τους Storn & Price (1995). Η DE μοιράζεται πολλά χαρακτηριστικά από την κλασική μέθοδο βελτιστοποίησης των γενετικών αλγορίθμων, εφαρμόζοντας στα χρωματοσώματα (chromosomes) του γονέα ένα τελεστή διαφορικής μετάλλαξης προκειμένου να δημιουργήσει τον απόγονο (offspring). Από την εισαγωγή της ως σήμερα, η DE αποτελεί αναμφισβήτητα έναν από τους πιο ισχυρούς στοχαστικούς αλγορίθμους βελτιστοποίησης πραγματικών παραμέτρων και έχει προσελκύσει την προσοχή πολλών ερευνητών σε όλο τον κόσμο με αποτέλεσμα να έχουν αναπτυχθεί αρκετές παραλλαγές του βασικού αλγορίθμου, με βελτιωμένη απόδοση. Ο κλασική ροή του αλγορίθμου της DE (Storn & Price, 1995; 1997) φαίνεται στο Σχήμα 22.

0.3.3 Αριθμητικές εφαρμογές

Προκειμένου να εξεταστούν οι δυνατότητες της προτεινόμενης μεθοδολογίας που περιγράφηκε στην Ενότητα 0.3.2 αναλύθηκε υπό κόπωση ένα δομικό μέλος από χάλυβα (Stolarska *et al.*, 2001). Στο Σχήμα 23 φαίνονται η γεωμετρία,η φόρτιση, και οι μεταβλητές σχεδιασμού του δομικού μέλους. Ο φορέας διακριτοποιήθηκε με 4πλευρικά – 4κομβικά ισοπαραμετρικά πεπερασμένα στοιχεία σταθερού πάχους ίσο με 5 mm και αναλύθηκε υπό συνθήκες επίπεδης έντασης για ισότροπο υλικό. Στη παρούσα διατριβή θεωρήθηκαν δύο περιπτώσεις συνοριακής στήριξης: στη πρώτη, που ονομάζεται 'άκαμπτο μέλος' (fillet rigid) δεσμεύθηκαν όλοι οι κόμβοι της κάτω πλευράς του μέλους, ενώ στη δεύτερη, που ονομάζεται 'εύκαμπτο μέλος' (fillet flexible), δεσμεύθηκαν οι δυο ακραίοι κόμβοι της κάτω πλευράς. Στην ενότητα αυτή παρουσιάζονται μόνο τα αποτελέσματα για την περίπτωση του άκαμπτου μέλους.

Και για τις δύο περιπτώσεις επιλύθηκαν ντετερμινιστικά και πιθανοτικά προβλήματα βελτιστοποίησης σχήματος. Η αντικειμενική συνάρτηση που ελαχιστοποιήθηκε, αντιστοιχούσε στον όγκο του υλικού, και τα δύο σύνολα των περιορισμών, ντετερμινιστικά και πιθανοτικά επιβλήθηκαν επί των κύκλων κόπωσης του μέλους. Επιπλέον, λόγω των κατασκευαστικών περιορισμών οι μεταβλητές σχεδιασμού αντιμετωπίστηκαν ως διακριτές κατά

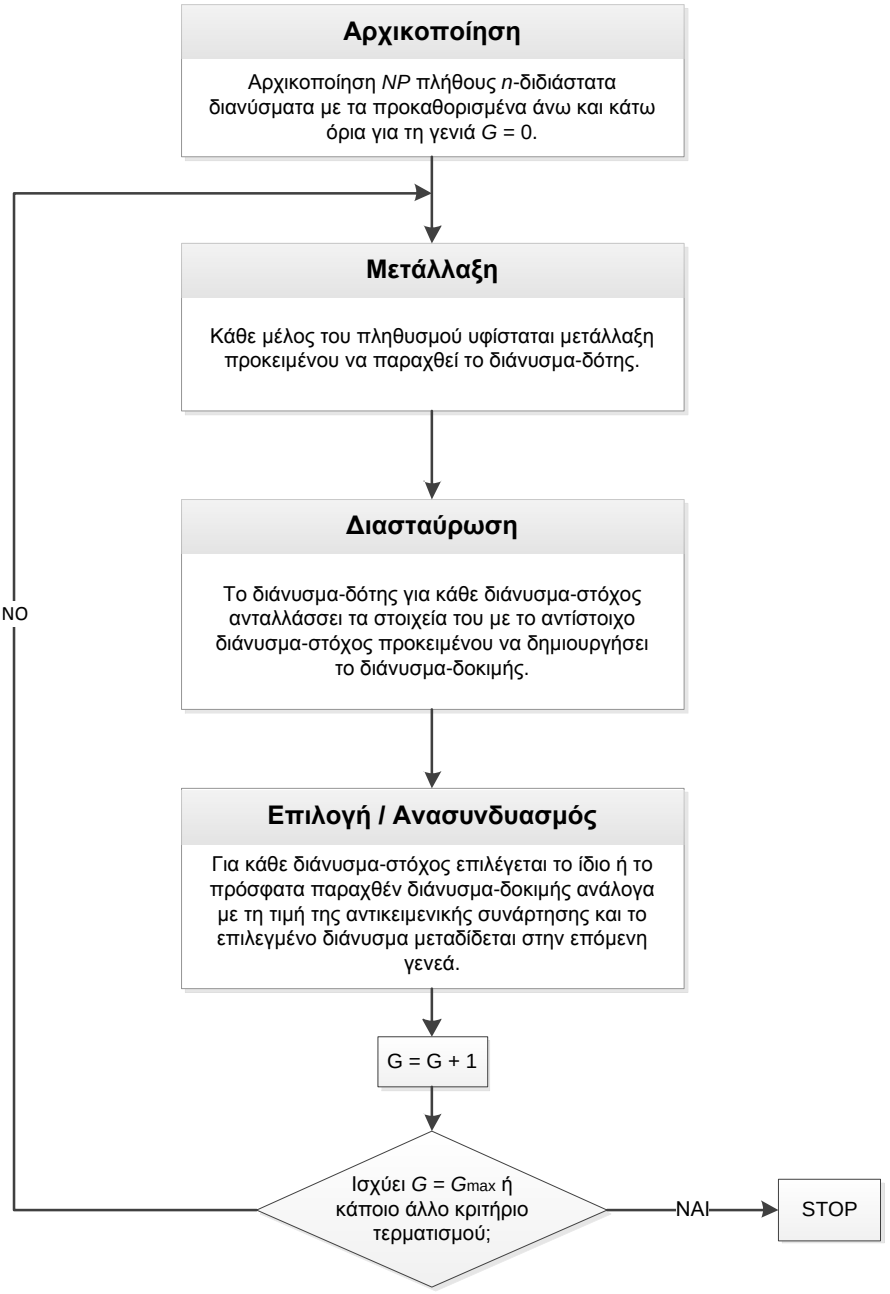

Σχήμα 22: Διάγραμμα ροής του κλασικού αλγόριθμου διαφορικής εξέλιξης (DE).

τον ίδιο τρόπο όπως και στη διακριτή διατύπωση προβλημάτων βελτιστοποίησης με Στρατηγικές Εξέλιξης (Lagaros *et al.*, 2004). Οι μεταβλητές σχεδιασμού που αντιστοιχούν στις διαστάσεις του μέλους ελήφθησαν από τον Πίνακα 1. Το φορτίο σχεδιασμού P ήταν με 20 KN (βλ. Σχήμα 23), και εφαρμόστηκε ως ένα συγκεντρωμένο εφελκυστικό φορτίο στο μέσο της άνω πλευράς .

Γενικά, στις πιθανοτικές αναλύσεις γίνεται διάκριση μεταξύ της αβεβαιότητας που οφείλεται στη διακύμανση του αποτελέσματος σε ένα επαναλαμβανόμενο πείραμα και της αβεβαιότητας που οφείλεται στην άγνοια. Η τελευταία αναφέρεται ως «τυχαιότητα» (randomness), κοινώς γνωστή ως 'αλεατορική αβεβαιότητα' (aleatoric uncertainty) η οποία

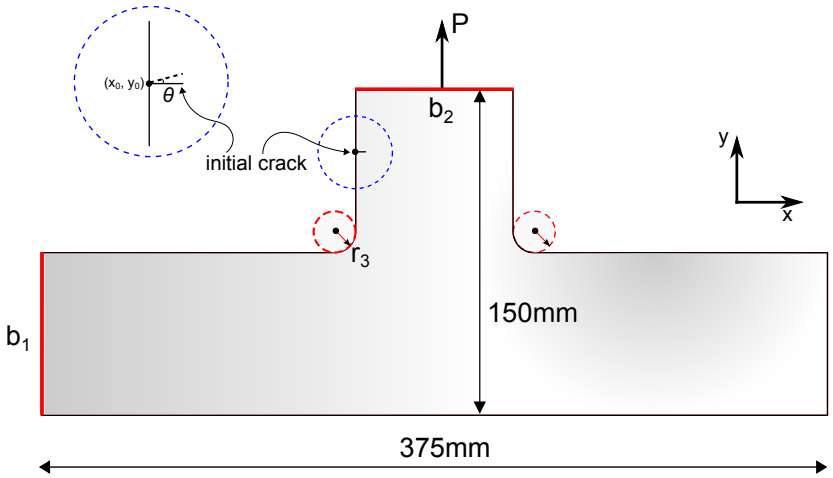

Σχήμα 23: Γεωμετρία και φόρτιση μεταλλικού μέλους και μεταβλητές σχεδιασμού του προβλήματος βελτιστοποίησης.

Μεταβλητή σχεδιασμού	l_{up}	l_{low}	βήμα
b_1	100.0	50.0	1.0
b_2	100.0	50.0	1.0
r_3	30.0	10.0	1.0

Πίνακας 1: Άνω και κάτω όρια των μεταβλητών σχεδιασμού και το αντίστοιχο βήμα τους (σε mm).

δε μπορεί να μειωθεί. Ωστόσο, οι ντετερμινιστικές όσο και οι πιθανοτικές θεωρήσεις βασίζονται σε διάφορες παραδοχές των παραμέτρων προσομοίωσης σύμφωνα με το υπάρχον επίπεδο γνώσης σχετικά με τη συμπεριφορά των δομικών συστημάτων υπό δεδομένες συνθήκες. Η αβεβαιότητα που συνδέεται με τις συνθήκες αυτές αναφέρεται ως «επιστημική αβεβαιότητα» (epistemic uncertainty).

Σε αυτή τη διατριβή εξετάζονται διάφορες πηγές αβεβαιότητας: ως προς την αρχικοποίηση της ρωγμής (ως προς τη θέση έναρξης), (αλεατορική αβεβαιότητα), η οποία επηρεάζει το σχήμα της μορφή διάδοσης της ρωγμής και ως προς την προσομοίωση (επιστημική αβεβαιότητα) η οποία επηρεάζει τη φέρουσα ικανότητα του μέλους. Η δυσκαμψία του μέλους συνδέεται άμεσα με το μέτρο ελαστικότητας E, του δομικού χάλυβα, ενώ ο αριθμός των κύκλων κόπωσης N_c επηρεάζεται από τις ιδιότητες του υλικού C και m. Η αύξηση του μήκους ρωγμής, ο λόγος Poisson και η ανθεκτικότητα K_c σε θραύση λαμβάνονται ίσες με 5.0 mm, 0.3 και 100 MPa/$\sqrt{m}$ αντίστοιχα, και αντιμετωπίζονται ντετερμινιστικά.

Ως εκ τούτου, για το δομικό μέλος χρησιμοποιήθηκαν πέντε τυχαίες μεταβλητές: η τεταγμένη y_0 του άκρου της αρχικής ρωγμής και η αντίστοιχη γωνία θ, (βλ. Σχήμα 23) το μέτρο ελαστικότητας E και οι παραμέτροι C, m του υλικού. Οι ιδιότητες του υλικού για το δομικό χάλυβα υλοποιήθηκαν ως ανεξάρτητες τυχαίες μεταβλητές των οποίων τα χαρακτηριστικά επιλέχθηκαν σύμφωνα με τους Ellingwood *et al.* (1980); Ellingwood & Galambos, (1982) και δίνονται στον Πίνακα 2.

Η αριθμητική μελέτη που ακολουθεί αποτελείται από δύο μέρη: στο πρώτο μέρος διεξήχθη μια παραμετρική διερεύνηση προκειμένου να βρεθεί ο κατάλληλος αριθμός των προσομοιώσεων που απαιτούνται για την υπολογιστική αποδοτικότητα και ευρωστία στην

Τυχαία μεταβλητή	μ	σ	COV	τύπος κατανομής
y_0 (σε mm)	$(150 - b_1)/(2 + b_1)$	-	5%	κανονική
θ (in degrees)	0.0	0.50	-	κανονική
E (in GPa)	207.0	35.19	17%	κανονική
C	2.45ε-11	4.16ε-12	17%	κανονική
m	2.37	0.40	17%	κανονική

Πίνακας 2: Τυχαίες μεταβλητές και κατανομή τους (μέση τιμή μ, τυπική απόκλιση σ και τύπος κατανομής).

εξαγωγή των στατιστικών ποσοτήτων για την επίδραση της τυχαιότητας επί των κύκλων κόπωσης του μέλους. Ενώ στο δεύτερο μέρος διερευνάται η απόδοση του μεταλλικού μέλους υπό κόπωση μέσα σε ένα πιθανοτικό πλαίσιο βελτιστοποίησης σχήματος.

0.3.3.1 Παραμετρική διερεύνηση

Στα πλαίσια της παραμετρικής διερεύνησης το άκαμπτο μέλος εξετάστηκε για τρεις τυχαίους σχεδιασμούς που αντιστοιχούν στα άνω (Design 1) και κάτω (Design 3) όρια των μεταβλητών σχεδιασμού καθώς και για έναν ενδιάμεσο (Design 2). Σκοπός της διερεύνησης αποτελεί η εύρεση του μικρότερου δυνατού αριθμού προσομοιώσεων για έναν αξιόπιστο υπολογισμό των στατιστικών ποσοτήτων που σχετίζονται με τον αριθμό των κύκλων κόπωσης. Έτσι για τις διαφορετικού πλήθους προσομοίωσεις Monte Carlo (MC) που διεξήχθησαν βάσει της τεχνικής LHS (βλέπε Παράρτημα A) υπολογίστηκαν η μέση τιμή και η τυπική απόκλιση των αριθμών των κύκλων κόπωσης οι οποίες φαίνονται στον Πίνακα 3.

Σχεδιασμός	Πλήθος MCS	Μέση τιμή	Διάμεσος	Τυπ. απόκλιση
Design 1	100	5382911.9	6895308.5	3176784.9
Design 1	200	6848983.6	7024024.0	11271233.5
Design 1	500	6568327.3	7026526.0	13717577.0
Design 1	1000	6533674.8	7026013.0	19043699.3
Design 2	100	90222.3	91794.2	27363.2
Design 2	200	94371.9	86020.0	28170.8
Design 2	500	96950.6	93982.8	109963.6
Design 2	1000	95214.8	94768.0	60920.3
Design 3	100	5260.5	4858.5	1141.3
Design 3	200	5371.9	4992.9	1308.9
Design 3	500	5369.6	5005.9	1278.3
Design 3	1000	5328.8	5360.0	994.2

Πίνακας 3: Στατιστικές μεγέθη για τους κύκλους κόπωσης της παραμετρικής διερεύνησης των τριών σχεδιασμών.

Η επίδοση για τον διαφορετικό αριθμό προσομοιώσεων MC του κάθε σχεδιασμού απεικονίζεται στα ιστογράμματα του Σχήματος 24. Στα πλαίσια της διερεύνησης οι τρεις σχεδιασμοί αποτιμώνται μέσω πλήθους ενός συνολικού πλήθους προσομοιώσεων (100 + 200 + 500 + 1000). Έτσι, επεξεργάστηκαν 5400 αναλύσεις XFEM προκειμένου να δημιουργηθεί μια αντιπροσωπευτική βάση απόκρισης για τις ενδιαφέρουσες παραμέτρους.

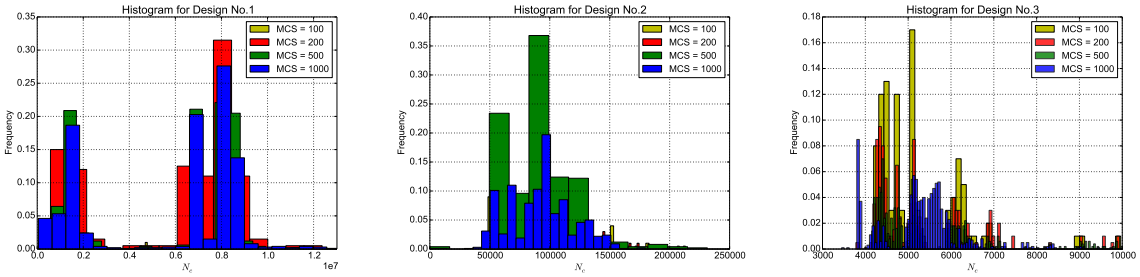

Σχήμα 24: Ιστογράμματα των τριων σχεδιασμών.

Η διάδοση των αβεβαιοτήτων πραγματοποιήθηκε μέσω της μεθόδου προσομοίωσης MC βάσει της τεχνικής LHS η οποία ενσωματώθηκε στο πλαίσιο της ανάλυσης με την μέθοδο XFEM όπως περιγράφεται στην Ενότητα 0.3.1. Σύμφωνα με τη τεχνική LHS ένας δεδομένος σχεδιασμός αναλύεται επαναληπτικά, για κάθε προσομοίωση MC χρησιμοποιώντας διαφορετικές τιμές των αβέβαιων παραμέτρων, που προέρχονται από τις αντίστοιχες κατανομές των πιθανοτήτων τους όπως προβλέπεται στον Πίνακα 2. Αξίζει να σημειωθεί ότι το μέγεθος του δικτύου πεπερασμένων στοιχείων στη περιοχή διάδοσης της ρωγμής, διατηρήθηκε σταθερό σε κάθε εμφωλευμένη (nested) ανάλυση XFEM που πραγματοποιήθηκε και στις δύο κατηγορίες (πιθανοτική ανάλυση και βελτιστοποίηση).

Στην ομάδα των ιστογραμμάτων του Σχήματος 24 απεικονίζεται η πιθανοτική κατανομή του αριθμού των κύκλων κόπωσης N_c για διαφορετικό πλήθος προσομοιώσεων για τους τρεις σχεδιασμούς. Η συχνότητα εμφάνισης του αριθμού των κύκλων κόπωσης ορίζεται ως ο λόγος του αριθμού των προσομοιώσεων, που αντιστοιχούν στις οριακές τιμές ενός συγκεκριμένου εύρους τιμών των κύκλων κόπωσης, προς το συνολικό αριθμό (N_{tot}) των προσομοιώσεων MC. Ο συνολικός αριθμός των προσομοιώσεων MC είναι ίσος με 100, 200, 500 ή 1000, ανάλογα με το πλήθος των προσομοιώσεων που χρησιμοποιήθηκαν κάθε φορά.

Συγκρίνοντας τα ιστογράμματα του Σχήματος 24, μπορεί να παρατηρήσει κανείς ότι το πλάτος των όριων εμπιστοσύνης που αντιστοιχούν στον ενδιάμεσο σχεδιασμό (Design 2) είναι περιορισμένο σε σύγκριση με τους άλλους δυο σχεδιασμούς, ενώ για τον σχεδιασμό που αντιστοιχεί στα ανώτερα όρια των μεταβλητών σχεδιασμού (Design 1) υπάρχουν δύο διακεκριμένες ζώνες συγκέντρωσης στις τιμές των συχνοτήτων. Επιπλέον, συγκρίνοντας τη μέση τιμή έναντι της διάμεσου του αριθμού των κύκλων κόπωσης, η τιμή της διαμέσου θεωρείται πιο αξιόπιστη, δεδομένου ότι δεν επηρεάζεται από τις ακραίες τιμές του αριθμού των κύκλων κόπωσης που υπολογίζονται. Συγκεκριμένα, στο πλαίσιο ενός προβλήματος βελτιστοποίησης οι τέτοιες ακραίες τιμές θα μπορούσαν να εμφανίζονται συχνά στη διαδικασία αναζήτησης του βέλτιστου, γεγονός το οποίο θα οδηγούσε σε ακραίους σχεδιασμούς. Από τη παραμετρική αυτή διερεύνηση προέκυψε τελικώς ότι οι 200 προσομοιώσεις MC αποτελούν έναν αποδεκτό συμβιβασμό μεταξύ υπολογιστικής αποδοτικότητας και ευρωστίας. Ο ίδιος αριθμός προσομοιώσεων θεωρήθηκε και για την επίλυση της πιθανοτικής διατύπωσης του προβλήματος βελτιστοποίησης σχήματος που περιγράφεται στο δεύτερο μέρος αυτής της ενότητας.

Στα Σχήματα 25 - 27 απεικονίζεται η επίδραση των αβέβαιων παραμέτρων στις διαδρομές διάδοσης των ρωγμών, λαμβάνοντας τα νέφη των 'τυπικών διαδρομών' των ρωγμών για τις 200 προσομοιώσεις MC. Μια διαδρομή ρωγμής ορίζεται ως 'τυπική' αν το σχήμα της είναι

όμοιο με το αντίστοιχο ντετερμινιστικό (Stolarska *et al.*, 2001). Ειδικά, για το σχεδιασμό Design 1, στο Σχήμα 25 εμφανίζονται μόνο οι τυπικές διαδρομές αφού παρατηρήθηκαν πολλές μη-τυπικές διαδρομές ρωγμών λόγω των γεωμετρικών χαρακτηριστικών του. Το γεγονός αυτό οδηγεί σ' ένα πρόσθετο λόγο επιλογής της διάμεσου έναντι της μέσης τιμής, ως κρίσιμη στατιστική ποσότητα στις πιθανοτικές διατυπώσεις του προβλήματος που ακολουθούν στη παρούσα διατριβή.

Η παραμετρική διερεύνηση έδειξε ότι οι διαδρομές ρωγμών που λαμβάνονται από την ανάλυση με τη μέθοδο XFEM επηρεάζονται από τις τυχαίες παράμετρους που ελήφθησαν υπόψη στη διαδικασία της ανάλυσης, και εν συνέχεια εξετάζεται η σημασία ενσωμάτωσης τους στη διαδικασία σχεδιασμού.

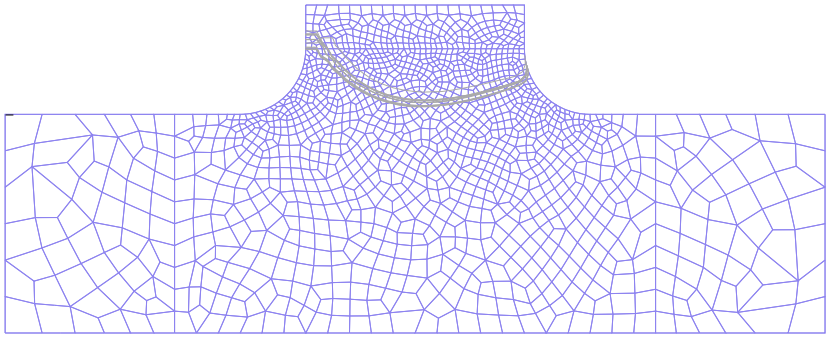

Σχήμα 25: Νέφη διαδρομών ρωγμών για το σχεδιασμό Design 1.

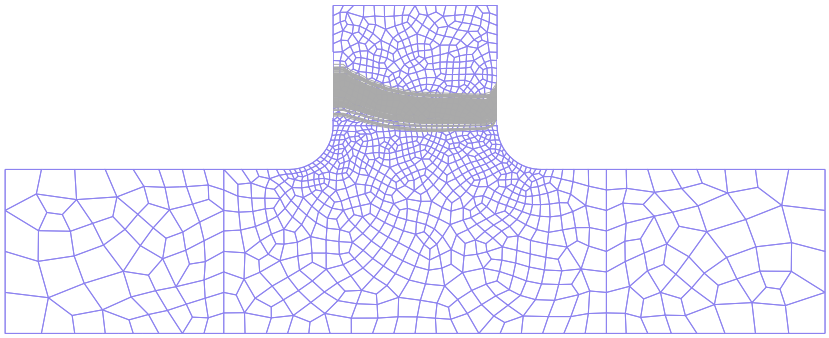

Σχήμα 26: Νέφη διαδρομών ρωγμών για το σχεδιασμό Design 2.

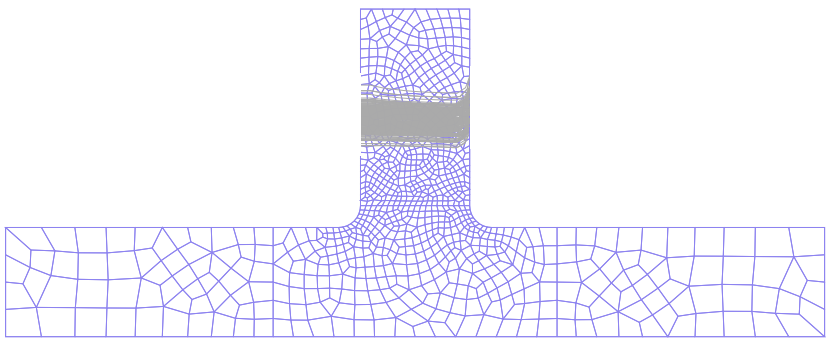

Σχήμα 27: Νέφη διαδρομών ρωγμών για το σχεδιασμό Design 3.

0.3.3.2 Διαδικασία βελτιστοποίησης

Μετά την παραμετρική διερεύνηση, επιλύθηκαν τέσσερα προβλήματα βελτιστοποίησης με το μεταευρετικό αλγόριθμο βελτιστοποίησης της διαφορικής εξέλιξης (DE) (βλ. Ενότητα 0.3.2) Οι συντομογραφίες K∗DET και K∗PROB, αντιστοιχούν στους βέλτιστους σχεδιασμούς που λαμβάνονται από την ντετερμινιστική (DET) και πιθανοτική (PROB) διατύπωση του προβλήματος, όπου ο μικρότερος επιτρεπτός αριθμός των κύκλων κόπωσης είναι ίσος με ∗ χιλιάδες. Στο Σχήμα 28 παρουσιάζεται η διαδικασία βελτιστοποίησης που βασίζεται στην ενσωμάτωση της μεθόδου XFEM στη ντετερμινιστική και πιθανοτική διατύπωση του προβλήματος. Εντός της κάθε επανάληψης της διαδικασίας αναζήτησης του βέλτιστου σχεδιασμού, υπάρχει ένας εμφωλευμένος βρόχος (nested loop) ανάλυσης με τη μέθοδο XFEM που πραγματοποιείται για τον κάθε υποψήφιο βέλτιστο σχεδιασμό. Έτσι, διεξάγεται μια πλήρης ανάλυση διάδοσης ρωγμών μέχρι να ικανοποιηθεί το κριτήριο αστοχίας, δηλαδή $K_{eq} < K_c$, υπολογίζοντας την αντίστοιχη διάρκεια ζωής μέσω του αριθμού των κύκλων κόπωσης (βλ. Ενότητα 0.3.1.7), πριν αποτιμηθεί ο υποψήφιος βέλτιστος σχεδιασμός.

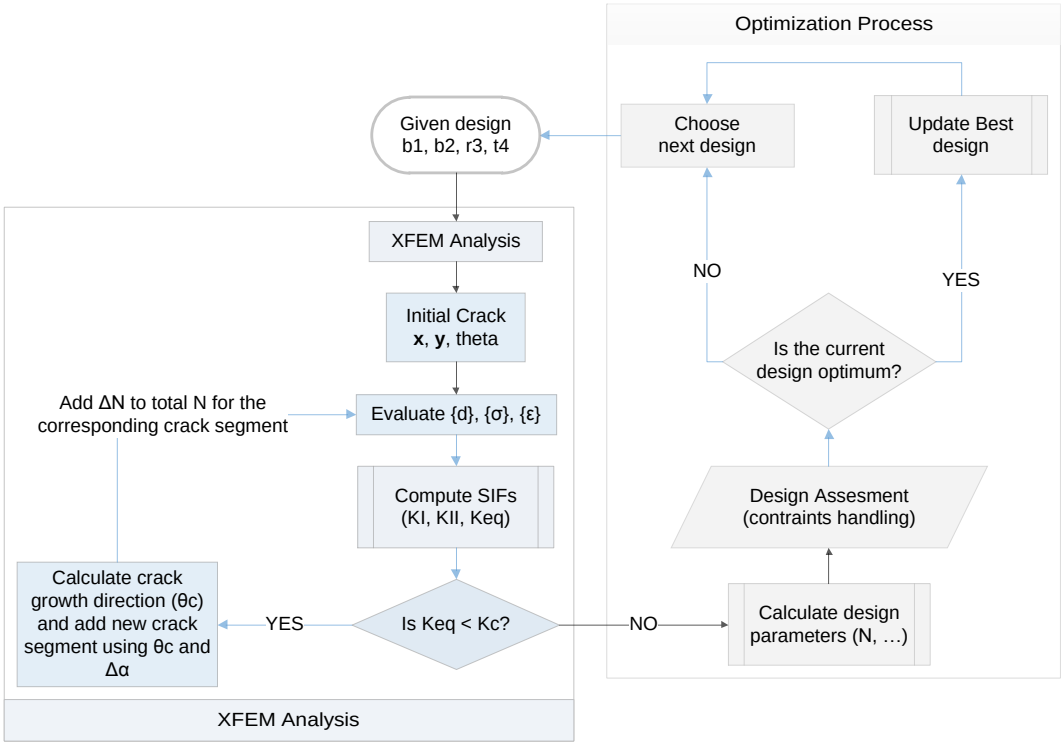

Σχήμα 28: Διαδικασία βελτιστοποίησης σχήματος XFEM για την ντετερμινιστική και την πιθανοτική διατύπωση του προβλήματος.

Οι παράμετροι που χρησιμοποιήθηκαν στον αλγόριθμο της DE έχουν ως εξής: μέγεθος πληθυσμού $NP = 30$, πιθανότητα $CR = 0.90$ και συντελεστής μετάλλαξης $F = 0.60$. Για συγκριτικούς λόγους, η μέθοδος που υιοθετήθηκε για την διαχείριση των περιορισμών και το κριτήριο τερματισμού είναι η ίδια σε όλες τις περιπτώσεις που αναλύθηκαν. Ειδικότερα

στη διαχείριση των περιορισμών, χρησιμοποιήθηκε η απλή αλλά αποτελεσματική πολλαπλή γραμμική τμηματική συνάρτηση ποινής (multiple linear segment penalty function) (Lagaros & Papadrakakis, 2012). Σύμφωνα με την θεώρηση αυτή, αν δεν υπάρχει παραβίαση, δεν επιβάλλεται καμιά ποινή στην αντικειμενική συνάρτηση, σε αντίθετη περίπτωση, εάν οποιοσδήποτε από τους περιορισμούς παραβιαστεί, εφαρμόζεται ποινή επί της αντικειμενικής συνάρτησης, σχετική με το μέγιστο βαθμό παραβίασης των περιορισμών. Η διαδικασία βελτιστοποίησης τερματίζεται όταν η βέλτιστη τιμή της αντικειμενικής συνάρτησης παραμένει αμετάβλητη στις τελευταίες 30 γενεές.

0.3.3.3 Αποτελέσματα βελτιστοποίησης

Ως αριθμητική εφαρμογή στο δεύτερο μέρος της παρούσας διατριβής, εξετάστηκε το άκαμπτο μεταλλικό μέλος όπως περιγράφηκε στην εισαγωγή της Ενότητας 0.3.3. Για την περίπτωση αυτή θεωρήθηκαν η ντετερμινιστική και η πιθανοτική διατύπωση όπως ορίζονται στις ακόλουθες εξισώσεις: Ο ελάχιστος αριθμός των κύκλων κόπωσης N_{min} ελήφθη ίσος με 100, 200 και 500 χιλιάδες και ως αντικειμένη συνάρτηση ελαχιστοποίησης ο όγκος V του απαιτούμενου υλικού.

$$
\begin{aligned}
\text{ελαχιστοποίηση:} \quad & V(b_1, b_2, r_3) \\
\text{υπό:} \quad & N(b_1, b_2, r_3) \geq N_{min} \\
& 50.0 \leq b_1 \leq 100.0, \\
& 50.0 \leq b_2 \leq 100.0, \\
& 10.0 \leq r_3 \leq 30.0
\end{aligned}
$$

$$
\begin{aligned}
\text{ελαχιστοποίηση:} \quad & V(b_1, b_2, r_3) \\
\text{υπό:} \quad & \bar{N}(b_1, b_2, r_3, y_0, \theta, E, C, m) \geq N_{min} \\
& 50.0 \leq b_1 \leq 100.0, \\
& 50.0 \leq b_2 \leq 100.0, \\
& 10.0 \leq r_3 \leq 30.0, \\
& y_0 \sim N((150 - b_1)/(2 + b_1), COV = 5\%) \\
& \theta \sim N(0, 0.50) \\
& E \sim lnN(207.0, 35.19) \\
& C \sim lnN(2.45^{-11}, 4.16^{-12}) \\
& m \sim lnN(2.37, 0.40)
\end{aligned}
$$

Όπως φαίνεται στα Σχήματα 29, 30 ο αλγόριθμος της DE κατάφερε να συγκλίνει στον βέλτιστο σχεδιασμό για την ντετερμινιστική και πιθανοτική διατύπωση αντίστοιχα. Συγκρίνοντας τις ιστορίες σύγκλισης στα σχήματα αυτά, παρατηρείται ότι για το ντετερμινιστικό πρόβλημα απαιτείται μικρότερος αριθμός γενεών για την εύρεση της βέλιστης λύσης που οφείλεται ενδεχομένως στο περιορισμένο χώρο αναζήτησης των εφικτών σχεδιασμών σε σχέση με αυτόν της πιθανοτικής διατύπωσης. Οι βέλτιστοι σχεδιασμοί που προέκυψαν σε κάθε περίπτωση παρουσιάζονται στον Πίνακα 4 μαζί με τον αντίστοιχο όγκο απαιτούμενου υλικού. Επίσης, στα Σχήματα 31, 33 απεικονίζονται τα βέλτιστα σχήματα που

προέκυψαν στη περίπτωση της ντετερμινισττικής διατύπωσης.

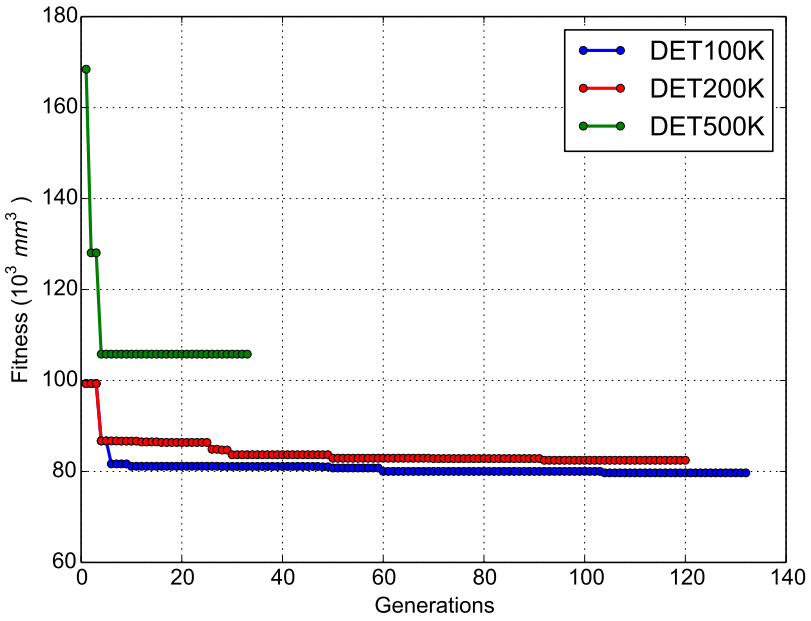

Σχήμα 29: Άκαμπτο μέλος: Αντικειμενική συνάρτηση συναρτήσει των γενεών για τη ντετερμινιστική περίπτωση (DET).

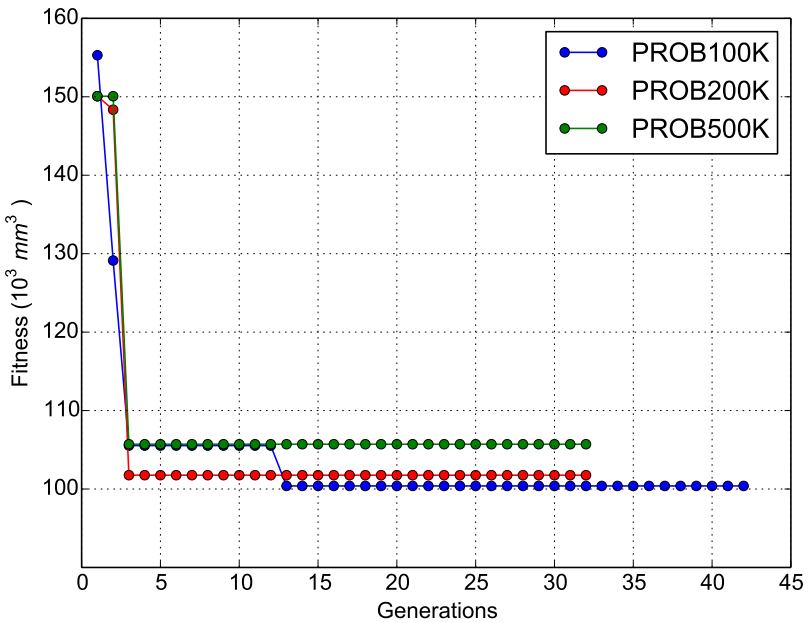

Σχήμα 30: Άκαμπτο μέλος: Αντικειμενική συνάρτηση συναρτήσει των γενεών για την πιθανοτική περίπτωση (PROB).

Συγκρίνοντας τους τρεις σχεδιασμούς (βλ. Πίνακας 4) της ντετερμινιστικής διατύπωσης προκύπτει ότι ο όγκος του υλικού στη περίπτωση DET500K αυξάνεται κατά 33% και 28% έναντι των περιπτώσεων DET100K και DET200K αντίστοιχα, ενώ για την περίπτωση DET200K αυξάνεται μόλις κατά 3.5% σε σύγκριση με DET100K. Επιπλέον, τα

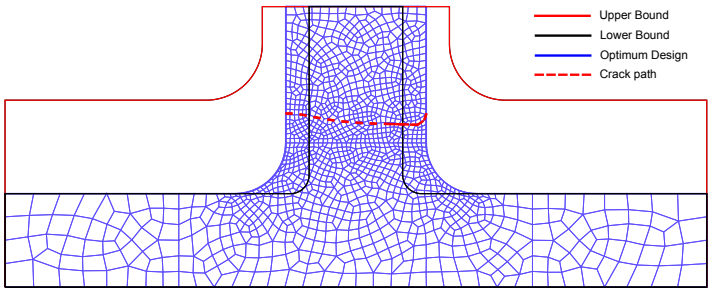

Σχήμα 31: Άκαμπτο μέλος: Βέλτιστο σχήμα για τη ντετερμινιστική διατύπωση DET100.

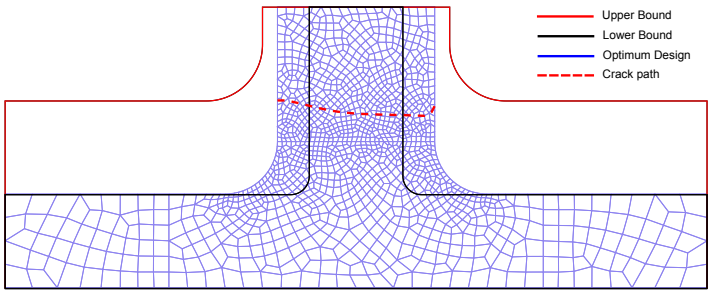

Σχήμα 32: Άκαμπτο μέλος: Βέλτιστο σχήμα για τη ντετερμινιστική διατύπωση DET200.

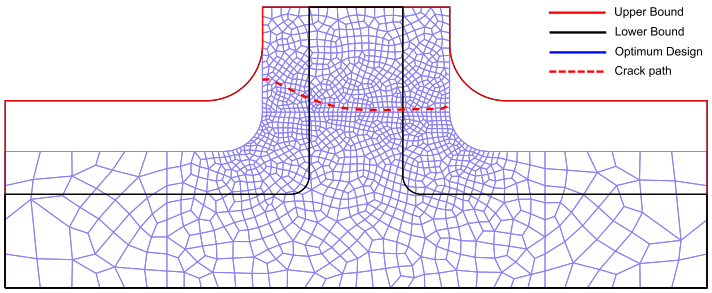

Σχήμα 33: Άκαμπτο μέλος: Βέλτιστο σχήμα για τη ντετερμινιστική διατύπωση DET500.

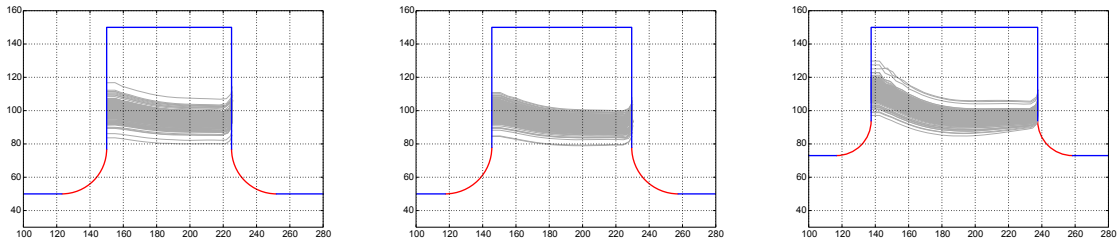

Σχήμα 34: Άκαμπτο μέλος: Νέφη διαδρομών ρωγμών για τις περιπτώσεις DET100, DET200 και DET500 αντίστοιχα.

αποτελέσματα που ελήφθησαν για την περίπτωση της πιθανοτικής διατύπωσης φανερώνουν ότι απαιτείται μεγαλύτερος όγκος υλικού για την περίπτωση PROB500K κατά 68% και 43% σε σύγκριση με τις περιπτώσεις PROB100K και PROB200K αντίστοιχα, ενώ για της περίπτωση PROB200K απαιτείται μόλις 17.5% αύξηση του όγκου. Τέλος, συγκρίνοντας τους βέλτιστους σχεδιασμούς της ντερμινιστικής διατύπωσης DET100K, DET200K και DET500K, με τους αντίστοιχους βέλτιστους σχεδιασμούς PROB100K, PROB200K και

PROB500K της πιθανοτικής διατύπωσης προκύπτει ότι απαίτείται αύξηση του όγκου του υλικού κατά αυξάνεται κατά 26%, 43% και 60% αντίστοιχα.

Σχεδιασμός	b_1	b_2	r_3	V	$N_c^{(det)}$	$\overline{N}_c$	N_c^{med}	COV (%)
DET100K	50.0	75.0	27.0	79690	136024	99055	106573	30.43
DET200K	50.0	84.0	28.0	82461	201728	261604	198703	36.84
DET500K	73.0	100.0	21.0	105793	553038	506188	505190	33.02
PROB100K	66.0	100.0	27.0	100390	118124	107584	100894	45.14
PROB200K	88.0	100.0	19.0	118065	83143	353434	200288	23.55
PROB500K	100.0	93.0	18.0	169157	498856	269721	554890	47.19

Πίνακας 4: Άκαμπτο μέλος: Βέλτιστος σχεδιασμός για κάθε διατύπωση και οι αντίστοιχες στατιστικές παράμετροι (MCS = 200).

Προκειμένου να αξιολογηθεί η διατύπωση του προβλήματος βελτιστοποίησης σχήματος λαμβάνοντας υπόψη τις αβεβαιότητες, πραγματοποιήθηκαν επιπλέον πιθανοτικές αναλύσεις για τους έξι βέλτιστους σχεδιασμούς που ελήφθησαν σε κάθε περίπτωση. και υπολογίστηκαν οι στατιστικές ποσότητες σχετικές με τον αριθμό των κύκλων κόπωσης (βλ. Πίνακας 4). Όπως προκύπτει από τον πίνακα αυτόν, υπάρχουν περιπτώσεις όπου η ντετερμινιστική διατύπωση υπερεκτιμά τον αριθμό των κύκλων κόπωσης σε σύγκριση με την τιμή της διαμέσου όταν λαμβάνεται υπόψη η αβεβαιότητα. Γίνεται σαφές λοιπόν ότι η μέση τιμή των κύκλων κόπωσης δεν αποτελεί μια αξιόπιστη στατιστική ποσότητα, δεδομένου ότι επηρεάζεται σε μεγάλο βαθμό από τη συμπεριφορά των ρωγμών.

This page intentionally left blank

Preface

This dissertation is submitted for the degree of Doctor of Philosophy at the National Technical University of Athens (NTUA). The research described herein was conducted under the supervision of Professor M. Papadrakakis in the School of Civil Engineering, NTUA. This work is to the best of my knowledge original, except where acknowledgments and references are made to previous work. Furthermore, no part of my dissertation has already been or is currently submitted for any such degree, diploma or other qualification.

Part of this work has been presented in the following publications:

- M. Georgioudakis, N.D. Lagaros and M. Papadrakakis. Probabilistic shape design optimization of structural components under fatigue, *Structural and Multidisciplinary Optimization*, 2014, (submitted for publication).
- G. Stefanou, M. Georgioudakis and M. Papadrakakis, Sequentially linear analysis of structures with stochastic material properties, in M. Papadrakakis and G. Stefanou (eds.), *Multiscale Modeling and Uncertainty Quantification of Materials and Structures*, Springer International Publishing, Switzerland, 2014.
- G. Stefanou, M. Georgioudakis and M. Papadrakakis. Response variability of structures with softening materials in a sequentially linear analysis framework, 7th Computational Stochastic Mechanics Conference, Santorini Greece, June 15–18, 2014.
- M. Georgioudakis, N.D. Lagaros and M. Papadrakakis. Shape design optimization for structural components under fatigue considering uncertainties, OPT-i 2014, Kos Island, Greece, June 4-6, 2014.
- M. Georgioudakis, G. Stefanou and M. Papadrakakis. Stochastic failure analysis of structures with softening materials, *Engineering Structures*, **61**, pp. 13–21, 2014.
- G. Stefanou, M. Georgioudakis and M. Papadrakakis, Sequentially linear analysis of structures with stochastic material properties, IUTAM Symposium 2013, Santorini Island, September 9-11, 2013.
- M. Georgioudakis, N.D. Lagaros, M. Papadrakakis, Multi-Objective shape design optimization into an extended finite element method (XFEM) framework, SEECCM 2013, Kos Island, Greece, June 12-14, 2013.
- M. Georgioudakis, G. Stefanou, M. Papadrakakis, Modeling failure of structures with stochastic properties in a sequentially linear analysis framework, SEECCM 2013, Kos Island, Greece, June 12-14, 2013.

Manolis Georgioudakis
Athens, 2014

This page intentionally left blank

Acknowledgments

I am sincerely grateful to my supervisor, Prof. Manolis Papadrakakis, for his guidance, inspiration and help throughout my doctoral studies. The impetus for this research came from his desire to understand the simulation of fracture phenomena with advanced numerical techniques always within the context of finite element method. This research was greatly improved by his expertise, and I have thoroughly enjoyed tackling these challenging problems under his mentorship. I can thank him also for the opportunities he has provided me, and for truly looking out for my best interests.

I would like to express my gratefulness to the Onassis Foundation and the General Secretariat for Research and Technology (GSRT) in Greece, for their contributions towards my financial support.

Additionally, I am pleased to acknowledge several others who contributed directly or indirectly to this research. I thank my committee members, Associate Prof. M. Kavvadas and Assistant Prof. N.D. Lagaros, from the School of Civil Engineering, NTUA for reviewing this work.

Specifically, I am deeply indebted to Dr. N.D. Lagaros for sharing his experience on optimization techniques, and our endless fruitful scientific conversations. I am also grateful, to Assistant Prof. G. Stefanou, from the School of Civil Engineering, Aristotle University of Thessaloniki, for his assistance with the stochastic part and aspects of this research. It has been a privilege working with them with so much experience and intuition related to physical problem, allowing me to join them in their scientific research.

I would also like to thank all my colleagues from the School of Civil Engineering at NTUA, for creating a friendly and supportive environment. My time working with them improved my research, but also changed me personally and encouraged me to supervise many of their diploma and post-diploma theses.

Finally, I would like to take this opportunity to express my gratitude to my parents, who always believed in the value of learning and were patiently supportive through my prolonged education.

Manolis Georgioudakis

This page intentionally left blank

Contents

List of Figures

This page intentionally left blank

List of Tables

This page intentionally left blank

List of Algorithms

This page intentionally left blank

List of Acronyms

ACO Ant Colony Optimization
AI Artificial Intelligence
BEM Boundary Element Method
CDF Cumulative Distribution Function
CMA Covariance Matrix Adaptation
DE Differential Evolution
DEM Discrete Element Method
EA Evolutionary Algorithm
EAS Enhanced Assumed Strains
EP Evolutionary Programming
ES Evolution Strategy
FEM Finite Element Analysis
FEM Finite Element Method
GA Genetic Algorithm
GP Genetic Programming
IGA Isogeometric Analysis
LEFM Linear Elastic Fracture Mechanics
LHS Latin Hypercube Sampling
LSM Level Set Method
PDF Probability Density Function
PSO Particle Swarm Optimization
PU Partition of Unity
SA Simulated Annealing
SDA Strong Discontinuity Approach
SDF Spectral Density Function
SFEM Stochastic Finite Element Method
SI Swarm Intelligence
SIF Stress Intensity Factor
TS Tabu Search
XFEM Extended Finite Element Method
XIGA Extened Isogeometric Analysis

This page intentionally left blank

Nomenclature

(r, θ)	local crack tip polar coordinates
$\boldsymbol{\epsilon}$	strain tensor
$\mathbb{C}$	material constitutive tensor
$\mathbb{K}$	stiffness matrix
$\boldsymbol{\sigma}$	stress tensor
$\boldsymbol{B}$	deformation matrix (derivatives of shape functions)
$\boldsymbol{f}$	nodal force vector
$\boldsymbol{f}^b$	body force vector
$\boldsymbol{f}^{ext}$	external force vector
$\boldsymbol{f}^t$	external traction vector
$\boldsymbol{N}$	shape functions matrix
$\boldsymbol{n}$	normal vector
$\boldsymbol{u}(\boldsymbol{x})$	displacement vector
$\boldsymbol{x}$	vector position of a point
δ	Dirac delta function
ϵ_{ij}	strain components
κ	wave number
H	softening modulus
ω	frequency
ψ, ϕ	level set functions associated with the surface and front of the crack
ρ	normalized autocorrelation function
σ_{ij}	stress components
b	correlation length
C_{ff}	autocovariance function of a stochastic field $f(x)$
$E[\bullet]$	mean value of $\bullet$
G	shear modulus
G_f	fracture energy
$H(\boldsymbol{x})$	generalized Heaviside function
J	J-integral
J^{act}	actual J-integral
J^{aux}	auxiliary J-integral
K_I, K_{II}, K_{III}	stress intensity factors of modes I, II and III respectively
q	arbitrary smoothing function
R_{ff}	autocorrelation function of a stochastic field $f(x)$
S_{ff}	power spectral density function or power spectrum
t	time
$Var[\bullet]$	variance of $\bullet$

W	external work
W^{aux}	auxiliary work
W^{ext}	work of external loading
W^{int}	work of internal loading

1

Introduction

In the past decades numerical methods have gained wide popularity for the analysis of physical processes. One of the most flexible numerical method is certainly the Finite Element Method (FEM) (Hughes, 2000; Zienkiewicz et al., 2014). By means of the FEM approximate numerical solutions for problems involving complex geometry, boundaries, loading and material behavior can be computed. Hence, it may be primarily applied to problems for which analytical solutions do not exist. FEM has been applied successfully in many areas of engineering sciences to study, model and predict the behavior of structures. The area ranges from aeronautical to aerospace, mechanical and civil engineering, automobile industry, bio-mechanics, material sciences etc. In the field of structural mechanics the FEM allows to predict the deformation and stress states, ultimate loads etc. of structures both in civil and mechanical engineering problems.

The development of advanced finite element methods is accompanied by extensive research in the field of material modeling: The corresponding mathematical models capable to describe the nonlinear behavior of materials under different loading scenarios offers still increasing capabilities to the FEM. Hence, finite element methods are continuously improved with respect to a more realistic description of material behavior.

1.1 Motivation

Among the most interesting phenomena in material science is the failure processes caused by different mechanisms. Consequently, computational failure mechanics has attracted large interest over the past decades. Nowadays, the modeling of failure processes in structures along with an objective and efficient mathematical description, remains as a challenging problem in Mechanics, in spite of the advances made in the development of the FEM. It plays an important role in the development of new materials for industry as well as in the understanding of their durability and resistance. Some typical examples that have stimulated this challenge are presented in the remaining of this section.

Ship Failure In the beginning of the 20th century, interest increased in the behavior of steel (the most used material of that time) after fatigue and fracture mechanisms were detected in various types of structures including in ships. As examples one can mention: the *Olympic* (1911), the *Titanic* (1912) and several ships called *Liberty*, as a special class cargo ships, which were built very rapidly and in large numbers during World War II, but suffered from catastrophic cracks (Fig. 1.1).

Figure 1.1: An oil tanker that fractured in a brittle manner by crack propagation around its girth (Callister and Rethwisch, 2012).

Dam Collapse Most concrete dams develop cracks, giving a heterogeneous character to the material which can affect its integrity. Depending on the stress states, microcracks can develop into a macrocrack formation, which can result in inefficient operation or even in a complete collapse.
The Malpasset dam was built on the Reyran River located on the French Riviera in the southern portion of France. In 1959, the dam was breached and the entire wall collapsed into pieces. Waves of over 40 meters started flowing across the nearby areas causing heavy fatalities and structural damage (Fig. 1.2).

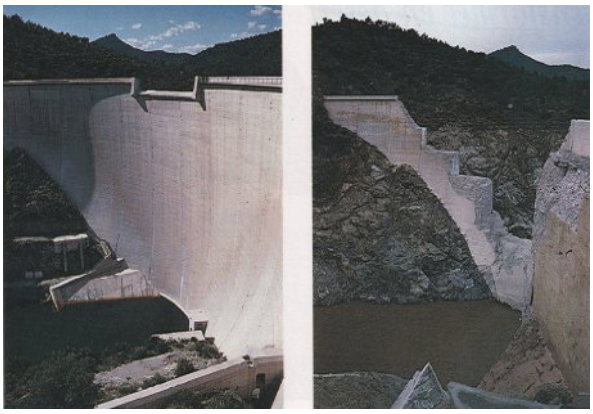

Figure 1.2: Malpasset Dam before and after failure (1959).

Oil/Gas pipeline rupture Thousands of kilometers of gas and oil transmission pipelines are currently in operation around the world. A rupture of a pipeline can release diesel fuel, gas, etc., which can kill or injure people or, sometimes, lead to an ecological disaster. In 2000, the Marathon Ashland Pipe Line LLC (Marathon Ashland), a 24-inch-diameter pipeline that runs 265 miles between Owensboro and Catlettsburg, Kentucky, ruptured near Winchester, Kentucky. The ruptured pipeline released about 489000 galons of crude oil onto a golf course and into Twomile Creek[1].

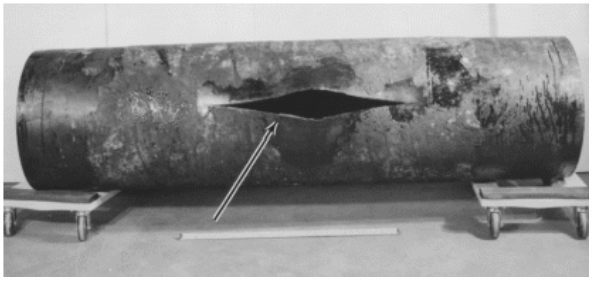

Figure 1.3: Ruptured pipe. The arrow indicates rupture site.

Landslides The downward and outward movement of slope-forming materials including rock, soil, artificial fill, or a combination of these. As the land slowly moves, it causes tension cracks in the earth and in the bedrock. As this tension increases and significant changes in moisture occur, from things like heavy rainfall or the fast melting of snow, the land begins to move more and more. Fig. 1.4 shows a graphic illustration of a landslide, with the commonly landforms and their different characteristic parts, such as toe, radial cracks (fissures), transverse cracks (fissures), and rupture, or slip, surface[2].

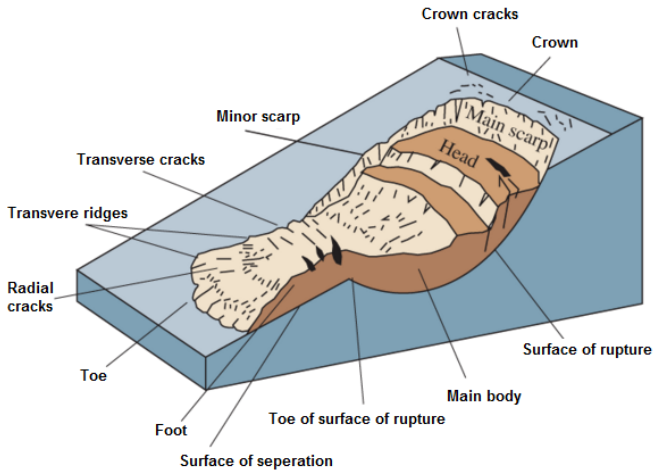

Figure 1.4: Commonly landforms and their characteristic parts of a landslide.

[1]Source: National Transportation Safety Board (Marathon Ashland Pipe Line Accident Report)
[2]Source: The Encyclopedia of Earth: http://www.eoearth.org

Fracture in bio-engineering A typical problem in the field of bio-engineering is the disease called *osteoporosis*, i.e. a condition involving decreased bone mass which strongly increases the risk of bone fracture (as age progresses). Hip fractures, which occur most frequently among older people, can be caused by minor falls. To prevent such fractures it is necessary to evaluate with a high degree of accuracy the strength of the bone and the propensity to fracture must be reliably estimated. Fig. 1.5 shows the two common types of hip fracture. When the topmost part (head) of the thighbone (femur) is badly damaged, it may be replaced with an artificial part (prosthesis), made of metal. This procedure is called *partial hip replacement*[3] (see Fig. 1.6).

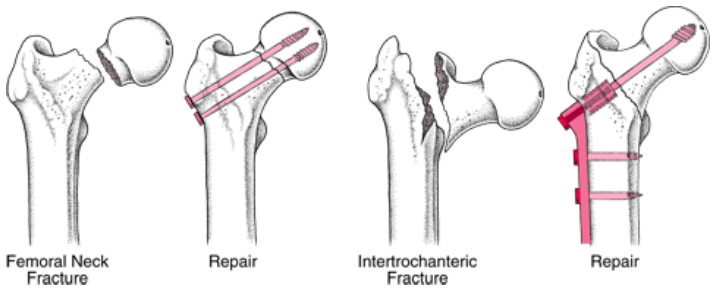

Figure 1.5: The two common types of hip fractures: *Femoral neck* and *Intertrochanteric* and their repairs.

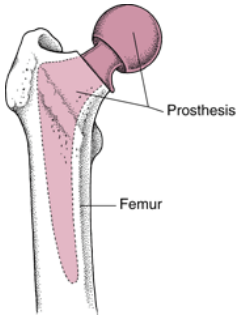

Figure 1.6: Partial hip replacement.

For the above reasons and many others that are not mentioned in this chapter, material behavior, especially material fracture problems have been of great interest to researchers. In the last decades there has been an increasing amount of interest in the study of the experimental and theoretical behavior of the response of materials under extreme load conditions.

Consequently, computational failure mechanics has attracted large interest over the past years. A multitude of approaches to the mathematical description of fracture and failure has been presented in the literature. Most of them, however, are characterized by certain restrictions with respect either to objectivity or to computational efficiency. Thus, their applicability to large scale structural analyses is most often questionable.

[3] Source: The Merck Manuals, http://www.merckmanuals.com.

1.2 Modeling failure of structures

1.2.1 Multiscale material description

Material Science has been studied on different scales (see Fig. 1.7) (Willam, 2002) and several theories have been formulated at these different scales to simulate the problem of crack initiation/propagation. This thesis will concentrate on the material behavior at a macroscopic point of view (material failure mechanics), in simulating the fracture process.

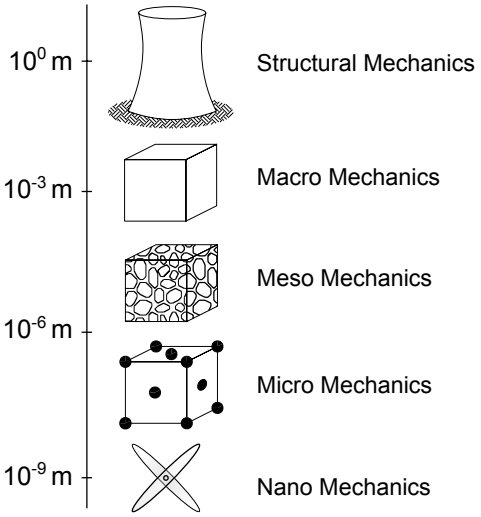

Figure 1.7: Multiscale material description.

1.2.2 Material behavior at macroscopic scale

In 1911 von Kármán demonstrated the mechanical behavior of rocks caused by different confining pressures. He showed that rocks, when compressed under high hydrostatic pressure, undergo a transition of plastic deformation characterized by the appearance of crossed net shear bands at approximately 45°. This phenomenon became fundamental in geophysical, rock engineering and rock mechanical knowledge. Later, the same effect was observed in other materials like soil, sand, ceramics, composites, ice, etc. The morphology of bands in rocks is very similar to the one observed in metals (see Fig. 1.8a). In soils, when a set of forces provokes instability, a zone with a concentration of deformations is observed. This zone where there is a concentration of strain is called the *localization zone* and specially in soils is called the slip line (see Fig. 1.8b).

Although localization is a phenomenon that has its origins at a microscopic level, caused by the presence of voids, microcracks, and other phenomena, cracks in concrete or rocks, slip lines in soils and shear bands in metals are observed at the macroscopic level. The localization zone is characterized by the concentration of inelastic strains in a narrow discrete band while the surrounding material undergoes unloading, a fact that causes numerical instabilities in the solution process.

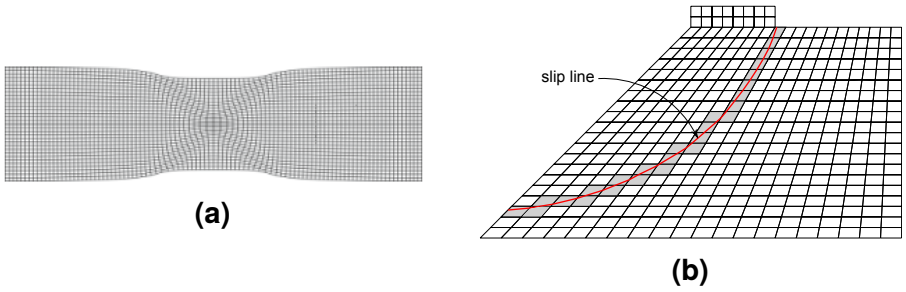

Figure 1.8: (a) Shear bands in metals and (b) slip lines in soils.

1.2.2.1 Brittle vs ductile materials

The behavior of materials can be broadly classified into two categories: *brittle* and *ductile*. The material response for ductile and brittle materials are exhibited by both qualitative and quantitative differences in their respective stress-strain curves. The terms brittle and ductile relate to the relative values of the elastic limit and failure threshold (see Fig. 1.9). The material is said to have brittle behavior, if the failure threshold nearly coincides with the elastic limit. This material will experience only negligible plastic deformation before fracture. In contrast, for a ductile material the failure threshold is significantly larger than the elastic limit so that as the material deforms it experiences an elastic domain, followed by a plastic domain, and then finally it fractures.

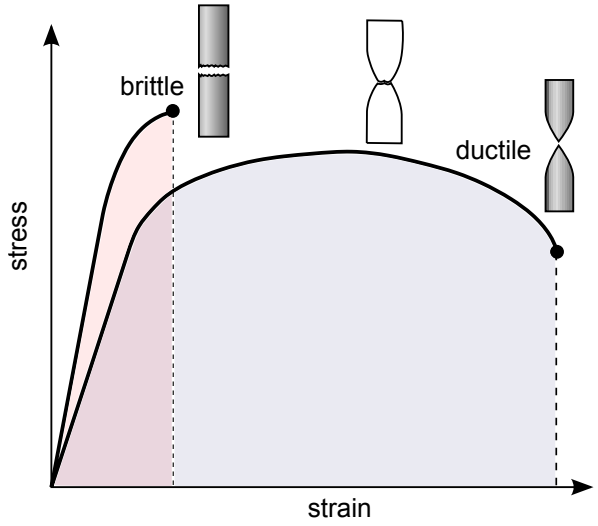

Figure 1.9: Brittle vs ductile material and typical stress-strain curves.

The following are the most relevant features of these two types of materials:

Brittle Materials: small deformations, no warning before failure (abrupt). (examples: concrete, ceramic, glass, ice, rocks, etc.)

Ductile Materials: large deformations, warning before failure (Not abrupt). (examples: steel, aluminum, etc.)

1.2.3 Fracture and continuum mechanics

To simulate the material failure mechanisms at a macroscopic level, the most accepted frameworks are: *Fracture Mechanics* and *Continuum Mechanics*. These methods, however, are applied to fundamentally different classes of failure problems. While the theory of plasticity and damage mechanics are basically designed for problems where the displacement field and usually the strain field remain continuous everywhere (continuous problems), fracture mechanics is essentially formulated to deal with strong discontinuities (cracks) where both the displacement and strain fields are discontinuous across a crack surface (cf. Fig. 1.10).

Basically, the main difference between these two general approaches is that in Fracture Mechanics after failure initiation a traction-separation relationship is invoked, whereas Continuum Mechanics assumes a stress-strain relationship ($\sigma - \epsilon$) after *strain localization*, which is a precursor to failure and macroscopic fracture of the material (as the stress vanishes). In practice, fracture mechanics is also used for weak discontinuity problems, and both damage mechanics and the theory of plasticity have been modified and adapted for failure/fracture analysis of structures with strong discontinuities.

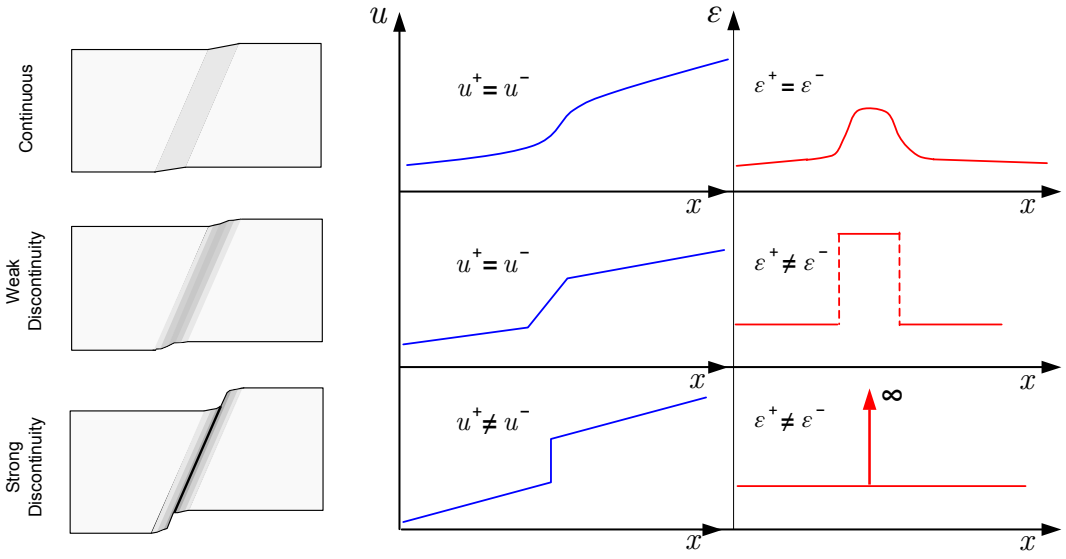

Figure 1.10: Weak vs Strong Discontinuities and the corresponding displacement and strain field.

1.3 Literature review

In order to predict not only the failure load but also the post-peak behavior correctly, robust and stable computational algorithms that are capable of dealing with the highly nonlinear set of governing equations are an essential requirement. Various methods have been developed over the years for simulation of the problems involved with creation and propagation of cracks. Analytical, semi-analytical and numerical approaches, each one provides advantages and drawbacks in handling certain parts of the simulation. In the following sections, the main approaches are briefly outlined.

1.3.1 Linear elastic fracture mechanics (LEFM)

Fracture mechanics was stimulated by Inglis (1913). Using elasticity fundamentals he studied the stress concentration in a large plate of elastic material with an elliptical hole. Later, Griffith (1921) used Inglis' stress analysis of an elliptical flaw in a linear elastic material to predict the critical stress under which a crack irreversibly grows, causing the material to fracture. He proposed an energy criterion of failure after considering that the stress value cannot be used as a failure criterion since the stress at the tip of a sharp crack in an elastic continuum is infinite. These concepts served as the basis of classical linear elastic fracture mechanics (LEFM) which came to the existence practically in naval laboratories during the World War I.

During the World War II, Irwin became interested in the fracture of steel armor plating during penetration by ammunition. His experimental work at the U.S. Naval Research Laboratory in Washington, D.C. led, to a theoretical formulation of fracture, to study the propagation of fissures where introduced the so-called Fracture Modes (see Section 3.1.4) whose combinations give rise to the mixed-mode cracks (Irwin, 1957).

The procedure used to determine the crack propagation is indicated as follows:

- Step 1: Determine the stress intensity factor
- Step 2: Verify the crack stability based on a criterion which is a function of the stress intensity factor, and determine the crack increase and its orientation
- Step 3: The crack tip is established in a new point.

The whole process is repeated until the crack stability is ensured. A detailed description of LEFM concepts is given in Chapter 3.

1.3.2 Discrete crack approach

In the discrete crack approach, introduced by Ngo and Scordelis (1967), existing cracks are simply defined along the finite element edges (cf. Fig. 1.11a). The strong discontinuity is automatically assumed in the displacement field, while an interface element or special boundary conditions between adjacent solid elements are required to simulate the crack propagation, avoiding the spurious stress across the discontinuities. However, it cannot account for the singular field around the crack tip, unless special singular finite elements are used. This approach is simple for predefined existing crack paths along the element edges (Ingraffea and Saouma, 1985), however, it becomes rather difficult for modeling general crack propagation paths as it requires a remeshing of the model. Accurate results for a fixed mesh can only be obtained if the crack pattern is known in advance and if elements have been oriented in the crack direction.

1.3.3 Smeared crack approach

In contrast, the smeared crack approach has been frequently used in the finite element simulation of fracture and crack propagation problems. It is in fact a continuous approach for a discontinuous/singular problem. In this model, the discontinuity caused by a discrete crack within an element is simulated by a distributed (smeared) equivalent field over the entire domain of the element (see Fig. 1.11b). The main advantage of the method is that it does not require any local or global remeshing in the pro-

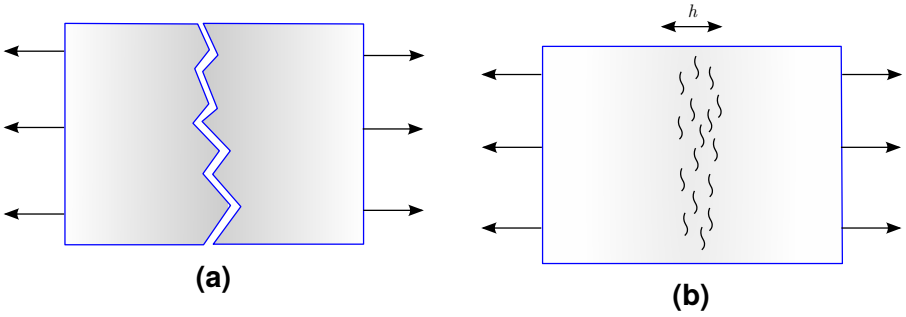

Figure 1.11: (a) Discrete vs (b) smeared crack approach.

cess of crack propagation. This approach was very well attracted because the FEM was getting powerful with the advance of computer development, and principally because this approach treated the two behaviors, continuum and fracture, in the same framework of the continuum. This approach has been further developed by several researchers (Bazant and Cedolin, 1979; Cervenka, 1970; Rots et al., 1985).

To simulate material behavior up to full fracture implies strain softening (after the load reaches the peak, the post-peak is characterized by stress declining with an increasing of strain). This behavior causes problems with certain theoretical difficulties, such as mesh dependency and localization instabilities. Such ideas appeared according to experiments, since the dimensions of the failure regions are independent of the structural size and they are assumed as fictitious planes. In the case of tensile cracks, this approach is known as “crack band model” (Bažant and Oh, 1983).

1.3.4 Intra-element crack

In this approach, which is similar to the Band Crack Model, the crack that propagates throughout the element (see Fig. 1.12) is concentrated in a band within the finite element. Different formulations have been adopted to for this concentration, and among them one can quote: assumed enhanced strain (AES) (e.g. weak discontinuity approach) and enhanced displacement (e.g. the strong discontinuity approach) (Simo et al., 1993). All these ramifications have one thing in common, which is that after localization a softening relation between traction and relative displacement can be reproduced by the stress-strain constitutive relation. To this end, Belytschko et al. (1988) have developed a method by which the localized zone can be embedded using a four-node quadrilateral element.

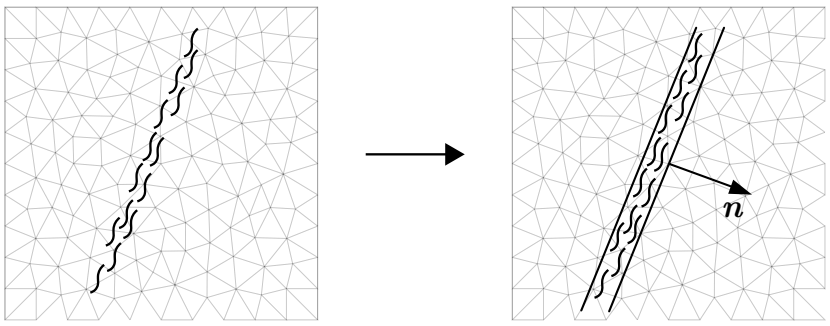

Figure 1.12: Intra-element crack model.

1.3.5 Enhanced continuum approaches

In the modeling of structures with strain softening within the framework of classical continuum, the corresponding boundary value problem (BVP) becomes ill-posed. To overcome these instabilities higher order continuum theories have been proposed. This kind of enrichment imposes a minimal width of the strain localization zone, which called *localization limiters* and aim to model the concentration of the strains in narrow bands, via the introduction of constitutive strain softening, whose propagation makes eventually the structure to fail.

Cosserat Continua The Cosserat theory of elasticity was originally developed in 1909 and can be useful in the modeling of heterogeneous materials when the size of the heterogeneities (internal length) and the size of the structure (external length) are of the same order of magnitude. Also, it can be useful in modeling size effects and as a regularization method for numerical computations where classical continua analysis breaks down. However, the limited range of applicability, the calibration of the internal length and the boundary conditions for the micro-rotations are curtailing their use (de Borst and Mühlhaus, 1992).

Non-local models In non-local models, the stress at a point depends on the state at this point and on the deformation in its neighborhood. The algorithm checks the stress state at the integration points against a material strength criterion, similar to hardening plasticity problems except for a negative hardening modulus to account for the softening effects of cracking. The behaviour of a point was only affected by its own stress state (cf. Fig. 1.13). This method were proposed to avoid mesh dependency of the plasticity based solutions for simulating crack problems (Bažant and Jirásek, 2002; Bažant and Planas, 1997).

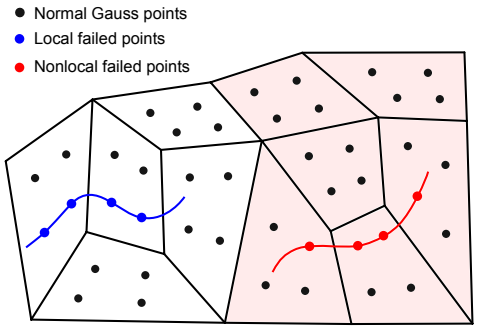

Figure 1.13: Local and non-local cracking state.

Gradient-enhanced models This model may be derived as an approximation of the nonlocal damage models. A characteristic of one class of gradient-enhanced model is the material parameter (material length) that introduced, where the displacement field and effective plastic strains are discretized using C^1-continuous shape functions. The addition of gradient terms becomes significant when modelling strain-softening solids and the pathological mesh dependence as obtained in finite element computations with conventional continuum models is no longer encountered (de Borst and Mühlhaus, 1992).

1.4 Numerical techniques for crack analysis

Due to the limitations and inflexible nature of the aforementioned analytical methods in handling arbitrary complex geometries and boundary conditions and general crack propagations, several numerical techniques have been developed for solving fracture mechanics problems.

In recent years, finite elements with enrichments have gained increasing interest in modeling material failure, due to their specific ability to provide, unlike standard finite elements, specific kinematics to capture weak and strong discontinuities. They essentially consist of enriching the (continuous) displacement modes of the standard finite elements, with additional (discontinuous) displacements. The discontinuity path is placed inside the elements irrespective of the size and specific orientation of them. Then, typical drawbacks of standard finite elements in modeling displacement discontinuities, like spurious mesh size and mesh bias dependencies, can be effectively removed. In addition, unlike with standard elements, mesh refinement isn't necessary to capture those discontinuities, and the simulation can be done with relatively coarse meshes. By using that technology, in conjunction with some additional refinements, realistic simulations of multiple strong discontinuities propagating in two as well as in three dimensional structures can be achieved, with small computers, in reasonable computational times. As for the enriching technique, two broad families can be distinguished in terms of the support of the enriching discontinuous displacement modes:

- the strong discontinuity approach (SDA) (a class of embedded finite elements)
- and the extended finite element method (XFEM).

Despite outstanding advantages, of these two families, alternative numerical techniques are also available, including the discrete element method (DEM), the boundary element method (BEM), the isogeometric analysis (IGA), a variety of meshless methods, the extended isogeometric analysis (XIGA) and more recently, advanced multiscale techniques, but all of them are out of the scope of this study.

1.4.1 The strong discontinuity approach (SDA)

From the class of assumed enhanced strain methods (AES), mentioned before, emerges the strong discontinuity approach (SDA) (Simo et al., 1993; Simo and Rifai, 1990). Lately, a discontinuous shape function (to capture the displacement field) into a triangular element was added, allowing the precise representation of the crack opening (Oliver, 1996a,b). The theory is based on AES framework and developed in the ambit of Continuum Mechanics using an isotropic continuum damage model (see Section 2.1.1) and its variations, which serves to simulate materials like concrete, ceramics, rocks and ice.

The SDA refers to the capture of jumps in the displacement field across a surface with zero bandwidth measure by using standard solid mechanics models with continuum constitutive equations. In Oliver (1996a,b) a discontinuous shape function (to capture the displacement field) into a triangular element has been used allowing a precise representation of the crack opening. It has been shown that the discrete theoretical model can be interpreted as the limit case of the continuum when the localization band goes to zero (discontinuity surface). In this case the strain has the sense

of a Dirac delta (δ) distributions. The interesting point is that the whole analysis is done in the Continuum Mechanics framework. The SDA leads to mesh-independent finite element discretization without introducing a material length scale (characteristic length of smeared crack models) which is a non-physical property.

This methodology has been used with many constitutive models (damage, Drucker-Prager, Rankine) (Armero and Garikipati, 1996; Larsson et al., 1996; Oliver, 1996a,b). Extensions of the method to localization analyses of saturated soils has been addressed (Steinmann, 1999) as well as the links with cohesive models (Oliver, 2000). Although, the SDA it is mesh-independent with respect to size and orientation, and as consequence, no remeshing is needed to capture the high strain gradients, special techniques are required for its implementation in a finite element code, regarding the robustness and convergence of the highly nonlinear system of equations.

1.4.2 The Extended Finite Element Method (XFEM)

In this method, the singular or discontinuous displacement field within a finite element is simulated by a special set of enriched shape functions at nodal level, that allow for accurate approximation of the displacement field. Presence of the crack is not geometrically modeled and the mesh does not need to conform to the crack path. Additional enrichment approximation is added to the classical finite element model to account for the effects of a crack or discontinuity.

The eXtended Finite Element Method (XFEM) is a numerical method for modeling strong (displacement) as well as weak (strain) discontinuities within a standard finite element framework. In XFEM, special functions are added to the finite element approximation. For crack modeling in isotropic linear elasticity, a discontinuous function and the two-dimensional asymptotic crack-tip displacement fields are used for accurate approximation of the displacement field. Presence of the crack is not geometrically modeled and the mesh does not need to conform to the crack path. This new proposal has lately been followed by several researchers because it presents certain attractive characteristics like:

- The implementation is done based on a standard FEA code,
- It is mesh-independent with respect to size and orientation,
- No remeshing is needed to capture the high strain gradients,
- There is no need to introduce any material length scale.

Unlike with standard finite elements, mesh refinement is not necessary to capture the discontinuities and the simulation can be performed with relatively coarse meshes. A comparative study of the two approaches can be found in Oliver et al. (2006) but a detailed assessment of relative errors, rates of convergence and computational cost is still an open area of research (Oliver et al., 2012).

1.4.3 Sequentially Linear Analysis (SLA)

In contrast, to the previous enriched techniques in the framework of the standard FEM, the sequentially linear analysis (SLA) has been also proposed (Rots, 2001). It is an alternative method to model the nonlinear fracture behavior of quasi-brittle materials. It's attractiveness consists in avoiding the well-known convergence and bifurcation problems that are often encountered when using incremental/iterative

schemes such as Newton-Raphson, with a sophisticated procedure on the discretization of the constitutive model for accurate description of the stiffness degradation due to damage (see Section 2.2.1).

1.5 Why stochastic analysis and optimum design?

Typical problems in all engineering fields, involving media with random properties, require complex mathematical predictions in order to be solved. The design of structures under static or dynamic loading cases, imperfections in the structural elements, random fluctuations in temperature, or other environmental conditions, life prediction of structures, crack growth in structures subjected to fracture etc. are characteristic examples in civil engineering field. Specifically, in structural engineering, materials with random properties are often used, such as, but not limited to steel, soil, and concrete. Thus, the natural responses of these structures may be completely unpredictable by deterministic models.

The advancements in reliability theory of the past three decades and the development of more accurate quantification of uncertainties associated with system loads, material properties and resistances have stimulated the interest in probabilistic treatment of systems (Schuëller, 2006). The reliability of a system or its probability of failure constitute important factors to be considered during the analysis and design procedure, since they characterize the system's capability to successfully accomplish its design requirements. Engineers have always been striving to design efficient structural systems which have to be economic yet strong enough to withstand all possible loads that will arise during their service life. The traditional trial-and-error design approach is not sufficient to determine economical satisfying as well as the safety criteria. Structural design optimization, on the other hand, provides a numerical procedure that can replace the traditional design approach with an automated one.

Hence, powerful analysis tools concerning random medium mechanics is very important to model uncertainties and random characteristics of the materials. Furthermore, the progress in analysis and design of structures has been invariably associated with the formulation of more detailed design optimization problems considering uncertainties in structures subjected to fracture.

1.6 Adopted approach and aim of the thesis

The present thesis is divided into two parts. In the first part, the influence of uncertain spatially varying material properties on the fracture behavior of structures with softening materials, is investigated. This is performed by coupling SLA method within the framework of a stochastic setting. Structural failure is modeled using the SLA, which replaces the incremental nonlinear finite element analysis by a series of scaled linear analyses and the nonlinear stress–strain law by a saw-tooth curve. The proposed approach alleviates the deficiencies of SDA, constituting an efficient procedure avoiding the convergence problems encountered in standard nonlinear FE analysis, providing also the minimum parameters required for defining the constitutive model in order to perform stochastic crack propagation analysis of the structures in reasonable computational times.

In the second part, the XFEM consists an appropriate framework which serves to simulate the fracture process in structural members caused by fatigue, into a shape optimization environment. Specifically, shape design optimization problems are formulated within the context of XFEM, which is adopted to solve the crack propagation problem as originally proposed by Moës et al. (1999) and Stolarska et al. (2001), avoiding the mesh difficulties encountered into a CAD-FEM shape optimization problem by working with a fixed mesh approach. Naturally associated to XFEM, the level set method (see Section 3.4.1) is used to describe the structural geometry providing also the ability to modify the CAD model topology during the optimization process. The whole process is performed, with nature inspired optimization techniques since they have been found to be robust and efficient even for complex mathematical problems.

1.7 Objectives of the present work

The present thesis deals with a unified framework for stochastic analysis and optimum design of structures subjected to fracture developed in the ambit of modern numerical techniques for crack growth simulation mainly based on enriched finite elements methods. This has been done within the context of the stochastic finite element method as well as within a modern optimization environment implementing metaheuristic search algorithms.

The main objectives of this thesis can be formulated as follows:

- to bridge different research fields related to crack growth simulation and analysis, stochastic analysis and optimum design into a contemporary design environment of structures,
- to investigate the influence of uncertain spatially varying structural properties on the fracture behavior of structures proposing an efficient coupled approach which allows the stochastic crack propagation analysis and highlighting the necessity of it, by quantification of this stochastic behavior,
- to develop and implement a shape optimization design framework able to investigate the relation between structural geometry and service life in the design process of structures, using state of the art optimization techniques (i.e. metaheuristic search algorithms),
- to demonstrate the feasibility and utility of the developed approaches in problems of a complexity relevant to industrial applications.

1.8 Outline of the thesis

This introductory chapter briefly introduced the subject of fracture in structures, and summarily reviewed the existing classes of analytical and numerical techniques. In each case, a short description and a number of reference works were presented without going into detail. Also, the necessity of the stochastic analysis and optimum design of structures subjected to fracture was discussed. A short outline of this thesis and its organization is given in Fig. 1.14. This organization serves on dividing the theory and the numerical applications, while keeping the coherent structure of the text.

Chapter 2, presents a general overview of the the damage models and the theo-

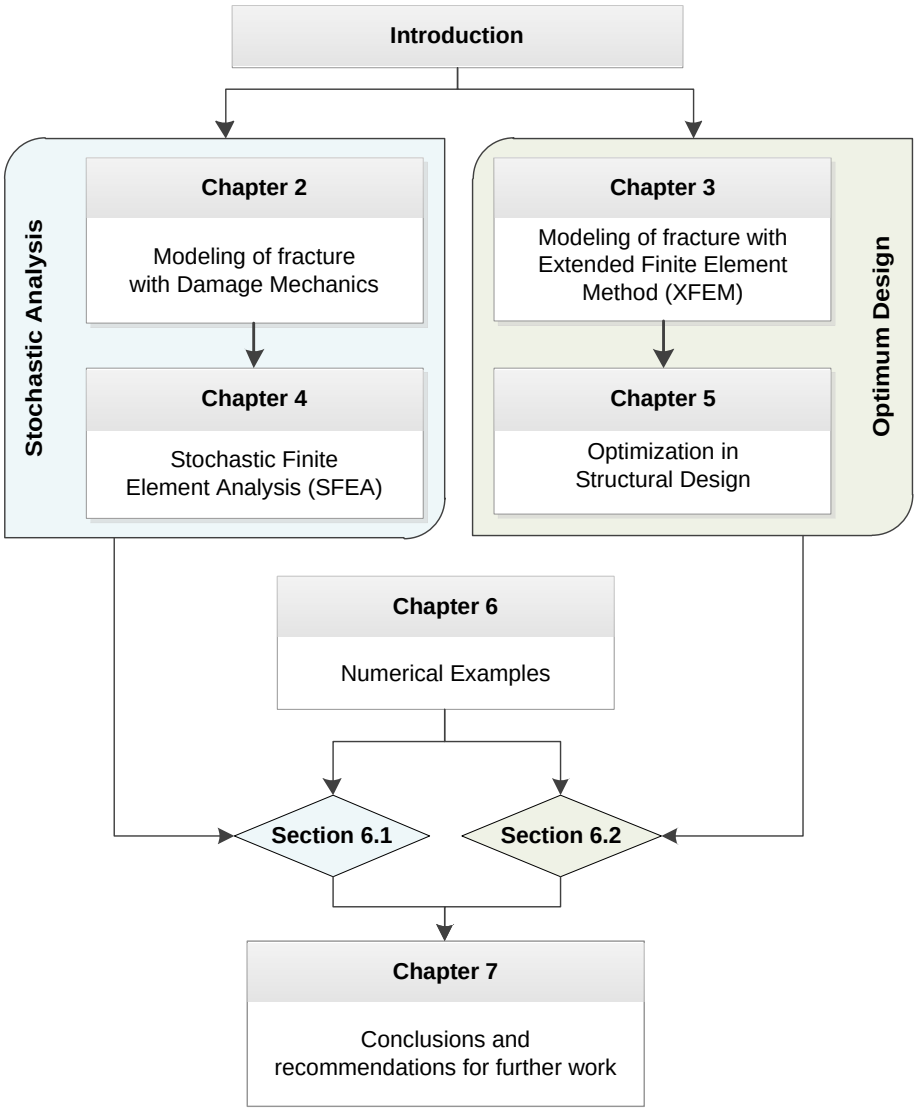

Figure 1.14: Outline of this thesis.

retical basis of the sequentially linear analysis (SLA) as an alternative method for incremental/iterative solution schemes to model the nonlinear fracture behavior of quasi-brittle materials. It is an attractive method since it avoids the well-known convergence and bifurcation problems that are often encountered when using incremental/iterative schemes such as Newton-Raphson. The general procedure, as well as the discretization of the constitutive model is outlined also.

Chapter 3, presents the extended finite element method (XFEM) as a numerical method to model internal (or external) boundaries such as holes, inclusions, or cracks, without requiring the mesh to conform to these boundaries. It begins with the basic concepts and fundamental formulations of the linear elastic fracture mechanics (LEFM). Asymptotic solutions for displacement and stress fields in different fracture modes are presented along with the basic concepts of stress intensity factors, energy release rate and the J-integral. The methodology of extracting mixed mode stress intensity factors is addressed and the maximum hoop (circumferential) stress criterion

for mixed mode fracture criteria is outlined.

The chapter continues with a detailed XFEM formulation for crack analysis in isotropic materials. The basic relations for modeling displacement discontinuity across a crack and the stress singularity at the crack tip are derived. A review of the level set method for tracking moving boundaries is provided before a short discussion on some numerical aspects of the method, such as the numerical integration and limitations of enrichments.

Chapter 4 deals with the modeling of uncertainties characterizing the structural parameters by using the theory of stochastic functions. A necessary mathematical background with a short presentation of fundamentals that characterize the stochastic functions, such as the mean value, autocovariance and autocorrelation functions, the correlation structure and the correlation length are defined. The mathematical background is followed by an overview of existing techniques for representing the Gaussian and non-Gaussian stochastic functions. The spectral representation method is discussed as it offers an elegant description of the translation fields used in the numerical examples of this thesis.

Furthermore, the basic aspects of stochastic finite element method (SFEM) are addressed comprising the three basic steps of the method: the discretization of the stochastic fields, the formulation of the stochastic matrix and the response variability calculation which is performed in the Monte Carlo simulation context, and the variability response function approach is presented as an alternate to the latter. Individual aspects of coupling SFEM with SLA are outlined.

In **Chapter 5**, a brief overview on structural optimization techniques is followed by the proposed formulations for the integration of XFEM into a shape design optimization framework. Basic aspects of the differential evolution algorithm which used for solving the crack optimization problems are outlined, after a sensitivity analysis of four metaheuristic search algorithms, which found to be very promising in multi-modal benchmarks.

Chapter 6 completes the thesis with representative numerical examples, to illustrate the applicability and potential of the proposed formulations presented in the previous chapters. These formulations are aiming to investigate the influence of uncertain spatially varying material properties on the fracture behavior of structures with softening materials, as well as the relation between structural geometry and service life in a shape design optimization process.

Finally, a summary of the work is given in **Chapter 7** along with a short discussion of possible improvements of the presented formulations.

2

Modeling of fracture with damage mechanics

In recent years, several numerical techniques have been developed to model the failure of structures in the framework of the finite element method (FEM), each of one incorporating a suitable constitutive model must in order to describe the nucleation of physical discontinuities (e.g. cracks, slip lines) and their subsequent growth.

In particular, for structures made of softening materials, a realistic representation of the softening behavior requires the accurate description of stiffness degeneration due to damage. This description can be achieved in a unified manner using *Damage Mechanics* approaches that have been proven advantageous for modeling failure phenomena due to their numerical efficiency. Damage mechanics has been increasingly adopted to analyze failure in various engineering application involving concrete, rock, metals, etc. In damage mechanics, both the strength and stiffness of a material point are decreased if it experiences some level of damage. This is in contrast to the classical theory of plasticity, where the stiffness remains unchanged and only the strength is updated according to the hardening/softening behaviour. The damage mechanics approach permits the incorporation of the description of damage into the constitutive equations, as well as the combination with different more specific simulation methods, such as the embedded finite element method (Oliver, 1996a; Oliver et al., 2012, 2006), extended finite element method (Mariani and Perego, 2003; Moës et al., 1999) and non-local theories (Jirásek, 1998).

The basic concepts of continuum damage mechanics are introduced in this chapter, with special reference to the isotropic damage model. This model, with its special treatment is used in the basis of the sequentially linear analysis (SLA) as an alternative method to standard nonlinear FEA, when dealing with material softening behavior. The latter method is particularly beneficial when brittle fracture causes convergence issues and will be adopted later for numerical examples, highlighting the attractiveness of it.

2.1 Damage mechanics

The term Damage Mechanics has been used to refer to models which characterized by a loss of stiffness, i.e. a reduction of the secant constitutive modulus. The concept

of effective stress $\overline{\sigma}$ was introduced in Kachanov (1986) pioneering work where the damage variable was treated as a scalar quantity (isotropic damage), whose value ranged from 0 to 1. Later, several researchers extended this theory by treating the damage variable as a tensor (anisotropic damage). Later, Rabotnov (1971) intended to include the loss of rigidity of the material as a consequence of the appearance of fissures, further called *Continuum Damage Mechanics* which became a very powerful and consistent theory based on the thermodynamics of irreversible processes.

2.1.1 Isotropic damage model

The so-called Continuum Damage Models have been used thoroughly to simulate the behavior of materials that present degradation of the mechanical properties due to small fissures that appear during the loading process. To characterize this, the concept of effective stress, $\overline{\sigma}$, is introduced (see Fig. 2.1).

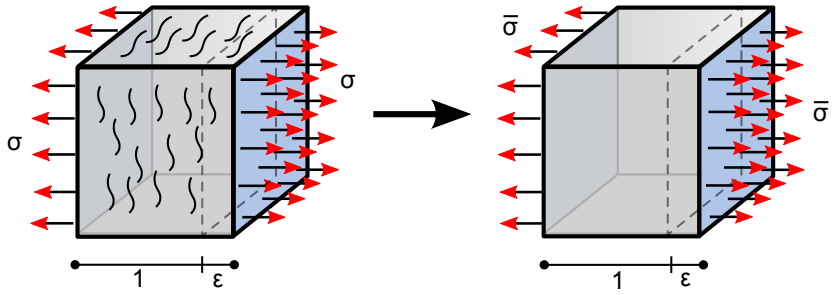

Figure 2.1: The effective stress concept.

For the one dimensional case the stress σ is given by:

$$\sigma = (1-d)\overline{\sigma}, \quad 0 \leq d \leq 1 \tag{2.1}$$

where $\overline{\sigma}$ is the effective stress and d is the scalar damage variable. The effective stress $\overline{\sigma}$ and the strain are related by the Hooke's law:

$$\overline{\sigma} = E\epsilon \tag{2.2}$$

where E is the elastic modulus of the material (Young's modulus). Substituting Eq. (2.2) into Eq. (2.1) yields:

$$\sigma = (1-d)E\epsilon \quad 0 \leq d \leq 1 \tag{2.3}$$

To derive the constitutive equation for the isotropic damage model a generalization of the damage model to $3D$ cases is made through the continuum mechanics concepts. Hence, for an isotropic damage model a family of constitute equations is defined by:

$$\Psi = (1-d)\Psi_0, \quad \Psi_0 = \frac{1}{2}\boldsymbol{\epsilon} : \mathbb{C} : \boldsymbol{\epsilon} \tag{2.4}$$

$$\sigma = \frac{\partial \Psi}{\partial \epsilon} = (1-d)\mathbb{C} : \epsilon \tag{2.5}$$

where Ψ is the Helmholtz's density of free energy, $\mathbb{C}$ the elastic constitutive tensor, $\boldsymbol{\sigma}$ and $\boldsymbol{\epsilon}$ the stress and strain tensor correspondingly. The value of the damage variable d is given by the corresponding damage condition and evolution laws. According to Oliver et al. (1990) the damage variable evolution can by integrated in close form at time t giving,

$$\begin{aligned} d_t &= G(r_t) \\ r_t &= \max_{s\in(-\infty,t)} \{r_0, \tau_s^\epsilon\} \end{aligned} \tag{2.6}$$

In Eq. (2.6), τ^ϵ is an appropriate norm of the strains described below, r_0 is an initial threshold value and $G(\cdot)$ is a non-decreasing scalar function such that $G(r_0) = 0, G'(\infty) \leq 1$ and $G(\mu) \geq 0,\ \forall \mu \in [r_0, \infty)$. The internal variable r_t describes, at time t, the size of elastic domain in the strain E_ϵ space, while the internal variable q_t describes the size of elastic domain in stress E_σ space (cf. Fig. 2.2) and can be defined as:

$$E_\epsilon := \{\boldsymbol{\epsilon} | \tau^\epsilon \leq r_t\} \tag{2.7}$$

$$E_\sigma := \{\boldsymbol{\sigma} | \tau^\sigma \leq q_t\} \tag{2.8}$$

Consequently, the damage criterion, which defines the elastic limits, reads:

$$\underbrace{\tau^\epsilon - r \leq 0}_{\text{Strain space}} \quad \text{or} \quad \underbrace{\tau^\sigma - q(r) \leq 0}_{\text{Stress space}} \tag{2.9}$$

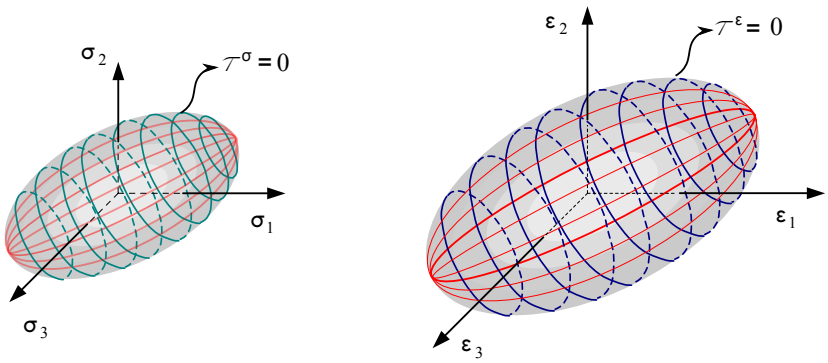

Figure 2.2: Stress and strain spaces and elastic limit.

Under such conditions it is straightforward to check that both d and r always increase along time, so that:

$$\begin{aligned} \dot{d} &\geq 0 \\ \dot{r} &\geq 0 \end{aligned} \tag{2.10}$$

where $\dot{d} = 0$ for unloading and elastic loading, whereas $\dot{d} > 0$ corresponds to inelastic loading.

Finally, from Eq. (2.4) and Eq. (2.5) the dissipation $\mathscr{D}$ can be computed as:

$$\mathscr{D} = -\dot{\Psi} + \boldsymbol{\sigma} : \dot{\boldsymbol{\epsilon}} = d\Psi_0 \geq 0 \tag{2.11}$$

For the case of a linear strain hardening-softening law with symmetric tension-compression behavior the constitutive equation takes the form:

$$\tau^{\epsilon} = \sqrt{\boldsymbol{\epsilon} : C : \boldsymbol{\epsilon}} \tag{2.12}$$

and the corresponding damage is defined by:

$$d = G(r) = \begin{cases} 0, & r < r_0 = \sigma_y/\sqrt{E} \\ \frac{1}{1+\mathsf{H}}(1 - \frac{r_0}{r}), & r_0 < r < r_{max} \\ 1, & r_{max} < r \end{cases} \tag{2.13}$$

where H plays the role of the softening parameter, σ_y is the uniaxial peak stress. A typical curve for damage evolution is depicted in Fig. 2.3 ($\mathsf{H} < 0$, strain softening case), while the corresponding uniaxial stress-strain law is depicted in Fig. 2.4.

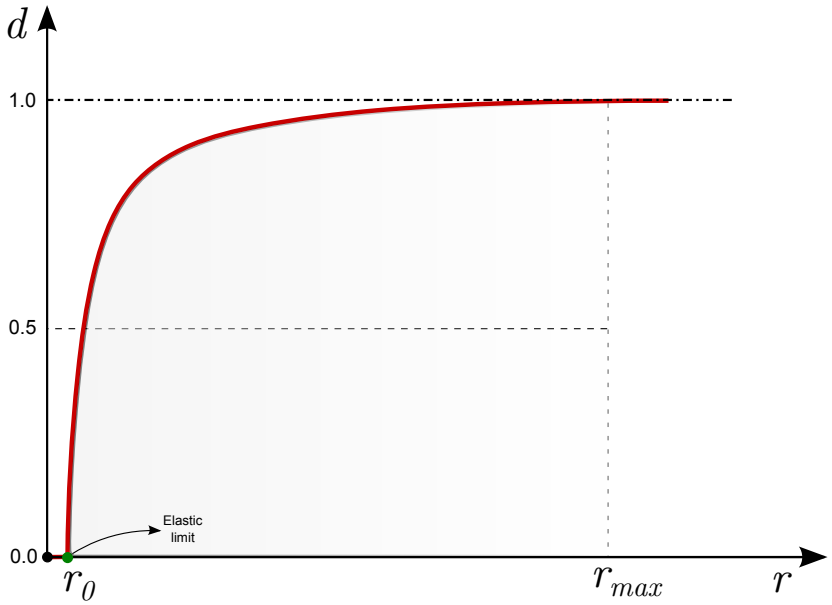

Figure 2.3: Damage variable evolution.

Similar to the strain τ^{ϵ} norm one can define also the stress τ^{σ} norm in the stress domain as:

$$\tau^{\sigma} = \sqrt{\boldsymbol{\sigma} : C^{-1} : \boldsymbol{\sigma}} = (1-d)\sqrt{\boldsymbol{\epsilon} : C^{-1} : \boldsymbol{\epsilon}} = (1-d)\tau^{\epsilon} \tag{2.14}$$

After some algebraic computations, the corresponding incremental stress-strain law can be computed as:

$$\dot{\boldsymbol{\sigma}} = \mathbb{C}^d : \dot{\boldsymbol{\epsilon}} \tag{2.15}$$

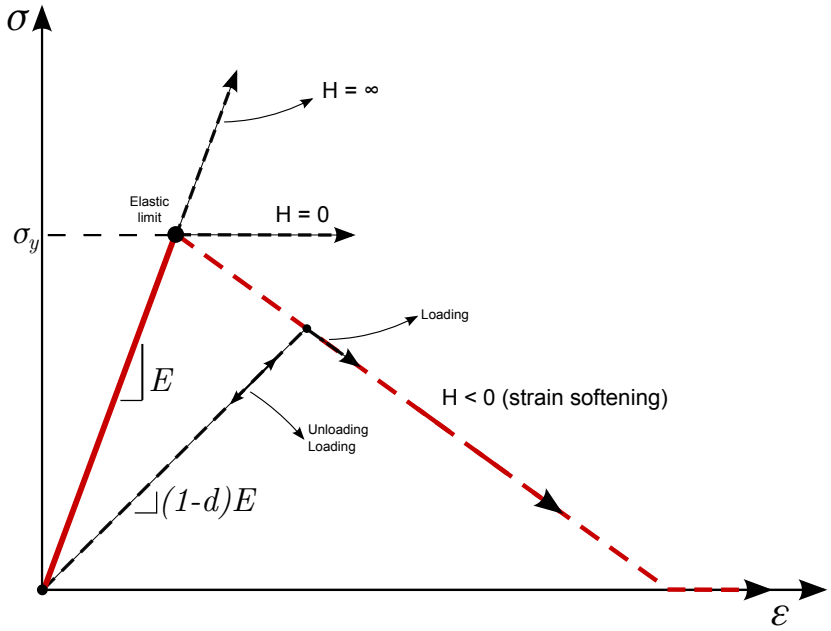

Figure 2.4: Stress-strain curve for isotropic damage model.

where $\mathbb{C}^d$ is the tangent constitutive operator computed as:

$$\mathbb{C}^d = \begin{cases} (1-d)\mathbb{C}, & \dot{d} = 0 \text{ (unloading)} \\ (1-d)\left[\mathbb{C} - \frac{1}{1+\mathsf{H}}\frac{\tau_0}{(\tau^\sigma)^3}\right]\boldsymbol{\sigma}\otimes\boldsymbol{\sigma}, & \dot{d} \neq 0 \text{ (loading)} \end{cases} \tag{2.16}$$

2.2 Sequentially linear analysis (SLA)

In failure mechanics, material softening is often responsible for unstable structural behavior (Bažant and Cedolin, 2010). This instability can lead to secondary equilibrium states or bifurcation of the equilibrium path, which require more elaborate incremental-iterative solution schemes (Borst et al., 2012). As a consequence, the robustness of the numerical procedure used for solving the nonlinear problem is strongly affected. In order to overcome these problems, an alternative method, called sequentially linear analysis (SLA), has been introduced by Rots (2001).

SLA is an *event-by-event* strategy based on a secant stiffness procedure which does not require iterations and replaces the incremental nonlinear finite element analysis by a series of scaled linear analyses and the nonlinear stress-strain law by a saw-tooth curve. The advantage of this replacement is that the secant linear (saw-tooth) stiffness is always positive and the analysis does always converge. The method is generally applicable for materials with nonlinear softening behavior, but it is particularly beneficial when brittle fracture causes convergence issues and has been successfully applied within the scope of the smeared crack approach (cf. Section 1.3.3). The method has been applied to masonry structures (DeJong et al., 2009; Rots, 2001; Rots et al., 2008, 2009; van De Graaf et al., 2009), reinforced concrete beams (Graça-e Costa and Alfaiate, 2006), composite beams (Billington, 2009), structures composed by extremely brittle materials (e.g. glass) (Invernizzi et al., 2011; van De Graaf et al., 2009) and

concrete in general, providing good results in problems which are difficult to solve due to nonconvergence problems.

Improvements of SLA for the case of non-proportional loading has also been proposed by Eliáš et al. (2010); Graça-e Costa et al. (2012) and Graça-e Costa et al. (2013), as well as for the concrete beams with shear failure by Slobbe et al. (2012).

In this study, SLA is adopted as the acceptable failure analysis method implemented in the framework of a stochastic setting. The proposed approach constitutes an efficient procedure for investigating the influence of uncertain spatially varying material properties on the fracture behavior of structures with softening materials.

2.2.1 Review of sequentially linear analysis

Modeling fracture through an *event-by-event* cracking procedure by imposing an increment of damage, is an attractive alternative to standard nonlinear FEA, where modeling proceeds by imposing increments of displacements or forces. To capture brittle events directly, rather than trying to iterate around these critical points in a Newton-Raphson scheme, SLA was developed specifically to address the difficulty of modeling snap-back behavior.

In this approach, a tensile softening curve of negative slope is replaced by a saw-tooth curve (cf. Fig. 2.4) which maintains a positive tangent stiffness (see Fig. 2.5). The incremental/iterative Newton-Raphson method is no longer required since a series of linear analyses are performed, each with a reduced positive stiffness, until the global equilibrium position is achieved. It has been shown, that this "event-by-event" strategy is robust and reliable (Rots and Invernizzi, 2004), and circumvents bifurcation problems, in contrast to regular nonlinear FE analysis.

In summary, the SLA model can be thought of as discretizing the space via finite elements, discretizing the local softening via a saw-tooth diagram and re-computing the load via a scaling technique. Standard incremental/iterative Newton-Raphson techniques rather discretize the space via finite elements, discretize the load via increments and re-compute the local softening on a continuous smooth diagram.

The general procedure of SLA is provided in the following section. More details about this method can be found in the studies by DeJong et al. (2009); Rots (2001); Rots and Invernizzi (2004); van De Graaf et al. (2009).

2.2.2 General procedure

In the framework of FEM a structural system is discretized, using standard continuum elements and the material properties (Young's modulus, Poisson's ratio and initial strength) are assigned to them. Subsequently, the following steps are carried out sequentially without the need of changing the initial mesh:

- Perform a linear-elastic FE analysis with a unit external load and calculate the principal stresses,
- Loop over all integration points for all elements and find the *critical element* for which the stress level divided by its current strength is the highest in the whole structure,
- Calculate the load multiplier, belonging to the critical integration point, i.e. the current strength divided by the stress level,

- Scale the reference load proportionally by the critical load multiplier,
- Increase the damage in the critical integration point by reducing the stiffness E and strength f_t according to the saw-tooth tensile-based constitutive relation (see Section 2.2.3),
- Repeat the previous cycle of steps continuously, until the damage has spread sufficiently into the structure.

An extended description of the above algorithm is provided in Algorithm 1: Initially, a linear-elastic FE analysis is performed ($\mathbf{K}_N$: stiffness matrix of the structure and $\mathbf{d}_N$: vector of unknown displacements in analysis step N) with a reference proportional load $\mathbf{P}$ (line 2). After the calculation of maximum principal tensile stresses ($\sigma_{t_{pr}}$), through the linear elastic analysis, a loop over all integration points for all elements is performed in order to find the *critical element* for which its current strength $f_{t_i}^+$ divided by the maximum principal tensile stress is the highest in the whole structure (lines 3–7). Subsequently (line 8), the reference load $\mathbf{P}$ (also, the displacements and stress resultants correspondingly) is scaled proportionally by the critical load multiplier λ_{cr_N} belonging to the critical integration point. Finally (lines 9–13), the damage in the critical integration point is increased by reducing the stiffness E and strength f_t according to the saw-tooth tensile-based constitutive relation (see Section 2.2.3). The aforementioned procedure is repeated sequentially, until the damage has spread sufficiently into the structure.

Algorithm 1 Sequentially linear analysis algorithm

1: **repeat**
2: $\mathbf{K}_N\mathbf{d}_N = \mathbf{P} \rightarrow \sigma_{t_{pr}}$
3: **for** $element = 1, ..., TotalElements$ **do**
4: **for** $GaussPoint = 1, ..., TotalGPperElement$ **do**
5: Calculate $\frac{f_{t_i}^+}{\sigma_{t_{pr}}}$ and find $\lambda_{cr_N} = max\{\frac{f_{t_i}^+}{\sigma_{t_{pr}}}\}$
6: **end for**
7: **end for**
8: Scale displacements and stress resultants $(\mathbf{d}_N, \sigma_N)$ by factor λ_{cr_N}
9: **for** $element = 1, ..., TotalElements$ **do**
10: **for** $GaussPoint = 1, ..., TotalGPperElement$ **do**
11: Find new $f_{t_{i+1}}^+, E_{i+1}$ according to Section 2.2.3
12: **end for**
13: **end for**
14: Update structure stiffness matrix $\mathbf{K}_{N+1} \leftarrow \mathbf{K}_N$
15: **until** damage has spread sufficiently into the structure

In this way, the nonlinear response is extracted by linking consecutively the results of each cycle. The smoothness of $P-\delta$ curves depends on the smoothness (number N_t of teeth) of the saw-tooth model (see Section 2.2.3). The SLA procedure allows only one integration point to change its status from elastic to softening at each time, while in nonlinear FE analysis, the use of load increments implies that multiple integration points may crack simultaneously and the local stiffnesses at these points switch from positive to negative, following the softening constitutive laws for quasi-brittle materials.

2.2.3 Saw-tooth model

In the SLA, the update of the secant stiffness leads to a *saw-tooth* stress-strain envelope (see Fig. 2.5) and requires mesh regularization in order to prevent deviations of the dissipated energy in the crack. In this study, the generalized tooth size approach (MODEL C) (Rots et al., 2008) is adopted, which does not require special techniques to handle mesh-size objectivity in order to obtain objective results with respect to the mesh as well as to overcome the lack of consistency. The way in which the stiffness and strength of the critical elements are progressively reduced at each "event", is shown schematically in Fig. 2.5 where the softening curve of negative slope in the constitutive stress-strain relation is replaced by a discretized, saw-tooth diagram of positive slopes which provides the correct energy dissipation. The linear tensile softening stress-strain curve is defined by the Young's modulus E, the tensile strength f_t and the area under the saw-tooth diagram. This area (cf. Fig. 2.5) is always equal to the fracture energy G_f, which is considered here as a material property, divided by the crack bandwidth h, which is associated with the size, orientation and integration scheme of the finite element.

In case of linear softening, ultimate strain ϵ_u is given by:

$$\epsilon_u = \frac{2G_f}{f_t h} \tag{2.17}$$

Both Young's modulus E and strength f_t can be reduced at the same time in the sequentially linear strategy by a factor a, according to:

$$E_i = \frac{E_{i-1}}{a}, \quad for \quad i = 1, 2, ..., N \tag{2.18}$$

where i and $i-1$ denote the current and previous step, respectively, in the saw-tooth diagram. To find the rule of reducing Young's modulus E as well as strength f_t, by

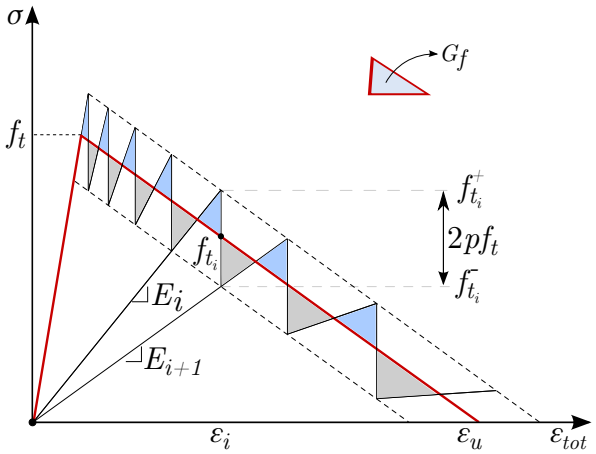

Figure 2.5: Stress-strain curve for linear softening and saw-tooth model definitions.

ratio a_i in step i according to Fig. 2.5, we have:

$$f_{ti}^- = f_{ti}^+ - 2pf_t \tag{2.19}$$

$$E_{i+1} = \frac{f_{ti}^{-}}{\epsilon_i} \tag{2.20}$$

$$a_{i+1} = \frac{E_i}{f_{ti}^{-}}\epsilon_i = \frac{f_{ti}^{+}}{f_{ti}^{-}} = \frac{f_{ti}^{+}}{f_{ti}^{+} - 2pf_t} \tag{2.21}$$

Thus, for the case of linear softening (Fig. 2.5) the value of f_{ti}^{+} can be easily defined as:

$$f_{ti}^{+} = \epsilon_u^{+} E_i \frac{D}{E_i + D} \tag{2.22}$$

where,

$$\epsilon_u^{+} = \epsilon_u + p\frac{f_t}{D} \tag{2.23}$$

and D is the tangent to the tensile stress-strain softening curve. The number N_t of teeth is automatically evaluated, depending on the user specified parameter p. For smaller values of p, a higher N_t is needed to cover the softening branch, leading to more exact results. The procedure ends, regarding the corresponding Gauss point, when the difference between the sum of *positive* triangles above the real curve and the sum of *negative* triangles below the real curve vanishes, as shown in Fig. 2.5.

This page intentionally left blank

3

Modeling of fracture with extended finite element method

Modeling crack growth in a conventional finite element framework is cumbersome due to the need for the mesh to match the geometry of the discontinuity. This becomes a major difficulty when treating problems with evolving discontinuities where the mesh must be regenerated at each step. Moreover, the crack tip singularity needs to be accurately represented by the approximation. Due to the fact that standard finite element methods are based on piecewise differentiable polynomial approximations, they are not well suited to problems with discontinuous and/or singular solutions. Typically, finite element methods require significant mesh refinement or meshes which conform with these features to get accurate results. In response to this deficiency of standard finite element methods, extended finite elements have been developed.

The extended finite element method (XFEM) is a numerical method for modeling strong (displacement) as well as weak (strain) discontinuities within the standard finite element framework. With XFEM internal (or external) boundaries such as holes, inclusions, or cracks, can be modeled without requiring the mesh to conform to these boundaries. It is based on a standard Galerkin procedure, and uses the concept of partition of unity (PU) (Melenk and Babuška, 1996) to accommodate the internal boundaries in the discrete model. Since its introduction in 1999, the XFEM method has enjoyed a considerable level of success and popularity from researchers in the computational and applied mechanics communities.

The method was originally proposed by Belytschko and Black (1999), who presented a method for enriching finite element approximations so that crack growth problems can be solved with minimal remeshing. Dolbow (1999); Dolbow et al. (2000) and Moës et al. (1999), introduced a much more elegant technique by adapting an enrichment that includes the asymptotic crack tip field and a Heaviside function, while Sukumar et al. (2000), extended the concepts of this method to the three-dimensional static crack modeling.

In the following sections, the basic ingredients of the XFEM for two-dimensional computational fracture mechanics problems are presented. After a brief review of the fundamental concepts in Fracture Mechanics, (Griffith theories, Stress Intensity

Factors and J-Integral) the rest of chapter, is dedicated to discussing the basic ideas and formulation for the XFEM, dealing with the enriched approximations, the governing equations, as well as the discrete form of the equilibrium equation in order to derive the element stiffness matrix. Moreover, the algorithm which couples the level set method (LSM) with the XFEM to model crack growth is also outlined. This combined method requires no remeshing as the crack progresses, making the algorithm very efficient and accurate, demonstrating a tremendous potential for a wide range of crack propagation problems which may be practically impossible to solve using the standard finite element method. Finally, some individual numerical aspects of the XFEM such the selection of enrichment nodes, the numerical integration and the limitations of the method are also addressed.

3.1 Fracture mechanics

Structures are designed to withstand the loads they are expected to be subject to while in service. Large stress concentrations are avoided, and a reasonable margin of security is taken to ensure that values close to the maximum admissible stress are never attained. However, material imperfections which arise at the time of production or usage of the material are unavoidable, and hence must be taken into account. Various kinds of geometric discontinuity, such as holes, notches, cracks, sharp changes in geometry, etc. are known to be the main source of failure in a large number of catastrophic failures of structures. Such discontinuities generate substantial stress concentrations which reduce the overall strength of a material. In this setting Fracture Mechanics plays a central role, as it provides useful tools which allow for an analysis of materials which exhibit cracks. The goal is to predict wether and in which manner failure might occur.

3.1.1 Linear elastic fracture mechanics (LEFM)

Linear Elastic Fracture Mechanics (LEFM) first assumes that the material is isotropic and linear elastic. Based on this assumption, the stress field near the crack tip is calculated using the theory of elasticity. When the stresses near the crack tip exceed the material fracture toughness, the crack will grow. LEFM is valid only when the inelastic deformation is small compared to the size of the crack, what we called small-scale yielding. If large zones of plastic deformation develop before the crack grows, Elastic Plastic Fracture Mechanics (EPFM) must be used, which is out of the scope of this study.

In order to explain the fundamental differences of LEFM and the conventional theory of the strength of materials, a simple infinite tensile plate is considered, as depicted in Fig. 3.1. The plate is assumed to include a number of isolated defects, such as a tiny hole and a microcrack, while the rest of the specimen is presumed flawless. The average stress field far from the flaws (region around point A) is equal to the applied tensile stress, σ_0. Limiting the internal stress field to the material yield stress σ_{yield} results in determination of the maximum allowable traction from the following simple material strength criterion:

$$\sigma_0 = \sigma_{yield} \tag{3.1}$$

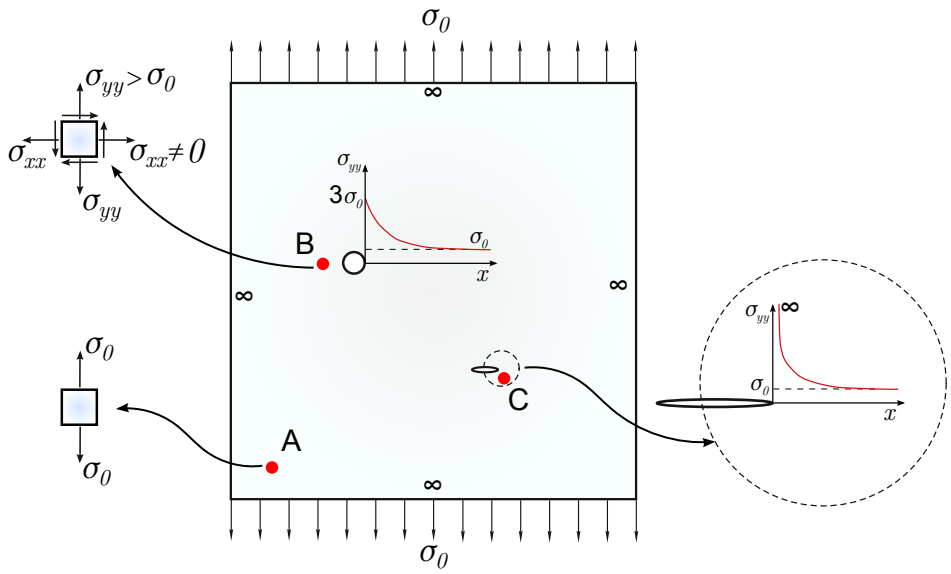

Figure 3.1: An infinite tensile plate and the stress states around an intact point A, a tiny hole B and a microcrack-tip C.

In the region around point B, the LFEM gives a solution for an infinite plate with a circular hole and a biaxial non-uniform stress field with a stress concentration factor of 3 at the centre of the plate, regardless of the size of the hole. In the limiting case of a line crack, the solution from a degenerated elliptical hole shows an infinite stress state at the crack tip (point C). While no material can withstand such an infinite stress state, real life observations show that many materials with internal cracks remain stable. As a result, instead of comparing the existing maximum stress field with a critical strength value, a different approach based on finite values is required. These fracture-based parameters define the way a crack affects the behaviour of a cracked specimen.

3.1.2 Griffith theory

The early strength theories were based on maximum tensile stress and in this connection uniaxial tensile strength were used to find the material fracture strength. Griffith himself performed experiments on glass fibers and observed that the fracture strength increases with a decrease in thickness of the fiber and vice versa. He found that the breaking load of a thin plate of glass having in it sufficiently long crack normal to the applied stress, is inversely proportional to the square root of the flaw length, i.e. $C = \sigma\sqrt{\alpha}$, where C is a constant, and α is the flaw length.

In order to find constant C, Griffith made use of energy balance of a body and derived also the critical stress level σ_{cr} that a cracked body can sustain, as:

$$\sigma_{cr} = \sqrt{\frac{2\gamma E}{\pi\alpha}} \tag{3.2}$$

$$C = \sqrt{\frac{2\gamma E}{\pi}} \tag{3.3}$$

where, γ is the surface energy per unit area (material constant).

3.1.3 Energy release rate

An infinite uniformly loaded plate with an elliptical crack of length 2α is considered (see Fig. 3.2). According to law of conservation of energy the work done per unit time

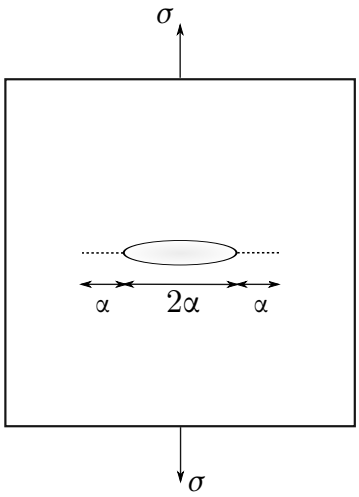

Figure 3.2: An infinite uniformly loaded plate with an elliptical crack of length 2α.

by the applied loads ($\dot{W}$) must be equal to the rates of change of the internal elastic energy ($\dot{U}_e$), plastic energy ($\dot{U}_p$), kinetic energy (K) of the body and the energy per unit time ($\dot{\Gamma}$) spent in increasing the crack area. Assuming the propagation is slow and plastic deformations are negligible, the conservation of energy can then be written in mathematical form as:

$$\dot{W} = \dot{U}_e + \dot{\Gamma} \tag{3.4}$$

If $\Pi = U_e - W$ be the potential energy of the system, Eq. (3.4) becomes:

$$-\dot{\Pi} = \dot{\Gamma} \tag{3.5}$$

As all the changes with respect to time are caused by change in flaw size, Eq. (3.5) can be re-written as:

$$G = \frac{\partial \Pi}{\partial \alpha} = \frac{\partial \Gamma}{\partial \alpha} \tag{3.6}$$

where G is known as *energy release rate* and characterizes the amount of energy available for crack propagation. The crack propagation can be occur when the energy release rate, G reaches a critical value, G_{cr}, which is the basic failure criteria for mixed mode fracture of materials (Nuismer, 1975).

3.1.4 Fracture modes

The theory of fracture mechanics uses a local stress intensity factor or a global fracture energy release rate in comparison with their critical values to assess the stability of a

flawed specimen. These fracture-based parameters define the way a crack affects the behavior of a cracked specimen. A force may be applied to the plate in several manners in which might enable the crack to propagate, but this is primarily achieved by classifying the general complex behavior of a crack into three independent situations, as depicted in Fig. 3.3. This classification corresponding to the three situations was proposed by Irwin (1958).

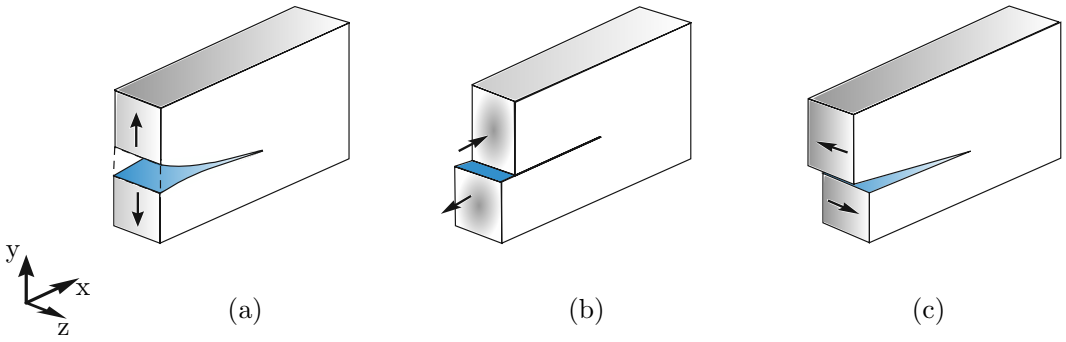

Figure 3.3: Crack failure modes: a) Mode I (opening mode), b) Mode II (shearing Mode), c) Mode III (tearing mode)

Accordingly, we consider three distinct modes: Mode I, Mode II and Mode III. According to the opening Mode I, crack surfaces are pulled apart in the normal direction (y) but remain symmetric about the xz and xy planes. The shearing Mode II represents the sliding mode of movement of crack surfaces in the x direction, while remaining symmetric about the xy plane and skew symmetric about the xz plane. Finally, in the tearing Mode III, the crack surfaces slide over each other in the z direction, while remaining skew symmetric about the xy and xz planes.

For each of these modes, crack extension may only take place in the direction of the x axis, the original orientation of the crack. In a more general situation, we typically find a mixed mode situation, where there is a superposition of the modes. In a linear elastic mixed mode problem, the principle of stress superposition states that the individual contributions to a given stress component $\sigma_{i,j}$ are additive, so that:

$$\sigma_{i,j} = \sigma^{I}_{i,j} + \sigma^{II}_{i,j} + \sigma^{III}_{i,j} \quad \text{for } i,j = \{x,y\} \tag{3.7}$$

where, $\sigma^{I}_{i,j}, \sigma^{II}_{i,j}, \sigma^{III}_{i,j}$ are respectively the stress components associated to the modes I, II and III.

3.1.5 Stress intensity factors (SIFs)

The concept of stress intensity factor K (SIF), introduced by Irwin (1957), as a measure of the strength of the singularity. He illustrated that all elastic stress fields around a crack tip are distributed similarly, and $K \propto \sigma\sqrt{\pi r}$ controls the local stress intensity. The elastic stress state around a crack in a plate, assuming that the crack surfaces are free of stress (cf. Fig. 3.4) can be represented (Westergaard, 1939) in polar coordi-

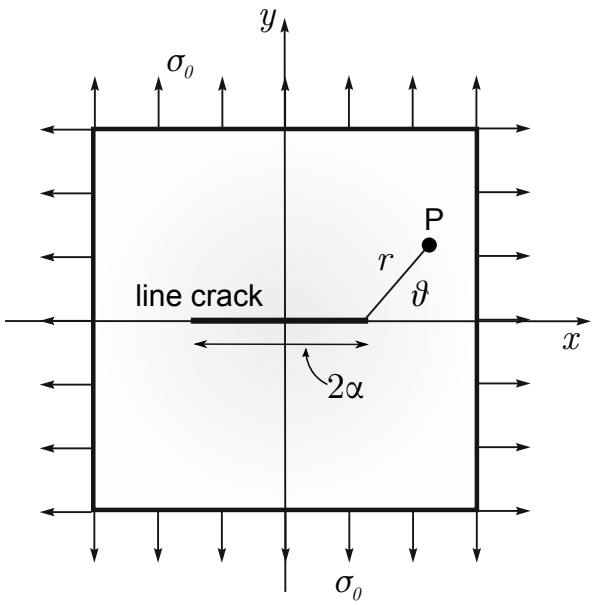

Figure 3.4: Westergaard infinite plate with a crack subjected to uniform normal tractions.

nates as:

$$\sigma_{xx}(r,\theta) = \sigma_0\sqrt{\frac{\alpha}{2r}}cos\frac{\theta}{2}(1 - sin\frac{\theta}{2}sin\frac{3\theta}{2}) + O(\sqrt{r}) \tag{3.8}$$

$$\sigma_{yy}(r,\theta) = \sigma_0\sqrt{\frac{\alpha}{2r}}cos\frac{\theta}{2}(1 + sin\frac{\theta}{2}sin\frac{3\theta}{2}) + O(\sqrt{r}) \tag{3.9}$$

$$\sigma_{xy}(r,\theta) = \sigma_0\sqrt{\frac{\alpha}{2r}}sin\frac{\theta}{2}cos\frac{\theta}{2}cos\frac{3\theta}{2}) + O(\sqrt{r}) \tag{3.10}$$

or in the more general form of:

$$\sigma_{ij}(r,\theta) = r^{-\frac{1}{2}}\{K_I f_{ij}^I(\theta) + K_{II} f_{ij}^{II}(\theta) + K_{III} f_{ij}^{III}(\theta)\} + O(\sqrt{r}) \tag{3.11}$$

where, σij are the near crack tip stresses, σ_0 is the finite applied tensile stress, r is the radial distance of point P of query from the crack tip, θ is the angle formed between the vector $\vec{r}$ and the plane of the crack and K_I, K_{II}, K_{III} are the SIFs associated with three three independent modes of movement of crack surfaces (cf. Fig. 3.3), such as:

$$K_I = \lim_{r\to 0}\sqrt{2\pi r}\sigma_{yy}(r,0) \tag{3.12}$$

$$K_{II} = \lim_{r\to 0}\sqrt{2\pi r}\sigma_{xy}(r,0) \tag{3.13}$$

$$K_{III} = \lim_{r\to 0}\sqrt{2\pi r}\sigma_{yz}(r,0) \tag{3.14}$$

e.g. for the infinite tensile plate with a central crack, based on Eq. (3.12) can then be simplified to:

$$K_I = \sigma_0\sqrt{\pi a} \tag{3.15}$$

The final stress and displacement fields at the crack tip ($\theta = 0$) in terms of the SIFs, for the three pure modes of fracture, can be described by substituting Eqs. (3.8)-(3.10) into Eqs. (3.12)-(3.14) (Saouma, 2000):

Mode I

Displacements field:

$$u_x = \frac{K_I}{2\mu}\sqrt{\frac{r}{2\pi}}cos\frac{\theta}{2}(\kappa - 1 + 2sin^2\frac{\theta}{2}) \tag{3.16}$$

$$u_y = \frac{K_I}{2\mu}\sqrt{\frac{r}{2\pi}}cos\frac{\theta}{2}(\kappa + 1 - 2cos^2\frac{\theta}{2}) \tag{3.17}$$

$$u_z = \begin{cases} 0, & \text{plain strain} \\ -\frac{\nu z}{E}(\sigma_{xx} + \sigma_{yy}), & \text{plain stress} \end{cases} \tag{3.18}$$

Stresses field:

$$\sigma_{xx} = \frac{K_I}{\sqrt{2\pi r}}cos\frac{\theta}{2}(1 - sin\frac{\theta}{2}sin\frac{3\theta}{2}) \tag{3.19}$$

$$\sigma_{yy} = \frac{K_I}{\sqrt{2\pi r}}cos\frac{\theta}{2}(1 - sin\frac{\theta}{2}sin\frac{3\theta}{2}) \tag{3.20}$$

$$\sigma_{xy} = \frac{K_I}{\sqrt{2\pi r}}cos\frac{\theta}{2}(1 + sin\frac{\theta}{2}sin\frac{3\theta}{2}) \tag{3.21}$$

$$\sigma_{zz} = \begin{cases} \nu(\sigma_{xx} + \sigma_{yy}), & \text{plain strain} \\ 0, & \text{plain stress} \end{cases} \tag{3.22}$$

$$\sigma_{xz} = 0 \tag{3.23}$$

$$\sigma_{yz} = 0 \tag{3.24}$$

Mode II

Displacements field:

$$u_x = \frac{K_{II}}{2\mu}\sqrt{\frac{r}{2\pi}}sin\frac{\theta}{2}(\kappa + 1 + 2cos^2\frac{\theta}{2}) \tag{3.25}$$

$$u_y = -\frac{K_I}{2\mu}\sqrt{\frac{r}{2\pi}}cos\frac{\theta}{2}(\kappa - 1 - 2sin^2\frac{\theta}{2}) \tag{3.26}$$

$$u_z = \begin{cases} 0, & \text{plain strain} \\ -\frac{\nu z}{E}(\sigma_{xx} + \sigma_{yy}), & \text{plain stress} \end{cases} \tag{3.27}$$

Stresses field:

$$\sigma_{xx} = -\frac{K_{II}}{\sqrt{2\pi r}} sin\frac{\theta}{2}(2 + cos\frac{\theta}{2}cos\frac{3\theta}{2}) \tag{3.28}$$

$$\sigma_{yy} = \frac{K_{II}}{\sqrt{2\pi r}} sin\frac{\theta}{2}cos\frac{\theta}{2}cos\frac{3\theta}{2} \tag{3.29}$$

$$\sigma_{xy} = \frac{K_{II}}{\sqrt{2\pi r}} cos\frac{\theta}{2}(1 - sin\frac{\theta}{2}sin\frac{3\theta}{2}) \tag{3.30}$$

$$\sigma_{zz} = \begin{cases} \nu(\sigma_{xx} + \sigma_{yy}), & \text{plain strain} \\ 0, & \text{plain stress} \end{cases} \tag{3.31}$$

$$\sigma_{xz} = 0 \tag{3.32}$$

$$\sigma_{yz} = 0 \tag{3.33}$$

Mode III

Displacements field:

$$u_x = 0 \tag{3.34}$$

$$u_y = 0 \tag{3.35}$$

$$u_z = \frac{K_{III}}{\mu}\sqrt{\frac{r}{2\pi}} sin\frac{\theta}{2} \tag{3.36}$$

Stresses field:

$$\sigma_{xx} = 0 \tag{3.37}$$

$$\sigma_{yy} = 0 \tag{3.38}$$

$$\sigma_{xy} = 0 \tag{3.39}$$

$$\sigma_{zz} = 0 \tag{3.40}$$

$$\sigma_{xz} = -\frac{K_{III}}{\sqrt{2\pi r}} sin\frac{\theta}{2} \tag{3.41}$$

$$\sigma_{yz} = \frac{K_{III}}{\sqrt{2\pi r}} cos\frac{\theta}{2} \tag{3.42}$$

where, $\mu = G$, represents the shear modulus of the elastic material, ν is the poisson ratio, while the parameter κ is defined as:

$$\kappa = \begin{cases} 3 - 4\nu, & \text{plain strain} \\ \frac{3-\nu}{1+\nu}, & \text{plain stress} \end{cases} \tag{3.43}$$

The stresses field can also be expressed in polar coordinates as:

Mode I

$$\sigma_{rr} = \frac{K_I}{\sqrt{2\pi r}} cos\frac{\theta}{2}(1 + sin^2\frac{\theta}{2}) \tag{3.44}$$

$$\sigma_{\theta\theta} = \frac{K_I}{\sqrt{2\pi r}} cos^3\frac{\theta}{2} \tag{3.45}$$

$$\sigma_{r\theta} = \frac{K_I}{\sqrt{2\pi r}} sin\frac{\theta}{2} cos^2\frac{\theta}{2} \tag{3.46}$$

Mode II

$$\sigma_{rr} = \frac{K_{II}}{\sqrt{2\pi r}} sin\frac{\theta}{2}(1 - 3sin^2\frac{\theta}{2}) \tag{3.47}$$

$$\sigma_{\theta\theta} = -\frac{3K_{II}}{2\sqrt{2\pi r}} sin\theta cos\frac{\theta}{2} \tag{3.48}$$

$$\sigma_{rr} = \frac{K_{II}}{\sqrt{2\pi r}} cos\frac{\theta}{2}(1 - 3sin^2\frac{\theta}{2}) \tag{3.49}$$

$$\tag{3.50}$$

3.1.6 J-integral

In order to compute the energy release rate G, Rice (1968) developed a way that called J-Integral and noticed the importance of the J-integral as a criterion for crack growth in fracture mechanics. The J-integral also known as conservation integral represents a way to compute the strain energy release rate for the material where the crack tip deformation does not obey linear elastic laws. In this approach a line integral is identified, which has the same value for all integration paths surrounding the crack tip. J-integral is path independent, hence evaluating the J-integral in a far field around a crack tip can be related to the crack-tip deformations. In this way crack tip complications can be avoided by evaluating the energy release rate in the domain where the results are reliable. In the absence of of the body force and crack tractions,

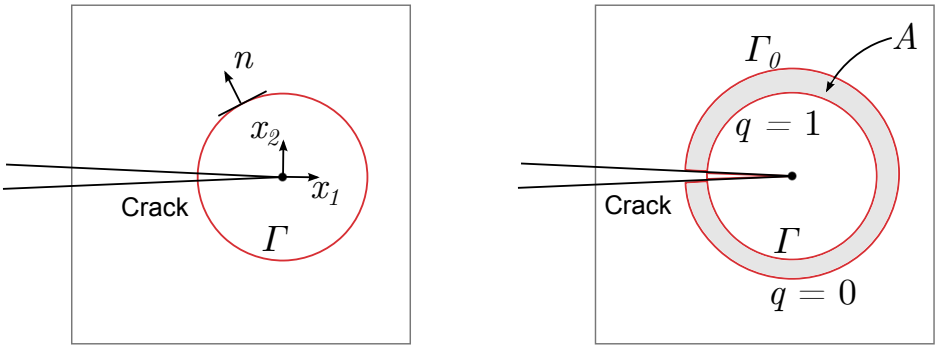

Figure 3.5: Definition of J-integral and the equivalent domain A.

the two-dimensional form of one of J-integral can be written as:

$$J = \oint_{\Gamma} (W dy - \boldsymbol{t} \frac{\partial \boldsymbol{u}}{\partial x} ds) \tag{3.51}$$

where

$$W(\epsilon) = \int_0^{\epsilon_{ij}} \sigma_{ij} d\epsilon_{ij} = \frac{1}{2} \sigma_{ij} \epsilon_{ij} \tag{3.52}$$

is the is the strain energy density, Γ is a closed counter-clockwise contour, ds is the differential element of the arc along the path Γ, $\boldsymbol{t} = \boldsymbol{\sigma n}$ is the traction vector on a plane defined by the outward normal $\boldsymbol{n}$, and $\boldsymbol{u}$ is the displacement vector (see Fig. 3.5).

3.1.6.1 Interaction integral method

As has been explained earlier, J-integral was developed as an alternative approach to calculate the G or K (SIFs). The J-integral is related to K_I, K_{II}, K_{III}, as:

$$J = \begin{cases} \frac{K_I^2}{E^*}, & \text{for Mode I} \\ \frac{K_{II}^2}{E^*}, & \text{for Mode II} \\ \frac{K_I^2}{E^*} + \frac{K_{II}^2}{E^*}, & \text{for mixed mode} \end{cases} \tag{3.53}$$

where

$$E^* = \begin{cases} E, & \text{plain stress} \\ \frac{E}{1-\nu^2}, & \text{plain strain} \end{cases} \tag{3.54}$$

For mixed mode fracture it is thus clear that SIFs for the two modes cannot be obtained independent of each other and auxiliary fields must be introduced and superimposed onto the actual fields satisfying the boundary value problem (Sih et al., 1965). In this method called the *interaction integral*, stresses and strains for the auxiliary state should be chosen so as to satisfy both the equilibrium equation and the traction-free boundary condition on the crack surface in the A area. These auxiliary fields are suitably selected in order to find a relationship between the mixed mode SIFs and the interaction integrals. The contour J-integral for the sum of the two states can be defined as:

$$J = J^{act} + J^{aux} + M \tag{3.55}$$

where J^{act} and J^{aux} are associated with the actual and auxiliary states, respectively, and M is the interaction integral:

$$J^{act} = \int_A [\sigma_{ij}\frac{\partial u_i}{\partial x_1} - W_s\delta_{1j}]\frac{\partial q}{\partial x_j}ds \tag{3.56}$$

$$J^{aux} = \int_A [\sigma^{aux}_{ij}\frac{\partial u^{aux}_i}{\partial x_1} - W^{aux}\delta_{1j}]\frac{\partial q}{\partial x_j}ds \tag{3.57}$$

$$M = \int_A [\sigma_{ij}\frac{\partial u^{aux}_i}{\partial x_1} + \sigma^{aux}_{ij}\frac{\partial u_i}{\partial x_1} - W^M\delta_{1j}]\frac{\partial q}{\partial x_j}ds \tag{3.58}$$

where q is a weighting function, while the actual, auxiliary and interaction works defined as:

$$W_s = \frac{1}{2}\sigma_{ij}\epsilon_{ij} \tag{3.59}$$

$$W^{aux} = \frac{1}{2}\sigma^{aux}_{ij}\epsilon^{aux}_{ij} \tag{3.60}$$

$$W^M = \frac{1}{2}(\sigma_{ij}\epsilon^{aux}_{ij} + \sigma^{aux}_{ij}\epsilon_{ij}) \tag{3.61}$$

One of the choices for the auxiliary state is the displacement and stress fields in the vicinity of the crack tip. Hence, from Eq. (3.53) the interaction integral M takes the following form:

$$M = \frac{2}{E^*}(K_I K^{aux}_I + K_{II}K^{aux}_{II}) \tag{3.62}$$

The M-integral shown above deals with interaction terms only and will be used for evaluating SIFs independently. An important thing here is that, M-integral is related to the crack-tip fields (i.e K_I and K_{II}) but yet may be evaluated in the region away from the crack tip, where such calculations (stress and deformations) can be performed with greater accuracy and convenience as compare to the crack tip region. Therefore, the mode I and II SIFs can be obtained from:

$$K = \frac{E^*}{2}M \tag{3.63}$$

The M-integral is then evaluated by determining the actual state parameters from the usual finite element analysis, and the auxiliary state parameters are evaluated using the asymptotic stress and displacement fields expressions of LEFM by inserting by choosing $K^{aux}_I = 1$, $K^{aux}_{II} = 0$ for Mode I, and $K^{aux}_{II} = 0$, $K^{aux}_{II} = 1$ for Mode II.

It should be noted that evaluation of the interaction integral M requires careful attention as the main fields are usually obtained from the finite element solution in a global or local (but crack independent) coordinate system, while the auxiliary fields are defined in the local crack-tip polar coordinate system. Therefore, necessary transformations are required to use a unified coordinate system.

3.1.6.2 Domain form of the interaction integral

For numerical purposes it is more advantageous to recast the conservation integral in a form best suited to finite element calculations, which is actually a line/contour integral into an area/domain integral. This is done by introducing a weighting function q in Eq. (3.58) such that, it has a value equal to 1 on the path Γ and 0 at the outer path Γ_0 (cf. Fig. 3.5).

For numerical evaluation of the integral the domain A is set from the collection of elements about the crack tip. This is done by selecting all elements which have nodes within a circle radius r_d with the center at the crack tip. As the J-integral is path independent, hence integral can be evaluated in the far field, so radius r_d for the domain A could be selected large enough to avoid complications of the crack tip. A thumb rule for the radius r_d is selected to be 2 to 3 time the square root of the area of an element size.

3.1.7 Fracture toughness

Similar to the conventional theory of strength of materials where the existing stress is compared with an allowable material stress/strength, fracture mechanics assumes that unstable fracture occurs when the stress intensity factor K reaches a critical value K_c, called the *fracture toughness*, which represents the potential ability of a material to withstand a given stress field at the tip of a crack and to resist progressive tensile crack extension. In other words K_c behaves as a threshold value for SIFs and for each pure fracture mode, the stress intensity factor K_i should be compared with its relevant toughness K_{ic}, a mixed mode criterion is required to account for the combined effect of all individual modes.

3.1.8 Fatigue crack growth

The concept of SIFs is also useful to compute the characteristics of a structural members subjected to fracture under fatigue. The fatigue crack growth is estimated by using Paris law (Paris et al., 1961), which is originally proposed for single mode deformation cases, relating the crack propagation rate under fatigue loading to the SIFs. For mixed-mode loading, a modified the Paris law can be expressed using the effective stress intensity factor (SIF) range $\Delta K_{\text{eff}} = K_{max} - K_{min}$. For a given fatigue loading, where the crack grows by length Δa in ΔN cycles, the Paris law becomes:

$$\frac{\Delta a}{\Delta N} \approx \frac{da}{dN} = C(\Delta K_{\text{eff}})^m \tag{3.64}$$

where C and m are empirical material constants. m is often called the *Paris exponent* and is typically in the range 3 to 4 for common steels and aluminium alloys. Eq. (3.64) represents a linear relationship between $log(\Delta K_{\text{eff}})$ and $log(\frac{da}{dN})$ which is used to describe the fatigue crack propagation behavior in region II (see Fig. 3.6).

For the calculation of effective mixed-mode stress intensity factor K_{eff}, various criteria have been proposed in the literature. In this thesis, however, the energy

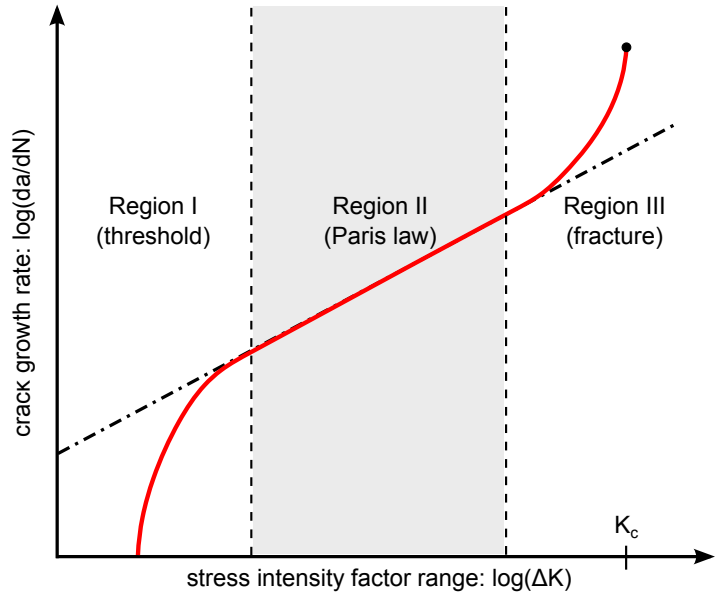

Figure 3.6: Logarithmic crack growth rate and effective region of Paris law.

release rate model has been adopted, leading to:

$$\Delta K_{\text{eff}} = \sqrt{\Delta K_I^2 + \Delta K_{II}^2} \tag{3.65}$$

and consequently, the number of corresponding cycles is computed according to (Anderson, 2004):

$$\Delta N = \frac{\Delta a}{C(\Delta K_{\text{eff}})^m} \tag{3.66}$$

3.2 The basic XFEM concept

The basic idea of XFEM is to enrich the approximation space so that it becomes capable of reproducing certain features of the problem of interest, in particular discontinuities such as cracks or interfaces. Naturally, the first XFEM approximations were also developed for simulation of strong discontinuities in fracture mechanics. XFEM can be assumed to be a classical FEM capable of handling arbitrary strong and weak discontinuities. In the XFEM, first, the usual finite element mesh is produced and then by considering the location of discontinuities, additional degrees of freedom, are added to the standard finite element model in selected nodes near to the discontinuities to provide a higher level of accuracy.

3.2.1 Enriched approximations

Enriched approximations have been the subject of several computational studies in the past two decades. Most of them are discussed within the framework of PU (Melenk and Babuška, 1996). The essential idea in XFEM is to add discontinuous enrichment functions to the finite element approximation using the PU. In XFEM, the following approximation is utilized to calculate the displacement for the point $\boldsymbol{x}$ locating within

the domain (Belytschko and Black, 1999), including discontinuities:

$$u(\boldsymbol{x}) = \boldsymbol{u}^{\text{std}} + \boldsymbol{u}^{\text{enr}} = \sum_{j=1}^{n} N_j(\boldsymbol{x})\boldsymbol{u}_j + \sum_{k=1}^{m} N_k(\boldsymbol{x})\psi(\boldsymbol{x})\boldsymbol{a}_k \tag{3.67}$$

where $\boldsymbol{u}_j$ is the vector of regular nodal degrees of freedom in the FEM, $\boldsymbol{a}_k$ is the set of degrees of freedom added to the standard FE model and $\psi(\boldsymbol{x})$ is the set of artificial enrichment functions defined for the set of nodes included in the influence (support) domain of the discontinuity.

The first term on the right-hand side of Eq. (3.67) is the standard finite element approximation to determine the displacement field, while the second term is the enrichment approximation which takes into account the existence of any discontinuities. This second term utilizes additional degrees of freedom to facilitate modeling of the existence of any discontinuous field, such as cracks, without modeling it explicitly in the FE mesh.

3.2.2 Modeling the crack

For modeling of cracks in the XFEM, two types of enrichment functions are used: (i) The Heaviside (step) function and (ii) the asymptotic crack-tip enrichment functions from LEFM. The approximate displacement function in Eq. (3.67) can be expressed in terms of the standard u^{std}, crack-split u^{H} and crack-tip u^{tip} components as:

$$u(\boldsymbol{x}) = \boldsymbol{u}^{\text{std}} + \boldsymbol{u}^{\text{H}} + \boldsymbol{u}^{\text{tip}} \tag{3.68}$$

or more explicitly:

$$u(\boldsymbol{x}) = \sum_{j=1}^{n} N_j(\boldsymbol{x})\boldsymbol{u}_j + \sum_{h=1}^{mh} N_h(\boldsymbol{x})H(\boldsymbol{x})\boldsymbol{a}_h + \sum_{k=1}^{mt} N_k(\boldsymbol{x})\Big(\sum_{l=1}^{mf} F_l(\boldsymbol{x})\boldsymbol{b}_k^l\Big) \tag{3.69}$$

where n is the number of nodes of each finite element with standard degrees of freedom $\boldsymbol{u}_j$ and shape functions $N_j(\boldsymbol{x})$, mh is the number of nodes in the elements containing the crack face (but not crack tip), $\boldsymbol{a}_h$ is the vector of additional nodal degrees of freedom for modeling crack faces (not crack tips) by the Heaviside function $H(\boldsymbol{x})$ (see Section 3.2.2.1), m_t is the number of nodes associated with the crack tip in its influence domain, $\boldsymbol{b}_k^l$ is the vector of additional nodal degrees of freedom for modeling crack tips and $F_l(\boldsymbol{x})$ are the crack-tip enrichment functions (see Section 3.2.2.2).

3.2.2.1 Heaviside function

The elements which are completely cut by the crack, such that they split into two, are enriched with the Heaviside (step) function H. The Heaviside function is a discontinuous function across the crack surface and is constant on each side of the crack. The splitting of the domain by the crack causes a displacement jump and the Heaviside function gives the desired behavior to approximate the true field. Mathematically the

Heaviside function is defined as:

$$H = \begin{cases} +1, & \text{for } (\boldsymbol{x} - \boldsymbol{x}^*) \cdot \boldsymbol{n} > 0 \\ -1, & \text{for } (\boldsymbol{x} - \boldsymbol{x}^*) \cdot \boldsymbol{n} < 0 \end{cases} \tag{3.70}$$

where $\boldsymbol{x}$ is the point of interest, $\boldsymbol{x}^*$ is nearest point to the crack segment Γ and $\boldsymbol{n}$ is the unit normal vector at $\boldsymbol{x}^*$. In other words, Heaviside function can define whether the point x^* is above or below the crack segment. This can be determined also by finding the minimum signed distance function to the crack geometry (see also Section 3.4.1). The function will have a positive value if the dot product of the two vectors is a positive value and negative otherwise. If no unique normal is defined then the function will have a positive value if $(x - x^*)$ belong to the cone of normals (see Fig. 3.7).

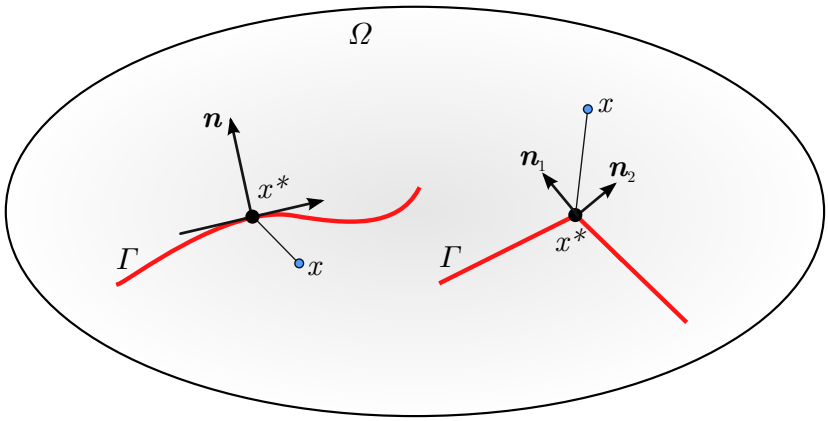

Figure 3.7: Evaluation of Heaviside function for a smooth and kink crack.

3.2.2.2 Crack-tip enrichment

Heaviside enrichment is good when the element is totally cut by the crack, such that it divides the element into two. In case the element contains the crack tip, then part of the element is cut and part of it not. Hence in such cases the step function cannot be used to enrich the domain. From LEFM, the exact solution of the displacement field around the crack tip (see Section 3.1.5), is given by:

$$u_x = \frac{K_I}{2\mu}\sqrt{\frac{r}{2\pi}}cos\frac{\theta}{2}(\kappa - 1 + 2sin^2\frac{\theta}{2}) + \frac{K_{II}}{2\mu}\sqrt{\frac{r}{2\pi}}sin\frac{\theta}{2}(\kappa + 1 + 2cos^2\frac{\theta}{2}) \tag{3.71}$$

$$u_y = \frac{K_I}{2\mu}\sqrt{\frac{r}{2\pi}}cos\frac{\theta}{2}(\kappa + 1 - 2cos^2\frac{\theta}{2}) - \frac{K_I}{2\mu}\sqrt{\frac{r}{2\pi}}cos\frac{\theta}{2}(\kappa - 1 - 2sin^2\frac{\theta}{2}) \tag{3.72}$$

where K_I, K_{II} are the SIFs for Mode I and II fracture, (r, θ) is a polar coordinate system with origin at the crack tip and κ the Kolsov constant. The above displacement fields are contained within the span of the following four functions, which forms the basis of the asymptotic field around the crack tip (Fleming et al., 1997):

$$\{F_l(r,\theta)\}_{l=1}^4 = \left\{\sqrt{r}\sin(\frac{\theta}{2}); \sqrt{r}\cos(\frac{\theta}{2}); \sqrt{r}\sin(\frac{\theta}{2})\sin(\theta); \sqrt{r}\cos(\frac{\theta}{2})\sin(\theta)\right\} \tag{3.73}$$

In addition to standard degrees of freedom, the above functions giving rise to four additional degrees of freedom in each direction at a node and are used for enriching the field near the crack tip. Note that the first function (Fig. 3.8a) is discontinuous across the crack and and represents the discontinuity near the crack-tip, while the other three functions (Figs. 3.8b - 3.8d) are added to get accurate result with relatively coarse meshes. The inclusion of $\sqrt{r}$ term in the enrichment function gives the required singularity in the stress field. Furthermore, the enrichment functions are discontinuous along the ray, $\theta = \pm\pi$.

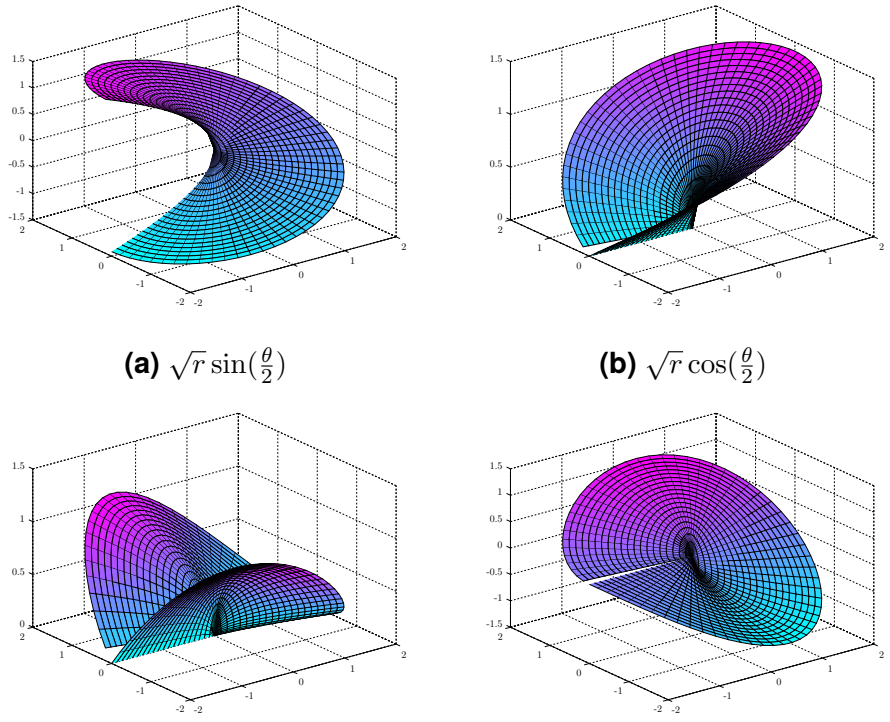

(a) $\sqrt{r}\sin(\frac{\theta}{2})$ **(b)** $\sqrt{r}\cos(\frac{\theta}{2})$

(c) $\sqrt{r}\sin(\frac{\theta}{2})\sin(\theta)$ **(d)** $\sqrt{r}\cos(\frac{\theta}{2})\sin(\theta)$

Figure 3.8: Crack tip enrichment functions.

3.2.3 Governing equations

A body in the state of equilibrium with the boundary conditions in the form of traction and displacement conditions, is considered (see Fig. 3.9). The strong form of the equilibrium equation can be written as:

$$\nabla \cdot \sigma + \boldsymbol{f}^b = 0 \quad \text{in } \Omega \tag{3.74}$$

with the following boundary conditions:

$$\begin{cases} \boldsymbol{\sigma} \cdot \boldsymbol{n} = \boldsymbol{f}^t, & \text{on } \Gamma_t\text{: external traction} \\ \boldsymbol{u} = \overline{\boldsymbol{u}}, & \text{on } \Gamma_u\text{: prescribed displacement} \\ \boldsymbol{\sigma} \cdot \boldsymbol{n} = 0, & \text{on } \Gamma_c\text{: traction free crack} \end{cases} \tag{3.75}$$

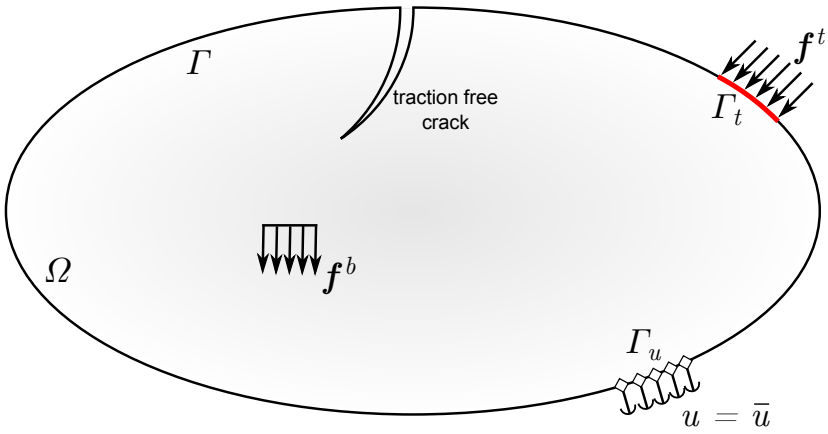

Figure 3.9: A body in the state of equilibrium.

where Γ_t, Γ_u and Γ_c are traction, displacement and crack boundaries, respectively, $\boldsymbol{\sigma}$ is the stress tensor and $\boldsymbol{f}^b$, $\boldsymbol{f}^t$ are the body force and external traction vectors, respectively.

Thus, the variational formulation of the boundary value problem (BVP) can be defined as:

$$W^{int} = W^{ext} \tag{3.76}$$

or

$$\int_\Omega \boldsymbol{\sigma} \cdot \delta\boldsymbol{\epsilon} d\Omega = \int_\Omega \boldsymbol{f}^b \cdot \delta\boldsymbol{u} d\Omega + \int_{\Gamma_t} \boldsymbol{f}^t \cdot \delta\boldsymbol{u} d\Gamma \tag{3.77}$$

3.2.4 Discrete form of equilibrium equation

Discretization of Eq. (3.77) using the XFEM approximations, results in the following discrete system of linear equilibrium equations:

$$\boldsymbol{K}\boldsymbol{u}^h = \boldsymbol{f} \tag{3.78}$$

where $\boldsymbol{K}$ is the stiffness matrix, $\boldsymbol{u}^h$ is the vector of degrees of nodal freedom (for both standard and enriched ones) and $\boldsymbol{f}$ is the vector of external force. The global matrix and vectors are calculated by assembling the matrix and vectors of each element. The elemental stiffness matrix $\boldsymbol{K}^e$ and external force vector $\boldsymbol{f}^e$ are defined as:

$$\boldsymbol{K}^e_{ij} = \begin{bmatrix} \boldsymbol{K}^{\boldsymbol{uu}}_{ij} & \boldsymbol{K}^{\boldsymbol{ua}}_{ij} & \boldsymbol{K}^{\boldsymbol{ub}}_{ij} \\ \boldsymbol{K}^{\boldsymbol{au}}_{ij} & \boldsymbol{K}^{\boldsymbol{aa}}_{ij} & \boldsymbol{K}^{\boldsymbol{ab}}_{ij} \\ \boldsymbol{K}^{\boldsymbol{bu}}_{ij} & \boldsymbol{K}^{\boldsymbol{ba}}_{ij} & \boldsymbol{K}^{\boldsymbol{bb}}_{ij} \end{bmatrix} \tag{3.79}$$

$$f^e_i = \{\boldsymbol{f}^u_i \ \boldsymbol{f}^{\boldsymbol{a}}_i \ \boldsymbol{f}^{b1}_i \ \boldsymbol{f}^{b2}_i \ \boldsymbol{f}^{b3}_i \ \boldsymbol{f}^{b4}_i\}^T \tag{3.80}$$

and $\boldsymbol{u}^h$ is the vector of nodal parameters:

$$\boldsymbol{u}^h = \{\boldsymbol{u}\ \boldsymbol{a}\ \boldsymbol{b}_1\ \boldsymbol{b}_2\ \boldsymbol{b}_3\ \boldsymbol{b}_4\}^T \tag{3.81}$$

with

$$\boldsymbol{K}_{ij}^{rs} = \int_{\Omega_e} (\boldsymbol{B}_i^r)^T \mathbb{C} \boldsymbol{B}_j^s d\Omega \quad \{r,s\} = \{\boldsymbol{u}, \boldsymbol{a}, \boldsymbol{b}\} \tag{3.82}$$

and

$$f_i^{\boldsymbol{u}} = \int_{\Gamma_t} N_i \boldsymbol{f}^t d\Gamma + \int_{\Omega^e} N_i \boldsymbol{f}^b d\Omega \tag{3.83}$$

$$f_i^{\boldsymbol{a}} = \int_{\Gamma_t} N_i H \boldsymbol{f}^t d\Gamma + \int_{\Omega^e} N_i H \boldsymbol{f}^b d\Omega \tag{3.84}$$

$$f_i^{\boldsymbol{b}\alpha} = \int_{\Gamma_t} N_i F_\alpha \boldsymbol{f}^t d\Gamma + \int_{\Omega^e} N_i F_\alpha \boldsymbol{f}^b d\Omega \quad (\alpha = 1,2,3,4) \tag{3.85}$$

In Eq. (3.82), $\boldsymbol{B}$ is the matrix of shape function derivatives, i.e:

$$\boldsymbol{B}_i^{\boldsymbol{u}} = \begin{bmatrix} N_{i,x} & 0 \\ 0 & N_{i,y} \\ N_{i,y} & N_{i,x} \end{bmatrix} \tag{3.86}$$

$$\boldsymbol{B}_i^{\boldsymbol{a}} = \begin{bmatrix} (N_i H(\phi))_{,x} & 0 \\ 0 & (N_i H(\phi))_{,y} \\ (N_i H(\phi))_{,y} & (N_i H(\phi))_{,x} \end{bmatrix} \tag{3.87}$$

$$\boldsymbol{B}_i^{\boldsymbol{b}} = \begin{bmatrix} \boldsymbol{B}_i^{\boldsymbol{b}1} & \boldsymbol{B}_i^{\boldsymbol{b}2} & \boldsymbol{B}_i^{\boldsymbol{b}3} & \boldsymbol{B}_i^{\boldsymbol{b}4} \end{bmatrix} \tag{3.88}$$

$$\boldsymbol{B}_i^{\alpha} = \begin{bmatrix} (N_i F_\alpha)_{,x} & 0 \\ 0 & (N_i F_\alpha)_{,y} \\ (N_i F_\alpha)_{,y} & (N_i F_\alpha)_{,x} \end{bmatrix} \quad (\alpha = 1,2,3,4) \tag{3.89}$$

Taking into account the effects of interpolation, Eq. (3.87) and Eq. (3.91) become:

$$\boldsymbol{B}_i^{\boldsymbol{a}} = \begin{bmatrix} (N_i[H(\phi) - H(\phi_i)])_{,x} & 0 \\ 0 & (N_i[H(\phi) - H(\phi_i)])_{,y} \\ (N_i[H(\phi) - H(\phi_i)])_{,y} & (N_i[H(\phi) - H(\phi_i)])_{,x} \end{bmatrix} \tag{3.90}$$

$$\boldsymbol{B}_i^{\alpha} = \begin{bmatrix} (N_i[F_\alpha - F_{\alpha i}])_{,x} & 0 \\ 0 & (N_i[F_\alpha - F_{\alpha i}])_{,y} \\ (N_i[F_\alpha - F_{\alpha i}])_{,y} & (N_i[F_\alpha - F_{\alpha i}])_{,x} \end{bmatrix} \quad (\alpha = 1,2,3,4) \tag{3.91}$$

In addition, the following vectors of nodal forces are modified to:

$$f_i^{\boldsymbol{a}} = \int_{\Gamma_t} N_i[H(\phi) - H(\phi_i)]\boldsymbol{f}^t d\Gamma + \int_{\Omega^e} N_i[H(\phi) - H(\phi_i)]\boldsymbol{f}^b d\Omega \tag{3.92}$$

$$f_i^{\boldsymbol{b}\alpha} = \int_{\Gamma_t} N_i[F_\alpha - F_{\alpha i}]\boldsymbol{f}^t d\Gamma + \int_{\Omega^e} N_i[F_\alpha - F_{\alpha i}]\boldsymbol{f}^b d\Omega \quad (\alpha = 1,2,3,4) \tag{3.93}$$

3.2.5 Derivatives of enrichment functions

Computation of the matrix of shape function derivatives $\boldsymbol{B}$, in Section 3.2.4 depends on the definition of the enrichment function. Hence, the following types are considered:

3.2.5.1 Derivatives of strong discontinuity enrichment

In case of strong discontinuity enrichment, the derivative of the Heaviside function is the Dirac delta function δ:

$$H_{,i}(\phi) = \delta(\phi) \tag{3.94}$$

which vanishes except at the position of the crack interface, taking the following form:

$$H_{,i}(\phi) = \begin{cases} 1, & \text{at crack} \\ 0, & \text{otherwise} \end{cases} \tag{3.95}$$

As a result, Eq. (3.87) can be rewritten as:

$$\boldsymbol{B}_i^{\boldsymbol{a}} = \begin{bmatrix} N_{i,x}H(\phi) & 0 \\ 0 & N_{i,y}H(\phi) \\ N_{i,y}H(\phi) & N_{i,x}H(\phi) \end{bmatrix} \tag{3.96}$$

3.2.5.2 Derivatives of crack-tip enrichment

Derivatives of $F_\alpha(r,\theta)$ with respect to the crack tip polar coordinates (r,θ), are:

$$F_{1,r} = \frac{1}{2\sqrt{r}} sin\frac{\theta}{2}, \quad F_{1,\theta} = \frac{\sqrt{r}}{2} cos\frac{\theta}{2} \tag{3.97}$$

$$F_{2,r} = \frac{1}{2\sqrt{r}} cos\frac{\theta}{2}, \quad F_{2,\theta} = -\frac{\sqrt{r}}{2} sin\frac{\theta}{2} \tag{3.98}$$

$$F_{3,r} = \frac{1}{2\sqrt{r}} sin\frac{\theta}{2} sin\theta, \quad F_{3,\theta} = \sqrt{r}(\frac{1}{2} cos\frac{\theta}{2} sin\theta + sin\frac{\theta}{2} cos\theta) \tag{3.99}$$

$$F_{4,r} = \frac{1}{2\sqrt{r}} cos\frac{\theta}{2} sin\theta, \quad F_{4,\theta} = \sqrt{r}(-\frac{1}{2} sin\frac{\theta}{2} sin\theta + cos\frac{\theta}{2} cos\theta) \tag{3.100}$$

and the derivatives of $F_\alpha(r,\theta)$ with respect to the local crack coordinate system $(x^{'}, y^{'})$ can be defined as (see Fig. 3.10):

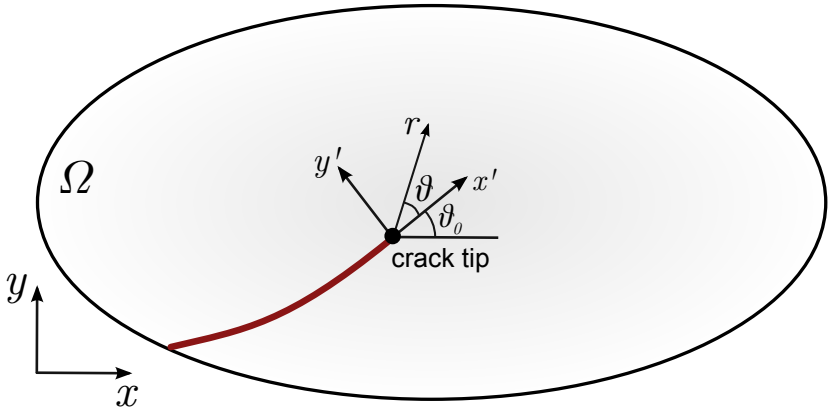

Figure 3.10: Global, local and polar coordinates at the crack tip.

$$F_{1,x'} = \frac{1}{2\sqrt{r}} sin\frac{\theta}{2}, \quad F_{1,y'} = \frac{1}{2\sqrt{r}} cos\frac{\theta}{2} \tag{3.101}$$

$$F_{2,x'} = \frac{1}{2\sqrt{r}} cos\frac{\theta}{2}, \quad F_{2,y'} = -\frac{1}{2\sqrt{r}} sin\frac{\theta}{2} \tag{3.102}$$

$$F_{3,x'} = -\frac{1}{2\sqrt{r}} sin\frac{3\theta}{2} sin\theta, \quad F_{3,y'} = \frac{1}{2\sqrt{r}} (sin\frac{\theta}{2} + sin\frac{3\theta}{2} cos\theta) \tag{3.103}$$

$$F_{4,x'} = -\frac{1}{2\sqrt{r}} cos\frac{3\theta}{2} sin\theta, \quad F_{4,y'} = \frac{1}{2\sqrt{r}} (cos\frac{\theta}{2} + cos\frac{3\theta}{2} cos\theta) \tag{3.104}$$

$$\tag{3.105}$$

Finally, the derivatives in the global coordinate system (x, y) are:

$$F_{\alpha,x} = F_{\alpha,x'} cos\theta_0 - F_{\alpha,y'} sin\theta_0 \tag{3.106}$$

$$F_{\alpha,x} = F_{\alpha,x'} sin\theta_0 - F_{\alpha,y'} cos\theta_0 \tag{3.107}$$

where $\theta 0$ is the angle of the crack with respect to the x axis.

3.3 Crack initiation and growth

The accuracy and reliability of the analysis of a cracked body primarily depends upon the accurate determination and continuity of the crack path. It is therefore very much important to select the crack growth criteria very carefully. Some of the commonly used crack growth criteria are:

- Minimum strain energy density criteria (Sih, 1974),
- Maximum energy release rate criteria (Nuismer, 1975),
- Maximum hoop stress or maximum principal stress criteria (Erdogan and Sih, 1963),
- Global tracking algorithm (Oliver and Huespe, 2004).

In this study the maximum hoop stress crack growth criteria was considered, coupled with XFEM.

3.3.1 Maximum hoop (circumferential) stress criterion

The most commonly used crack growth criteria in LEFM is the maximum hoop stress criteria (Erdogan and Sih, 1963). The criteria is based on the evaluation of mixed mode SIFs, K_I and K_{II}. According to this criteria it is assumed that (i) the crack initiation will occur when the maximum hoop stress reaches to a critical value, (ii) the crack will grow in a direction θ_{cr} in which circumferential stress $\sigma_{\theta\theta}$ is maximum.

The direction is determined by evaluating the SIFs, K_I and K_{II} using the domain form of interaction integral (cf. Section 3.1.6.2) around the crack tip assuming the crack surfaces are traction free. The circumferential stress in the direction of crack propagation is a principal stress, hence the crack propagation direction is determined by setting the shear stress equal to zero, i.e.:

$$\sigma_{r\theta} = \frac{1}{2\pi r} cos\frac{\theta}{2}\Big(\frac{1}{2}K_I sin\theta + \frac{1}{2}K_{II}(3cos\theta - 1\Big) = 0 \tag{3.108}$$

This leads to the equation for the critical crack propagation direction θ_{cr} in local crack tip coordinate system as:

$$\theta_{cr} = 2atan\frac{1}{4}\Big(\frac{K_I}{K_{II}} \pm \sqrt{\frac{K_I^2}{K_{II}} + 8}\Big) \tag{3.109}$$

It is worth mentioning that according to this criteria maximum propagation angle θ_{cr} is limited to 70.5° for pure Mode II cracks. The criteria basically works well for traction free crack surfaces. A more efficient expression for θ_{cr} for numerical computations, was implemented by Liang et al. (2003):

$$\theta_{cr} = 2atan\frac{-2\frac{K_{II}}{K_I}}{1 + \sqrt{1 + 8(\frac{K_{II}}{K_I})^2}} \tag{3.110}$$

3.4 Tracking discontinuities

The most important aspect of problems dealing with moving interfaces (such as cracks) is to track them as they evolve. To avoid instabilities around points of high curvature and cusps, two different techniques have been developed based on idea of tracking evolving fronts with the equations of motion forms: (i) the level set method (LSM) and (ii) the fast marching method (FMM). The first method is more general but slowed, while the latter is very efficient but limited to specific range of geometries. Both methods are designed to handle problems in which the separating interfaces develop sharp corners and cusps, change topology, break apart and merge together. These techniques have been used in a range of applications, including problems in fluid mechanics, computer animation, as well as in image processing.

3.4.1 Level set method (LSM)

The level set approach, introduced by Osher and Sethian (1988), for tracking moving interfaces. This method builds a surface from the original curve, instead of following

the curve interface itself. Though it is not mandatory to use level sets in XFEM, many XFEM formulations take advantage of this powerful technique for tracking interfaces. This method is also adopted in this study. To construct a level set set function ϕ a do-

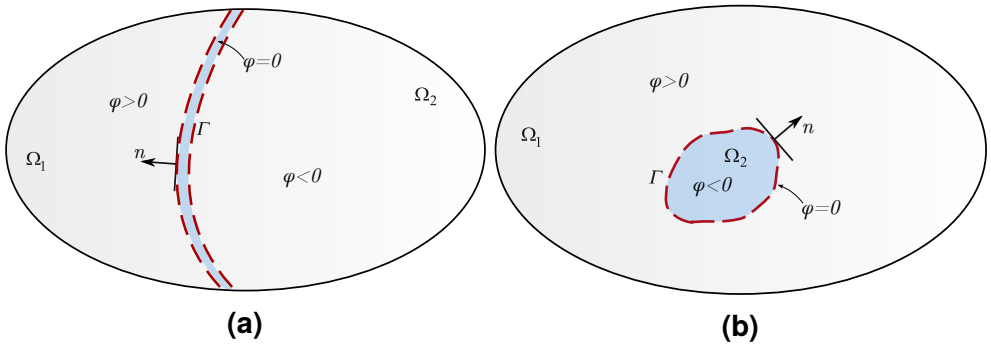

Figure 3.11: Domain Ω with (a) an open discontinuity and with (b) a closed discontinuity.

main Ω is defined, which is divided into two non-overlapping and distinct subdomains, Ω_1 and Ω_2, sharing an open or closed interface Γ (see Figs. 3.11a-3.11b, respectively), which is moving outward with a velocity $\boldsymbol{v}$ normal to the interface. The key point in the LSM is to represent this interface at any time t, with a zero level set function i.e $\phi(x,t) = 0$, where $\phi(x,t)$ is the level set function. The evolution equation for the interface Γ using the material time derivative (total derivative) can be written as:

$$\frac{\partial \phi}{\partial t} + \boldsymbol{v}|\nabla \phi| = 0 \tag{3.111}$$

with the initial condition $\phi(x,0) =$ given.

3.4.1.1 Signed distance function

One common choice for the initial condition is usually the signed distance function such that the level set function has positive values on one side of the interface and negative values at the other side of the interface and the interface is identified by the zero level set function, i.e.:

$$\phi(\boldsymbol{x}) = \begin{cases} > 0, & \boldsymbol{x} \in \Omega_1 \\ = 0, & \boldsymbol{x} \in \Gamma \\ < 0, & \boldsymbol{x} \in \Omega_2 \end{cases} \tag{3.112}$$

The interface Γ can be regarded as the zero level contour of the level set function $\phi(\boldsymbol{x})$. The distance d from a point $\boldsymbol{x}$ to the interface Γ is defined as:

$$d = \|\boldsymbol{x} - \boldsymbol{x}_\Gamma\| \tag{3.113}$$

where, $\boldsymbol{x}_\Gamma$ is the normal projection of $\boldsymbol{x}$ on Γ. The signed distance function $\phi(\boldsymbol{x})$ can then be defined as,

$$\phi(\boldsymbol{x}) = \min \|\boldsymbol{x} - \boldsymbol{x}_\Gamma\| \, sign(\boldsymbol{n} \cdot (\boldsymbol{x} - \boldsymbol{x}_\Gamma)) \tag{3.114}$$

where $\boldsymbol{n}$ is the unit normal vector (see Fig. 3.12).

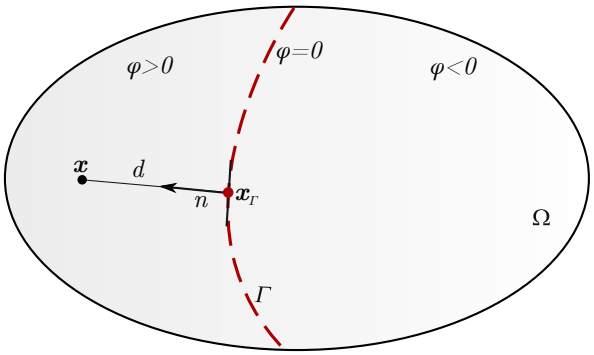

Figure 3.12: Definition of the signed distance function.

3.4.1.2 Crack representation by level sets

Level set method offers also an elegant way of modeling cracks. For the modeling of crack the level set function is defined as a signed distance function. As the crack is a discontinuity in order to fully characterize it, two level set functions are defined: (i) a normal level set function ϕ and (ii) a tangential level set function ψ. Both the two level set functions are defined as a signed distance functions.

To construct these two level sets functions the approach proposed by Stolarska et al. (2001) was also adopted in this thesis. The crack tip segment is extended to meet the boundary of the domain. The normal level set function ϕ is then computed using Eq. (3.114), from the original crack segment Γ (at crack tip j) and the virtual segments (extensions) (see Fig. 3.13). The tangential level set function ψ is computed

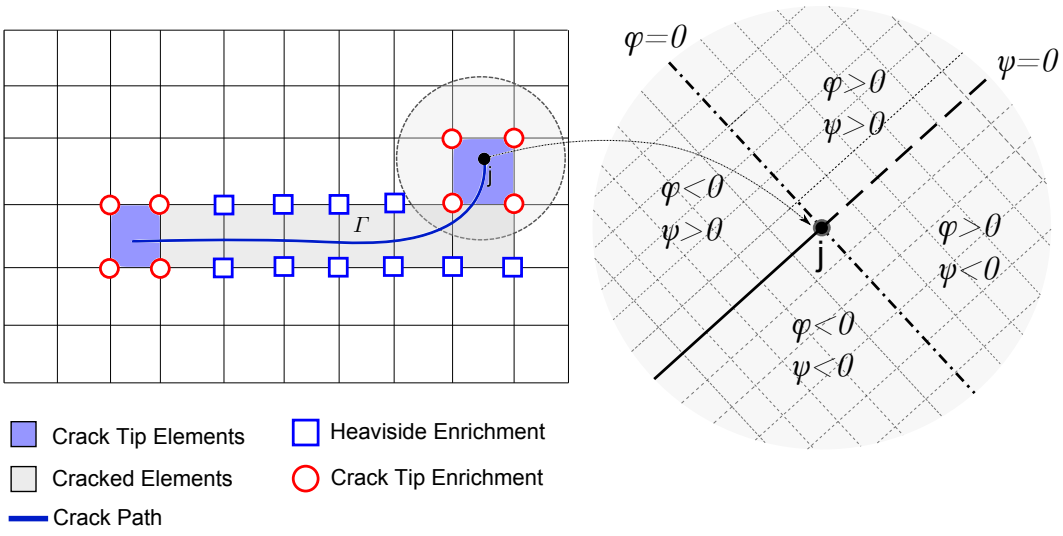

Figure 3.13: Level set functions ϕ and ψ for crack representation.

by finding the minimum signed distance to the normal vector at the crack tip. If the crack is an interior crack then we need to define two tangential level set functions ψ_1 and ψ_2 corresponding to each crack tip. In this case, one can define a unique

tangential level set function in order to make further computations easy, as:

$$\psi = \max[\psi_1, \psi_2] \tag{3.115}$$

It is now evident that the crack can now be fully characterized by the two level set functions ϕ and ψ such that $\phi = 0$ and $\psi < 0$ at the crack surface Γ. Consequently, the crack tip is identified on an intersection of normal and tangential zero level set functions, i.e intersection of $\phi = 0$ and $\psi = 0$. In the rest of the domain ϕ has a positive value above the crack and a negative value below the crack, while ψ has a positive value to the right of the normal at the crack tip.

The crack tip level set ψ is generally assumed to be orthogonal to ϕ, i.e. $\phi\psi = 0$. Although the actual crack is embedded inside a domain, the zero level set of ψ cuts through the entire domain. It is also assumed that once a part of a crack has formed, that part will no longer change shape or move.

Within the framework of finite elements the level set functions ϕ and ψ, defined above, can be interpolated within an element using the standard shape functions (Stolarska and Chopp, 2003) as:

$$\phi(\boldsymbol{x}) = N_i(\boldsymbol{x})\phi_i \tag{3.116}$$

where ϕ_i are the nodal values of the level set function. Furthermore, the level set functions can also be used for determining the Heaviside enrichment function H, such that:

$$H = sign(\phi) = \begin{cases} +1, & \phi > 0 \\ -1, & \phi < 0 \end{cases} \tag{3.117}$$

Similar, the crack tip field which enriched with crack-tip enrichment functions in the framework of XFEM can be expressed in terms of level set functions. If the position of a point is expressed in polar coordinates (r, θ) of the crack tip coordinate system, then in order to align the discontinuity in the enrichment function a sequence of mapping is required to rotate each crack segment onto the crack (Belytschko and Black, 1999). However the use of level set functions alleviate the need for such mapping and the position of a point in the crack tip polar coordinate system can be written as:

$$r = \sqrt{\phi^2 + \psi^2} \tag{3.118}$$

$$\theta = atan\frac{\phi}{\psi} \tag{3.119}$$

It can be seen that the θ is aligned with the discontinuity and varies from $-\pi$ to $+\pi$.

Also, level set functions ϕ and ψ can also be used to identify the elements completely cut by the crack and the elements containing the crack tip (Stolarska et al., 2001). The elements that are completely cut by the crack can be found by the conditions:

$$\phi_{min}\phi_{max} \leq 0 \tag{3.120}$$

$$\psi_{max} < 0 \tag{3.121}$$

while the elements containing the crack tip can be found by the conditions:

$$\phi_{min}\phi_{max} \leq 0 \tag{3.122}$$
$$\psi_{min}\psi_{min} \leq 0 \tag{3.123}$$

3.5 Numerical aspects of XFEM

3.5.1 Selection of enrichment nodes

There have been different approaches proposed in literature, for the selection of nodes to be enriched and the most accepted ones are described in this section.

3.5.1.1 Heaviside enrichment

One method, called *Heaviside enrichment* allows the discontinuity to be modelled across the crack over the points along the crack surface. The value of the enriched shape function remains zero at all nodes and edges that do not intersect with the crack, in order to satisfy the inter-element continuity requirement. This method only affects the element containing the crack, and does not directly influence adjacent elements, even if they share a common node with the enriched element. A simple procedure for selection of nodes for this type of enrichment is shown in Fig. 3.14, where enriched nodes are marked by blue squares. At each stage of the propagation, nodes on edges cut by the crack path are enriched. Even if the crack tip locates just on an edge, the corresponding nodes are not enriched, but if a crack path passes along the finite element edges this might be a potential source of instability.

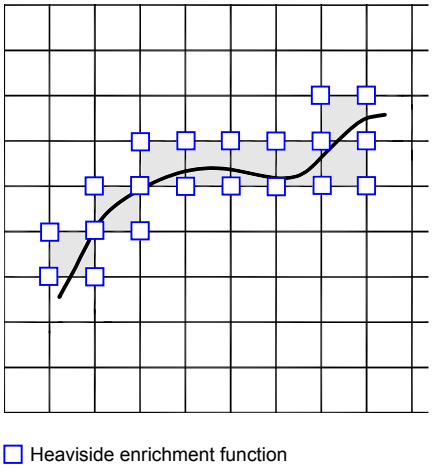

Figure 3.14: Heaviside enrichment type A.

3.5.1.2 Crack-tip enrichment

In an alternative procedure, the enrichment with Heaviside function is applied onto all nodal points of elements that contain part of the crack as shown in Fig. 3.15.

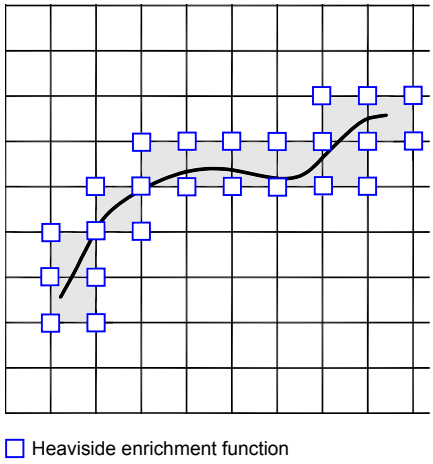

Figure 3.15: Heaviside enrichment type B.

3.5.1.3 Full enrichment

The most appropriate choice, however, is to use both Heaviside and crack-tip enrichments where required. Accordingly, the crack-tip enrichment functions in the crack-tip element also allow accurate representation of discontinuity in that element. The sets of nodes that must be enriched with Heaviside or crack-tip functions are marked by blue squares and red circles, respectively, as depicted in Fig. 3.16.

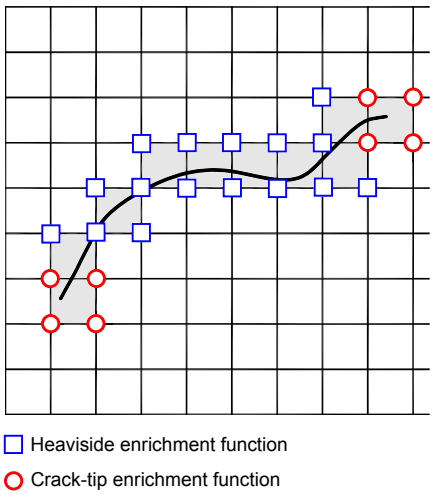

Figure 3.16: Heaviside and crack-tip enrichments.

3.5.2 Numerical integration

The Gauss quadrature rule is widely used in finite element analysis for numerical evaluation of various integrals over a specified domain of interest such as a finite element and for polynomial integrands, the is proved to be exact. But, when singularities are introduced within a finite element, this lead to transform the displacement and stress fields into highly nonlinear fields. Also, the usual Gauss quadrature rule fails

to integrate the field in the elements cut by the crack accurately and correctly. Thus, a modified integration scheme is required to define the necessary points needed for the integration within an enriched element. Hence, the enriched element is necessary to be partitioned, in order to integrate the field properly on both sides of the discontinuity. This approach has to be consistent with the geometry of the crack as well as the order of the enrichment functions. The partitioning of elements cut by the crack in the XFEM, is different from the re-meshing in standard FEM and is performed in the following ways:

- The partition is done only for the integration purpose and no extra degrees of freedoms are added to the system unlike the convetional FEM, where such re-meshing becomes not only cumbersome but also computationally costly in case of crack growth problems.
- The partition is done only for the purpose of integration and no conditions on the shape of sub-quads or sub-triangles is imposed, while re-meshing in FEM requires the construction of well shaped elements.

3.5.2.1 Sub-quad approach

Dolbow (1999) proposed a method to subdivide the element into sub-quads (see Fig. 3.17a). Each sub-quad is then integrated by a conventional Gauss integration rule. There is no limit in how many different number of sub-quads can be used for elements that are cut by a crack or include a crack tip.

3.5.2.2 Sub-triangle approach

Dolbow (1999) proposed also a second method to subdivide the element at both sides of the crack into sub-triangles whose edges are adapted to crack faces (see Fig. 3.17b). For a crack-tip element, more sub-triangles are required in front of the crack tip because of the existence of a highly nonlinear and singular stress field. This method has been also adopted in this study.

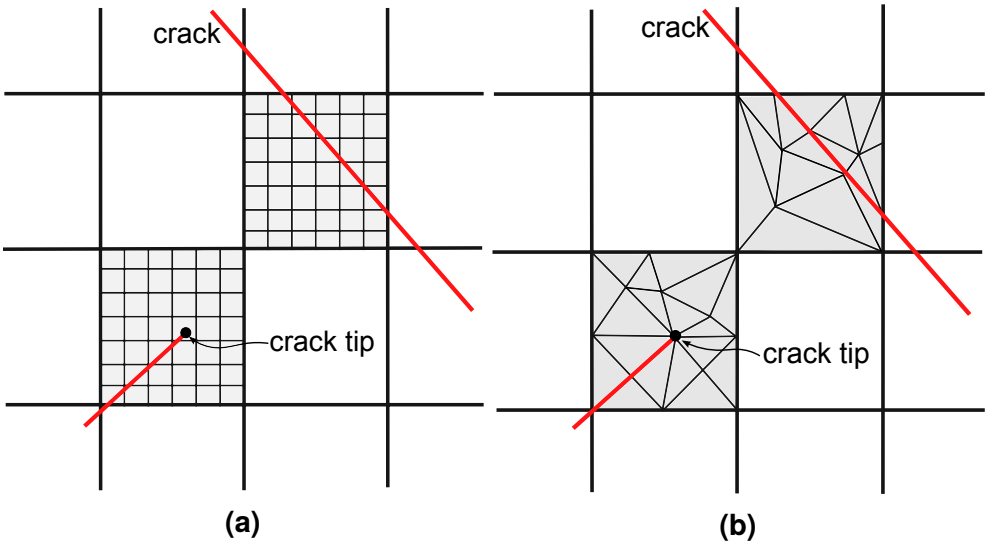

Figure 3.17: Partitioning the cracked element into (a) sub-quads and (b) sub-triangles.

3.5.2.3 Limitations of enrichments

It is well-known that the XFEM approximation may become ill-conditioned, or even fail, if the enrichment is adopted for a case where the crack passes through or very close to a node. To avoid such a numerical difficulty, Dolbow (1999) proposed a simple geometric criterion to determine the candidacy of a node for enrichment. The two extreme cases of the relative position of a crack within a cracked element are shown in Fig. 3.18. For both cases the following ratios are defined as a measure of candidacy, as:

$$r_{A^-} = \frac{A^-}{A^+ + A^-} \tag{3.124}$$

$$r_{A^+} = \frac{A^+}{A^+ + A^-} \tag{3.125}$$

where A^+ and A^- are the area of the influence domain of a node above and below the crack, respectively. If values of r_{A^-} or r_{A^+} are smaller than an allowable tolerance value, the node must not be enriched. Dolbow (1999) proposed a tolerance of 0.01%, although the value of it should be set according to each specific problem. An alternative approach based on the existence of Gauss points within its support

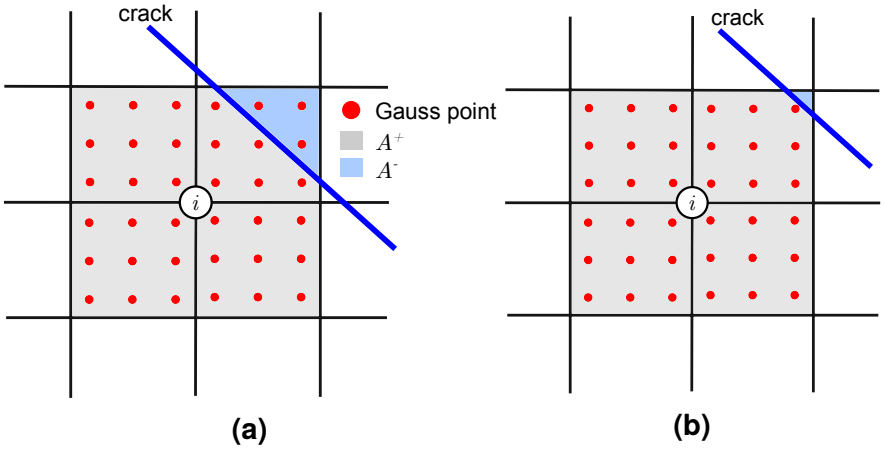

Figure 3.18: Criteria for node enrichment: (a) based on Dolbow (1999) definition, (b) based on the existence of Gauss points within its support domain.

domain. In this approach, a node is enriched if each side of the crack in its influence domain includes at least one Gauss point. Hence, node i in Fig. 3.18a must not be enriched because there is no Gaussian point above the crack, although the crack cuts the element where node i belongs. On the contrary, node i in Fig. 3.18b has to be enriched.

4

Stochastic Finite Element Analysis

Randomness is the lack of pattern or regularity. The two sources of randomness are: (i) the impracticality of a comprehensive deterministic description and the inherent irregularity in the phenomenon being observed (aleatoric uncertainty), and (ii) the generalized lack of knowledge about the processes concerned (epistemic uncertainty) (Ghanem and Spanos, 2003).

Typical problems in all engineering fields, involve media with random properties (random media), and require complex mathematical tools for their solution. The design of structures under static, dynamic (earthquake and wind loadings), imperfections in the structural elements, random fluctuations in temperature, or other environmental loading conditions, life prediction of structures, etc. are characteristic examples in the field of civil engineering. Specifically, in structural engineering, materials with random properties are often used, such as, soils, rocks, and concrete. The natural responses of these structures may be completely unpredictable by deterministic models. Hence, powerful analysis tools based on the mechanics of random media are very important to model these uncertainties and random characteristics of the materials.

Mathematicians and engineers study and discover independently the theoretical and/or numerical aspects of random medium mechanics from different points of view, developing different methods. The stochastic finite element method (SFEM) is a powerful tool rendering possible the efficient treatment of large-scale stochastic problems due to the spectacular growth of computational power in recent years. SFEM is an extension of the classical deterministic FE approach to the stochastic framework i.e. to the solution of stochastic (static and dynamic) problems involving finite elements whose properties are random. In this thesis, SFEM is implemented for the first time within the framework of the SLA, described in Section 2.2.1, providing solutions to the stochastic nonlinear static problems for structures made with softening materials whose properties are randomly distributed in the whole structure, as well as providing specific information on the probability of failure.

In this chapter, stochastic functions are used for modeling structures with random spatially varying material properties. The necessary mathematical background is presented first involving the definition of the fundamental concepts of the stochastic

functions, such as the mean value, the autocovariance and autocorrelation functions, the correlation structure and the correlation length. This is followed by an overview of existing techniques for the representation of the Gaussian and non-Gaussian stochastic processes and fields. The spectral representation method is discussed in detail and used to represent the stochastic fields describing the uncertain material properties.

Furthermore, the basic aspects of SFEM are presented comprising the three basic steps of the method: The discretization of the stochastic fields, the formulation of the stochastic stiffness matrix and the response variability calculation using either Monte Carlo simulation or the variability response function approach. Finally, particular aspects of coupling SFEM with SLA and useful conclusions are outlined.

4.1 Stochastic processes and fields

In computational structural mechanics, different types of problems will arise based on what information is available. From an engineering mechanics point of view, the most common stochastic system problem involves a linear differential equation with random coefficients, in which the properties of the system under study are represented by these coefficients and can be interpreted as random variables. The problem can be mathematically expressed as:

$$\boldsymbol{\Lambda u} = \boldsymbol{f} \tag{4.1}$$

where $\boldsymbol{\Lambda}$ is a linear stochastic differential operator, $\boldsymbol{u}$ is the random response, and $\boldsymbol{f}$ is possibly deterministic/random excitation. Fig. 4.1 illustrates the sequence of events leading to assigning a function to the response of a random experiment. First the experiment is run and then the resulting response is observed. Each response is associated with stochastic function f. The present study undertakes only the de-

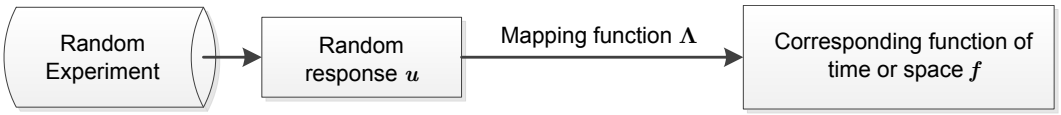

Figure 4.1: The sequence of events leading to assigning a stochastic function f to the response of a random experiment.

terministic input and random system type of problems in the context of SFEM. The quantification of uncertainty in parameter values, a key component in SFEM, is done using the mathematical theory of stochastic processes and fields.

4.1.1 Definitions

Each function of one or more variables, whose values are random variables, is called *stochastic function*. The stochastic function is a generalization of the known functions, and the difference between them, is that the former consists of a set of sample functions (realizations) and not univocal mappings. The stochastic functions are characterized as *processes* or *fields* depending on whether the independent variables are related to time or space, respectively. The loading of a structure, the environment temperature, a cross-section of a structural element are typical cases of stochastic

processes/fields. This thesis deals with stochastic functions where the outcome of a random experiment is associated with a function of space, i.e. stochastic field, which is described by (see Fig. 4.2):

- the sample space S which includes all possible outcomes s of a random experiment,
- the sample function $f(x, s)$ which is the function associated with an outcome s,
- the *ensemble* which is the set of all possible space functions produced by the random experiment,
- the space parameter x,
- the statistical dependencies among the stochastic field when x is changed.

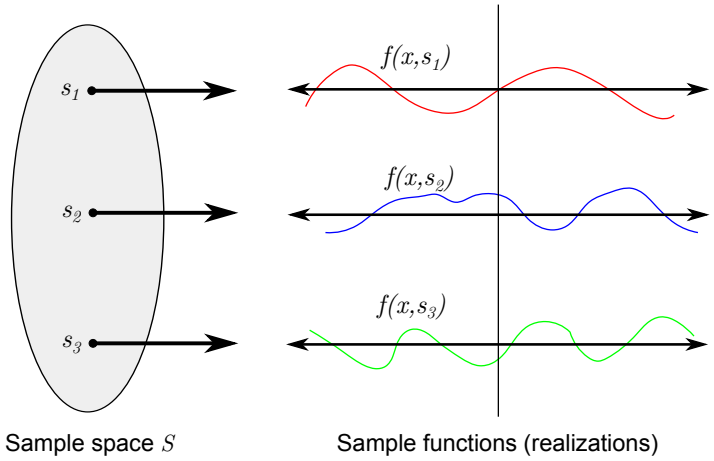

Figure 4.2: Conceptual representation of a stochastic field (sample space and three realizations of it).

In the following section, for the sake of simplicity, the basic properties of the stochastic functions will be defined in the case of one-dimensional continuous stochastic field, without loss of generality.

4.2 Mathematical background of stochastic fields

4.2.1 Mean value

The mean value $m(x)$ of a stochastic field $f(x)$ is defined as follows:

$$m(x) = E[f(x)] = \int_{-\infty}^{\infty} f(x)p(x)dx \tag{4.2}$$

where, $p(x)$ is the probability density function (PDF) of the random field.

4.2.2 Autocovariance function

The covariance of the random variables $f(x_1)$ and $f(x_2)$ is called *autocovariance function* C_{ff} of the stochastic field $f(x)$ and is defined as:

$$C_{ff}(x_1, x_2) = E\Big[[f(x_1) - m(x_1)] \cdot [f(x_2) - m(x_2)]\Big] \tag{4.3}$$

The variance of the stochastic field $f(x)$ is given by:

$$Var[f(x)] = \sigma^2(x) = C_{ff}(x,x) = E[f^2(x)] - m^2(x) \tag{4.4}$$

where σ is the standard deviation of the field.

The autocovariance function has the following useful properties:

- As follows from the definition in Eq. (4.3) it is a symmetric function, i.e.:

$$C_{ff}(x_1,x_2) = C_{ff}(x_2,x_1) \tag{4.5}$$

- It is a non-negative definite function.
- It verifies the relationship:

$$|C_{ff}(x_1,x_2)| \leq \sqrt{Var[f(x_1)] \cdot Var[f(x_1)]} = \sqrt{C_{ff}(x_1,x_1) \cdot C_{ff}(x_2,x_2)} \tag{4.6}$$

This last inequality allows to introduce the normalized autocovariance function c_{ff} as:

$$c_{ff}(x_1,x_2) = \frac{C_{ff}(x_1,x_2)}{\sqrt{C_{ff}(x_1,x_1) \cdot C_{ff}(x_2,x_2)}} = \frac{C_{ff}(x_1,x_2)}{\sigma(x_1) \cdot \sigma(x_2)} \tag{4.7}$$

that fullfils the following inequality:

$$|c_{ff}(x_1,x_2)| \leq 1 \tag{4.8}$$

4.2.3 Autocorrelation function

Autocorrelation function is the cross-correlation function of a field with itself. It is a mathematical tool for finding repeating patterns or identifying the missing fundamental frequency in a field implied by its harmonic frequencies. The autocorrelation function R_{ff} of a stochastic field $f(x)$ is defined as:

$$R_{ff}(x_1,x_2) = E[f(x_1) \cdot f(x_2)] \tag{4.9}$$

i.e. the mean value of the product of the stochastic field values at two different points of the x-axis. From Eq. (4.9) and Eq. (4.3) it is obvious that for a zero-mean stochastic field, the autocorrelation and autovariance functions are identical. In the case of $x = x_1 = x_2$, the autocorrelation function is written as:

$$R_{ff}(x,x) = E[f^2(x)] \tag{4.10}$$

The cumulative distribution function (CDF) of the stochastic fields that follow the normal distribution (Gaussian fields) is fully defined by its mean and the autocorrelation function. Gaussian fields also have the useful property that can be decomposed into the sum of a zero-mean field and the mean value function of it.

4.2.4 Homogeneous stochastic fields - stationary stochastic processes)

An important class of stochastic fields are the homogeneous fields, the CDF of which does not depend on the position x (see Fig. 4.3).

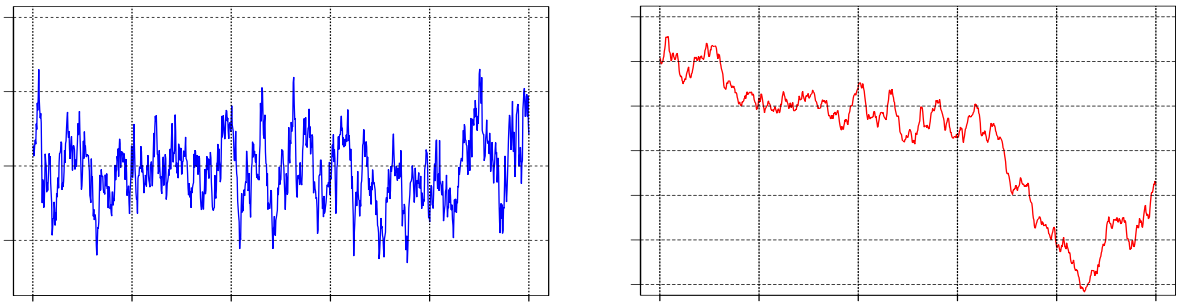

Figure 4.3: Sample functions of a homogeneous (left) and a non-homogeneous (right) stochastic field.

Therefore, both the mean and standard deviation of a homogeneous stochastic field are constant and independent of the position variable x:

$$E[f(x)] = m(x) = m$$
$$\sigma(x) = \sigma$$

As expected, the autocorrelation function of a homogeneous stochastic field depends only on the distance τ between two points x_1, x_2 on the x-axis and therefore:

$$R_{ff}(x_1, x_2) = R_{ff}(x_2 - x_1) = R_{ff}(\tau) \tag{4.11}$$

The correlation coefficient ρ between the values $f(x)$ and $f(x+\tau)$ of the stochastic field is given by:

$$\rho = \frac{E\Big[[f(x) - m] \cdot [f(x+\tau) - m]\Big]}{\sigma^2} = \frac{R_{ff}(\tau) - m^2}{\sigma^2} \tag{4.12}$$

From Eq. (4.12) it follows that $R_{ff}(\tau) = \sigma^2\rho + m^2$, and since $\rho \in [-1, 1]$, then:

$$-\sigma^2 + m^2 \leq R_{ff}(\tau) \leq \sigma^2 + m^2 \tag{4.13}$$

For large distances ($\tau \to \infty$), it is expected to be no relationship between the values of $f(x)$ and $f(x+\tau)$ and consequently, the correlation coefficient between these values will tend to zero. Also, from Eq. (4.12) it follows that:

$$\lim_{\tau \to \infty} R_{ff}(\tau) = m^2 \tag{4.14}$$

Since the autocorrelation function of a homogeneous field depends only on the distance between two points, then:

$$R_{ff}(\tau) = E[f(x) \cdot f(x+\tau)] = E[f(x) \cdot f(x-\tau)] = R_{ff}(-\tau) \tag{4.15}$$

and thus, $R_{ff}(\tau)$ is an even function. A typical autocorrelation function of a homogeneous stochastic field along with its properties, as described above, is shown in Fig. 4.4.

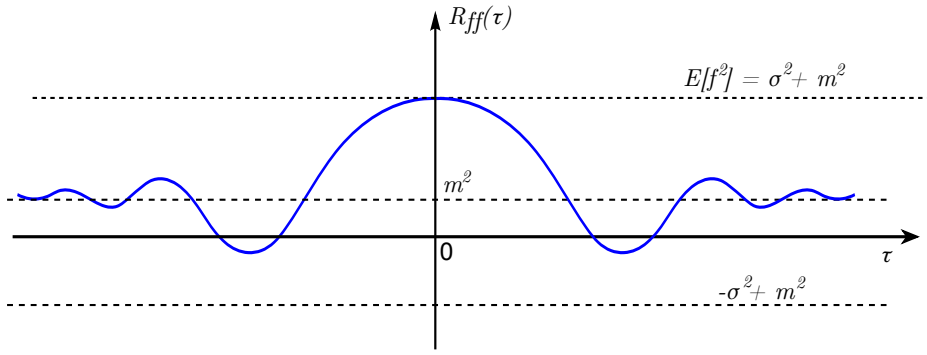

Figure 4.4: Autocorrelation function of a homogeneous stochastic field and its properties.

4.2.5 Ergodicity

To determine the *ensemble average* of a homogeneous stochastic field $f(x)$, a sufficiently large number of realizations of the field is necessary. However, researchers usually generate a sample function and calculate an estimator of the mean field value, i.e. the spatial average of the specific sample function (realization) as:

$$\langle f(x) \rangle_L = \frac{1}{L} \int_0^L f(x) dx \tag{4.16}$$

The determination of the probabilistic characteristics of a homogeneous stochastic field, from a single sample function is possible when the spatial average can be considered identical to the ensemble average. This can be done in the case of *ergodic* stochastic fields measured in a sufficiently long interval $(0, L)$.

4.2.6 Correlation structure

The *correlation structure* of a stochastic field is determined (in the Cartesian space) from the mathematical expression of the autocorrelation function R_{ff}. In many types of 2D-dimensional problems and based on the existing experimental data, it can be assumed that the variation of the test parameters (e.g. Young modulus, construction defect) in the x dimension is completely independent of the variation in the y dimension. Therefore, for the stochastic field $f(x, y)$ to be used in this thesis, a fully separable correlation structure can be adopted (Vanmarcke, 1983). Under this assumption, the autocorrelation function of the homogeneous stochastic field has the

following expression:

$$R_{ff}(\tau_x, \tau_y) = \sigma^2 \rho_x(\tau_x)\rho_y(\tau_y)$$
$$\tau_x = x_2 - x_1$$
$$\tau_y = y_2 - y_1$$

where, ρ_x, ρ_y are the correlation functions over the axes x, y, respectively, and σ is the standard deviation of the field. In this case, R_{ff} is defined only for positive values of τ_x and τ_y, and fully characterizes the correlation structure of the field (quadrant symmetry). Apart from the fully separable correlation structure, which is the most common in practical applications, there are other types of structures described in detail in Vanmarcke (1983).

4.2.7 Correlation length

An important parameter associated with the amplitude of the fluctuation of a stochastic field is the *correlation length*. This quantity determines the degree of correlation between the values $f(x_1)$ and $f(x_2)$ of the stochastic field in two different positions and constitutes a measure of the number of the uncorrelated random variables needed for the field description with a satisfactory quality.

In several technical problems, where homogeneous stochastic fields are used, the correlation length is usually defined as follows:

$$b = \int_0^\infty |\rho(\tau)| d\tau \tag{4.17}$$

where, $\rho(\tau)$ is the normalized (divided by the standard deviation) autocorrelation function of the stochastic field. For example, if:

$$\rho(\tau) = e^{-\alpha|\tau|}, \quad \alpha > 0$$

the correlation length is given by:

$$b = \int_0^\infty e^{-\alpha|\tau|} d\tau = \frac{1}{\alpha}$$

When the correlation length tends to infinity ($b \to \infty$), the field is considered as fully correlated. In this case, all the random variables are linearly dependent between them and thus the stochastic field degenerates to a random variable. If the correlation length tends to zero ($b \to 0$), the field tends to the ideal white noise and it is completely uncorrelated.

4.2.8 Power spectral density function

The Fourier analysis is fundamental in the application of stochastic fields since all of the properties of a stochastic field can be formulated in a simple and more elegant

manner in the space of frequencies. In particular, the Fourier transform of the autocorrelation function $R_{ff}(\tau)$ of a homogeneous stochastic field leads to the *power spectral density function* (SDF) of this field, i.e.:

$$S_{ff}(\omega) = \frac{1}{2\pi} \int_{-\infty}^{\infty} R_{ff}(\tau) e^{-i\omega\tau} d\tau \tag{4.18}$$

As expected, the inverse Fourier transform gives the autocorrelation function:

$$R_{ff}(\tau) = \int_{-\infty}^{\infty} S_{ff}(\omega) e^{i\omega\tau} d\omega \tag{4.19}$$

Eqs. (4.18)-(4.19) are the pair of Wiener-Khintchine transform pair.

The most important property of the SDF follows from Eq. (4.19) for $\tau = 0$, i.e.:

$$R_{ff}(0) = E[f^2(x)] = \int_{-\infty}^{\infty} S_{ff}(\omega) d\omega \tag{4.20}$$

This means that the mean square of the homogeneous field $f(x)$ is equal to the area

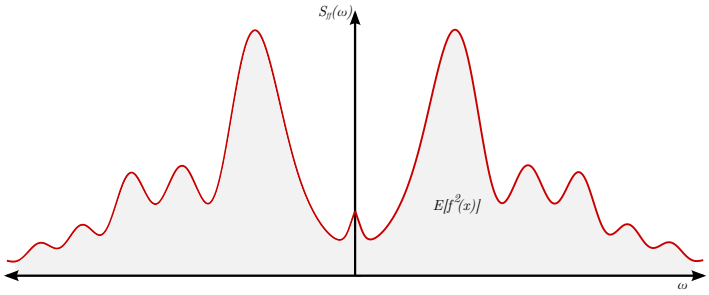

Figure 4.5: Power spectral density function: the area under the curve is equal to $E[f^2(x)]$.

enclosed by the graph of $S_{ff}(\omega)$ and the frequency axis ω, as depicted in Fig. 4.5. An even more interesting property obtained for zero-mean homogeneous stochastic fields is that their mean square value coincides with their variance, since $\sigma^2 = E[f^2(x)] - m^2$ and Eq. (4.20) becomes:

$$R_{ff}(0) = E[f^2(x)] = \sigma^2 = \int_{-\infty}^{\infty} S_{ff}(\omega) d\omega \tag{4.21}$$

Eq. (4.21) helps in understanding the physical meaning of the SDF, i.e. the values of this function correspond to the contribution of each frequency ω (or each wave number κ) in the total fluctuation of the stochastic field. S_{ff} is also called *power spectrum*, and is a real function and symmetric with respect to the vertical axis (see Fig. 4.5), thus, it is often characterized as *two-sided function*.

4.3 Representation of stochastic processes and fields

The first step in the analysis of uncertain systems (in the framework of SFEM) is the representation of the input of the system. This input usually consists of the mechanical and geometric properties as well as of the loading of the system (left and right hand side of the equilibrium equation, respectively). Characteristic examples are the Young modulus, Poisson ratio, yield stress, cross section geometry of physical systems, material and geometric imperfections of shells, earthquake loading, wind loads, waves etc. A convenient way for describing these uncertain quantities in time and/or space is the implementation of stochastic processes and fields, the probability distribution and correlation structure of which can be defined through experimental measurements. However, in most cases, due to the lack of relevant experimental data, assumptions are made regarding these probabilistic characteristics. Two main categories of stochastic processes and fields can be defined based on their probability distribution: (i) *Gaussian* and (ii) *non-Gaussian*.

In the next sections, a brief review of the techniques for the simulation of Gaussian stochastic fields, used for the purposes of this thesis, are presented. For the sake of simplicity, the presentation is made for one-dimensional stochastic fields (variable in space). The same expressions hold for stochastic processes but with time t as the independent variable.

4.4 Simulation methods for Gaussian stochastic processes and fields

Despite the fact that most of the uncertain quantities appearing in engineering systems are non-Gaussian in nature (e.g. material, geometric properties, wind, seismic loads), the Gaussian assumption is often used due to its simplicity and the lack of relevant experimental data. From the wide variety of methods developed for the simulation of Gaussian stochastic processes and fields, two are most often used in applications: (a) the spectral representation method (Shinozuka and Deodatis, 1991, 1996) and (b) the Karhunen-Loève (K-L) expansion (Ghanem and Spanos, 2003). A unified approach for generating Gaussian random field simulation methods (including spectral representation and K-L expansion) has been proposed by Poirion and Puig (2005).

Spectral representation algorithms are nowadays available covering various kinds of Gaussian stochastic fields (multi-dimensional, multi-variate, non-homogeneous) and the computational cost for the generation of homogeneous Gaussian sample functions can be drastically reduced by using the fast Fourier transform technique (FFT). Spectral representation has been successfully implemented in the framework of Monte Carlo Simulation (MCS) for the solution of realistic problems with the stochastic finite element approach.

The spectral representation method serves as the starting point to simulate the non-Gaussian random fields (see Section 4.5.1) used in the numerical examples of the thesis (see Section 6.1).

4.4.1 The spectral representation method

The spectral representation method is one of the most widely used methods for the simulation of Gaussian stochastic fields. Shinozuka and Jan (1972) applied the spectral representation method in simulation of multidimensional, vector and non-homogeneous fields, based on theoretical background of the method for one-dimensional scalar stochastic fields.

In the general case, the spectral representation method expands the stochastic field $f(x)$ as a sum of trigonometric functions with random phase angles and amplitudes. The version having only random phase angles is adopted in most applications because it leads to sample functions that are ergodic in the mean value and autocorrelation (Grigoriu, 1993). If $f(x)$ is a zero-mean one-dimensional uni-variate (1D-1V) homogeneous stochastic field with real values and two-sided SDF $S_{ff}(\omega)$, the spectral representation of the field is initially given by the following fundamental relation (Shinozuka and Deodatis, 1991):

$$f(x) = \int_0^\infty [cos(\omega x)du(\omega) + sin(\omega x)dv(\omega)] \tag{4.22}$$

where, $u(\omega)$ and $v(\omega)$ are two real zero-mean independent Gaussian fields, with orthogonal steps $du(\omega)$ and $dv(\omega)$, respectively, for which:

$$E[du^2(\omega)] = E[dv^2(\omega)] = 2S_{ff}(\omega)d(\omega) \tag{4.23}$$

The stochastic integral of Eq. (4.22) is defined as the limit in the mean square sense of the following sequence:

$$f(x) = \lim_{\max(\Delta\omega_k)\to 0} \sum_k [cos(\omega_k x)U_k + sin(\omega_k x)V_k] \tag{4.24}$$

where $U_k = u(\omega_{k+1}) - u(\omega_k), V_k = v(\omega_{k+1}) - v(\omega_k)$. Since the fields $u(\omega)$ and $v(\omega)$ have orthogonal steps, it can be shown that the sequences $\{U_k\}$ and $\{V_k\}$ are statistically independent with mean value equal to zero and variance equal to:

$$\sigma_k^2 = 2\int_{\omega_k}^{\omega_{k+1}} S_{ff}(\omega)d(\omega) \approx 2S_{ff}(\omega_k)\Delta\omega_k \tag{4.25}$$

For small values of $\Delta\omega_k$ the following approximation can be used:

$$f_{\text{appr}}(x) = \sum_{k=0}^{\infty} [cos(\omega_k x)U_k + sin(\omega_k x)V_k] \tag{4.26}$$

with the mean square error given by:

$$\begin{aligned} err &= E[(f(x) - f_{\text{appr}}(x))^2] \\ &= 2\sum_{k=0}^{\infty} \int_{\omega_k}^{\omega_{k+1}} \left[(cos\omega x - cos\omega_k x)^2 + (sin\omega x - sin\omega_k x)^2\right] S_{ff}(\omega) d\omega \end{aligned} \tag{4.27}$$

The error tends to 0 when the SDF has the special form of:

$$S_{ff}(\omega) = \sum_{k=0}^{\infty} S_{ff}(\omega_k)\delta(\omega - \omega_k) \tag{4.28}$$

where δ is the Dirac function. In applications, the field approximation given by Eq. (4.26) is used, for a finite number of terms:

$$f_{\text{appr}}(x) = \sum_{k=0}^{N-1} [cos(\omega_k x)U_k + sin(\omega_k x)V_k] \tag{4.29}$$

where N is an integer selected such that all the frequencies corresponding to non-negligible spectral power to contribute to the simulation of the field. Eq. (4.29) can be re-written also in the form of:

$$f_{\text{appr}}(x) = \sum_{k=0}^{N-1} A_k cos[(\omega_k x) + \Phi_k] \tag{4.30}$$

which gives the *spectral representation* of the stochastic field $f(x)$, with:

$$U_k = A_k cos\Phi_k \quad \text{and} \quad V_k = A_k sin\Phi_k$$

Eq. (4.30) leads to zero-mean homogeneous stochastic fields and the target second order moments of the fields are satisfactorily approximated if the error of Eq. (4.27) is not important. For a small number of terms N, the fields generated by Eq. (4.30) are quite different in the distribution and correlation structure (Spanos and Zeldin, 1998). The parameters involved in Eq. (4.30) are given in detail by (Shinozuka and Deodatis, 1991):

$$\begin{aligned} A_k &= \sqrt{2S_{ff}(\omega_k)\Delta\omega}, \quad k = \{0, 1, 2, \ldots, N-1\} \\ \omega_k &= k\Delta\omega, \quad k = \{0, 1, 2, \ldots, N-1\} \\ \Delta\omega &= \frac{\omega_u}{N} \end{aligned} \tag{4.31}$$

and,

$$\text{with } A_0 = 0 \text{ or } S_{ff}(\kappa_0 = 0) = 0 \tag{4.32}$$

where the parameter ω_u is a cut-off frequency defining the *active region* of the SDF

$S_{ff}(\kappa)$ of the stochastic field, i.e. beyond ω_u the SDF may be considered equal to zero because of the negligible values it takes. Usually for determining ω_u the following equation is used:

$$\int_0^{\omega_u} S_{ff}(\omega)d\omega = (1 - tol) \int_0^{\omega_u} S_{ff}(\omega)d\omega \tag{4.33}$$

where, tol is a small value, e.g. 0.0001. However, the simplest way of determining the cut-off frequency is the graphical way by a rough estimation of it on the S_{ff} plot. Since ω_u is constant, the frequency step $\Delta\omega \to 0$ when $N \to \infty$. Also, for a given number of terms N, the step $\Delta\omega$ is constant, see Eq. (4.31). $\Phi_0, \Phi_1, \ldots, \Phi_{N-1}$ in Eq. (4.30) are independent random phase angles uniformly distributed in the range $[0, 2\pi]$:

$$p_{\Phi_k}(\phi) = \begin{cases} \frac{1}{2\pi}, & \text{in } [0, 2\pi] \\ 0, & \text{otherwise} \end{cases} \tag{4.34}$$

Each sample function $f^{(i)}_{\text{appr}}(x)$ of the simulation can be obtained by substituting the random phase angles $\Phi_0, \Phi_1, \ldots, \Phi_{N-1}$ with the corresponding random values in the sample (i), $\phi^{(i)}_0, \phi^{(i)}_1, \ldots, \phi^{(i)}_{N-1}$ as these are produced by a random number generator:

$$f^{(i)}_{\text{appr}}(x) = \sum_{k=0}^{N-1} A_k cos[(\omega_k x) + \phi^{(i)}_k] \tag{4.35}$$

f_{appr} has the following properties (Shinozuka and Deodatis, 1991):

(i) It is asymptotically a Gaussian stochastic field as $N \to \infty$ due to the central limit theorem.

(ii) Its mean value and autocorrelation function are identical to the corresponding targets as $N \to \infty$, i.e. $E[f_{\text{appr}}(x)] = E[f(x)] = 0$ (see Eq. (4.9)).

(iii) Under the condition of $A_0 = 0$ or $S_{ff}(\kappa_0 = 0) = 0$, it can be shown that $f^{(i)}(x)$ is a periodic function with period $T_0 = 2\pi/\Delta\kappa$.

In the general case, the spectral representation method expands the stochastic field $f(x)$ as a sum of trigonometric functions with random phase angles and amplitudes. The version having only random phase angles is adopted in most applications because it leads to sample functions, that are ergodic in the mean value and autocorrelation (Grigoriu, 1993). The amplitudes are then deterministic and depend only on the prescribed power spectrum of the stochastic field (see Eq. (4.31)).

4.5 Simulation methods for non-Gaussian stochastic processes and fields

The problem of simulating non-Gaussian stochastic processes and fields has received considerable attention recently in the field of stochastic mechanics. This is due to the fact that several quantities arising in practical engineering problems exhibit non-Gaussian probabilistic characteristics. Especially the mechanical and geometrical properties of construction materials and soil properties are physical quantities that take

only positive values (e.g. Young's modulus, cross-sectional dimensions, density). The use of Gaussian distribution for their simulation, probably leads to negative values of these quantities. This probability is usually very small for small variations but may increase significantly in the case of large fluctuations of these quantities. If negative values occur even for a small part of a structure, numerical instabilities in the analysis of the structure will occur (e.g. non-positive definite stiffness matrices) that usually lead to incorrect results. It is therefore necessary to develop reliable algorithms for the production of samples of non-Gaussian stochastic processes/fields.

Despite the problems outlined above, the Gaussian distribution is still widely used in practical applications mainly due to its simplicity. Gaussian processes are fully defined by the first and second order moments, they are symmetrical with respect to zero and the generation of sample functions is directly related to the application of the central limit theorem. In contrast, to fully characterize a non-Gaussian stochastic field, all the joint multi-dimensional density functions are needed, and thus a number of studies have been focused on producing a more realistic definition of a non-Gaussian sample function from a simple transformation of some underlying Gaussian field with known second-order statistics.

Simulation methods for non-Gaussian stochastic processes and fields can be grouped into two main categories. Those which seek to produce sample functions matching the prescribed power SDF and lower-order statistics (mean, variance, skewness and kurtosis) of a target stochastic field (Gurley et al., 1997) and those seeking to generate sample functions compatible to complete probabilistic information (Deodatis and Micaletti, 2001; Grigoriu, 1998; Yamazaki and Shinozuka, 1988). The first type of methods are suitable for the simulation of wind and wave loads, for which non-Gaussian sample functions generated according to prescribed lower-order moments will provide accurate results for the stochastic response. However, sample functions having only the prescribed lower moments are not sufficient for the successful solution of problems where the accurate characterization of the tails of the distributions is of importance. When dealing with such types of problems, the use of methods belonging to the second category is required. The methods belonging to the second category is qualitatively superior to those of the first, because they lead to sample functions having the same distribution function which is equivalent to an infinite number of moments.

A non-Gaussian stochastic process which is defined by the lower order moments is likely to lead to sample functions with significantly different distributions as there are infinite distribution functions that have the same lower order moments. In general, the problem of deciding appropriate simulation for a non-Gaussian process doesn't have a unique solution. In the following section of this thesis a brief review of translation approach belonging to the second category of methods (Grigoriu, 1998) is outlined. The description of the method is done in two dimensions as implemented for the purposes of this thesis and is based on the concept of a nonlinear memory-less transformation of Gaussian to non-Gaussian process (Grigoriu, 1984).

4.5.1 Correlation distortion methods - Translation fields

If $g(\boldsymbol{x})$ is a homogeneous zero-mean Gaussian field with unit variance and spectral density function (SDF) $S_{gg}(\boldsymbol{\kappa})$, or equivalently autocorrelation function $R_{gg}(\xi)$, a homogeneous non-Gaussian stochastic field $f(\boldsymbol{x})$ with power spectrum $S_{ff}^{T}(\boldsymbol{\kappa})$ can be defined as:

$$f(\boldsymbol{x}) = F^{-1} \cdot \Phi[g(\boldsymbol{x})] \tag{4.36}$$

where Φ is the standard Gaussian cumulative distribution function and F is the non-Gaussian marginal cumulative distribution function of $f(\boldsymbol{x})$. The transform $F^{-1} \cdot \Phi$ is a memory-less translation since the value of $f(\boldsymbol{x})$ at an arbitrary point $\boldsymbol{x} = (x, y)$ depends on the value of $g(\boldsymbol{x})$ at the same point only and the resulting non-Gaussian field is called a *translation field* (Grigoriu, 1998).

Translation fields can be used to represent various non-Gaussian phenomena and have a number of useful properties such as the analytical calculation of crossing rates and extreme value distributions, but they also have some limitations, the most important one from a practical point of view is that the choice of the marginal distribution of $f(\boldsymbol{x})$ imposes constraints to its correlation structure. In other words, F and $S_{ff}^{T}(\boldsymbol{\kappa})$, or $R_{ff}^{T}(\boldsymbol{\xi})$, have to satisfy a specific compatibility condition derived directly from the definition of the autocorrelation function of the translation field:

$$R_{ff}^{T}(\boldsymbol{\xi}) = \int_{-\infty}^{\infty}\int_{-\infty}^{\infty} F^{-1}[\Phi(g_1)]F^{-1}[\Phi(g_2)] \cdot \phi[g_1, g_2; R_{gg}(\boldsymbol{\xi})]dg_1dg_2 \tag{4.37}$$

where $g_1 = g(\boldsymbol{x})$, $g_2 = g(\boldsymbol{x} + \boldsymbol{\xi})$, $\phi[g_1, g_2; R_{gg}(\boldsymbol{\xi})]$ denotes the joint density of g_1, g_2 and $\boldsymbol{\xi}$ is the space lag. If F and $S_{ff}^{T}(\boldsymbol{\kappa})$ are proven to be incompatible through Eq. (4.37), i.e. if $R_{ff}^{T}(\xi)$ has certain values lying outside a range of admissible values and/or the solution $R_{gg}(\xi)$ is not positive definite and therefore not admissible as an autocorrelation function, there is no translation field with the prescribed characteristics. In this case, one has to resort to translation fields that match the target SDF approximately (Shields et al., 2011).

In the present thesis, Eq. (4.36) is used for the generation of non-Gaussian translation sample functions representing the uncertain material properties of the problem. Sample functions of the underlying homogeneous Gaussian field $g(\boldsymbol{x})$ are generated using the spectral representation method. This method is well suited in the context of Monte Carlo simulation (MCS) technique used for calculating the response variability of stochastic structural systems, e.g. Stefanou and Papadrakakis (2004).

For a two-dimensional stochastic field, the i-th sample function is given by (Shinozuka and Deodatis, 1996):

$$g^{(i)}(x, y) = \sqrt{2}\sum_{n_1=0}^{N_1-1}\sum_{n_2=0}^{N_2-1}[A_{n_1n_2}^{(1)}cos(\kappa_{1n_1}x + \kappa_{2n_2}y + \phi_{n_1n_2}^{(1)(i)}) + \\ + A_{n_1n_2}^{(2)}cos(\kappa_{1n_1}x - \kappa_{2n_2}y + \phi_{n_1n_2}^{(2)(i)})] \tag{4.38}$$

where $\phi_{n_1n_2}^{(j)(i)}$, $j = 1, 2$ represent the realization for the i-th simulation of the indepen-

dent random phase angles uniformly distributed in the range $[0, 2\pi]$ and $A^{(1)}_{n_1 n_2}$, $A^{(2)}_{n_1 n_2}$ have the following expressions:

$$A^{(1)}_{n_1 n_2} = \sqrt{2 S_{gg}(\kappa_{1n_1}, \kappa_{2n_2}) \Delta\kappa_1 \Delta\kappa_2} \tag{4.39a}$$

$$A^{(2)}_{n_1 n_2} = \sqrt{2 S_{gg}(\kappa_{1n_1}, -\kappa_{2n_2}) \Delta\kappa_1 \Delta\kappa_2} \tag{4.39b}$$

where,

$$\kappa_{1n_1} = n_1 \Delta\kappa_1, \quad \kappa_{2n_2} = n_2 \Delta\kappa_2 \tag{4.40}$$

$$\Delta\kappa_1 = \frac{\kappa_{1u}}{N_1}, \quad \Delta\kappa_2 = \frac{\kappa_{2u}}{N_2} \tag{4.41}$$

$$\text{and} \quad n_1 = \{0, 1, \ldots, N_1 - 1\}, \quad n_2 = \{0, 1, \ldots, N_2 - 1\}$$

$N_j, j = \{1, 2\}$, represent the number of intervals in which the wave number axes are subdivided and $\kappa_{ju}, j = 1, 2$, are the upper cut-off wave numbers which define the active region of the power spectrum $S_{gg}(\kappa_1, \kappa_2)$ of the stochastic field. The last means that S_{gg} is assumed to be zero outside the region defined by:

$$-\kappa_{1u} \leq \kappa_1 \leq \kappa_{1u} \text{ and } -\kappa_{2u} \leq \kappa_2 \leq \kappa_{2u} \tag{4.42}$$

Typical shapes of realizations of a lognormal translation field for weak, medium and strong isotropic correlation ($b = b_1 = b_2$), respectively, are shown in Fig. 4.6.

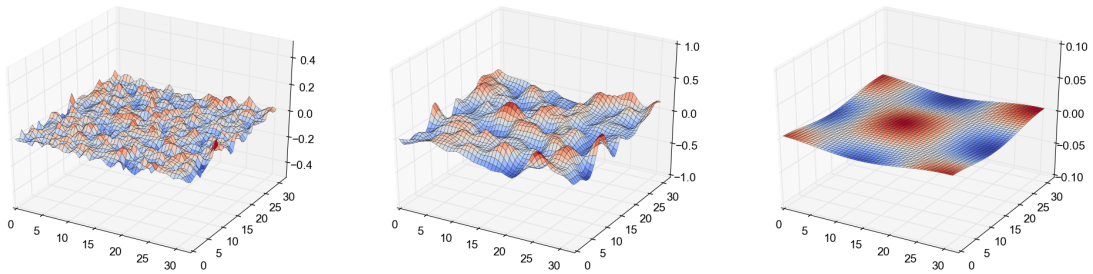

Figure 4.6: Realizations of a lognormal translation field for (a) weak, (b) medium and (c) strong correlation, respectively ($\sigma = 0.1$).

The SDF of the underlying Gaussian field used in the numerical examples (see Section 6.1) is of square exponential type (see Fig. 4.7):

$$S_{gg}(\kappa_1, \kappa_2) = \sigma_g^2 \frac{b_1 b_2}{4\pi} exp\Big[-\frac{1}{4}(b_1^2 \kappa_1^2 + b_2^2 \kappa_2^2) \Big] \tag{4.43}$$

where σ_g denotes the standard deviation of the stochastic field and b_1, b_2 denote the parameters that influence the shape of the spectrum, which are proportional to the correlation lengths of the stochastic field along the x, y axes, respectively. The squared exponential model is a realistic correlation model for softening materials (e.g. concrete) suggested by the Joint Committee on Structural Safety (Allaix and

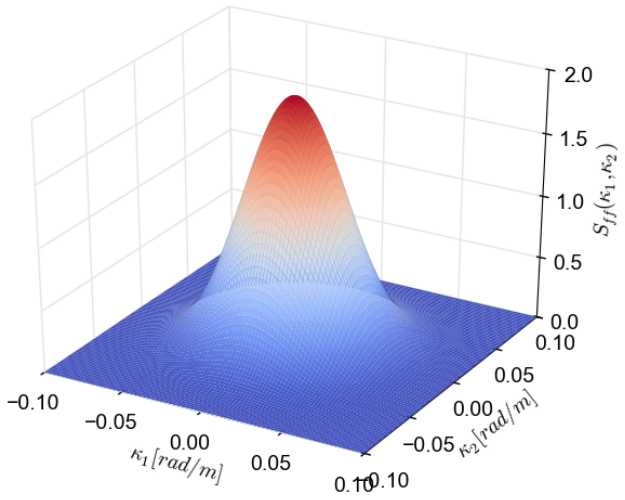

Figure 4.7: Spectral density function of square exponential type ($\sigma = 0.1$ and $b = b_1 = b_2 = 50$).

Carbone, 2009; JCSS, 2001) and also used for the same purpose in Vořechovský (2008); Yang and Xu (2008). In this case, the SDF of the translation field will be slightly different from S_{gg} due to the spectral distortion caused by the transform of Eq. (4.36) (Papadopoulos et al., 2009).

4.6 The stochastic finite element method (SFEM)

The most important issue in stochastic mechanics is the propagation of uncertainty through the system and the assessment of its stochastic response. Nowdays, this is mainly addressed in the framework of the stochastic finite element method (SFEM). SFEM is an extension of the classical deterministic approach for the solution of stochastic (static and dynamic) problems and has received considerable attention especially in the last two decades, due to the continuously rising computational power. SFEM involves finite elements whose properties are random and has been successfully applied in a wide variety of problems (e.g. solid, structural and fluid mechanics, acoustics, heat transfer).

The two main variants of SFEM as appearing in the literature are:

- the perturbation approach (Kleiber and Hien, 1993),
- the spectral stochastic finite element method (SSFEM) (Ghanem and Spanos, 2003)

The first approach is based on a Taylor series expansion of the response vector, while in the second, each response quantity is represented using a series of random Hermite polynomials. In these two SFEM variants, Monte Carlo simulation (MCS) can also be added (which is also used in the present thesis).

The SFEM comprises three basic steps:

(i) the formulation of the stochastic stiffness matrix (first at the element and then at the global-system level),

(ii) The discretization of the stochastic fields representing the uncertain system properties,

(iii) the response variability calculation (response statistics).
These steps along with their computational aspects are described in the following sections.

4.6.1 Formulation of the stochastic finite element matrix

The classical theory of finite elements based on the virtual work principle serves to to derive the stochastic stiffness matrix of the system by discretizing the continuous medium to a number of nodes and elements. With the use of the shape function matrix $\boldsymbol{N}$, the displacement field $\boldsymbol{u}$ inside each element is expressed in terms of the nodal displacements vector $\boldsymbol{d}$ as follows:

$$\boldsymbol{u} = \boldsymbol{N}\boldsymbol{d} \tag{4.44}$$

The displacement field is chosen so as to satisfy the compatibility of deformations at each element (kinematics compatibility). To ensure the equilibrium conditions, the principle of virtual work is used:

$$\delta W = W^{ext} - W^{int} = 0 \tag{4.45}$$

where, W^{ext} is the work of external loading, and W^{int} is the work of internal loading. The strain field $\boldsymbol{\epsilon}$ of an element is given by:

$$\boldsymbol{\epsilon} = \boldsymbol{B}\boldsymbol{d} \tag{4.46}$$

where, $\boldsymbol{B}$ is the deformation (strain-displacement) matrix (derivative of the shape function matrix). Neglecting the effect of thermal, the stress vector $\boldsymbol{\sigma}$ can be written as:

$$\boldsymbol{\sigma} = \mathbb{C}\boldsymbol{B}\boldsymbol{d} \tag{4.47}$$

where, $\mathbb{C}$ is the constitutive matrix.

When the material properties are involving randomness, they fluctuate spatially and their variation can be described in the general case, from a $nD - mV$ stochastic field. The constitutive tensor is then written as follows:

$$\mathbb{C} = \mathbb{C}_0[1 + f(\boldsymbol{x})] \tag{4.48}$$

where $f(\boldsymbol{x})$ is a zero-mean homogeneous stochastic field with autocorrelation function R_{ff}, and $\mathbb{C}_0$ is the mean value of $\mathbb{C}$.

By imposing into an element (e) a virtual displacement field $\widetilde{\boldsymbol{u}}^{(e)}$:

$$\widetilde{\boldsymbol{u}}^{(e)} = \boldsymbol{N}^{(e)}\widetilde{\boldsymbol{d}}^{(e)} \tag{4.49}$$

and introducing the external loading vector $\boldsymbol{f}^{ext}$, the principle of virtual work gives:

$$\widetilde{\boldsymbol{d}}^{(e)^T}\boldsymbol{f}^{ext} = \int\limits_{V^{(e)}} \widetilde{\boldsymbol{\epsilon}}^{(e)^T}\boldsymbol{\sigma}^{(e)}dV^{(e)} \tag{4.50}$$

and substituting Eqs. (4.46) - (4.48) into Eq. (4.50):

$$\widetilde{\boldsymbol{d}}^{(e)^T}\boldsymbol{f}^{ext} = \widetilde{\boldsymbol{d}}^{(e)^T}\left[\int_{V^{(e)}} \boldsymbol{B}^{(e)^T}\mathbb{C}^{(\boldsymbol{e})}\boldsymbol{B}^{(e)}dV^{(e)}\right]\boldsymbol{d}^{(e)} \tag{4.51}$$

$$= \widetilde{\boldsymbol{d}}^{(e)^T}\left[\int_{V^{(e)}} \boldsymbol{B}^{(e)^T}\mathbb{C}_{\mathbf{0}}^{(\boldsymbol{e})}\boldsymbol{B}^{(e)}dV^{(e)} + \int_{V^{(e)}} \boldsymbol{B}^{(e)^T}\mathbb{C}_{\mathbf{0}}^{(\boldsymbol{e})}\boldsymbol{B}^{(e)}f^{(e)}(\boldsymbol{x})dV^{(e)}\right]\boldsymbol{d}^{(e)}$$

Eq. (**??**) contains the stochastic stiffness matrix of an element (e) which can be written as:

$$\mathbb{k}^{(e)} = \underbrace{\int_{V^{(e)}} \boldsymbol{B}^{(e)}\mathbb{C}_0^{(e)}\boldsymbol{B}^{(e)}dV^{(e)}}_{\mathbb{k}_0^{(e)}} + \underbrace{\int_{V^{(e)}} \boldsymbol{B}^{(e)T}\mathbb{C}_0^{(e)}\boldsymbol{B}^{(e)}f^{(e)}(\boldsymbol{x})dV^{(e)}}_{\Delta\mathbb{k}^{(e)}} \tag{4.52}$$

where $\mathbb{k}_0^{(e)}$ and $\Delta\mathbb{k}^{(e)}$ are the deterministic and fluctuating parts of the stochastic finite element matrix, respectively, $B^{(e)}$ is the deterministic deformation (strain-displacement) matrix, $\mathbb{C}_0^{(e)}$ is the mean value of the constitutive matrix and $V^{(e)}$ is the volume of the finite element.

The global stochastic matrix of the system has a similar form and is formed by assembling all $\mathbb{k}^{(e)}$ as follows:

$$\mathbb{K} = \sum_{e=1}^{N_e}\mathbb{k}^{(e)} = \mathbb{K}_0 + \Delta\mathbb{K} \tag{4.53}$$

where N_e is the total number of finite elements. Finally, static analysis in the context of SFEM, results in the solution of the algebraic problem given below:

$$(\mathbb{K}_0 + \Delta\mathbb{K})\boldsymbol{u} = \boldsymbol{f}^{ext} \tag{4.54}$$

where $\boldsymbol{f}^{ext}$ and $\boldsymbol{u}$ are the loading and displacement vectors, respectively. In the case of large-scale systems, the solution of this problem is computationally demanding and thus constitutes the crucial point in the applicability and efficiency of the SFEM.

For the calculation of elemental stochastic stiffness matrix $\mathbb{k}^{(e)}$ the discretization of the stochastic field $f(\boldsymbol{x})$ is required, as it is clearly shown in Eq. (4.52).

4.6.2 Discretization of stochastic processes and fields

The second step of the SFEM is the discretization of the stochastic fields used to represent the uncertain mechanical and geometric system properties. The term *discretization* refers to the approximation of the continuous stochastic field $f(\boldsymbol{x})$ by a finite number of random variables f_i forming a random vector, i.e.:

$$f(\boldsymbol{x}) \Rightarrow \text{discretization} \Rightarrow \widetilde{f}(\boldsymbol{x}) = \{f_i\}, \quad i = \{1, 2, \ldots, n\} \tag{4.55}$$

The discretization methods can be split into two main categories:

- point discretization methods,
- average-type discretization methods

In the first category of methods, the final random variables are the values of the stochastic field at specific points of the system domain (element centroid, nodes, integration points), while in the second category of methods, the random variables are defined as (weighted) integrals of the stochastic field over each finite element. The main representatives of the first category are the midpoint (Der Kiureghian and Ke, 1988) (which is used in this study), nodal point, integration point (Brenner and Bucher, 1995) and interpolation methods (Liu et al., 1986), while the local average (Vanmarcke, 1983) and weighted integral methods (Deodatis, 1991) are the main representatives of the second group.

4.6.2.1 The midpoint method

The midpoint method is one of the most widespread discretization methods in stochastic finite element analysis (Der Kiureghian and Ke, 1988). The method consists in the approximation of the stochastic field in each finite element (e) from a random variable defined as the value of the field at the centroid of the element. The coordinates of the centroid x_e^* are given as a function of the coordinates of nodes x_j of the element (e) according to:

$$x_e^* = \frac{1}{q} \sum_{j=1}^{q} x_j^{(e)} \tag{4.56}$$

where q is the total number of nodes of the element. It has been proven that the method overestimates the variation of stochastic field within each element (Der Kiureghian and Ke, 1988).

4.6.2.2 Mesh size selection for discretization

In order to discretize the stochastic field, a suitable mesh is required. The meshes used for the discretization of the continuum and of the stochastic field should be selected based on different criteria. Specifically:

- The finite element grid is usually determined by geometry and expected changes in the stress field, e.g. in stress concentration areas, a mesh refinement is required.
- The mesh size for the discretization of the stochastic field is mainly determined by the correlation length which is directly related to its variability.

Therefore, it is possible and perhaps more effective to use two different meshes in practical applications. However, the use of a single mesh is very convenient. The ideal case is one in which the mesh size chosen for the correct description of the geometry of the structure and the changes of stress field can also describe adequately the variability of stochastic field.

Concerning the size of the stochastic mesh, Der Kiureghian and Ke (1988) proposed the value $L_{RF} \approx b/4 \div b/2$, where b is the correlation length parameter and L_{RF} is the typical element size in the random field mesh. This result has been obtained by repeatedly evaluating the reliability index of a beam with stochastic rigidity using

meshes with decreasing element size. This range of L_{RF} was also confirmed by Li and Der Kiureghian (1993) and Zeldin and Spanos (1998) who arrived to this conclusion by comparing the power spectra of the random fields before and after discretization.

Since the correlation length is a constant, discretization mesh of the stochastic field can have a "regular" form, i.e. subdivide the domain into equal length segments, squares or cubes depending on the dimension of the problem. Several researchers construct the discretization mesh of the stochastic field with a simple composition of two or more finite elements (Liu and Kiureghian, 1991). This leads to a drastic reduction in the number of random variables of the problem and any discretization version $\widetilde{f}(\boldsymbol{x})$ of the field can easily be represented in the existing finite element mesh.

4.6.3 Response variability calculation

In the third and last step of the SFEM, Monte Carlo simulation is used, as the simplest method for computing the response variability in the framework of SFEM. In the framework of MCS (Gentle, 2003; Rubinstein and Kroese, 2007), the deterministic problem is solved a (large) number of times and the response variability is calculated using simple relationships of statistics. Due to its robustness and simplicity, MCS is often used in the literature as a reference method in order to check the accuracy of other approaches and is sometimes combined with the two aforementioned SFEM variants (Ghanem and Pellissetti, 2002) (cf. Section 4.6).

4.6.3.1 Direct Monte Carlo simulation (MCS)

In this method, N_{sim} samples of the stochastic system matrix are generated using a random number generator and the final equilibrium Eq. (4.54) is solved N_{sim} times, leading to a population (sample) of the response vector. Based on this population, the response variability of the system is calculated using simple relationships of statistics. For example, if u_i is the displacement at the i-th d.o.f., then the unbiased estimates of the mean value and variance of the sample are:

$$E(u_i) = \frac{1}{N_{sim}} \sum_{n=1}^{N_{sim}} u_i(n) \tag{4.57}$$

$$\sigma^2(u_i) = \frac{1}{N_{sim}-1} \Big[\sum_{n=1}^{N_{sim}} u_i^2(n) - N_{sim} \cdot E^2(u_i) \Big] \tag{4.58}$$

It is obvious that the accuracy of the estimation depends on the number of samples and, in particular, the estimate of standard deviation σ is inversely proportional to $\sqrt{N_{sim}}$. A small number of samples e.g. $N_{sim} \approx 50$ permits only a rough approximation of the mean value and variance of the response, while with a larger sample size e.g. $N_{sim} \approx 500$, it is possible to estimate the CDF of the response (Schuëller, 2006). The solution of N_{sim} deterministic problems has a significant computational cost especially in the combined case of large-scale systems and of considerable stochastic dimension. It is therefore desirable to combine MCS with discretization methods that do not involve a large number of random variables such as the midpoint or the local average method, which lead to only one random variable per finite element. However,

the development of robust and efficient solution algorithms in conjunction with the increasing availability of powerful computers and the suitability of the method to parallel processing with ideal efficiency, alleviate this limitation to a large extent. Thus, direct MCS is today a powerful (and perhaps the only universal) tool for treating complex SFEM applications.

4.6.3.2 Variability response function approach

The response variability of stochastic systems can alternatively be computed using the concept of variability response function (VRF), introduced by Shinozuka (1987). VRFs have been established for an efficient evaluation of the variance and sensitivity of the response of stochastic systems where properties are modeled by random fields, in contrast to computationally expensive Monte Carlo simulations. It has been applied in a variety of structural systems including trusses, frames, plane stress/plane strain systems, plates and shells with a single or with multiple correlated random properties.

The VRF for the structural system can be calculated by *fast MC* simulation (Shinozuka, 1987), considering the covariance of the response displacement at a point of interest in a statically determinate structure with randomly fluctuating material properties modeled using random fields. To this end, it is possible to express the vector of displacement variances as a function of the VRF of the system:

$$Var(\boldsymbol{u}) = \int_{-\infty}^{\infty} \mathbf{VRF}(\boldsymbol{\kappa}) S_{ff}(\boldsymbol{\kappa}) d\boldsymbol{\kappa} \tag{4.59}$$

The numerical estimation of the VRF through a fast MCS procedure based on Eq. (4.59) (see below), is very important as the closed-form analytic expressions existing in the literature involve modulating functions that are very difficult to establish even in the simplest cases of statically indeterminate linear beams (Papadopoulos et al., 2006) or statically determinate beams with nonlinear (power) constitutive laws (Teferra and Deodatis, 2012), as well as for plane stress/strain systems (Arwade and Deodatis, 2011; Wall and Deodatis, 1994). In these studies, it is shown that the VRF is a function of the deterministic parameters describing the geometry, material properties and loading of the structure. VRFs are useful mainly for two reasons: (i) they provide insight into the mechanisms controlling the response of stochastic systems and, (ii) they allow the establishment of spectral-distribution-free upper bounds on the response variability, i.e.:

$$Var(\boldsymbol{u}) = \int_{-\infty}^{\infty} \mathbf{VRF}(\boldsymbol{\kappa}) S_{ff}(\boldsymbol{\kappa}) d\boldsymbol{\kappa} \leq \mathbf{VRF}(\hat{\boldsymbol{\kappa}}) \int_{-\infty}^{\infty} S_{ff}(\boldsymbol{\kappa}) d\boldsymbol{\kappa} = \mathbf{VRF}(\hat{\boldsymbol{\kappa}}) \sigma_f^2 \tag{4.60}$$

where $\hat{\boldsymbol{\kappa}}$ is the wave number at which the VRF takes its maximum value. This upper bound is physically realizable and corresponds to the case in which the random field $f(x, y)$ becomes a random sinusoid:

$$f(x, y) = \sqrt{2}\sigma_f cos(\hat{\kappa}_1 x + \hat{\kappa}_2 y + \phi) \tag{4.61}$$

where ϕ is a random phase angle uniformly distributed between 0 and 2π and σ_f is the standard deviation of the random sinusoid. It is worth noting that (Papadopoulos et al., 2005, 2006) established exact expressions for the upper bound of the displacement variability of statically determinate and indeterminate beams using VRFs based on the inverse of the elastic modulus.

In addition to providing a means for computing spectral-distribution-free upper bounds on the response variability, the VRF can qualitatively reveal which types of spectral density function will cause significant response variances (see Eq. 4.59). That is, VRFs provide insight into the importance of the shape of the spectral density functions of the random properties on the response variance. The proof of VRF existence in the nonlinear problems considered in this thesis is not straightforward and requires the application of a generalized VRF methodology described by Teferra and Deodatis (2012).

The basic steps of the fast MCS approach used in the numerical example of this study, are described in the following:

- Generate N realizations of a random sinusoid with standard deviation σ_f and wave number $\hat{\boldsymbol{\kappa}} = (\hat{\kappa_1}, \hat{\kappa_2})$ that describes the elastic modulus:

$$f_j(x, y) = \sqrt{2}\sigma_f cos(\hat{\kappa}_1 x + \hat{\kappa}_2 y + \phi_j), \quad j = \{1, 2, ..., N\} \tag{4.62}$$

  Rather than picking up the ϕ_j's randomly in $[0, 2\pi]$, they can be selected at N equal intervals in this range for significant computational savings.
- Compute N sample responses using the N realizations of $f(x, y)$.
- Compute the variance of the response from the N sample responses.
- Determine **VRF**$(\hat{\boldsymbol{\kappa}})$ from:

$$\textbf{VRF}(\hat{\boldsymbol{\kappa}}) = \frac{Var(\boldsymbol{u})}{\sigma_f^2} \tag{4.63}$$

- Repeat the previous four steps for different values of $\hat{\boldsymbol{\kappa}}$ until the VRF is estimated over a sufficient range of wave numbers.

The fast MCS procedure described above can be implemented into the framework of a deterministic FE code making this approach very general. In addition, this approach is usually very efficient as convergence is achieved with N as low as 10–20 for each wave number.

5

Optimization in Structural Design

One of the most fundamental principles in our world is the search for an *optimal state*. The scientific field of optimization has been the focus of much attention in recent years primarily because of the rapid progress in computer technology, including the development and availability of user-friendly software and high-speed processors with parallel computing capabilities. Engineers, analysts, and managers are often faced with the challenge of making tradeoffs between different factors in order to achieve desirable outcomes. Optimization is the process of choosing these tradeoffs in the *optimum* way. Many engineering problems can be defined as optimization problems, e.g. the process of design, finding optimal thickness of steel in pressure vessels, designing a bridge by minimizing weight or maximizing strength, selecting a flight plan for an aircraft to minimize time or fuel use, or designing of water resources systems for maximum benefit.

Hence, optimization is viewed as a decision problem that involves finding the best values of the decision variables over all possibilities. The power of optimization methods to determine the best case without actually testing all possible cases comes through the use of a modest level of mathematics and at the cost of performing iterative numerical calculations using clearly defined logical procedures or algorithms implemented on computing machines. That's why, these families of computational methods, which are sometimes collectively termed *soft computing* are among the top ten computational methods of the 20th century[1].

Components of optimization problem

Design vector

Any engineering system or component is defined by a set of parameters some of which are viewed as variables during the design process. In general, certain quantities are usually fixed at the outset and these are called pre-assigned parameters. All the other quantities are treated as variables in the design process and are called design or decision variables $x_i,\ i = 1, 2, \ldots, n$. The design variables are collectively represented as a design vector $\boldsymbol{X} = (x_1, x_2, \ldots, x_n)^T$.

[1] IACM Expressions Vol.19: http://www.cimne.com/iacm/News/Expressions.htm.

Objective Function (fitness)

The conventional design procedures aim at finding a feasible design that merely satisfies the functional and other requirements of the problem. In general, there will be more than one feasible design, and the purpose of optimization is to choose the best one of the many feasible designs available. Thus a criterion has to be chosen for comparing the different alternative feasible designs and for selecting the best one. The criterion with respect to which the design is optimized, when expressed as a function of the design variables, is known as the criterion or merit or objective function. The choice of objective function is governed by the nature of problem. The objective function for minimization is generally taken as weight in aircraft and aerospace structural design problems. In civil engineering structural designs, the objective is usually taken as the minimization of cost. The maximization of mechanical efficiency is the obvious choice of an objective in mechanical engineering systems.

Design constraints

Any optimization problem can be classified as *constrained* or *unconstrained*, depending on whether or not constraints exist in the problem. A problem that does not entail any equality or inequality constraints is said to be an unconstrained optimization problem. In many practical problems, the design cannot be chosen arbitrarily; rather, it has to satisfy certain specified functional and other requirements. The restrictions that must be satisfied to produce an acceptable design are collectively called *design constraints*. Moreover, the designs satisfying all design constraints are called *feasible designs*.

5.1 Structural optimization

Structural Optimization represents the scientific field where optimization techniques are used in order to achieve design goals in structural engineering field with a highly accurate modeling of reality. Its topics include structural design (e.g., pressure vessel design, welded beam design), shape optimization, topological optimization (e.g., airfoil), product designs and others. In structural optimization, design objectives are structural criteria used to evaluate the merit of a design such as minimum construction cost, minimum life-cycle cost, minimum weight, and maximum stiffness. Building code provisions, which provide safety and service ability requirements to the structure, usually appear as the design constraints.

There are three major structural optimization problems namely: (i) Sizing, (ii) Shape and (iii) Topology Optimization, respectively. Initially structural optimization was focused on sizing optimization, such as optimizing cross sectional areas of truss and frame structures, or the thickness of plates and shells. Later on, the problem of finding optimum boundaries of a structure and optimize its shape was considered. In the former case the structural domain is fixed, while in the latter case it is not fixed but it has a predefined topology. In both cases a non-optimal starting topology can lead to sub-optimal results. To overcome this deficiency structural topology optimization needs to be employed, which allows the designer to optimize the layout or the topology of a structure by detecting and removing the low-stressed material in the structure which is not used effectively.

In this study only shape optimization problems will be considered, where the shape problem is defined on a domain which is unknown *a priori*. Thus, the optimum shape of the domain is obtained so as to improve structural properties under consideration of specified constraints. Fig. 5.1, shows a typical example of a multi-step shape optimization of L-shaped bracket design problem[2] with the initial (Fig. 5.1a), as well as the optimum shape (Fig. 5.1b) of it.

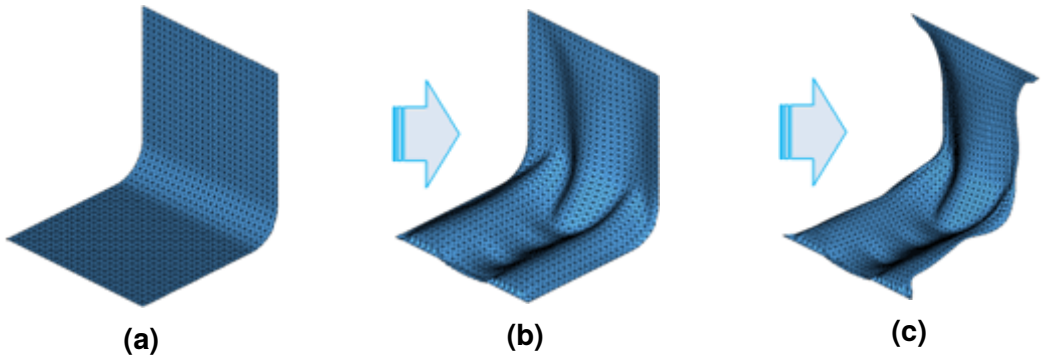

Figure 5.1: Multi-step shape optimization of L-shaped bracket design problem: (a) Initial shape, (b) Optimal surface (by out-of-plane variation), (c) Optimal boundary (by in-plane variation).

5.1.1 Problem definition

Structural optimization problems are characterized by objective and constraint functions that are generally non-linear functions of the design variables. These functions are usually implicit, discontinuous and non-convex. In general there are three classes of structural optimization problems: sizing, shape and topology or layout problems. Structural optimization was focused at the beginning on sizing optimization, such as optimizing cross sectional areas of truss and frame structures, or the thickness of plates and shells and subsequently later the problem of finding optimum boundaries of a structure and optimizing its shape was also considered. In the former case the structural domain is fixed, while in the latter case it is not fixed but it has a predefined topology.

The mathematical formulation of structural optimization problems can be expressed in standard mathematical terms as a non-linear programming problem, which in general form can be stated as follows:

$$\begin{aligned} \text{opt:} \quad & F(\boldsymbol{s}) \\ \text{subject to:} \quad & g_j(\boldsymbol{s}) \leq 0, \quad j = 1, ..., k \\ & s_i^{low} \leq s_i \leq s_i^{up}, \quad i = 1, ..., n \end{aligned} \tag{5.1}$$

where $\boldsymbol{s}$ is the vector of design variables, $F(\boldsymbol{s})$ is the objective function to be optimized (minimized or maximized), $g_j(\boldsymbol{s})$ are the behavioral constraint functions, s_i^{low} and s_i^{up} are the lower and upper bounds of the i^{th} design variable. Due to fabrication limitations the design variables are not always continuous but discrete since cross-sections

[2]Toyota Technology Institute, Solid Mechanics Laboratory (http://www.toyota-ti.ac.jp/english/research/labolatories/mech/post-24.html)

or dimensions belong to a certain design set. A discrete structural optimization problem can be formulated in the form of Eq. (5.1) where $s_i \in \Re_d,\ i = 1, 2, \ldots, n$ and $\Re_d^n$ is a given set of discrete values representing for example the available structural member cross-sections or dimensions and design variables $\boldsymbol{s}$ can take values only from this set.

5.1.2 Shape optimization

In structural shape optimization problems the aim is to improve the performance of the structural component by modifying its boundaries (Bletzinger and Ramm, 2001; Chen and Tortorelli, 1997; Haftka and Grandhi, 1986; Sienz and Hinton, 1997). All functions are related to the design variables, which are some of the coordinates of the key points in the boundary of the structure. The shape optimization methodology proceeds with the following steps:

(i) At the outset of the optimization, the geometry of the structure under investigation has to be defined. The boundaries of the structure are modeled using cubic B-splines that are defined by a set of key points. Some of the coordinates of these key points will be the design variables.

(ii) An automatic mesh generator is used to create a finite element model. A finite element analysis is carried out and the displacements and stresses are calculated.

(iii) The optimization problem is solved; the design variables are improved and the new shape of the structure is defined. If the convergence criteria for the optimization algorithm are satisfied, then the optimum solution has been found and the process is terminated, else a new geometry is defined and the whole process is repeated from step (ii).

5.1.3 Shape optimization considering cracks

In the case of the presence of cracks in structural components, when dealing with shape optimization problems, due to the limitations and inflexible nature of the analytical methods in handling arbitrary complex geometries and crack propagations, the XFEM (see Chapter 3) can be considered as a capable numerical method for the accurate solution of the problem of evolving discontinuities and moving boundaries. In this framework, Duysinx et al. (2006) proposed a method for an intermediate approach between parametric shape optimization and topology optimization which takes benefit of the fixed mesh work using XFEM and of the curves smoothness of the level set description. Lately, Edke and Chang (2010) presented a shape sensitivity analysis method for calculating gradients of crack growth rate and crack growth direction for 2D structural components under mixed-mode loading, by overcoming the issues of calculating accurate derivatives of both crack growth rate and direction. This research was further extended (Edke and Chang, 2011) in a novel crack propagation analysis technique into a shape optimization framework to support design of 2D structural components again under mixed-mode fracture for maximizing the service life and minimizing their weight. Furthermore, Li et al. (2012) proposed elegant XFEM schemes for LSM structural optimization, for improving the computational accuracy and efficiency of XFEM, while Su et al. (2013) considered a reanalysis algorithm based on incremental Cholesky factorization which is further used into an optimization al-

gorithm to predict the angle of crack initiation from a hole in a plate with inclusion. An extension also of this coupling (XFEM and LSM) from structural mechanics to electromagnetics, developed in a shape optimization framework, particularly tailored for 2D electric structures have been also proposed by Topa et al. (2012).

5.1.4 XFEM shape optimization considering uncertainties

In this thesis, two problem formulations are proposed for coupling XFEM in an optimization framework: a deterministic and a probabilistic one (Georgioudakis et al., 2014a,b). According to the deterministic formulation, the goal is to minimize the volume of structural components subject to constraints related to the minimum service life allowed and material volume expressed by optimized geometry. The minimum service life is calculated using fatigue cycles as described in Section 3.1.8.

5.1.4.1 Deterministic formulation (DET)

The design problem for the deterministic formulation (DET) is defined as:

$$\begin{aligned} \text{min:} \quad & V(\boldsymbol{s}) \\ \text{subject to:} \quad & N(\boldsymbol{s}) \geq N_{min} \\ & s_i^{low} \leq s_i \leq s_i^{up}, \quad i = 1, 2, \ldots, n \end{aligned} \tag{5.2}$$

V is the volume of the structural components, s_i are the shape design variables with lower and upper limits s_i^{low} and s_i^{up}, respectively, and N is the service life in number of fatigue cycles with the lower limit of N_{min}.

5.1.4.2 Probabilistic formulation (PROB)

In extension, the design problem of the probabilistic formulation (PROB) is defined as:

$$\begin{aligned} \text{min:} \quad & V(\boldsymbol{s}) \\ \text{subject to:} \quad & \bar{N}(\boldsymbol{s}, \boldsymbol{x}) \geq N_{min} \\ & s_i^{low} \leq s_i \leq s_i^{up}, \quad i = 1, 2, \ldots, n \\ & x_j \sim N(\mu_x, \sigma_x^2) \quad j = 1, 2, \ldots, nr \end{aligned} \tag{5.3}$$

where $\boldsymbol{s}$ and $\boldsymbol{x}$ are the vectors of the design and random variables, respectively, $\bar{N}$ is the mean number of fatigue cycles.

The probabilistic quantity x_j of Eq. (5.3) is calculated by means of the Latin hypercube sampling (LHS) method (see Appendix A). LHS was introduced by McKay et al. (2000) in an effort to reduce the required computational cost of purely random sampling methodologies. This sampling method can generate a variable number of samples well distributed over the entire range of interest. A Latin hypercube sample is constructed by dividing the range of each of the nr uncertain variables into M non-overlapping segments of equal marginal probability. Thus, the whole parameter space, consisting of M parameters, is partitioned into M^{nr} cells. A single value is selected randomly from each interval, producing M sample values for each input variable. The

values are randomly matched to create M sets from the M^{nr} space with respect to the density of each interval for the M simulations.

5.2 Classification of optimization algorithms

5.2.1 Local vs global optima

The optimization algorithms can be classified into two main categories, the *local* and *global* ones. In *local optimization* the algorithm attempts to find an optimized design (see Fig. 5.2), and there is no guarantee that the global minimum for the problem will be found. There are some cases (convex problems like linear programming problems) where the local minimum found will in fact be the global minimum. However, for the most situations, "the best answer" when using a local optimization algorithm is not guaranteed.

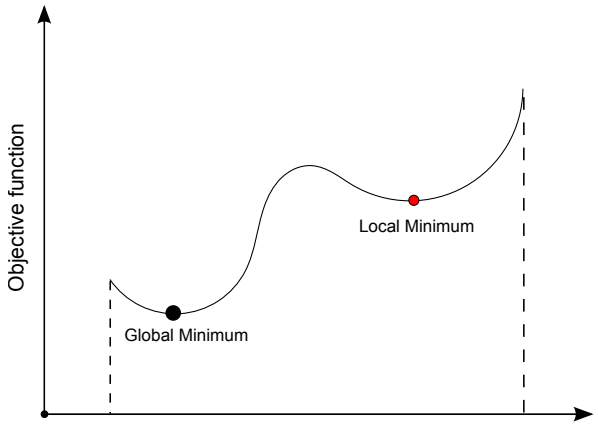

Figure 5.2: Local vs Global minimum.

In contrast, *global optimization* algorithms try to find the absolutely best set of parameters to optimize the objective function. In general, there can be solutions that are optimal locally, but not globally optimal. Consequently, global optimization problems are typically quite difficult to solve exactly. However, in structural optimization field, global optimization algorithms are mainly used, since many times the design space is extensive and in order to search the global design space, a global optimization method is mandatory and highly nonconvex.

5.2.2 Global optimization algorithms

During the last three decades many numerical methods have been developed to meet the demands of engineering optimization problems. These methods can be classified in two main classes, the *deterministic* and the *probabilistic* ones. In Fig. 5.3 a rough taxonomy of global optimization methods according to method of operation, is provided. Deterministic algorithms are most often used if a clear relation between the characteristics of the possible solutions and their utility for a given problem exists. Then, the search space can efficiently be explored using for example a divide and conquer scheme. Mathematical programming methods are the most popular methods of the first category and in particular the gradient-based optimizers. These methods

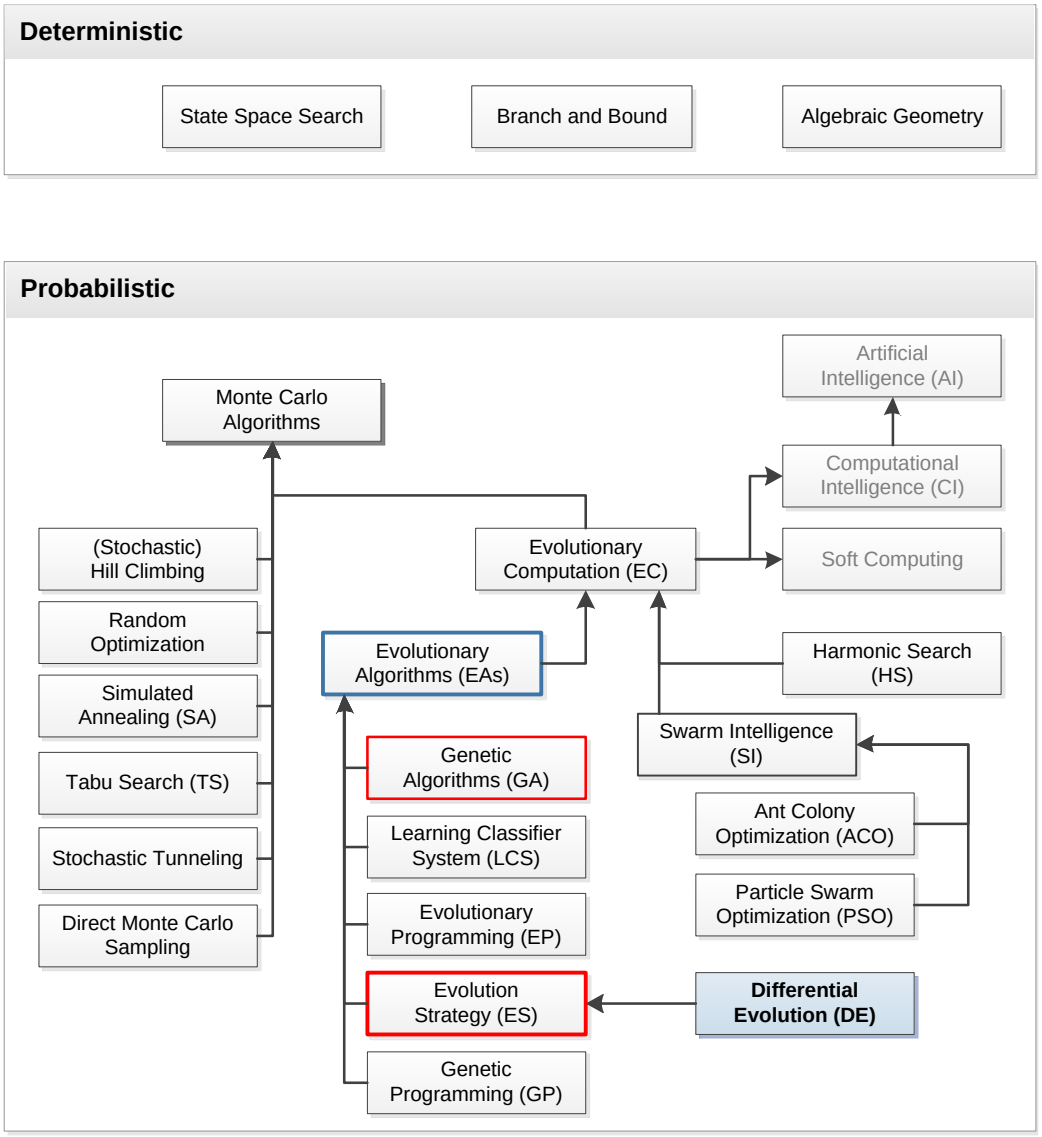

Figure 5.3: The taxonomy of global optimization algorithms.

make use of local curvature information, derived from linearization of the objective and constraint functions by using their derivatives with respect to the design variables at points obtained in the process of optimization, to construct an approximate model of the initial problem. If the relation between a solution candidate and its "fitness" are not so obvious or too complicated, or the dimensionality of the search space is very high, it becomes harder to solve a problem deterministically and would possible result in exhaustive enumeration of the search space, which is not feasible even for relatively small problems. Then, probabilistic algorithms come into play.

An especially relevant family of probabilistic algorithms are the Monte Carlo-based approaches. They trade in guaranteed correctness of the solution for a shorter run-time. The most widely used class of probabilistic category of methods are *heuristic* and *metaheuristic* algorithms, which are nature-inspired or bio-inspired as they have been developed based on the successful evolutionary behavior of natural systems by

learning from nature. Modern metaheuristic algorithms for engineering optimization include genetic algorithms (GA) (Holland, 1973), simulated annealing (SA), particle swarm optimization (PSO), ant colony algorithm (ACO), artificial bee colony algorithm (ABC) (Haddad et al., 2006), harmony search (HS), cuckoo search algorithm (CS) (Yang, 2010), firefly algorithm (FA), bat algorithm (BA), krill herd and many others. Evolutionary algorithms (EA) are the most widely used class of metaheuristic algorithms and in particular evolutionary programming (EP) (Fogel, 1992), genetic algorithms (Holland, 1973), evolution strategies (ES) and genetic programming (GP).

Gradient-based optimizers capture very fast the right path to the nearest optimum, irrespective if it is a local or a global optimum but it cannot assure that the global optimum can be found. On the other hand metaheuristics, due to their random search, are being considered more robust in terms of global convergence; they may suffer, however, from a slow rate of convergence towards the global optimum. When metaheuristics are adopted to perform the optimization, the solution of the finite element equations is of paramount importance since more than 95% of the total computing time is spent for the solution of the finite element equilibrium equations. A second characteristic is that in place of a single design point metaheuristics work simultaneously with a population of design points in the space of design variables. This allows for a natural implementation of the evolution procedure in parallel computer environments.

In single-objective optimization problems the optimal solution is usually clearly defined since it is the minimum or maximum value of the objective function. This does not hold in real world problems where multiple and conflicting objectives frequently exist. Instead of a single optimal solution, there is usually a set of alternative solutions, generally denoted as the set of Pareto optimal solutions. These solutions are optimal in the wider sense since no other solution in the search space is superior to them when all objectives are considered. In the absence of preference information, none of the corresponding trade-offs can be said to be better than the others. On the other hand, the search space can be too large and too complex, which is the usual case of real world problems, hence the implementation of gradient based optimizers for this type of problems becomes even more cumbersome.

Thus, efficient optimization strategies are required able to deal with the presence of multiple objectives and the complexity of the search space. Metaheuristics and in particular EA have several characteristics that are desirable for this kind of problems and most frequently outperform the deterministic optimizers such as gradient based optimization algorithms.

5.3 Evolutionary computation (EC)

In computer science, evolutionary computation (EC) is a subfield of artificial intelligence that involves continuous optimization and combinatorial optimization problems of computational systems drawing their inspiration from the process of natural evolution. Its algorithms can be considered global optimization methods with a metaheuristic or stochastic optimization character and are mostly applied for black box problems. EC uses iterative progress (trial-and-error), such as growth or development in a population. This population is then selected in a guided random search using par-

allel processing to achieve the desired end. As evolution can produce highly optimised processes and networks, it has many applications in computer science.

5.3.1 Brief history

The idea of applying Darwinian principles to automated problem solving dates back to the 1940s, long before the breakthrough of computers. During the 1960s three different implementations of the basic idea were developed in different places. In the USA, Fogel et al. (1966) introduced *evolutionary programming* (EP), while Holland (1973) called his method a *genetic algorithm* (GA). Meanwhile, in Germany, Rechenberg (1973) and Schwefel (1995) invented *evolution strategies* (ES).

For about 15 years these areas developed separately, but since the early 1990s they have been viewed as different representatives ("dialects") of one technology that has come to be known as *evolutionary computing* (Bäck, 1996; Bäck et al., 2000a,b; Eiben and Smith, 2003). In the early 1990s a fourth stream following the general ideas emerged, *genetic programming* (GP), championed by Koza (1992, 1994). The contemporary terminology denotes the whole field by EC, the algorithms involved are termed evolutionary algorithms (EA), and it considers EP, ES, GA and GP as subareas belonging to the corresponding algorithm variants (cf. Fig. 5.3).

5.3.2 Genetic algorithms (GA)

GA method is probably the best-known evolutionary algorithm, receiving substantial attention. The first attempt to use evolutionary algorithms took place in the 60's by a team of biologists (Barricelli, 1963) and was focused in developing a computer software that would simulate the evolution process of the nature. However, the model implemented in GA refers to that introduced and studied by Holland (1973). In the basic genetic algorithm each population member is a binary or real valued string, which is sometimes referred to as *genotype* or *chromosome*. The three main steps of basic GA are:

Initialization
: In this step a generation of the initial population members $\{X_1, X_2, ..., X_{NP}\}$ is generated, where NP is the population size, and each member of the population is evaluated by computing the corresponding objective and constraint functions.

Selection
: Selection operator is applied to the current population in order to create an intermediate one. In the first generation the initial population is considered as the intermediate one, while in the next generations this population is created by the application of the selection operator.

Crossover/Mutation
: In order to create the next generation crossover and mutation operators are applied to the intermediate population. Crossover operator forms new chromosomes by combining parts of each of the two parental chromosomes (p_c is the crossover probability). Mutation is a reproduction operator that forms one new chromosome by making (usually small, with mutation probability p_m) alterations to the values of the genes in a copy of a single parent chromosome and

serves to recover lost alleles. The purpose of mutation operator is to maintain diversity within the population and inhibit premature convergence.

The process of moving from the current population to the next population constitutes one generation in the evolution process of a GA model. If the termination criterion is satisfied the procedure stops otherwise returns to the selection step. The flowchart of the GA method is presented in Fig. 5.4.

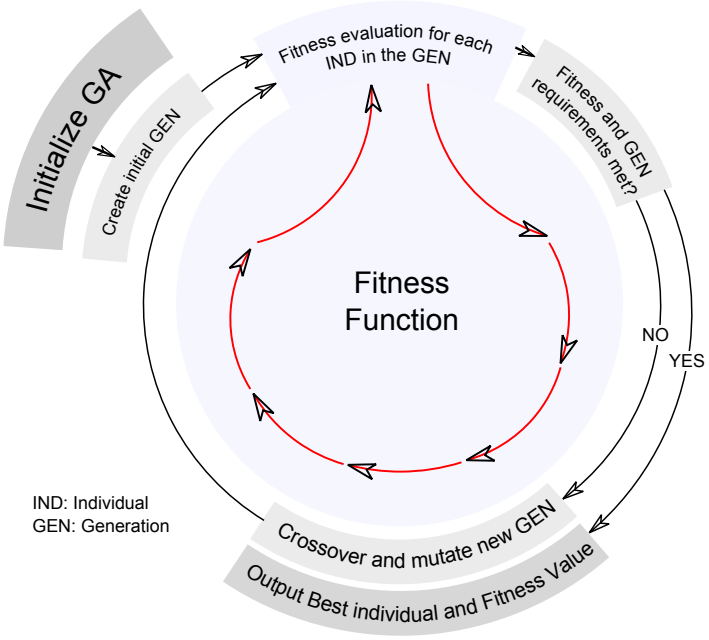

Figure 5.4: Flowchart for a genetic algorithm (GA).

5.4 Evolutionary algorithms (EAs)

Nature has been solving problems over millions or even billions of years. Only the best and robust solutions remain based on the principle of the survival of the fittest. Similarly, heuristic algorithms use the trial-and-error, learning and adaptation to solve problems. Modern metaheuristic algorithms are almost guaranteed to an efficient performance for a wide range of combinatorial optimization problems. The main aim of research in optimization and algorithm development is to design and/or choose the most suitable and efficient algorithms for a given optimization problem.

In the following sections metaheuristics based on the evolution process called *Evolutionary Algorithms* (EAs) and used in the framework of this thesis are presented. More specifically, four metaheuristic search optimization algorithms are tested and appear to be very promising as they have been implemented in various challenging structural optimization problems with success. A short description of these algorithms is presented, giving greater emphasis in the algorithm used for the numerical examples (see Section 6.2), i.e. the differential evolution algorithm.

5.4.1 Evolution strategies (ES)

Evolutionary strategies are population-based probabilistic direct search optimization algorithm gleaned from principles of Darwinian evolution. Starting with an initial population of μ candidate designs, an offspring population of λ designs is created from the parents using variation operators. Depending on the manner in which the variation and selection operators are designed and the spaces in which they act, different classes of ES have been proposed. In ES algorithm employed in this study (Rechenberg, 1973; Schwefel, 1995), each member of the population is equipped with a set of parameters:

$$\begin{aligned} \boldsymbol{a} &= [(\boldsymbol{s}_d, \boldsymbol{\gamma}), (\boldsymbol{s}_c, \boldsymbol{\sigma}, \boldsymbol{\alpha})] \in (I_d, I_c) \\ I_d &= D^{n_d} \times R_+^{n_\gamma} \\ I_c &= D^{n_c} \times R_+^{n_\sigma} \times [-\pi, \pi]^{n_\alpha} \end{aligned} \tag{5.4}$$

where $\boldsymbol{s}_d$ and $\boldsymbol{s}_c$, are the vectors of discrete and continuous design variables defined in the discrete and continuous design sets D^{n_d} and R^{n_c}, respectively. Vectors $\boldsymbol{\gamma}, \boldsymbol{\sigma}$ and $\boldsymbol{\alpha}$, are the distribution parameter vectors taking values in $R_+^{n_\gamma}$, $R_+^{n_\sigma}$ and $[-\pi, \pi]^{n_\alpha}$, respectively. Vector $\boldsymbol{\gamma}$ corresponds to the variances of the Poisson distribution. Vector $\boldsymbol{\sigma} \in R_+^{n_\sigma}$ corresponds to the standard deviations $(1 \leqslant n_\sigma \leqslant n_c)$ of the normal distribution. Vector $\boldsymbol{\alpha} \in [-\pi, \pi]^{n_\alpha}$ is related to the inclination angles $(n_\alpha = (n_c - n_\sigma/2)(n_\sigma - 1))$ defining linearly correlated mutations of the continuous design variables $\boldsymbol{s}_d$, where $n = n_d + n_c$ is the total number of design variables.

Let $P(t) = \{a_1, ..., a_\mu\}$ denotes a population of individuals at the t^{th} generation. The genetic operators used in the ES method are denoted by the following mappings:

$$\begin{aligned} rec &: (I_d, I_c)^\mu \longrightarrow (I_d, I_c)^\lambda \quad (recombination) \\ mut &: (I_d, I_c)^\lambda \longrightarrow (I_d, I_c)^\lambda \quad (mutation) \\ sel_\mu^k &: (I_d, I_c)^k \longrightarrow (I_d, I_c)^\mu \quad (selection, k \in \{\lambda, \mu + \lambda\}) \end{aligned} \tag{5.5}$$

A single iteration of the ES, which is a step from the population P_p^t to the next parent population P_p^{t+1} is modelled by the mapping:

$$opt_{EA} : (I_d, I_c)_t^\mu \longrightarrow (I_d, I_c)_{t+1}^\mu \tag{5.6}$$

A general pseudo code of the ES algorithm is given in Algorithm 2.

5.4.2 Covariance matrix adaptation (CMA)

The covariance matrix adaptation, proposed by Hansen and Ostermeier (2001) is a completely de-randomized self-adaptation scheme. First, the covariance matrix of the mutation distribution is changed in order to increase the probability of producing the selected mutation step again. Second, the rate of change is adjusted according to the number of strategy parameters to be adapted. Third, under random selection the expectation of the covariance matrix is stationary. Further, the adaptation mechanism is inherently independent of the given coordinate system. The transition from generation g to $g + 1$, given in the following steps, completely defines the Algorithm 3).

Algorithm 2 ES algorithm

$t = 0$
initialize$(P(t = 0))$
evaluate$(P(t = 0))$
repeat:
    $P_p(t) =$ selectBest$(\mu, P(t))$
    $P_c(t) =$ reproduce$(\lambda, P_p(t))$
    mutate$(P_c(t))$
    evaluate$(P_c(t))$
    if *UsePlusStrategy* **then**
        $P(t+1) = P_c(t) \cup P_p(t)$
    else
        $P(t+1) = P_c(t)$
    end if
    $t = t + 1$
until *isNotTerminated()*

Algorithm 3 CMA algorithm

initialize $\lambda, \mu, w_{i=1,\dots,\mu}, \mu_{\text{eff}}, c_\sigma, d_\sigma, c_c, \mu_{cov}, c_{cov}$
initialize $\mathbb{C}(t) \in \mathbb{I}^n, \vec{m}(t) = ones(n \times 1), \vec{p}(t) = zeros(n \times 1)$
repeat:
    $\vec{x}_i(t) \sim N(\vec{m}(t), \sigma^2(t)\mathbb{C}(t))$ for $i = 1, \dots, \lambda$
    $\vec{m}(t+1) = \sum_{i=1}^{\mu} w_i \vec{x}_i(t)$
    $\vec{p}_c(t) = (1 - c_c)\vec{p}_c(t-1) + \sqrt{c_c(2 - c_c)\mu_{\text{eff}}}\big(\frac{\vec{m}(t+1) - \vec{m}(t)}{\sigma(t)}\big)$
    $\mathbb{C}(t+1) = (1 - c_{cov})\mathbb{C}(t) + c_{cov}(1 - \frac{1}{\mu_{cov}}) \sum_{i=1}^{\mu} w_i \text{OP}\big(\frac{\vec{x}_i(t) - \vec{m}(t)}{\sigma(t)}\big) + \frac{c_{cov}}{\mu_{cov}} \text{OP}(\vec{p}_c(t))$
    $\vec{p}_\sigma(t) = (1 - c_\sigma)\vec{p}_\sigma(t-1) + \sqrt{c_\sigma(2 - c_\sigma)\mu_{\text{eff}}}\mathbb{C}(t)^{-\frac{1}{2}} \frac{\vec{m}(t+1) - \vec{m}(t)}{\sigma(t)}$
    $\sigma(t+1) = \sigma(t) exp\big(\frac{c_\sigma}{d_\sigma}\big(\frac{\|\vec{p}_\sigma(t)\|}{\mathbb{E}(\|N(0,\mathbb{I})\|)} - 1\big)\big)$
until stopping criterion is met

Generation of offsprings. Creation of λ new offsprings as follows:

$$s_k^{g+1} \sim N(\vec{m}^{(g)}, \sigma^{(g)^2}\mathbb{C}^{()}) \sim \vec{m}^{(g)} + \sigma^{(g)} N(\vec{0}, \mathbb{C}^{(g)}) \tag{5.7}$$

where $s_k^{g+1} \in \Re^n$ is the design vector of the k^{th} offspring in generation $g + 1, (k = 1, ..., \lambda)$, $N(\vec{m}^{(g)}, \mathbb{C}^{()})$ are normally distributed random numbers where $\vec{m}^{(g)} \in \Re^n$ is the mean value vector and $\mathbb{C}^{(g)}$ is the covariance matrix while $\sigma^{(g)} \in \Re_+$ is the global step size. To define a generation step, the new mean value vector $\vec{m}^{(g+1)}$, global step size $\sigma^{(g+1)}$, and covariance matrix $\mathbb{C}^{(g+1)}$ have to be defined.

New mean value vector. After selection scheme (μ, λ) operates over the λ offsprings, the new mean value vector $\vec{m}^{(g+1)}$ is calculated according to the following expression:

$$\vec{m}^{(g+1)} = \sum_{i=1}^{\mu} w_i \vec{s}_{i:\lambda}^{(g+1)} \tag{5.8}$$

where $\vec{s}_{i:\lambda}^{(g+1)}$ is the i^{th} best offspring and w_i are the weight coefficients.

Global step size. The new global step size is calculated according to the following expression:

$$\sigma^{(g+1)} = \sigma^{(g)} exp\left(\frac{c_\sigma}{d_\sigma}\left(\frac{\|\vec{p}_\sigma^{(g+1)}\|}{E\|N(,\mathbb{I})\|} - 1\right)\right) \tag{5.9}$$

while the matrix $\mathbb{C}^{(g)^{-\frac{1}{2}}}$ is given by:

$$\mathbb{C}^{(g)^{-\frac{1}{2}}} = \mathbb{B}^{(g)}\mathbb{D}^{(g)^{-1}}\mathbb{B}^{(g)^T} \tag{5.10}$$

where the columns of $\mathbb{B}^{(g)}$ are an orthogonal basis of the eigenvectors of $\mathbb{C}^{(g)}$ and the diagonal elements of $\mathbb{D}^{(g)}$ are the square roots of the corresponding positive eigenvalues.

Covariance matrix update. The new covariance matrix $\mathbb{C}^{(g+1)}$ is calculated from the following equation:

$$\begin{aligned}\mathbb{C}^{(g+1)} = (1 - c_{\text{cov}})\mathbb{C}^{(g)} + \frac{c_{\text{cov}}}{\mu_{\text{cov}}}\vec{p}_c^{(g+1)}\vec{p}_c^{(g+1)^T} \\ + c_{\text{cov}}\left(1 - \frac{1}{\mu_{\text{cov}}}\right)\sum_{i=1}^{\mu} w_i OP\left(\frac{s_{i:\lambda}^{(g+1)} - \vec{m}^{(g)}}{\sigma^{(g)}}\right)\end{aligned} \tag{5.11}$$

OP denotes the outer product of a vector with itself and $\vec{p}_c^{(g)} \in \Re^n$ is the evolution path ($\vec{p}_c^{(0)} = 0$).

5.4.3 Elitist covariance matrix adaptation (ECMA)

Elitist CMA evolution strategies algorithm is a combination of the well-known $(1+\lambda)$-selection scheme of evolution strategies (Rechenberg, 1973), with covariance matrix adaptation (Igel et al., 2007). The original update rule of the covariance matrix is applied to the $(1+\lambda)$-selection while the cumulative step size adaptation (path length control) of the CMA$(\mu/\mu, \lambda)$ is replaced by a success rule based step size control. Every individual a of the ECMA algorithm is comprised of five components:

$$a = \{s, \overline{p}_{succ}, \sigma, \vec{p}_c, \mathbb{C}\} \tag{5.12}$$

where s is the design vector, $\overline{p}_{succ}$ is a parameter that controls the success rate during the evolution process, σ is the step size, $\vec{p}_c$ is the evolution path and $\mathbb{C}$ is the covariance matrix. Contrary to CMA, each individual has its own step size σ, evolution path $\vec{p}_c$ and covariance matrix $\mathbb{C}$. A pseudo code of the ECMA algorithm is shown in Algorithm 4. In line #1 a new parent $a_{parent}^{(g)}$ is generated. In lines #4-6, λ new offsprings are

Algorithm 4 $(1+\lambda)$-ECMA

1: $\vec{g} = \vec{0}$, initialize $a^{(g)}_{\text{parent}}$
2: **repeat**
3: $\quad a^{(g+1)}_{\text{parent}} \leftarrow a^{(g+1)}_{\text{parent}}$
4: $\quad$ **for** $k = 1, ..., \lambda$ **do**
5: $\quad\quad s^{(g+1)}_{k} \sim N(\vec{s}^{(g)}_{\text{parent}}, \sigma^{(g)^2}\mathbb{C}^{()})$
6: $\quad$ **end for**
7: $\quad$ *UpdateStepSize*$\left(a^{(g+1)}_{\text{parent}}, \frac{\lambda^{(g+1)}_{succ}}{\lambda}\right)$
8: $\quad$ **if** $f(s^{(g+1)}_{1:\lambda}) < f(s^{(g)}_{\text{parent}})$ **then**
9: $\quad\quad \vec{x}^{(g+1)}_{\text{parent}} \leftarrow \vec{x}^{(g+1)}_{1:\lambda}$
10: $\quad\quad$ *UpdateCovariance*$\left(a^{(g+1)}_{\text{parent}}, \frac{s^{(g+1)}_{\text{parent}} - s^{(g)}_{\text{parent}}}{\sigma^{(g)}_{\text{parent}}}\right)$
11: $\quad$ **end if**
12: **until** stopping criterion is met

generated from the parent vector $a^{(g)}_{parent}$. The new offsprings are sampled according to Eq. (8), with variable $\vec{m}^{(g)}$ being replaced by the design vector $s^{(g)}_{parent}$ of the parent individual. After the λ new offsprings are sampled, the parent's step size is updated by means of $UpdateStepSize$ subroutine (see Procedure 5). The arguments of the subroutine are the parent $a^{(g)}_{parent}$ and the success rate $\lambda^{(g+1)}_{succ}/\lambda$, where $\lambda^{(g+1)}_{succ}$ is the number of offsprings having better fitness function than the parent. The step size update is based upon the $1/5$ success rule, thus when the ratio $\lambda^{(g+1)}_{succ}/\lambda$ is larger than $1/5$ step size increases, otherwise step size decreases. If the best offspring has a better fitness value than the parent, it becomes the parent of the next generation (see lines $\#8-9$), and the covariance matrix of the new parent is updated by means of $UpdateCovariance$ subroutine (see Procedure 6). The arguments of the subroutine are the current parent and the step change:

$$\frac{s^{(g+1)}_{parent} - s^{(g)}_{parent}}{\sigma^{(g)}_{parent}} \tag{5.13}$$

The update of the evolution path and the covariance matrix depends on the success rate:

$$\overline{p}_{succ} = \frac{\lambda_{succ}}{\lambda} \tag{5.14}$$

If the success rate is below a given threshold value p_{thresh} then the step size is taken into account and the evolution path and the covariance matrix is updated (see lines #2-3 of Procedure 6). If the success rate is above the given threshold p_{thresh} the step change is not taken into account and evolution path and covariance matrix happens are updated (see lines #5-6).

Procedure 5 *UpdateSizeState*$(a = \{s, \overline{p}_{succ}, \sigma, \vec{p}_c, \mathbb{C}\}, p_{succ})$

1: $\overline{p}_{succ} \leftarrow (1 - c_p)\overline{p}_{succ} + c_p p_{succ}$

2: $\sigma \leftarrow \sigma exp\left(\frac{1}{d}\left(\overline{p}_{succ} - \frac{p_{succ}^{target}}{1 - p_{succ}^{target}}(1 - \overline{p}_{succ})\right)\right)$

Procedure 6 *UpdateCovariance*$(a = \{s, \overline{p}_{succ}, \sigma, \vec{p}_c, \mathbb{C}\}, s_{step} \in \Re^n)$

1: **if** $\overline{p}_{succ} < p_{thresh}$ **then**

2: $\quad \vec{p}_c \leftarrow (1 - c_c)\vec{p}_c + \sqrt{c_c(2 - c_c)}\vec{x}_{step}$

3: $\quad \mathbb{C} \leftarrow (1 - c_{\text{cov}})\mathbb{C} + c_{\text{cov}}\vec{p}_c\vec{p}_c^T$

4: **else**

5: $\quad \vec{p}_c \leftarrow (1 - c_c)\vec{p}_c$

6: $\quad \mathbb{C} \leftarrow (1 - c_{\text{cov}})\mathbb{C} + c_{\text{cov}}(\vec{p}_c\vec{p}_c^T + c_c(2 - c_c)\mathbb{C})$

7: **end if**

5.5 Differential evolution (DE)

DE is a population-based stochastic method for global optimization over continuous spaces introduced by (Storn and Price, 1995, 1997). DE shares many features of the classical GA and applies a kind of differential mutation operator on parent *chromosomes* to generate the *offspring*. Since its inception, DE is arguably one of the most powerful stochastic real-parameter optimization algorithms in current use and has drawn the attention of many researchers all over the world, resulting in a lot of variants of the basic algorithm, with improved performance. In the next sections a conceptual of classical DE is outlined, followed by several significant variants of the algorithm in greater details.

5.5.1 DE: a first glance

DE works through a simple cycle of stages, presented in Fig. 5.5. As with all evolutionary algorithms, it operates using a set or population $\{X_1, X_2, ..., X_{NP}\}$ of potential solutions or points to explore the solution space. The size of the population, given by the value NP, remains constant throughout. At each generation the algorithm aims to create a new population by replacing points in the current population with better points. In essence, the population is simply a set of points X_i^G, where i is the index of the member in the population and G indicates the generation or iteration to which the population belongs. Each X_i^G consists of n components, where n is the dimension of the problem. Through a repeated process of reproduction (mutation and crossover) and selection, the population is guided toward the global minimum. In the next sections, a detailed look at the different processes involved in the DE algorithm is given.

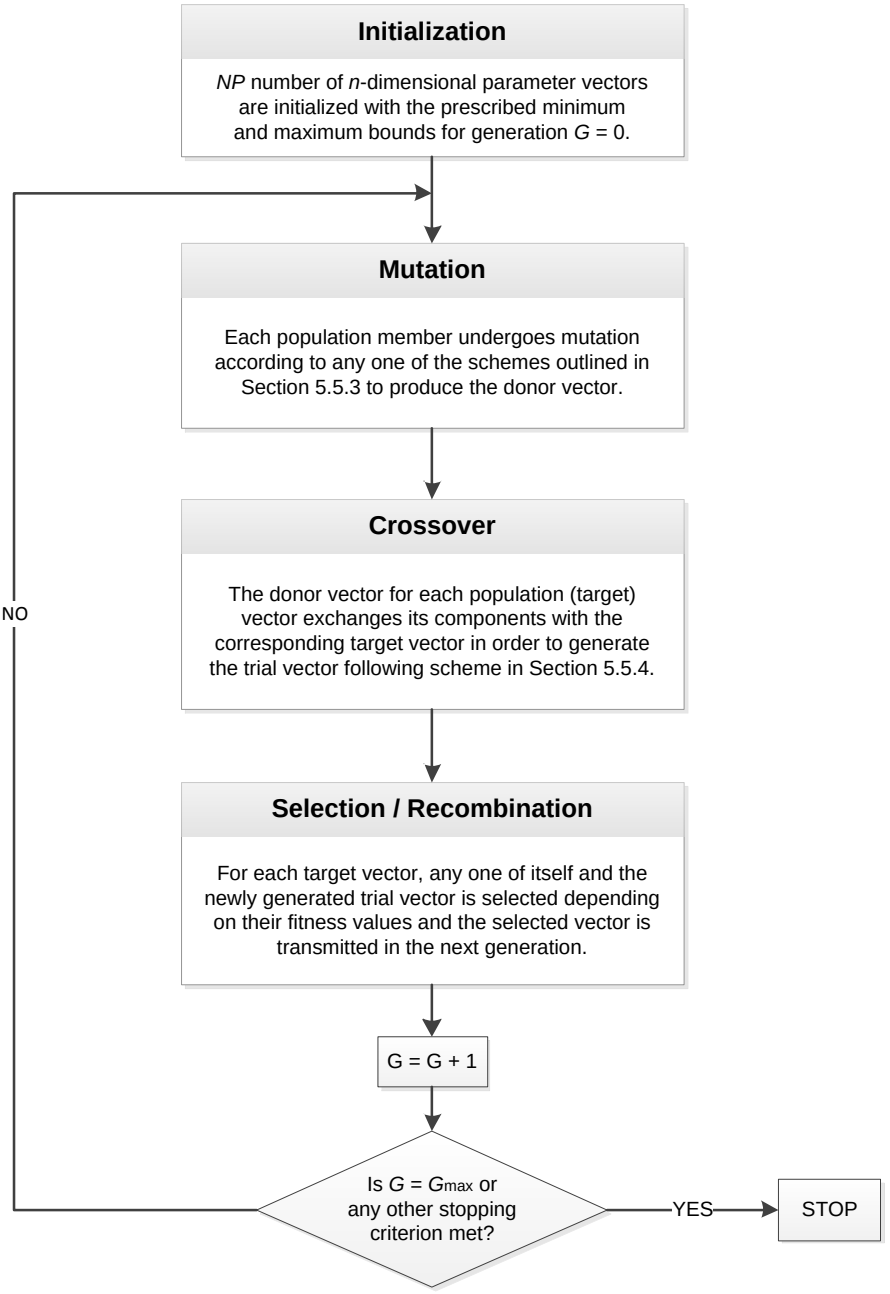

Figure 5.5: Flowchart for the differential evolution algorithm.

5.5.2 Initialization of the parameter vectors

DE searches for a global optimum point in a n-dimensional continuous hyperspace. It begins with a randomly initiated population of NP n-dimensional real-valued parameter vectors. Each vector, also known as *genome/chromosome*, forms a candidate solution to the multi dimensional optimization problem. Subsequent generations in DE is denoted by $G, G+1, G+2, ..., G_{max}$. Since the parameter vectors are likely to be changed over different generations, we adopt the following notation for representing

the i-th vector of the population at the current generation G as:

$$\vec{X}_i^G = [x_{i,1}^G, x_{i,2}^G, \ldots, x_{i,D}^G], \text{ where } i = \{1, 2, \ldots, NP\} \tag{5.15}$$

For each parameter of the problem, there may be a certain range within which the value of the parameter should be restricted, often because parameters are related to physical components or measures that have natural bounds (for example if one parameter is a length or mass, it cannot be negative). The initial population (at $G = 0$) should cover this range as much as possible by uniformly randomizing individuals within the search space constrained by the prescribed minimum and maximum bounds: $X_{min} = [x_{min,1}, x_{min,2}, \ldots, x_{min,D}]$ and $X_{max} = [x_{max,1}, x_{max,2}, \ldots, x_{max,D}]$. Hence we may initialize the j-th component of the i-th vector as:

$$x_{i,j}^0 = x_{min,j} + rand_{i,j}[0, 1] \cdot (x_{max,j} - x_{min,j}) \tag{5.16}$$

where $rand_{i,j}[0, 1]$ is a uniformly distributed random number lying between 0 and 1 and is instantiated independently for each component of the i-th vector. In Fig. 5.6 a population of $NP = 10$ points, is shown, for the $2D$ parametric space case.

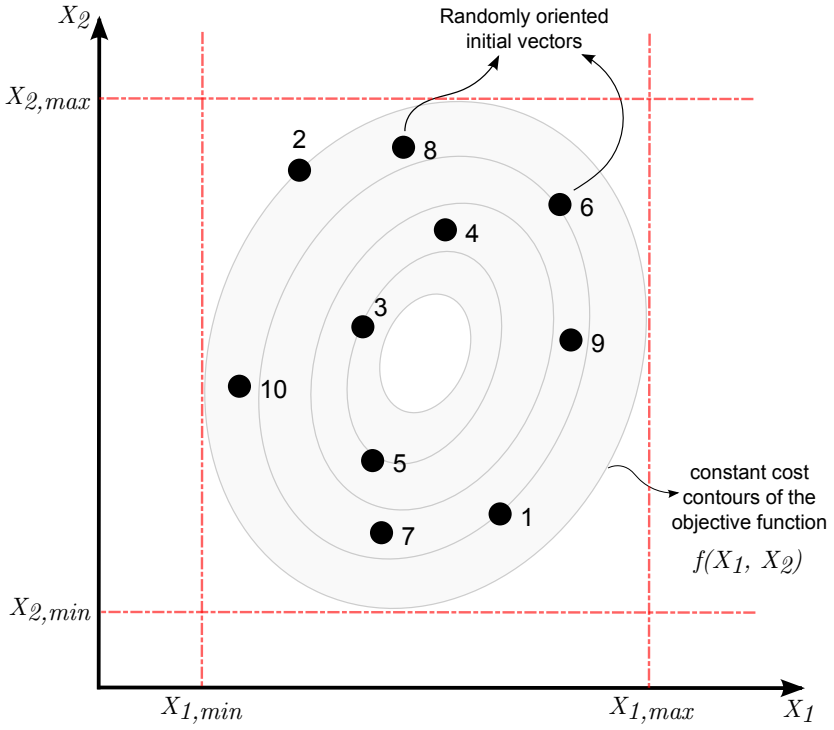

Figure 5.6: Initializing a DE population of $NP = 10$, on a $2D$ parametric space.

5.5.3 Mutation with differential operators

In Biology, *mutation* denotes a sudden change in the gene characteristics of a chromosome. In the context of the evolutionary computing field, however, mutation is also seen as a change or perturbation with a random element. In DE literature, a parent vector from the current generation is called *target* vector, and a *mutant* vector obtained

through the differential mutation operation is known as *donor* vector and finally an offspring formed by recombining the donor with the target vector is called trial vector. The simplest form of DE-mutation implies in creation a donor vector $\vec{V}_i^G$ for each i-th target vector X for changing each population member $\vec{X}_i^G$, in each generation (or in one iteration of the algorithm). To create $\vec{V}_i^G$ three other distinct parameter vectors, say the vectors $\vec{X}_{r_1^i}, \vec{X}_{r_2^i}, \vec{X}_{r_3^i}$ are picked up randomly from the current population. The indices r_1^i, r_2^i, r_3^i mutually exclusive integers randomly chosen from the range [1, NP], which are also different from the base vector index i. These indices are randomly generated once for each mutant vector. Now the difference of any two of these three vectors is scaled by a scalar number F (mutation factor, typically lies in the interval [0.4, 1], see Section 5.5.7) and the scaled difference is added to the third one whence we obtain the donor vector $\vec{V}_i^G$. We can express the process as:

$$\vec{V}_i^G = \vec{X}_{r_1^i}^G + F \cdot (\vec{X}_{r_2^i}^G - \vec{X}_{r_3^i}^G) \tag{5.17}$$

This mutation scheme is the simplest scheme among the different kinds of DE schemes (cf. Section 5.5.8) and a graphical representation of it, in $2D$ parametric space, is shown in Fig. 5.7.

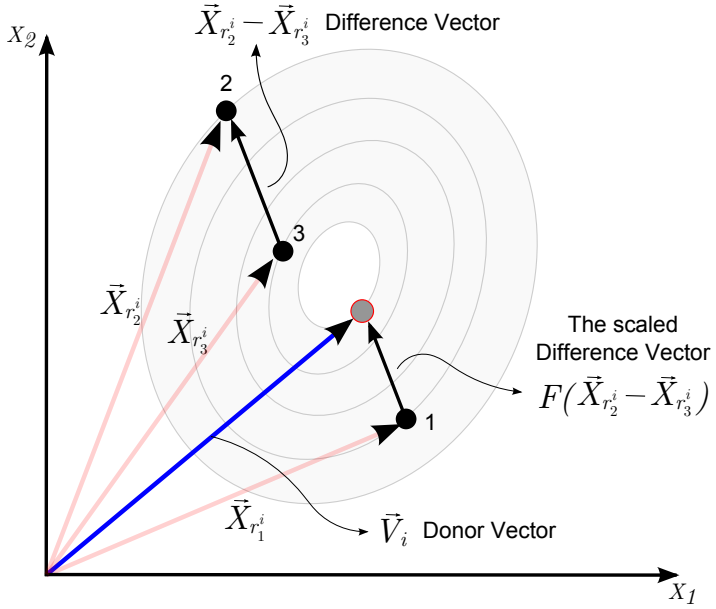

Figure 5.7: The simplest DE mutation scheme in $2D$ parametric space.

5.5.4 Crossover

To increase the potential diversity of the population, a crossover operation comes into play after generating the donor vector through mutation. The DE family of algorithms can use two kinds of crossover schemes, *exponential* and *binomial* [6, 7]. The donor vector exchanges its components with the target vector $\vec{X}_i^G$ under this operation to form the *trial* vector $\vec{U}_i^G = [u_{i,1}^G, u_{i,2}^G, \ldots, u_{i,D}^G]^T$.

5.5.4.1 Exponential crossover

In exponential crossover, we first choose an integer n randomly among the numbers [0, D-1]. This integer acts as a starting point in the target vector, from where the crossover or exchange of components with the donor vector starts. We also choose another integer L from the interval [1, D]. L denotes the number of components (the donor vector actually contributes to the target). After choosing n and L each component of the trial vector is obtained as:

$$u_{i,j}^{G} = \begin{cases} v_{i,j}^{G}, & \forall\, j \in \langle n \rangle_D, \langle n+1 \rangle_D, \ldots, \langle n+L-1 \rangle_D \\ x_{i,j}^{G}, & \forall\, j \in [0, D-1] \end{cases} \tag{5.18}$$

where the angular brackets $\langle\rangle_D$ denote a modulo function with modulus D. The integer L is drawn from $[1, 2, \ldots, D]$ according to the following pseudo-code:

```
L = 0
do while ((rand[0, 1] < CR) .AND. (L < D))
    {
        L = L + 1;
    }
```

CR is called the *crossover rate* and appears as a control parameter of DE just like F. Hence in effect, the probability $P(L \geq v)$ is equal to $(CR)^{v-1}$ for any positive integer $v \in [1, D]$. For each donor vector, a new set of n and L must be chosen randomly as shown above.

5.5.4.2 Binomial crossover

On the other hand, binomial crossover is performed on each of the D variables whenever a randomly picked number between 0 and 1 is less than or equal to the CR value. In this case the number of parameters inherited from the donor has a (nearly) binomial distribution. The scheme may be outlined as:

$$u_{i,j}^{G} = \begin{cases} v_{i,j}^{G}, & \text{if } \; rand_{i,j}[0,1] \leq CR \;\text{ or }\; j = j_{rand} \\ x_{i,j}^{G}, & \text{otherwise} \end{cases} \tag{5.19}$$

where $rand_{i,j}[0,1] \in [0,1]$ is a uniformly distributed random number, which is called a new for each j-th component of the i-th parameter vector, and $j_{rand} \in [1, 2, \ldots, D]$ is a randomly chosen index, which ensures that $\vec{U}_i^G$, gets at least one component from $\vec{V}_i^G$, where is instantiated once for each vector in one generation. For this additional demand, CR is only approximating the true probability p_{CR} that a component of the trial vector will be inherited from the donor. A visual feel of this process is given in Fig. 5.8.

5.5.5 Selection

To keep the population size constant over subsequent generations, the last step of the algorithm calls for *selection* to determine whether the target $\vec{X}_i^G$ or the newly formed

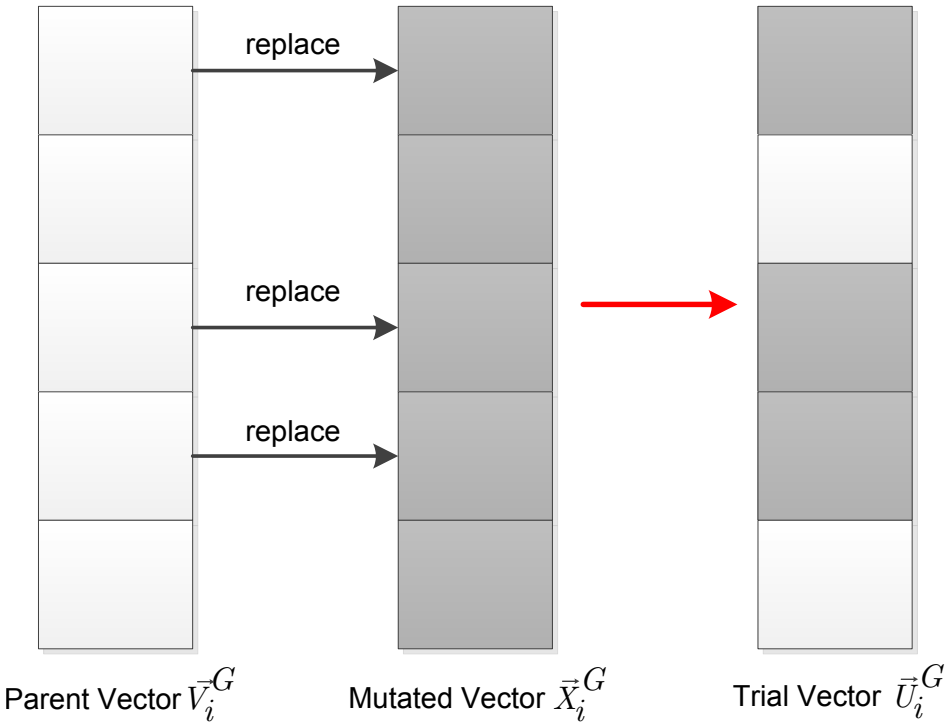

Figure 5.8: Illustrating the binomial crossover in DE.

trial vector $\vec{U}_i^G$ will survive to the next generation, i.e., at $G = G + 1$. The selection operation is described as:

$$\vec{X}_i^{G+1} = \begin{cases} \vec{U}_i^G, & \text{if } f(\vec{U}_i^G) \leq \vec{X}_i^G \\ x_{i,j}^G, & \text{if } f(\vec{U}_i^G) > \vec{X}_i^G \end{cases} \tag{5.20}$$

where $f(\vec{X})$ is the objective function to be minimized. Since the selection process employs a binary decision, i.e. any one between the target vector and its offspring survives the population size remains fixed through out generations. Hence, the population either gets better (with respect to the minimization of the objective function) or remains the same in fitness status, but never deteriorates.

5.5.6 Termination criteria

An important aspect for a stochastic algorithm is deciding when to stop the algorithm. Stochastic methods converge with a probability of 100% to an optimal value as time goes to infinity (Törn and Zhilinskas, 1989; Zhigljavsky and Zilinskas, 2007). However upholding such a convergence guarantee is impractical. Therefore the user will need to decide on some preset conditions that will terminate the algorithm. Deciding on what termination criteria to use is dependent on many factors such as the application of the algorithm, accuracy required, cost and time constraints. Some of the most common termination criteria used for the DE algorithm include:

- a preset number of maximum generations
- the difference between the best and worst function values in the population is very small

- the best function value has not improved beyond some tolerance value for a predefined number of generations
- the distance between solution vectors in the population is small.

5.5.7 Parameter selection

In DE algorithm three main control parameters have to be set: the mutation scale factor (F), the crossover constant (CR) and the population size (NP). Each of these parameters can effect the performance of the DE as well as the state-of-the-art methods for tuning these parameters.

A lot of research work has been undertaken so far to improve the ultimate performance of the DE by tuning its control parameters. General guidelines for the values of parameters that work reasonably well on a wide range of problems are known. Storn and Price (1997) have indicated that a reasonable value for NP could be chosen between $5D$ and $10D$ (D is the dimensionality of the problem).

The scale factor F controls the magnitude of the difference vector and consequently the amount by which the base vector is perturbed. Large values of F encourage large scale exploration of the fitness landscape but could lead to premature convergence, while small values result in a more detailed exploration of the local fitness landscape (exploitation) while increasing convergence time. A good initial choice of F is 0.5, while the effective value range of F is usually between 0.4 and 1. The upper limit of the scale factor F is empirically taken as 1. Although that does not necessarily mean that a solution is not possible with $F > 1$, however, no benchmark function that was successfully optimized with DE required $F > 1$.

Also, mathematical convergence analysis regarding parameter selection (Zaharie, 2002) showed on three test functions that the smallest reliable value for F is 0.3 when $CR = 0.2$ and $NP = 50$. Storn and Price (1997), also showed that $0 \leq CR \leq 0.2$ worked well on decomposable functions, while $0.9 \leq CR \leq 1.0$ worked well on functions that are not decomposable. Gämperle et al. (2002) evaluated different parameter settings for DE on the three benchmark functions (Sphere, Rosenbrock's, and Rastrigin's). Their experimental results revealed that the global optimum searching capability and the convergence speed are very sensitive to the choice of control parameters NP, F and CR. Furthermore, a reasonable choice of the population size NP is between $3D$ and $8D$, the scaling factor $F = 0.6$ and the crossover rate CR is between $[0.3, 0.9]$. Also, Rönkkönen et al. (2005), claim that typically $0.4 < F < 0.95$ with $F = 0.9$ being a good first choice and CR always lies in $(0, 0.2)$ when the function is separable, while in $(0.9, 1)$ when the function's parameters are dependent.

Other recommendations may found in the literature (Pedersen, 2010; Storn and Price, 1997), however, best results in terms of accuracy and convergence time are found if the parameters are tuned for each problem individually (Engelbrecht, 2007). Therefore researchers naturally consider some techniques such as self-adaptation to avoid manual tuning of the parameters of DE, for engineers who try to solve real-world optimization problems with the DE.

5.5.8 Other mutation schemes

The process of mutation demarcates one DE scheme from another. The mutation scheme used in Eq. (5.17) uses a randomly selected $\vec{X}_{r_1}$ vector and only one weighted difference vector $F \cdot (\vec{X}_{r_2} - \vec{X}_{r_3})$ is used to perturb it. Hence, in literature, the particular mutation scheme given by Eq. (5.17) referred to as DE/rand/1.

The general convention of how the different DE schemes are named is DE/x/y. DE stands for Differential Evolution, x represents a string denoting the type of the vector to be perturbed (whether it is randomly selected or it is the best vector in the population with respect to fitness) and y is the number of difference vectors considered for perturbation of x. The other four different mutation schemes, suggested by Price et al. (2005) are summarized below.

5.5.8.1 DE/target-to-best/1

The DE/target-to-best/1 (or DE/current-to-best/1) scheme follows the same procedure as that of the classical DE scheme (cf. Eq. (5.17)), and the only difference being that, now the donor vector, used to perturb each population member, is created using any two randomly selected member of the population as well as the best vector of the current generation (i.e. the vector yielding best suited objective function value at $G = G$). This can be expressed for the i-th donor vector at generation $G = G + 1$ as,

$$\vec{V}_i^G = \vec{X}_i^G + F \cdot (\vec{X}_{best}^G - \vec{X}_i^G) + F \cdot (\vec{X}_{r_1^i}^G - \vec{X}_{r_2^i}^G) \tag{5.21}$$

where $\vec{X}_i^G$, it the target vector and $\vec{X}_{best}^G$ is the best member of the population regarding fitness at current generation $G = G$.

5.5.8.2 DE/best/1

In this scheme everything is identical to DE/rand/1 except the fact that the trial vector is formed as,

$$\vec{V}_i^G = \vec{X}_{best}^G + F \cdot (\vec{X}_{r_1^i}^G - \vec{X}_{r_2^i}^G) \tag{5.22}$$

5.5.8.3 DE/best/2

Under this scheme, the donor vector is formed by using two difference vectors as following:

$$\vec{V}_i^G = \vec{X}_{best}^G + F \cdot (\vec{X}_{best}^G - \vec{X}_{r_1^i}^G - \vec{X}_{r_2^i}^G) + F \cdot (\vec{X}_{r_3^i}^G - \vec{X}_{r_4^i}^G) \tag{5.23}$$

5.5.8.4 DE/rand/2

Finally, in DE/rand/2 scheme, the vector to be perturbed is selected randomly and two weighted difference vectors are added to the same to produce the donor vector. Thus, for each target vector, five other distinct vectors in total, are selected from the rest of the population. The process can be expressed in the form of an equation as:

$$\vec{V}_i^G = \vec{X}_{r_1^i}^G + F_1 \cdot (\vec{X}_{r_2^i}^G - \vec{X}_{r_3^i}^G)) + F_2 \cdot (\vec{X}_{r_3^i}^G - \vec{X}_{r_5^i}^G) \tag{5.24}$$

where, F_1 and F_2 are two weighing factors selected in the range from 0 to 1. To reduce the number of parameters one may choose $F1 = F2 = F$. The indices $r_j^i,\ j \in \{1, 2, 3, 4, 5\}$ are mutually exclusive integers randomly chosen from the range [1, NP], which are also different from the index i. These indices are randomly generated once for each mutant vector.

Also, Storn and Price (1997) suggested ten different working strategies of DE, as well as useful guidelines in applying these strategies to any given problem. These strategies were derived from the five different DE mutation schemes outlined before. Each mutation strategy was combined with either the exponential type crossover or the binomial type crossover. This yielded a total of ten DE strategies, which are listed below:

1. DE/best/1/exp
2. DE/rand/1/exp
3. DE/rand-to-best/1/exp
4. DE/best/2/exp
5. DE/rand/2/exp
6. DE/best/1/bin
7. DE/rand/1/bin
8. DE/rand-to-best/1/bin
9. DE/best/2/bin
10. DE/rand/2/bin

The general convention used above is again DE/x/y/z, where DE stands for Differential Evolution, x represents a string denoting the vector to be perturbed, y is the number of difference vectors considered for perturbation of x, and z stands for the type of crossover being used (exp: exponential; bin: binomial).

5.6 Towards the selection of the optimization algorithm

In the past a number of studies have been published where structural optimization with single and multiple objectives are solved implementing metaheuristics. A literature survey can be found in the following subsection, before a sensitivity analysis is performed for the four metaheuristics described previously in benchmark multimodal constrained functions highlighting the proper search algorithm for solving the structural optimization problem.

5.6.1 Literature survey on metaheuristic based structural optimization

Perez and Behdinan (2007) presented the background and implementation of a particle swarm optimization algorithm suitable for constraint structural optimization problems, while improvements that effect of the setting parameters and functionality of the algorithm were shown. Hasançebi (2008) investigated the computational performance of adaptive evolution strategies in large-scale structural optimization. Bureerat and Limtragool (2008) presented the application of simulated annealing for solving structural topology optimization, while a numerical technique termed as multiresolution design variables was proposed as a numerical tool to enhance the searching performance. Hansen et al. (2008) introduced an optimization approach

based on an evolution strategy that incorporates multiple criteria by using nonlinear finite-element analyses for stability and a set of linear analyses for damage-tolerance evaluation, the applicability of the approach was presented for the window area of a generic aircraft fuselage. Kaveh and Shahrouzi (2008) proposed a hybrid strategy combining indirect information share in ant systems with direct constructive genetic search, for this purpose some proper coding techniques were employed to enable testing the method with various sets of control parameters. Farhat et al. (2009) proposed a systematic methodology for determining the optimal cross-sectional areas of buckling restrained braces used for the seismic upgrading of structures against severe earthquakes, for this purpose single-objective and multi-objective optimization problems were formulated. Chen and Chen (2009) proposed modified evolution strategies for solving mixed-discrete optimization problems, in particular three approaches were proposed for handling discrete variables.

Gholizadeh and Salajegheh (2009) proposed a new metamodeling framework that reduces the computational burden of the structural optimization against the time history loading, for this purpose a metamodel consisting of adaptive neuro-fuzzy inference system, subtractive algorithm, self-organizing map and a set of radial basis function networks were used to accurately predict the time history responses of structures. Wang et al. (2010) studied an optimal cost base isolation design or retrofit design method for bridges subject to transient earthquake loads. Hasançebi et al. (2010) utilized metaheuristic techniques like genetic algorithms, simulated annealing, evolution strategies, particle swarm optimizer, tabu search, ant colony optimization and harmony search in order to develop seven optimum design algorithms for real size rigidly connected steel frames. Manan et al. (2010) employed four different biologically inspired optimization algorithms (binary genetic algorithm, continuous genetic algorithm, particle swarm optimization, and ant colony optimization) and a simple meta-modeling approach on the same problem set. Gandomi and Yang (2011) provide an overview of structural optimization problems of both truss and non-truss cases. Martínez et al. (2011) described a methodology for the analysis and design of reinforced concrete tall bridge piers with hollow rectangular sections, which are typically used in deep valley bridge viaducts. Kripakaran et al. (2011) presented computational approaches that can be implemented in a decision support system for the design of moment-resisting steel frames, while trade-off studies were performed using genetic algorithms to evaluate the savings due to the inclusion of the cost of connections in the optimization model. Gandomi et al. (2013) used the cuckoo search (CS) method for solving structural optimization problems, furthermore, for the validation against structural engineering optimization problems the CS method was applied to 13 design problems taken from the literature.

Kunakote and Bureerat (2011) dealt with the comparative performance of some established multi-objective evolutionary algorithms for structural topology optimization, four multi-objective problems, having design objectives like structural compliance, natural frequency and mass, and subjected to constraints on stress, were used for performance testing. Su et al. (2011) used genetic algorithm to handle topology and sizing optimization of truss structures, in which a sparse node matrix encoding approach is used and individual identification technique is employed to avoid duplicate structural analysis to save computation time. Gandomi and Yang (2011) used firefly

algorithm for solving mixed continuous/discrete structural optimization problems, the results of a trade study carried out on six classical structural optimization problems taken from literature confirm the validity of the proposed algorithm. Degertekin (2012) proposed two improved harmony search algorithms for sizing optimization of truss structures, while four truss structure weight minimization problems were presented to demonstrate the robustness of the proposed algorithms. The main part of the work by Muc and Muc-Wierzgoń (2012) was devoted to the definition of design variables and the forms of objective functions for multi-layered plated and shell structures, while the evolution strategy method was used as the optimization algorithm. Comparative studies of metaheuristics on engineering problems can be found in two recent studies by Lagaros and Papadrakakis (2012) and in the edited book by Yang and Koziel (2011).

5.6.2 Sensitivity analysis of metaheuristics

Choosing the proper search algorithm for solving an optimization problem is not a straightforward procedure. In this section a sensitivity analysis of the four algorithms described above is performed for five constrained multimodal benchmark test functions in order to identify the best algorithm and to be used for solving the structural shape optimization problem studied in the next section. This sensitivity analysis is carried out to examine the influence of the four metaheuristic algorithms and thus proving their robustness. In particular, for the solution of the five problems ES, CMA, ECMA and DE methods are implemented, since they were found robust and efficient in previous numerical tests (Lagaros and Papadrakakis, 2012). This should not been considered as an implication related to the efficiency of other algorithms, since any algorithm available can be considered for the solution of the optimization problem based on user's experience.

The control parameters for DE are the population size (NP), probability (CR) and constant (F), while for ES, CMA and ECMA the control parameters are the number of parents (μ) and offsprings (λ). The characteristic parameters adopted for the implementation are as follows: (i) for DE method, population size $NP = 15$, probability $CR = 0.90$ and constant $F = 0.60$, while (ii) for all three ES, CMA and ECMA methods, number of parents $\mu = 1$ and offsprings $\lambda = 14$ for the case of ES and ECMA and number of parents $\mu = 5$ and offsprings $\lambda = 15$ for the case of CMA.

For all four algorithms the initial population is generated randomly using LHS in the range of design space for each test example examined, while for the implementation of all algorithms, the real valued representation of the design vectors is adopted. For the purposes of the sensitivity analysis 50 independent optimization runs were performed, for the combination of the algorithmic parameters. The 50 independent optimization runs, represents a necessary step since non deterministic optimization algorithms do not yield the same results when restarted with the same parameters (Riche and Haftka, 2012). Using the optimum objective function values achieved for the 50 independent optimization runs, mean and coefficient of variation of the optimum objective function are calculated.

For comparative reasons the method adopted for handling the constraints and the termination criterion is the same for all metaheuristic optimization algorithms. In

particular, the simple yet effective, multiple linear segment penalty function (Lagaros and Papadrakakis, 2012) is used in this study for handling the constraints. According to this technique if no violation is detected, then no penalty is imposed on the objective function. If any of the constraints is violated, a penalty, relative to the maximum degree of constraints' violation, is applied to the objective function, otherwise the optimization procedure is terminated after 10000 function evaluations. For the results found in the literature and used for our comparative study different constraint handling techniques and termination criteria were implemented.

5.6.2.1 Test case S-6ACT

The first test case considered in this sensitivity analysis study is the so called S-6ACT (Hock and Schittkowski, 1980) problem that is defined as follows:

$$
\begin{aligned}
\text{min:} \quad & F(x) = x_1^2 + x_2^2 + x_1 x_2 - 14x_1 - 16x_2 + (x_3 - 10)^2 + 4(x_4 - 5)^2 \\
& + (x_5 - 3)^2 + 2(x_6 - 1)^2 + 5x_7^2 + 7(x_8 - 11)^2 + 2(x_9 - 10)^2 \\
& + (x_{10} - 7)^2 + 45 \\
\text{subject to:} \quad & g_1(\vec{x}) = 105 - 4x_1 - 5x_2 + 3x_7 - 9x_8 \geq 0 \\
& g_2(\vec{x}) = -10x_1 + 8x_2 + 17x_7 - 2x_8 \geq 0 \\
& g_3(\vec{x}) = 8x_1 - 2x_2 + 17x_7 - 2x_8 \geq 0 \\
& g_4(\vec{x}) = -3(x_1 - 2)^2 - 4(x_2 - 3)^2 - 2x_3^2 + 7x_4 + 120 \geq 0 \\
& g_5(\vec{x}) = -5x_2 - 8x_2 - (x_3 - 6)^2 + 2x_4 + 40 \geq 0 \\
& g_6(\vec{x}) = -x_1^2 - 2(x_2 - 2)^2 + 2x_1 x_2 - 14x_5 + 6x_6 \geq 0 \\
& g_7(\vec{x}) = -0.5(x_1 - 8)^2 - 2(x_2 - 4)^2 + 3x_5^2 + x_6 + 30 \geq 0 \\
& g_8(\vec{x}) = 3x_1 - 6x_2 - 12(x_9 - 8)^2 \geq 0 \\
& -10 \leq x_i \leq 10, \; i = 1, \ldots, 10
\end{aligned}
$$

It is a 10 design variables problem with 8 inequality constraints. As it can be observed in Table 5.1 the better COV value is achieved by CMA and the worst one by ES algorithm, while the best mean value is obtained by DE algorithm and the worst by ES.

Algorithm	μ	λ	Selection	Obj. Function		
				Best	Mean	COV (%)
ES	1	14	+	14.962	49.0379	1.56E+02
CMA	5	15	,	14.257	15.1669	8.57E-02
ECMA	1	14	+	14.436	14.2681	5.17E+00
DE				14.257	14.2608	3.42E-01

Table 5.1: Results comparison for test case S-6ACT.

The best optimized designs achieved by the four metaheuristics among the 50 independent optimization runs is given in Table 5.2. Although, the best optimized design is achieved by CMA and DE algorithm, DE algorithm had slightly better performance

based on statistical data of Table 5.1 with reference to the mean value achieved, while with respect to COV performed slightly better compared to DE. It should be noted also that for all 50 independent optimization runs performed for each algorithm, feasible optimized designs were obtained.

x	Deb (2000)	ES	CMA	ECMA	DE
x_1	2.171996	1.5859	1.576076	1.6996902	1.5760762
x_2	2.363683	2.8712	2.731987	2.6947086	2.7319869
x_3	8.773926	8.7952	8.791763	8.7832448	8.7917633
x_4	5.095984	5.0471	5.059531	4.9932193	5.0595309
x_5	0.990655	1.1745	0.976753	1.0675614	0.9767532
x_6	1.430574	1.9129	1.436430	1.6072484	1.4364296
x_7	1.321644	0.7489	0.783778	0.8738167	0.7837782
x_8	9.828726	9.6163	9.709677	9.7054379	9.7096767
x_9	8.280092	9.7648	9.774489	9.7654962	9.7744885
x_{10}	8.375927	7.1255	7.064255	6.9290318	7.0642553
F	24.30621	14.962	14.257	14.436	14.257

Table 5.2: Results comparison for test case S-6ACT.

5.6.2.2 Test case S-CRES

This test case problem proposed by Deb (2000) and is characterized by 2 design variables and 2 inequality constraints. It is defined by the following relations:

$$\begin{aligned} \text{min:} \quad & F(x) = (x_1^2 + x_2 - 11)^2 + (x_1 + x_2^2 - 7)^2 \\ \text{subject to:} \quad & g_1(\vec{x}) = 4.84 - (x_1 - 0.05)^2 - (x_2 - 2.5)^2 \geq 0 \\ & g_2(\vec{x}) = x_1^2 + (x_2 - 2.5)^2 - 4.84 \geq 0 \\ & 0 \leq x_1 \leq 6 \\ & 0 \leq x_2 \leq 6 \end{aligned}$$

In Fig. 5.9 the feasible and infeasible domain of the problem is shown. The feasible domain is approximately 0.7% of the total search space. The two constraint functions g_1, g_2 create a crescent shape for the feasible domain, as it is shown in Fig. 5.10 with the zoomed area around the optimal point.

Similar to the previous test case, statistical results (mean value and standard deviation) are given in Table 5.3. Also, in Table 5.4, the results are compared with the best result found in literature (Deb, 2000). It should be noted also that for all 50 independent optimization runs performed for each algorithm, feasible optimized designs were obtained.

The CMA and DE algorithms had better performance, since the standard deviation values of the objective function at the end of the evolution process was orders of magnitude smaller than the other two algorithms.

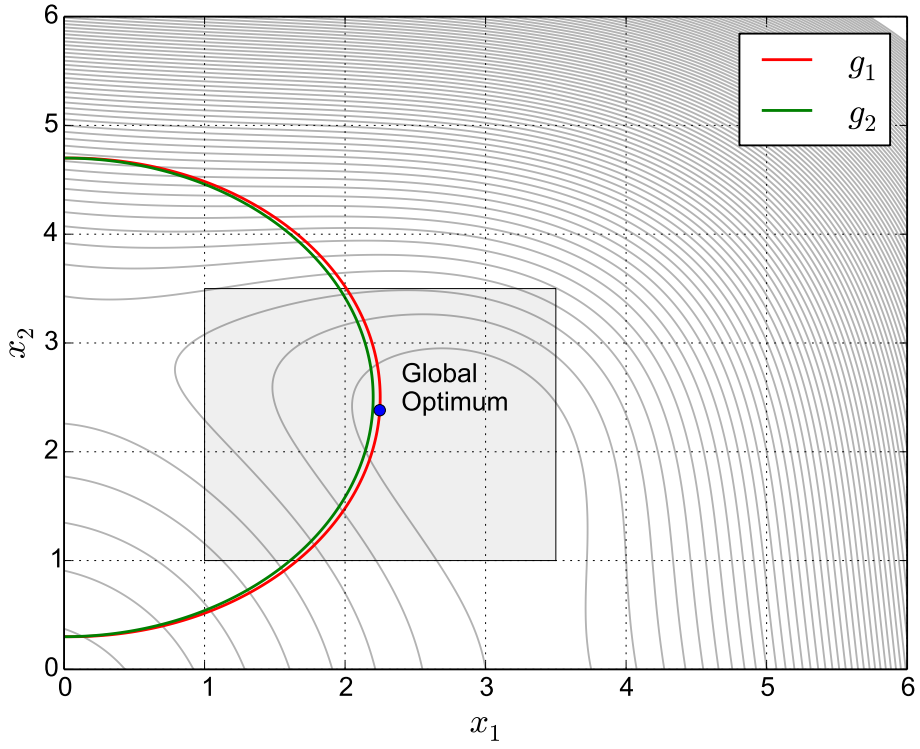

Figure 5.9: Feasible and infeasible domain for S-CRES problem.

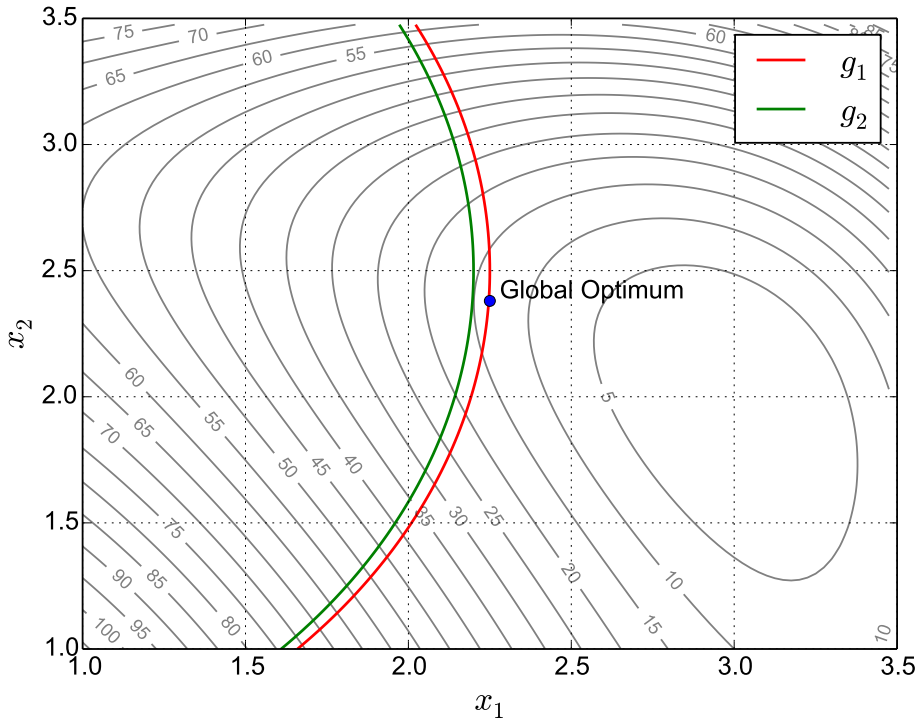

Figure 5.10: Enlarged space around the optimal point.

Algorithm	μ	λ	Selection	Obj. Function		
				Best	Mean	COV (%)
ES	1	14	+	13.59085	13.6897	2.53E+00
CMA	5	15	,	13.59084	13.5909	1.34E-03
ECMA	1	14	+	13.59087	13.6096	3.49E-01
DE				13.59084	13.5957	1.79E-02

Table 5.3: Results comparison for test case S-CRES.

x	Deb (2000)	ES	CMA	ECMA	DE
x_1	2.246826	2.246841	2.246826	2.246811	2.246826
x_2	2.381865	2.382141	2.381865	2.381597	2.381865
F	13.59085	13.59085	13.59084	13.59087	13.59084

Table 5.4: Results comparison for test case S-CRES.

5.6.2.3 Test case S-0.5F

The optimization problem S-0.5F (Coelho, 2004) is characterized by 7 design variables and 4 inequality constraints, and is defined by the following relations:

$$
\begin{aligned}
\text{min:} \quad & F(x) = (x_1 - 10)^2 + 5(x_2 - 12)^2 + x_3^4 + 3(x_4 - 11)^2 \\
& \quad + 10x_5^6 + 7x_6^2 + x_7^4 - 4x_6x_7 \\
\text{subject to:} \quad & g_1(\vec{x}) = 127 - 2x_1^2 - 3x_2^2 - x_3 - 4x_4^2 - 5_x5^2 \geq 0 \\
& g_2(\vec{x}) = 282 - 7x_1 - 3x_2 - 10x_3^2 - x_4 - x_5 \geq 0 \\
& g_3(\vec{x}) = 196 - 23x_1 - x_2^2 - 6x_6^2 + 8x_7 \geq 0 \\
& g_4(\vec{x}) = -4x_1^2 - x_2^2 + 3x_1x_2 - 2x_3^2 - 5x_6 + 11x_7 \geq 0 \\
& -10 \leq x_i \leq 10, \; i = 1, \ldots, 7
\end{aligned}
$$

In this problem, only 0.5% of the space defined by the design variables is feasible. Again for all 50 independent optimization runs performed for each algorithm, feasible optimized designs were obtained. Statistical results (mean value and COV) are given in Table 5.5. Table 5.6 shows that even thought all algorithms found the optimal

Algorithm	μ	λ	Selection	Obj. Function		
				Best	Mean	COV (%)
ES	1	14	+	680.7721	705.7945	1.24E+01
CMA	5	15	,	680.6301	680.6301	1.20E-07
ECMA	1	14	+	680.6848	681.5228	6.33E-02
DE				680.6301	680.6551	1.67E-01

Table 5.5: Results for test case S-0.5F.

design domain, only the CMA algorithm found the global optimum design. CMA algo-

x	Deb (2000)	ES	CMA	ECMA	DE
x_1	2.330499	2.320378	2.330501	2.299430	2.330501
x_2	1.951372	1.967625	1.951373	1.947076	1.951373
x_3	-0.477541	-0.281803	-0.477539	-0.468747	-0.477539
x_4	4.365723	4.319129	4.365723	4.382807	4.365723
x_5	-0.624487	-0.615799	-0.624484	-0.611883	-0.624484
x_6	1.038131	1.057470	1.038125	1.001823	1.038125
x_7	1.594227	1.560759	1.594225	1.541608	1.594225
F	680.63	680.77	680.63	680.69	680.63

Table 5.6: Results comparison for test case S-0.5F.

rithm had the best performance, since the standard deviation values of the objective function at the end of the evolution process is almost zero.

5.6.2.4 Test case S-HIM

The optimization problem S-HIM (Coelho, 2004) is characterized by 5 design variables and 6 inequality constraints, and is defined by the following relations:

$$
\begin{aligned}
\text{min:} \quad & F(x) = 5.3578547x_3^2 + 0.8356891x_1x_5 + 37.293239x_1 - 40792.141 \\
\text{subject to:} \quad & g_1(\vec{x}) = 85.334407 + 0.0056858x_2x_5 + 0.0006262x_1x_4 \\
& \quad - 0.0022053x_3x_5 \geq 0 \\
& g_2(\vec{x}) = 92 - g_1(\vec{x}) \geq 0 \\
& g_3(\vec{x}) = 80.51249 + 0.0071317x_2x_5 + 0.0029955x_1x_2 \\
& \quad + 0.0021813x_3^2 - 90 \geq 0 \\
& g_4(\vec{x}) = 20 - g_3(\vec{x}) \geq 0 \\
& g_5(\vec{x}) = 9.300961 + 0.0047026x_3x_5 + 0.0012547x_1x_3 \\
& \quad + 0.0019085x_3x_4 - 20 \geq 0 \\
& g_6(\vec{x}) = 5 - g_4(\vec{x}) \geq 0 \\
& 78 \leq x_1 \leq 102 \\
& 33 \leq x_2 \leq 45 \\
& -27 \leq x_i \leq 45, \; i = 3, 4, 5
\end{aligned}
$$

Statistical results (mean value and COV) are given in Table 5.7. The optimal value of the objective function value is equal to -31005.7966 (Aguirre et al., 2004), which was achieved with computational cost of 350000 evaluations of the objective function. From Table 5.8 is shown that for all 50 independent optimization runs performed only for ES, CMA and DE algorithms, feasible optimized designs were obtained. In contrast, the CMA algorithm failed to find the area of the optimal solution.

Algorithm	μ	λ	Selection	Obj. Function		
				Best	Mean	COV (%)
ES	1	14	+	-30665.5	-30190.0	1.81E+00
CMA	5	15	,	-25273.7	-24258.6	2.07E+01
ECMA	1	14	+	-30665.5	-30477.6	8.45E-01
DE				-30665.5	-30700.5	2.68E-01

Table 5.7: Results for test case S-HIM.

x	ES	CMA	ECMA	DE
x_1	78.000	78.000	78.000	78.000
x_2	33.000	33.000	33.000	33.000
x_3	29.996	45.000	29.995	29.995
x_4	45.000	45.000	45.000	45.000
x_5	36.776	27.000	36.776	36.776
F	-30665.5	-25272.7	-30665.5	-30665.5

Table 5.8: Results comparison for test case S-HIM.

5.6.2.5 Test case S-G08

The optimization problem S-G08 (Aguirre et al., 2004) is characterized by 2 design variables and 2 inequality constraints, and is defined by the following relations:

$$\begin{aligned} \text{min:} \quad & F(x) = \frac{sin(2\pi x_1)^3 sin(2\pi x_2)}{x_1^3(x_1+x_2)} \\ \text{subject to:} \quad & g_1(\vec{x}) = x_1^2 - x_2 + 1 \geq 0 \\ & g_2(\vec{x}) = 1 - x_1 + (x_2 - 4)^2 \geq 0 \end{aligned}$$

In Fig. 5.11 the space defined by the design variables, is shown, while in Fig. 5.12 the area around the optimal solution related to the literature, is depicted. Similar to the previous test case, statistical results (mean value and standard deviation) are given in Table 3. The DE algorithm had better performance, since the standard deviation values

Algorithm	μ	λ	Selection	Obj. Function		
				Best	Mean	COV (%)
ES	1	14	+	-0.10546	-0.08413	4.14E+01
CMA	5	15	,	-0.10546	-0.06765	1.49E+02
ECMA	1	14	+	-0.10546	-0.10398	4.11E+01
DE				-0.10566	-0.10546	7.02E-01

Table 5.9: Results for test case S-G08.

of the objective function at the end of the evolution process was orders of magnitude smaller than the other three algorithms. The optimal value of the objective function

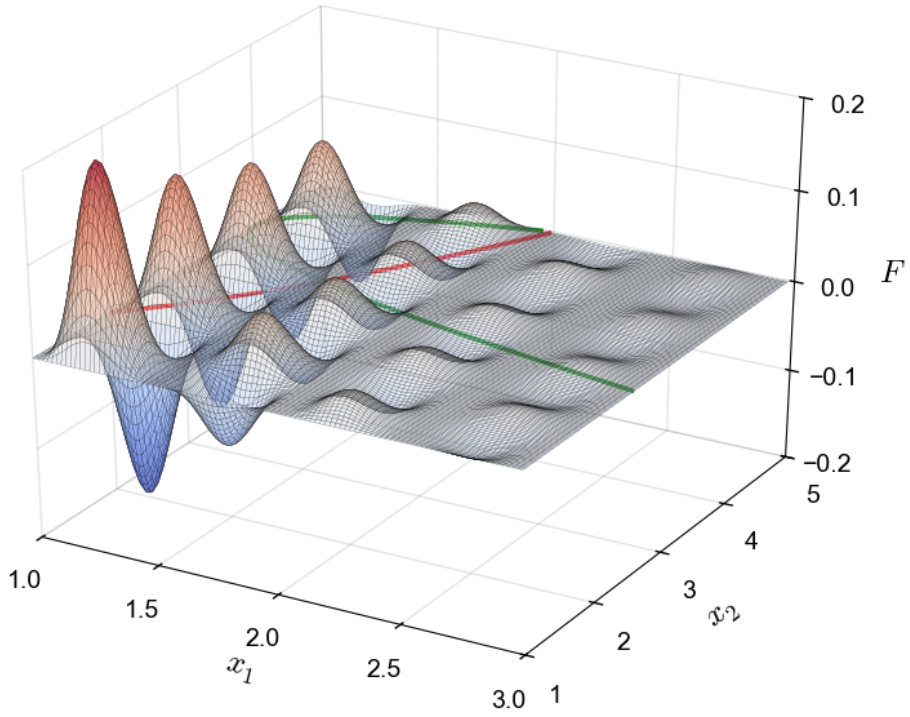

Figure 5.11: Design variables domain for test case S-G08.

found in the literature is equal to -0.09582 (Aguirre et al., 2004), which was achieved after 350000 evaluations of the objective function. Also, in Table 5.10 is shown that for all algorithms feasible optimized designs were obtained.

x	Aguirre et al. (2004)	ES	CMA	ECMA	DE
x_1	1.227971	1.227818	1.227818	1.227818	1.227817
x_2	4.245373	3.744911	3.744911	3.744911	3.744911
F	-0.09582	-0.10546	-0.10546	-0.10546	-0.10546

Table 5.10: Results comparison for test case S-G08.

5.6.3 Selection of the appropriate search algorithm

The sensitivity of the four algorithms with respect to different optimization runs characterized by the mean and coefficient of variation (COV) of the optimized objective function values for each metaheuristic algorithm was identified in the corresponding tables of Section 5.6.2. The lower mean and COV values are, the better the algorithm is. This is due to the fact that low COV values mean that the algorithm is not influenced by the independent runs. Overall, the algorithm resulting to the lower mean value (in case of minimization problem) and COV is used for performing the optimization run with the specific algorithm, i.e. the DE algorithm.

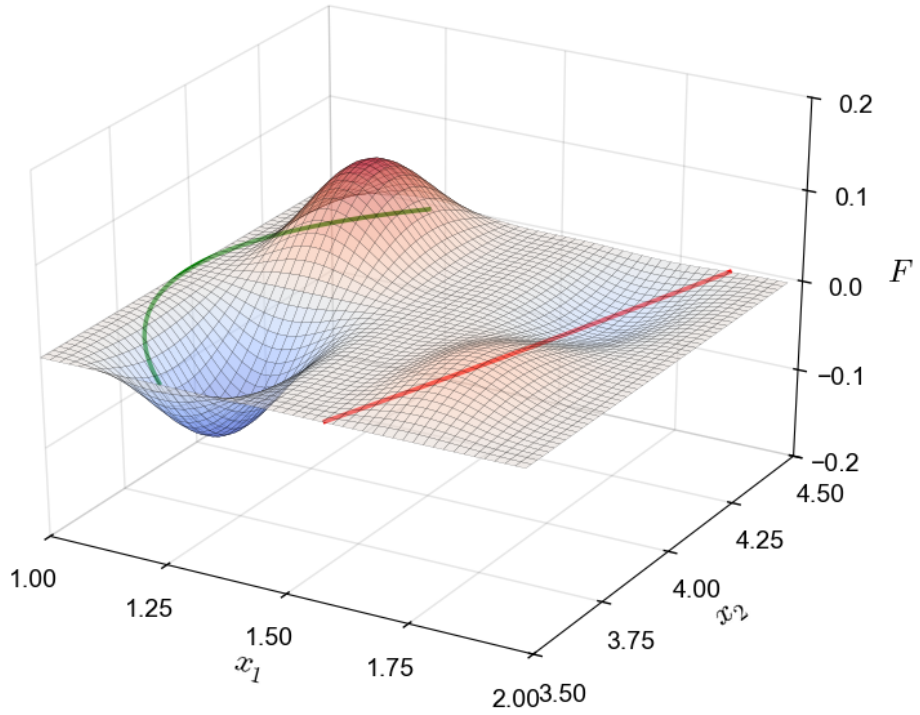

Figure 5.12: Domain around global minimum for test case S-G08.

This page intentionally left blank

6

Numerical Examples

In this chapter representative numerical examples are chosen to investigate and demonstrate the capabilities of the proposed formulations presented in Chapters 4 and 5. The chapter is divided into two sections: the first section presents the results from the investigation of the influence of uncertain spatially varying material properties on the fracture behavior of two benchmark structures with softening materials, while in the second section structural shape optimization results are presented for a steel structural components under fatigue.

The numerical tools developed in this thesis are coded in a FORTRAN and PYTHON code which are used to carry out all presented simulations. Interactive post processing tasks are conducted with MATPLOTLIB, while the graphical representations of meshes and cracks paths are facilitated through GMSH (Geuzaine and Remacle, 2009).

6.1 Stochastic analysis results

For the numerical examples, in the first part of the present thesis, SFEM (cf. Section 4.6) is coupled with the SLA, described in Section 2.2.1, providing solutions of the stochastic nonlinear static problems for structures made of softening materials (Stefanou et al., 2014). It is assumed that the Young's modulus E, tensile strength f_t and fracture energy G_f of the material (cf. Section 2.2.3) are represented by two dimensional uni-variate (2D-1V) homogeneous stochastic fields. The variation of E is described as follows:

$$E(x, y) = E_0[1 + f(x, y)] \tag{6.1}$$

where E_0 is the mean value of the elastic modulus and $f(x, y)$ is a zero-mean homogeneous stochastic field. The discretized stochastic fields are used for the formulation of the stochastic matrix $\mathbb{k}^{(e)}$ of each finite element. The two other material properties (i.e. f_t and G_f) are varying in a similar way. The stochastic stiffness matrix is derived using the midpoint method (cf. Section 4.6.2.1), i.e. one integration point at the centroid of each finite element is used for the computation of the stiffness matrix. This approach gives accurate results for relatively coarse meshes keeping the computational cost at

reasonable levels (Stefanou, 2009).

Both Gaussian and non-Gaussian stochastic fields are used in this study for the representation of uncertain material properties. Using the procedure described in Section 4.4.1 and Section 4.5.1, a large number N_{sim} of sample functions are produced, leading to the generation of a set of stochastic stiffness matrices. The associated structural problem is solved N_{sim} times and the response is finally be calculated by obtaining the response statistics of the N_{sim} simulations or alternatively by using the VRF approach.

6.1.1 A 4-point bending notched beam

A symmetric notched beam (Rots and Invernizzi, 2004) is analyzed and the geometry, boundary conditions, loading are shown in Fig. 6.1. The thickness of the beam is 50 mm and the notch depth is 10 mm. Four-node linear quadrilateral elements under plane stress conditions are used and a 2x2 Gaussian integration rule. The uncertain parameters of the problem are the Young's modulus E, tensile strength f_t and fracture energy G_f of the material with mean values equal to 38 GPa, 3 MPa and 0.06 N/mm, respectively. Note that the displacement is monitored at the point where the load is applied.

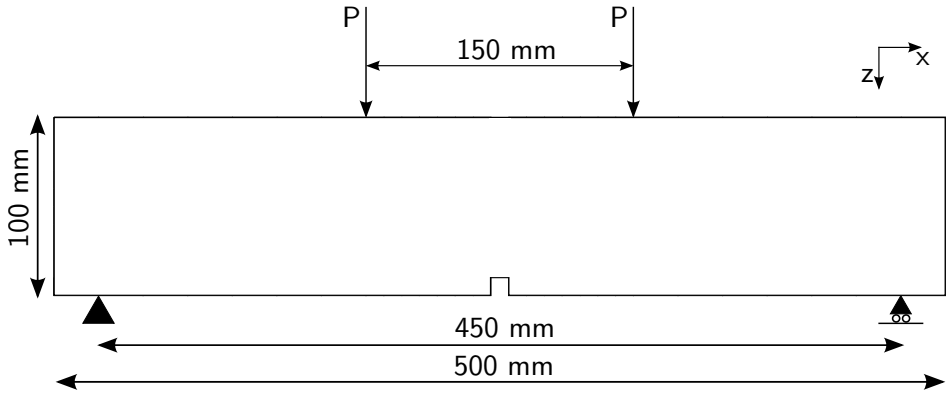

Figure 6.1: Notched beam geometry.

The spatial fluctuation of the uncertain parameters is described by 2D-1V homogeneous Gaussian as well as lognormal translation stochastic fields, sample functions of which are generated using Eqs.(4.36, 4.38). Three different values ($b = 1, 10, 100$) of the correlation length parameter b ($= b_1 = b_2$) are used, corresponding to stochastic fields of low, moderate and strong correlation (all values of b are in mm). Based on the assumption of Papadopoulos et al. (2009); Yang and Xu (2008), the same value of correlation length is adopted for both the underlying Gaussian and lognormal translation fields with reasonable accuracy. The number of terms N_j used in the spectral representation series is equal to 20 and the upper cut-off wave numbers $\kappa_{ju}, j = 1, 2$ are equal to 2π, 0.2π and 0.02π for b equal to 1, 10 and 100, respectively.

A mesh convergence study is performed in order to define the appropriate finite element mesh size that combines accuracy and computational efficiency. Stress contours are shown in Fig. 6.2 for a randomly selected realization and for various mesh sizes to illustrate the convergence of the results. As a result of this parametric investigation, a mesh of 1237 nodes and 1156 elements is finally used for the analyses.

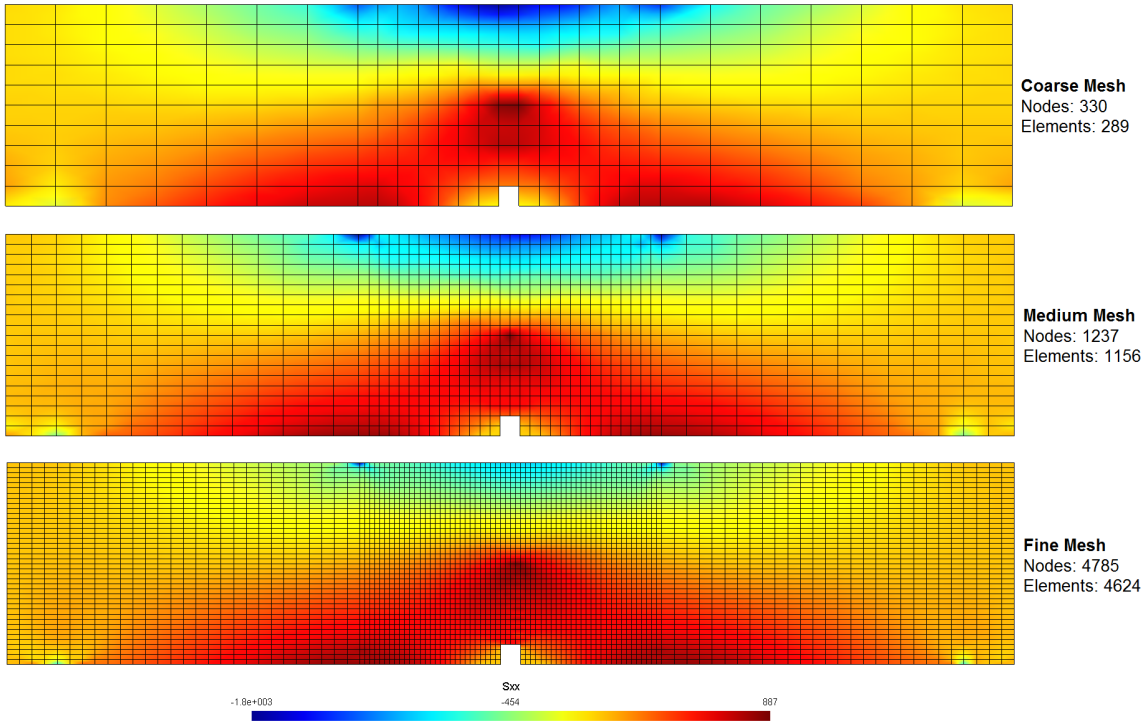

Figure 6.2: Notched beam: Normal stress (σ_{xx}) contours just after the peak load for a randomly selected realization and for different mesh sizes.

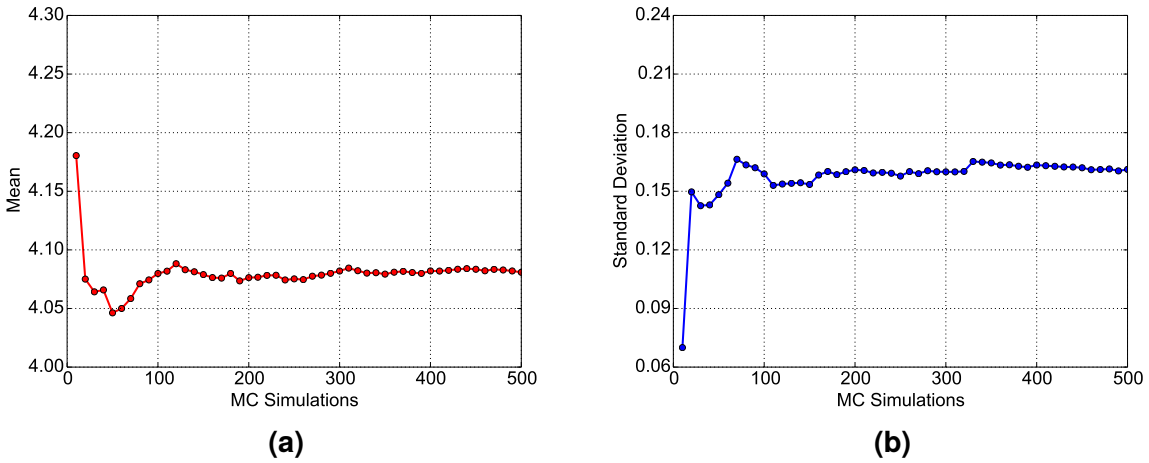

Figure 6.3: Notched beam: Statistical convergence for a) mean and b) standard deviation of the peak load (stochastic G_f with $\sigma = 20\%$ and $b = 100$, lognormal case).

The response variability is computed using MCS with a sample size equal to 500. The statistical convergence achieved within this number of samples is illustrated in Fig. 6.3, where the mean value and standard deviation of the peak load are plotted as a function of the number of Monte Carlo simulations. Load-displacement curves corresponding to a 10% variation of E, G_f with $b = 1$ are shown in Fig. 6.4 for lognormal fields. Moreover, load-displacement curves corresponding to a 20% variation of E, G_f with $b = 100$ are presented in Fig. 6.5 and Fig. 6.6 for Gaussian and lognormal

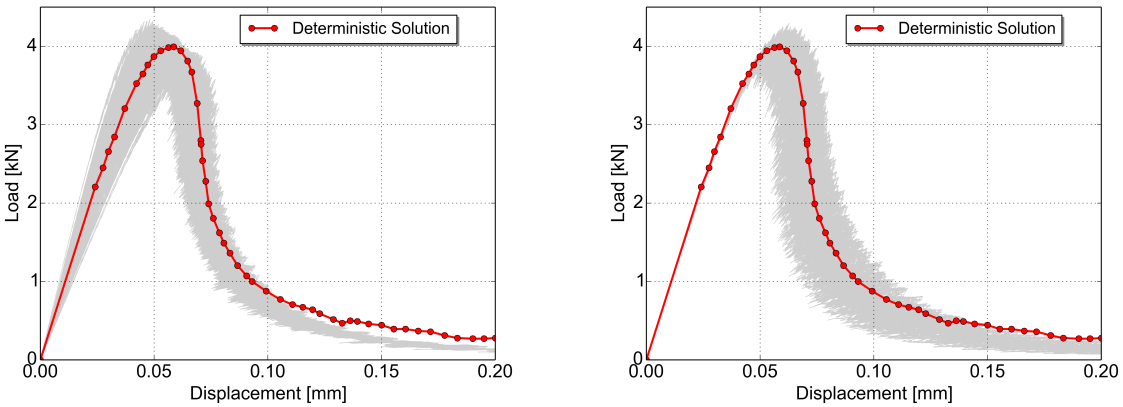

(a) Stochastic E **(b)** Stochastic G_f

Figure 6.4: Notched beam: Load-displacement curves for stochastic parameters E and G_f with $\sigma = 10\%$ and $b = 1$ (Lognormal case).

fields, respectively. The effect of probability distribution is rather important in this case. Comparisons with the deterministic nonlinear solution of (Rots and Invernizzi, 2004) are also provided in these figures.

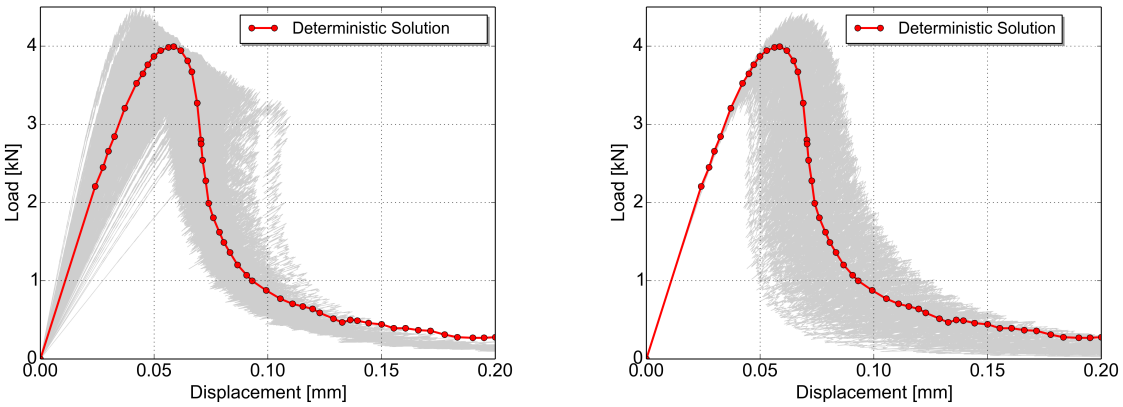

(a) Stochastic E **(b)** Stochastic G_f

Figure 6.5: Notched beam: Load-displacement curves for stochastic parameters E and G_f with $\sigma = 20\%$ and $b = 100$ (Gaussian case).

As shown in Figs. 6.4a - 6.6a, the variation of E affects the stiffness of the structure. The Gaussian assumption leads to a significant, unrealistic reduction of the stiffness in some cases (Fig. 6.5a). Larger values of the coefficient of variation and of the correlation length of the stochastic fields lead to more significant variability of the load-displacement curves, as expected (Figs. 6.5, 6.6). In the case the probability of failure p_f of the beam is defined as the probability of the peak load not exceeding that of the deterministic solution (which means that the structure fails at a smaller load), then p_f is equal to 16% and 31% for the cases described in Figs. 6.4b, 6.6b, respectively.

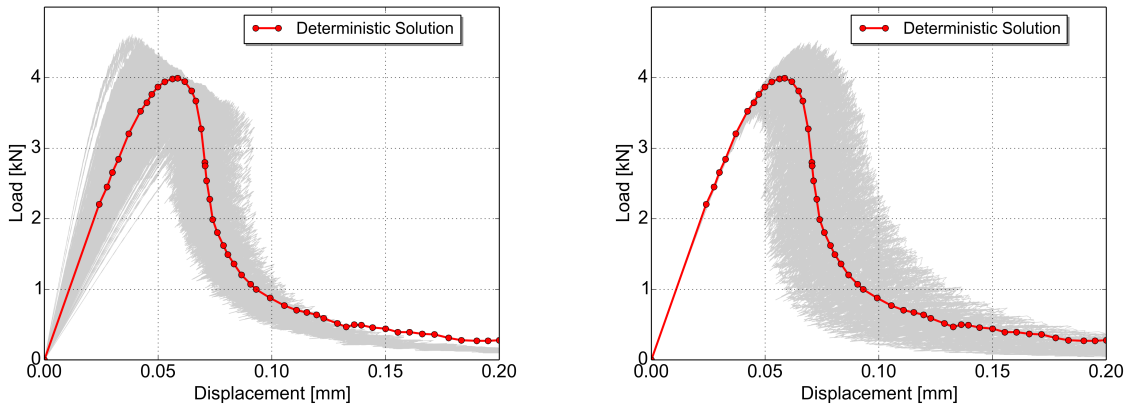

(a) Stochastic E **(b)** Stochastic G_f

Figure 6.6: Notched beam: Load-displacement curves for stochastic parameters E and G_f with $\sigma = 20\%$ and $b = 100$ (Lognormal case).

Variability Response Function

The response variability can also be determined using the concept of VRF. This function has been computed using the fast MCS procedure described in Section 4.6.3.2 for each pair of wave numbers $\hat{\kappa}_1$ and $\hat{\kappa}_2$, where $\hat{\kappa}_1, \hat{\kappa}_2 \in [0, 1, 2, \ldots, 20]$.

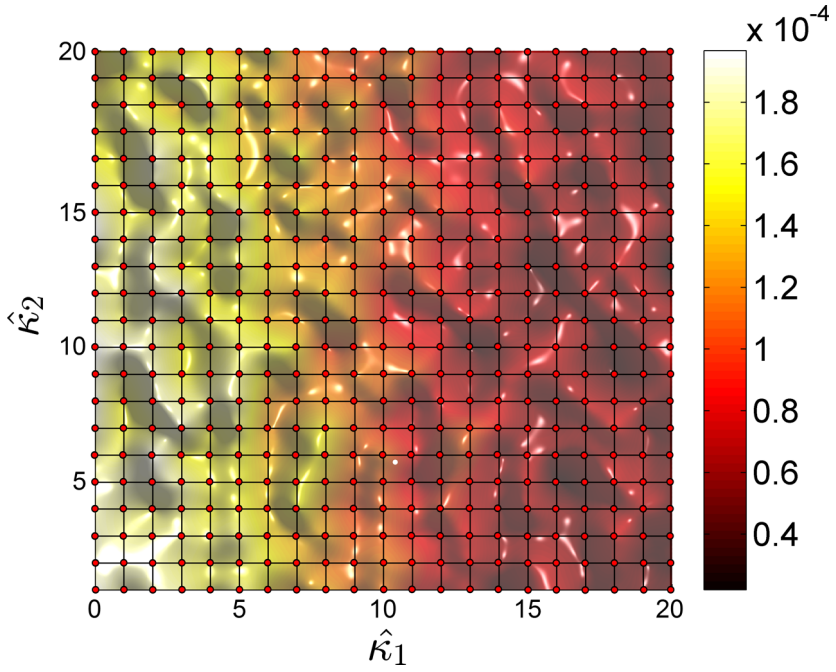

Figure 6.7: VRF calculation in the discrete space $\hat{\kappa}_1, \hat{\kappa}_2$.

The VRF (after smoothing) is shown in Fig. 6.8 for stochastic Young's modulus. Due to its quadrant symmetry, only a quarter of this function is shown in the figure. It is worth noting the irregular shape of the VRF, which can be attributed to the "rippled" load-displacement curves used for its computation. In addition, the computation of VRF through fast MCS has been more expensive than direct MCS in this case (where

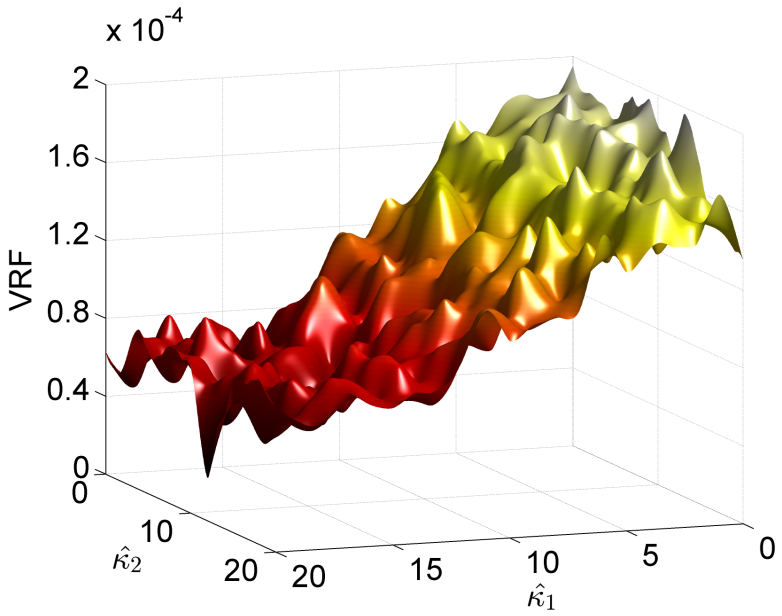

Figure 6.8: Variability response function of displacement at peak load.

a small number of MC samples is generated). This is due to the fact that the whole load-displacement curve is computed for each wave number pair in the fast MCS procedure (cf. Section 4.6.3.2). Using the VRF approach, the upper bound of the standard deviation of the displacement at the monitoring point is computed from Eq. 4.60 as 0.0028 for $\sigma_f = 0.2$.

6.1.2 A double-edge notched specimen

As a second example, the double-edge notched specimen under tension (Nguyen, 2008; Shi et al., 2000) shown in Fig. 6.9 is analyzed. The specimen is fixed in both directions at the bottom edge, and in horizontal direction at the top edge. The numerical analyses were carried out using four-node quadrilateral finite elements. The uncertain parameters of the problem are again the Young's modulus E, tensile strength f_t and fracture energy G_f of the material with mean values equal to 24 GPa, 2.4 MPa and 0.059 N/mm, respectively.

The spatial fluctuation of the uncertain parameters is described by 2D-1V homogeneous lognormal translation fields. Three different values ($b = 1.2, 12, 120$) of the correlation length parameter b proportional to the dimensions of the structure are used, corresponding to stochastic fields of low, moderate and strong correlation. The values of N_j, $\kappa_{ju}, j = 1, 2$ are the same with those of the first example. Sample functions of a lognormal field for $\sigma = 20\%$ and $b = 1.2$, $b = 120$ are shown in Figs. 6.10a, 6.10b, respectively.

The case of anisotropic correlation ($b_1 \neq b_2$) has also been examined to highlight its effect on the response variability, which is computed using direct MCS with a sample size equal to 500. The statistical convergence achieved within this number of samples is illustrated in Fig. 6.11 where the mean value and standard deviation of the peak load are plotted as a function of the number of Monte Carlo simulations.

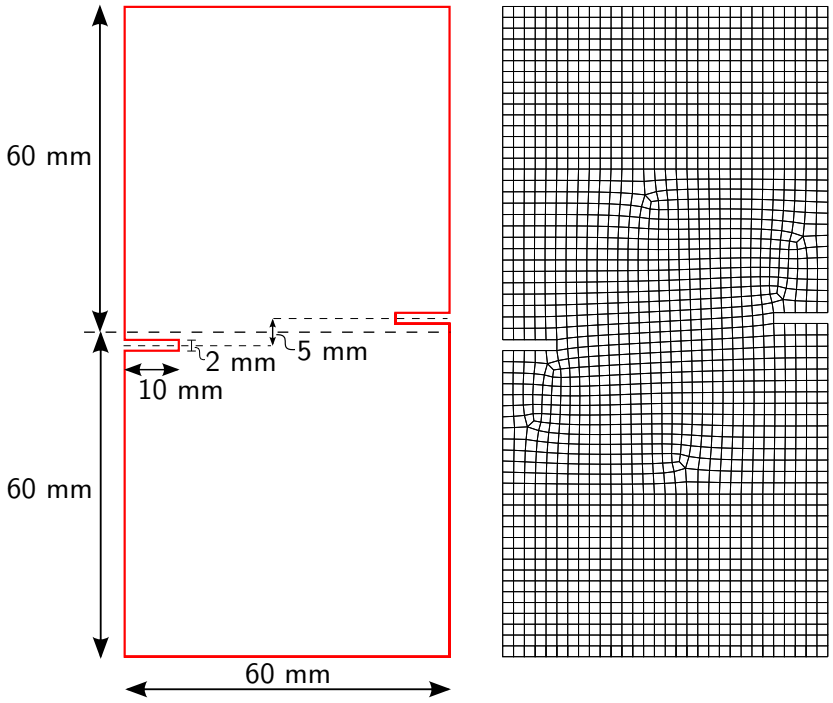

Figure 6.9: Double-edge notched specimen (Geometry and FE mesh with 1950 nodes and 1850 elements).

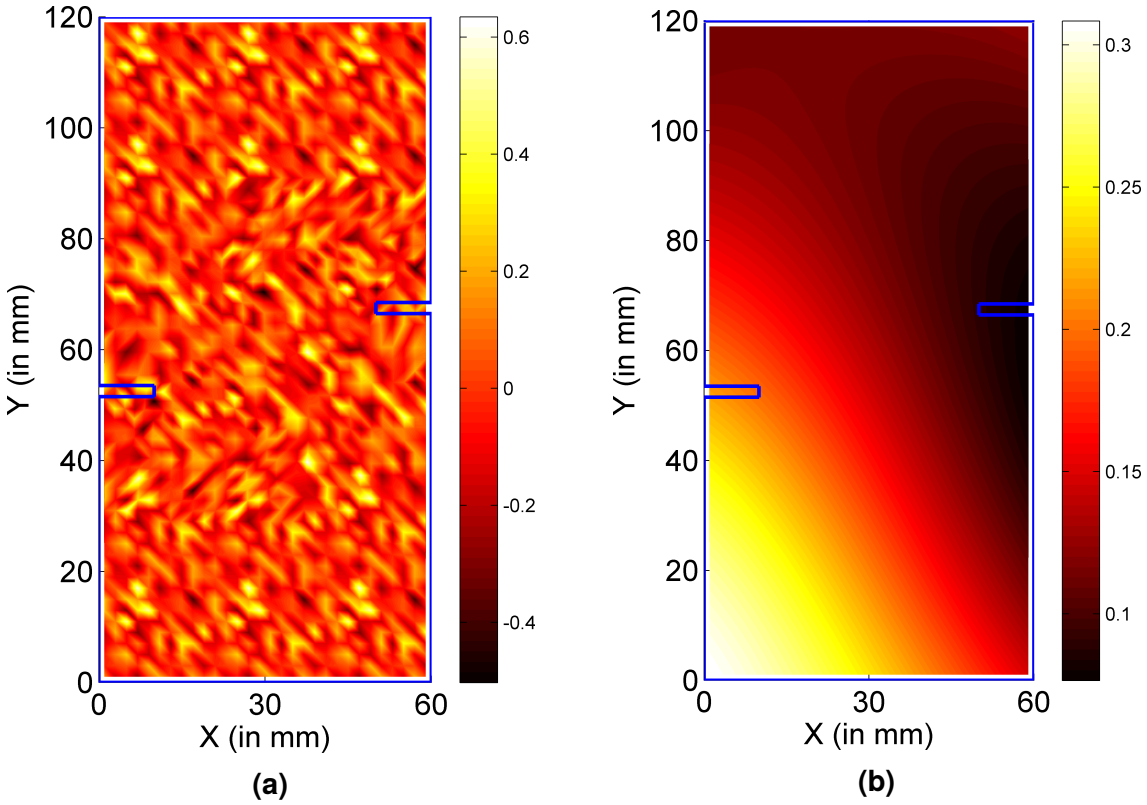

Figure 6.10: Notched specimen: Realizations of a lognormal field for $\sigma = 20\%$ and (a) $b = 1.2$, (b) $b = 120$.

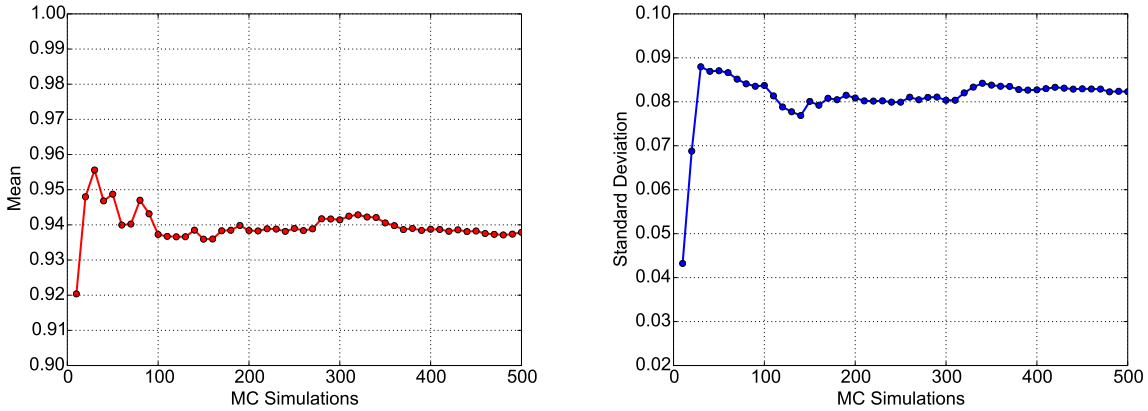

Figure 6.11: Notched specimen: Statistical convergence for a) mean and b) standard deviation of the peak load (E, f_t, G_f fully correlated with $\sigma = 10\%$ and $b = 120$, lognormal case).

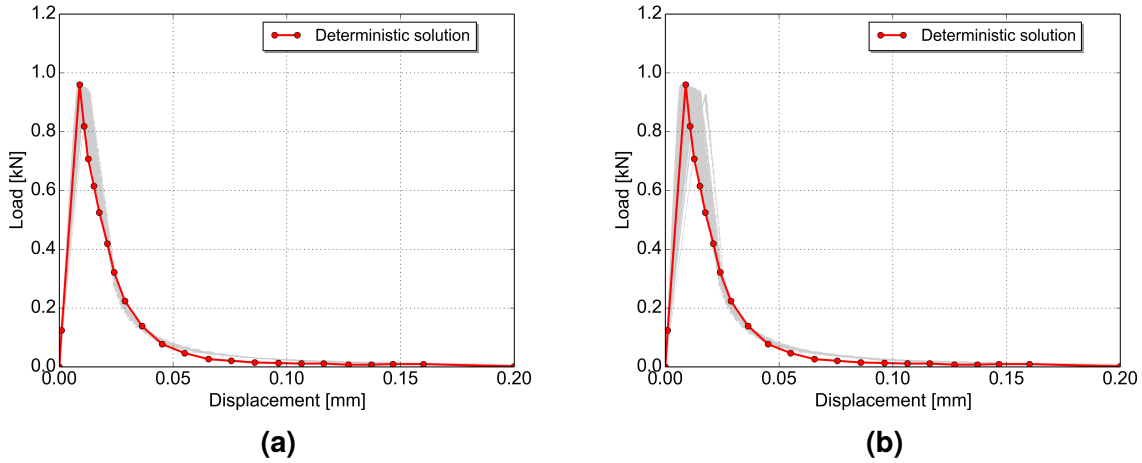

Figure 6.12: Notched specimen: Load-displacement curves for stochastic parameter E with (a) $\sigma = 10\%$ and (b) $\sigma = 20\%$ (lognormal case, b = 120).

Figs. 6.12, 6.13 show the load-displacement curves obtained from different stochastic simulations with variable E, G_f. Comparisons with the deterministic nonlinear solution of (Nguyen, 2008) are provided in these figures. The results obtained with the assumption of anisotropic correlation were very similar and therefore isotropic correlation ($b = b_1 = b_2$) is finally adopted.

As a final step, two cases of combined variation of E, f_t, G_f are considered. In the first case, the lognormal stochastic fields representing the three parameters are fully correlated while in the second case there is no cross-correlation between them. The corresponding load-displacement curves shown in Fig. 6.14 are highly variable and thus lead to a large probability of failure of the structure. For $b = 1.2$, the peak load of all realizations is smaller than the deterministic one, while p_f is equal to 87% and 61% for $b = 12$ and 120, respectively (case of fully correlated properties).

Finally, crack patterns for a randomly selected realization and for different values of correlation length b are shown in Fig. 6.15 (the crack paths are formed by elements with zero stiffness at the end of SLA). The unrealistic crack pattern obtained for

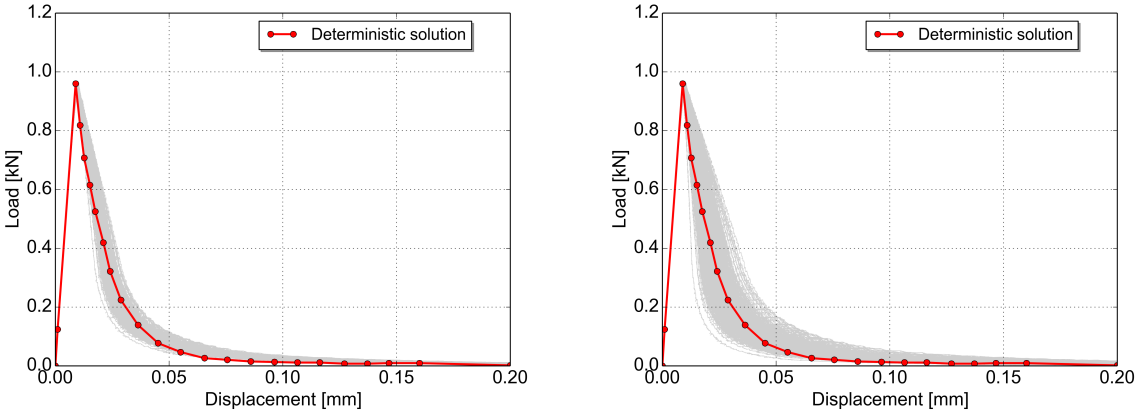

Figure 6.13: Notched specimen: Load-displacement curves for stochastic parameter G_f (a) $\sigma = 10\%$ and (b) $\sigma = 20\%$ (lognormal case, b = 120).

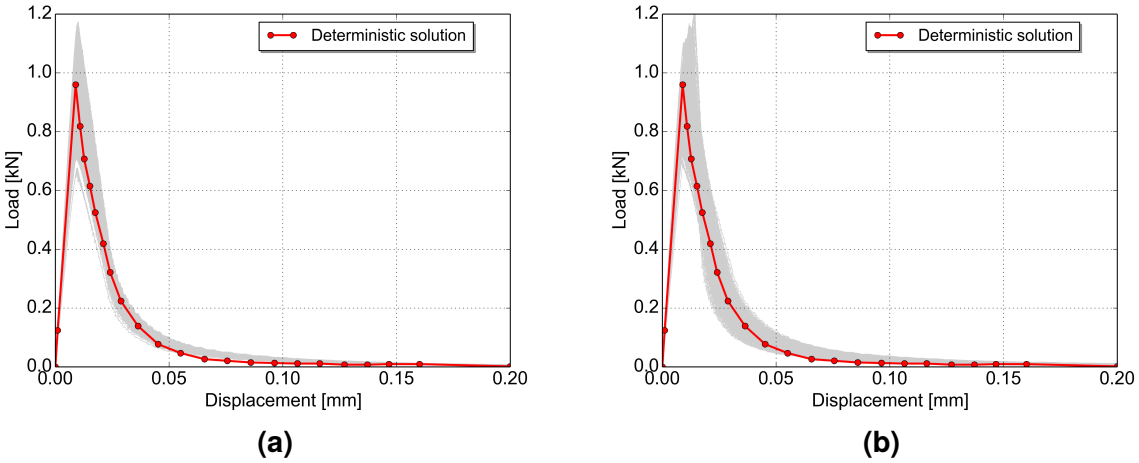

Figure 6.14: Notched specimen: Load-displacement curves for combined variation of the three parameters for $\sigma = 10\%$ (lognormal case, b = 120): (a) E, f_t, G_f fully correlated, (b) E, f_t, G_f uncorrelated.

$b = 1.2$ is due to the high variability of the elastic modulus in this case which leads to neighboring elements with substantially different E.

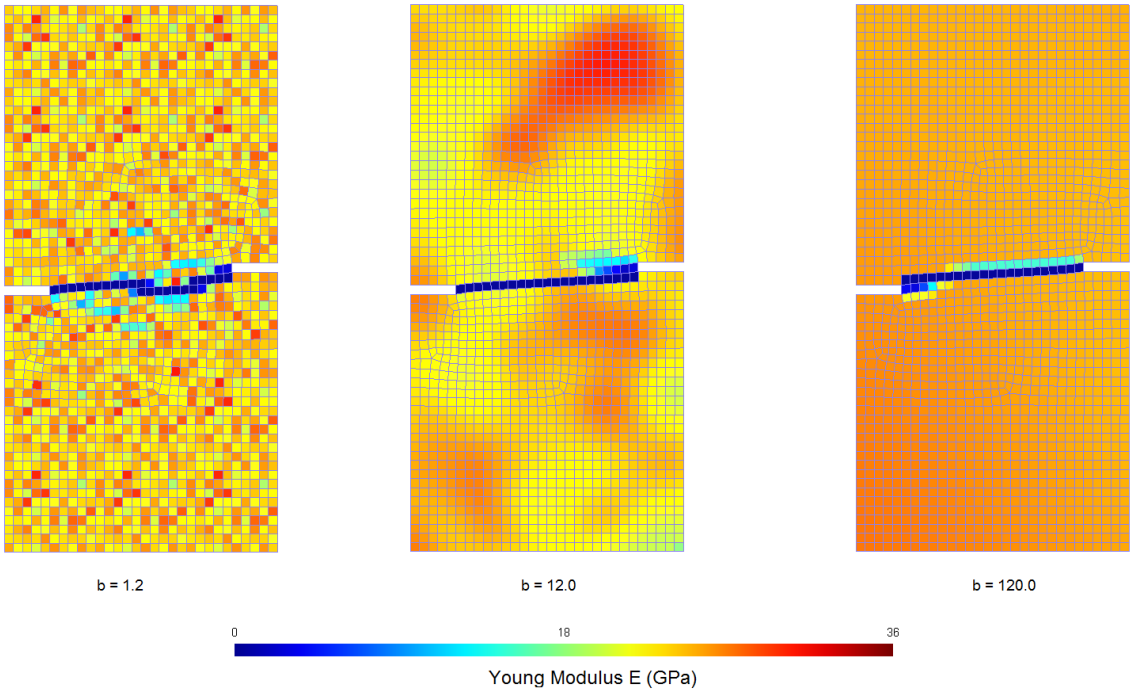

Figure 6.15: Notched specimen: Crack paths for a randomly selected realization and for different values of correlation length b (E, f_t, G_f fully correlated).

6.2 Optimization results

In the second part of this thesis, a fillet from a steel structural member (Stolarska et al., 2001) is analyzed to illustrate the capabilities of the proposed methodology described in Section 5.1.4. The geometry, loading conditions, and design variables of the structural component are shown in Fig. 6.16. Four-node linear quadrilateral elements under plane stress conditions with constant thickness equal to 5 mm and isotropic material properties are assumed. For the purposes of this thesis, two boundary conditions are considered; in the first one, designated as *fillet rigid*, all nodes of the bottom edge are fixed while in the second one, denoted as *fillet flexible*, the two end nodes of the bottom edge of the component are fixed.

For both test examples deterministic and probabilistic shape optimization problems are solved. The objective function to be minimized, corresponds to the material volume for both, while two sets of constraints are enforced, i.e. deterministic and probabilistic constraints on the fatigue cycles. Furthermore, due to manufacturing limitations the design variables are treated as discrete in the same way as in single objective design optimization problems with the discrete version of evolution strategies (Lagaros et al., 2004). The design variables correspond to the dimensions of the structural component taken from Table 6.1. The design load P (see Fig. 6.16), is applied as a concentrated tensile load at the midpoint of the top edge and is equal to 20 KN.

It is common in probabilistic analysis to distinguish between uncertainty that reflects the variability of the outcome of a repeatable experiment and uncertainty due to ignorance. The last one is sometimes referred as “randomness”, commonly known

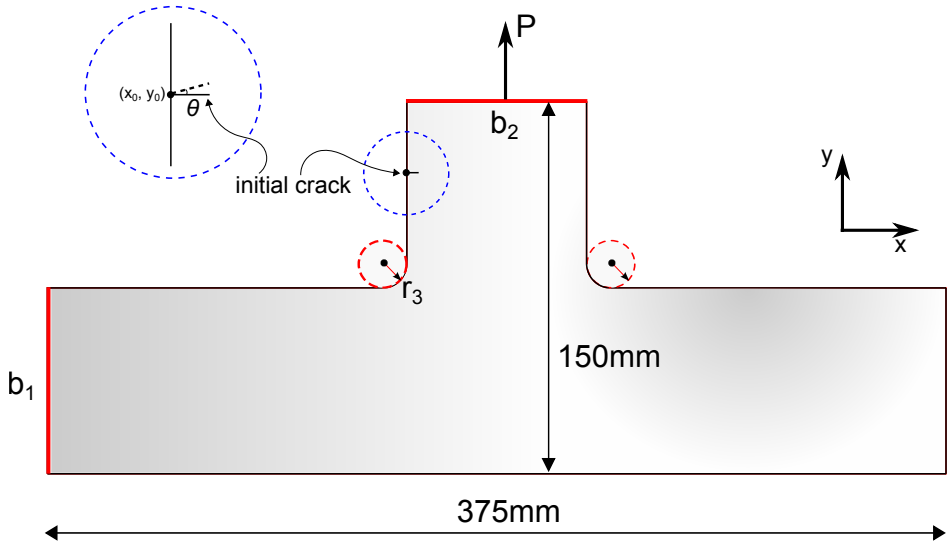

Figure 6.16: Fillet geometry, loading and design variables of the problem.

Design variable	l_{up}	l_{low}	step
b_1	100.0	50.0	1.0
b_2	100.0	50.0	1.0
r_3	30.0	10.0	1.0

Table 6.1: Upper and lower bounds of design variables and corresponding steps (in mm).

as "aleatoric uncertainty" , which cannot be reduced. However, both deterministic and probabilistic approaches rely on various model assumptions and model parameters that are based on the current state of knowledge on the behavior of structural systems under given conditions. There is uncertainty associated with these conditions, which depends upon the state of knowledge that is referred as "epistemic uncertainty".

In this thesis various sources of uncertainty are considered: on crack tip initialization (aleatoric randomness) which influences the shape of the crack propagation path and on modeling (epistemic uncertainty) which affects the structural capacity. The structural stiffness is directly connected to the Young modulus E, of the structural steel, while the number of fatigue cycles is influenced by the material properties C and m. The crack length increment Δa and the poison ratio and fracture toughness are taken equal to 5.0mm, 0.3 and 100MPa/$\sqrt{m}$ respectively, treated as deterministic.

Hence, for the structural component five random variables are used, i.e. the ordinate y_0 of the crack tip initialization and the corresponding angle θ along (see Fig. 6.16) with the Young modulus E and the parameters C, m. The material properties for the structural steel of the component are implemented as independent random variables whose characteristics were selected according to Ellingwood et al. (1980); Ellingwood and Galambos (1982) and are given in Table 6.2.

The numerical study that follows comprises two parts: in the first part a parametric investigation is performed in order to find the number of simulations required for computational efficiency and robustness regarding the calculation of the statistical

Random variable	μ	σ	COV	distribution type
y_0 (in mm)	$(150 - b_1)/(2 + b_1)$	-	5%	normal
θ (in degrees)	0.0	0.50	-	normal
E (in GPa)	207.0	35.19	17%	lognormal
C	2.45e-11	4.16e-12	17%	lognormal
m	2.37	0.40	17%	lognormal

Table 6.2: Random variables with the type of distribution and each statistical parameters: mean value (μ) and standard deviation (σ).

quantities required and the identification of the most appropriate one that can be used in order to characterize the influence of randomness on the fatigue cycles. In the second part, performance of structural components under fatigue is investigated within a probabilistic shape design optimization framework.

6.2.1 Parametric investigation

For the purpose of the parametric investigation the fillet rigid case was examined and three designs, corresponding to the upper (Design 1), lower (Design 3) bounds of the designs variables and an intermediate one (Design 2) are chosen. The scope of this investigation is to find the lower number of simulations for a reliable calculation of certain statistical quantities that are related to the number of fatigue cycles. To this end, Monte Carlo (MC) simulations based on LHS (see Appendix A) are performed for the three designs described above and the mean, median and standard deviation of the number of fatigue cycles are calculated (see Table 6.3).

Design	MCS	mean	median	std. dev.
Design 1	100	5382911.9	6895308.5	3176784.9
Design 1	200	6848983.6	7024024.0	11271233.5
Design 1	500	6568327.3	7026526.0	13717577.0
Design 1	1000	6533674.8	7026013.0	19043699.3
Design 2	100	90222.3	91794.2	27363.2
Design 2	200	94371.9	86020.0	28170.8
Design 2	500	96950.6	93982.8	109963.6
Design 2	1000	95214.8	94768.0	60920.3
Design 3	100	5260.5	4858.5	1141.3
Design 3	200	5371.9	4992.9	1308.9
Design 3	500	5369.6	5005.9	1278.3
Design 3	1000	5328.8	5360.0	994.2

Table 6.3: Statistical quantities of the parametric investigation for the three designs.

The performance of the different number of MC samples is depicted in the histograms of Fig. 6.17. For the purpose of this investigation, the three designs are subjected to the ensemble of different number of simulations (100 + 200 + 500 + 1000). Thus, 5400 XFEM analyses have been postprocessed in order to create a response databank with the quantities of interest. The propagation of uncertainties is

performed by means of the MC simulation method in connection to the LHS technique which has been incorporated into the XFEM framework as described in Section 5.1.4. According to LHS a given design is run repeatedly, for each MC simulation using different values for the uncertain parameters, drawn from their probability distributions as provided in Table 6.2. It is worth mentioning that the characteristic mesh size generated for the nested XFEM analysis in both probabilistic analysis and optimization cases, is kept constant in the region of the crack path.

The group of histograms Fig. 6.17 show the probabilistic distribution of the fatigue cycles values N_c, for different number of MC simulations implemented into XFEM and for the three designs. The frequency on the occurrence of the number of fatigue cycles value is defined as the ratio of the number of simulations, corresponding to limit state values in a specific range, over the total number of simulations (N_{tot}). N_{tot} is equal to 100, 200, 500 or 1000 depending on the number of simulations used in each case.

Comparing the histograms of Fig. 6.17, it can be noticed that the width of the confidence bounds corresponding to the intermediate design is narrower compared to the other two, while for the case corresponding to the upper bounds of the design variables there are two zones of concentration for the frequency values. Furthermore, comparing the mean versus median values of the number of fatigue cycles, the median value is considered more reliable since it is not influenced by the extreme lower and upper values obtained. Specifically, in the framework of an optimization problem where such values might be often encountered due to search procedure that might also lead to extreme designs. Concluding, 200 LH simulations were considered as an acceptable compromise between computational efficiency and robustness. To this extend an equal number of simulations are applied for the solution of the probabilistic formulation of the shape optimization problem which is described in the second part of this study.

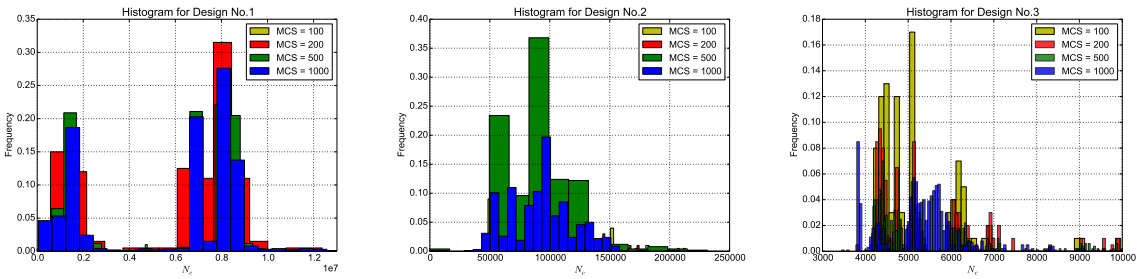

Figure 6.17: Histograms of each design

The influence of the uncertain variables on the shape of the crack propagation paths is depicted in Figs. 6.18 - 6.20, with the cloud of the typical crack paths obtained for 200 simulations. A crack path is defined as typical, if its shape is similar to deterministic one (Stolarska et al., 2001). Especially, for Design 1, due to its geometric characteristics, many not typical crack paths were obtained, however only the typical ones are shown in Fig. 6.18. This is an additional reason for choosing the median versus mean value as the statistical quantity to be incorporated into the probabilistic formulations of the problems studied in the following sections of this thesis.

From the results obtained, it can be concluded that the crack paths obtained by

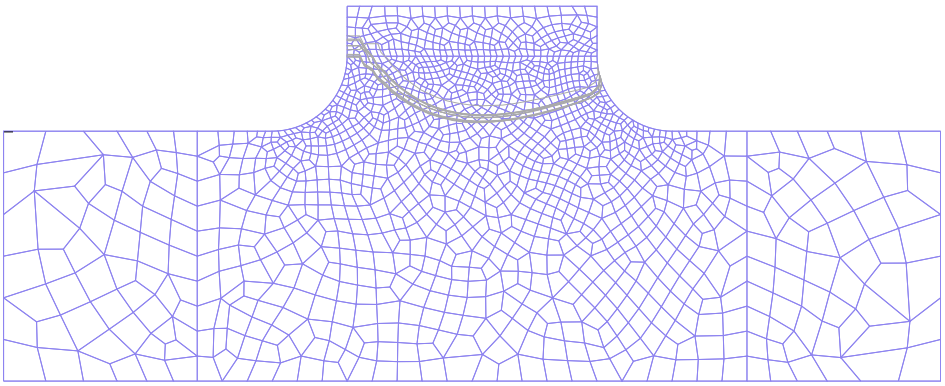

Figure 6.18: Design 1.

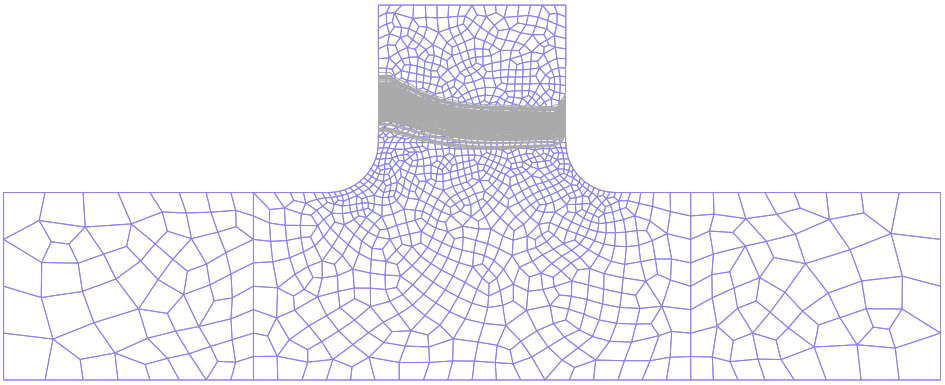

Figure 6.19: Design 2.

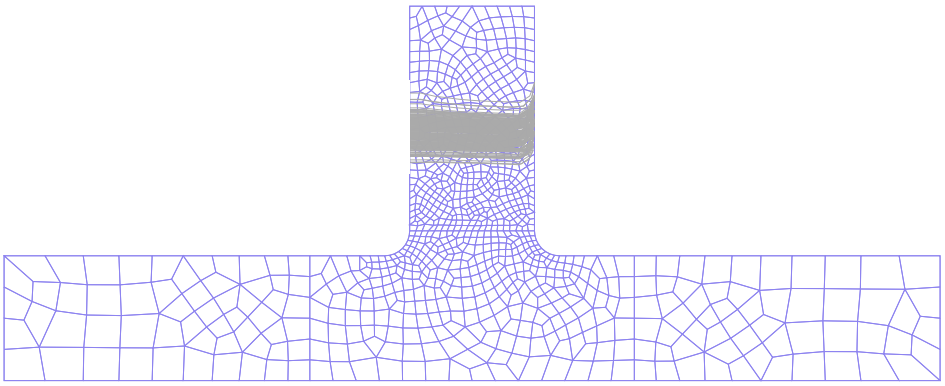

Figure 6.20: Design 3.

means of XFEM is highly in influenced by the random parameters considered in this study, thus the importance of incorporating them into the design procedure is examined in the following part.

6.2.2 Design optimization process

After the parametric investigation, four optimization problems are solved with the differential evolution (DE) metaheuristic optimization algorithm. The abbreviations DET$*$K and PROB$*$K correspond to the optimum designs obtained through a deterministic (DET) and probabilistic (PROB) formulation where the lower number of fatigue

cycles allowed is equal to $*$ thousands. The optimization process that is based on the integration of XFEM into a deterministic and a probabilistic formulation of structural shape optimization is shown in Fig. 6.21. Within each design iteration of the search process there is a nested crack growth analysis loop performed for each candidate optimum design. Thus, a complete crack growth analysis is conducted until the failure criterion is met, i.e. $K_{eq} < K_c$ and the corresponding service life is evaluated (see Section 3.1.8) in order to assess the candidate optimum design.

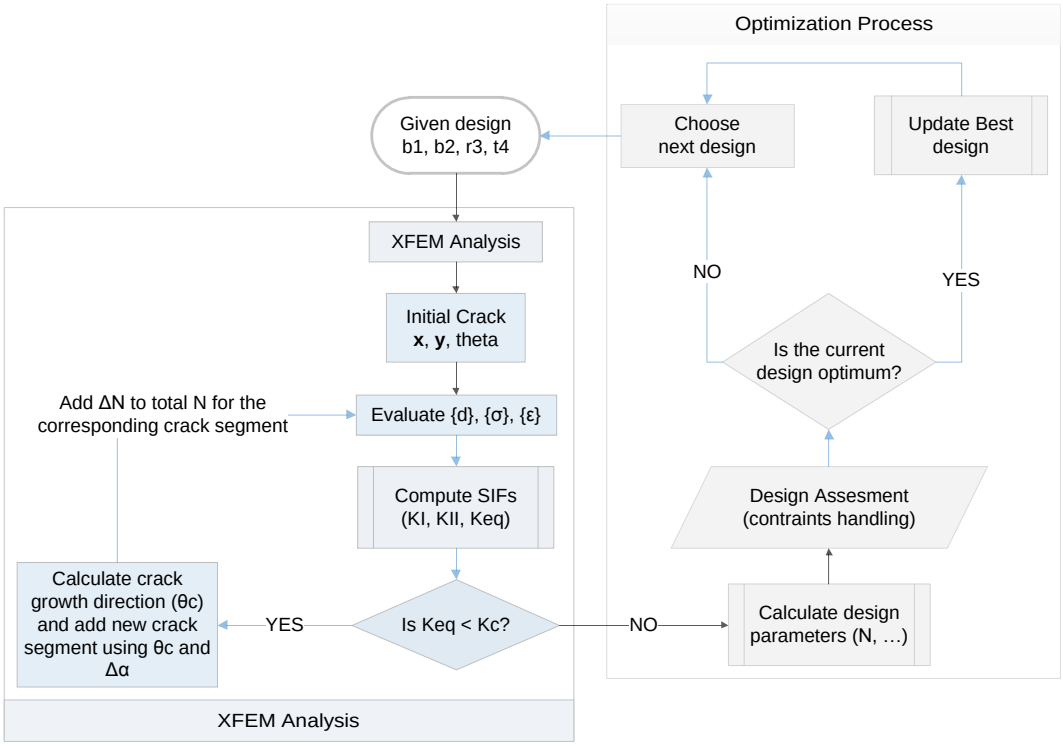

Figure 6.21: XFEM shape optimization process for deterministic and probabilistic formulation.

The parameters used for the DE algorithm are as follows: population size $NP = 30$, the probability $CR = 0.90$ and the mutation factor $F = 0.60$. For comparative reasons the method adopted for handling the constraints and the termination criterion is the same for all test cases. In particular, the simple yet effective, multiple linear segment penalty function (Lagaros and Papadrakakis, 2012) is used in this thesis for handling the constraints. According to this approach if no violation is detected, no penalty is imposed on the objective function. If any of the constraints is violated, a penalty, relative to the maximum degree of constraints violation, is applied to the objective function. The optimization procedure is terminated when the best value of the objective function in the last 30 generations remains unchanged.

6.2.3 Fillet rigid

The fillet rigid structural component examined in the previous section is the first test example of this study. For this case two groups of formulations: the deterministic, described in Eq. (6.2) and the probabilistic, defined in Eq. (6.3), respectively. N_{min} was taken equal to 100, 200 and 500 thousands of fatigue cycles and the objective function to be minimized is the material volume V.

$$\begin{aligned} \text{min:} \quad & V(b_1, b_2, r_3) \\ \text{subject to:} \quad & N(b_1, b_2, r_3) \geq N_{min} \\ & 50.0 \leq b_1 \leq 100.0, \\ & 50.0 \leq b_2 \leq 100.0, \\ & 10.0 \leq r_3 \leq 30.0 \end{aligned} \tag{6.2}$$

$$\begin{aligned} \text{min:} \quad & V(b_1, b_2, r_3) \\ \text{subject to:} \quad & \bar{N}(b_1, b_2, r_3, y_0, \theta, E, C, m) \geq N_{min} \\ & 50.0 \leq b_1 \leq 100.0, \\ & 50.0 \leq b_2 \leq 100.0, \\ & 10.0 \leq r_3 \leq 30.0, \\ & y_0 \sim N((150 - b_1)/(2 + b_1), COV = 5\%) \\ & \theta \sim N(0, 0.50) \\ & E \sim lnN(207.0, 35.19) \\ & C \sim lnN(2.45^{-11}, 4.16^{-12}) \\ & m \sim lnN(2.37, 0.40) \end{aligned} \tag{6.3}$$

DE managed to reach optimum designs as shown in Figs. 6.22 - 6.23 together with its optimization history for the deterministic and probabilistic formulation respectively. Comparing the optimization histories shown in these figures the probabilistic formulations require less generation steps compare to the deterministic one, probably, due to the narrower feasible design set of the probabilistic formulation. The optimized designs achieved are presented in Table 6.4 along with the material volume, while the shapes of deterministic optimized designs are shown in Figs. 6.24 - 6.26. Also, the clouds of crack patterns are shown in Fig. 6.27 for DET100, DET200 and DET500 cases respectively.

Comparing the three designs (see Table 6.4) by means of the deterministic formulation it can be said that the material volume of DET500K is increased by 33% and 28% compared to DET100K and DET200K respectively, while that of DET200K is increased by almost 3.5% compared to DET100K. Furthermore, it can be seen that there are differences to almost all design variables considered to formulate the optimization problem. The results obtained for the probabilistic formulation revealed that the material volume of PROB500K is increased by 68% and 43% compared to PROB100K and PROB200K respectively, while that of PROB200K is increased by almost 17.5% compared to PROB100K. In addition, it can be seen that the material volume of designs

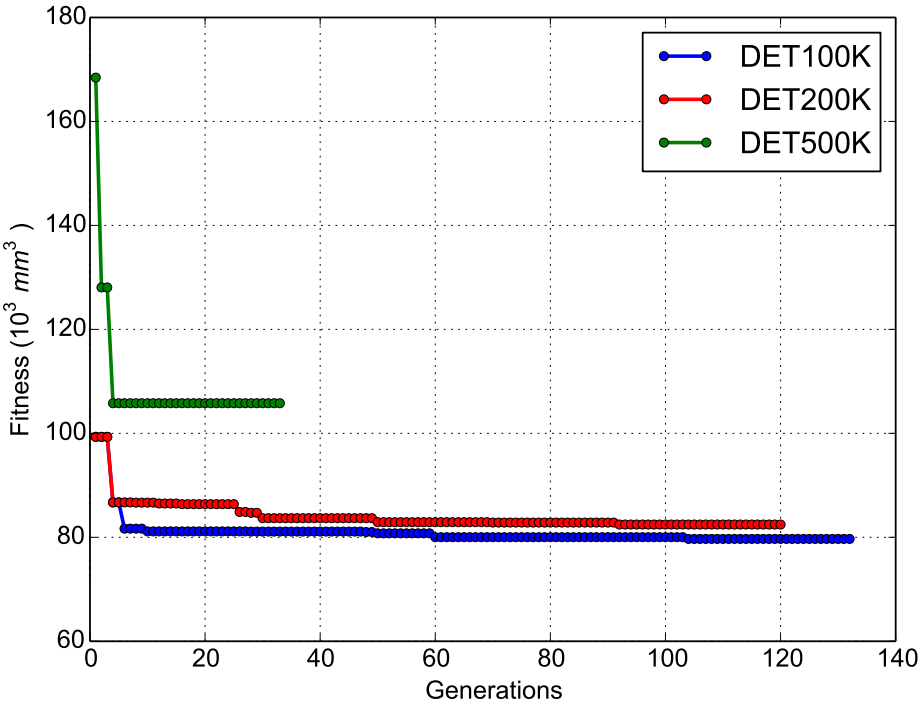

Figure 6.22: Objective function vs Generation for DET case (rigid fillet).

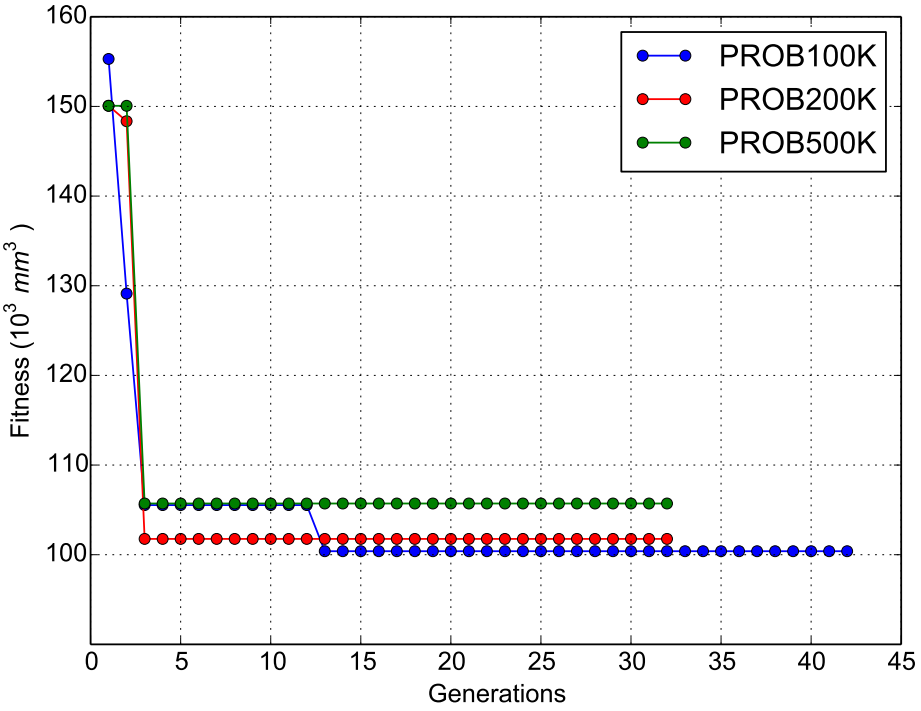

Figure 6.23: Objective function vs Generation for PROB case (rigid fillet).

PROB100K, PROB200K and PROB500K is increased by 26%, 43% and 60% compared to DET100K, DET200K and DET500K, respectively.

In order to justify the formulation of the shape optimization problem considering

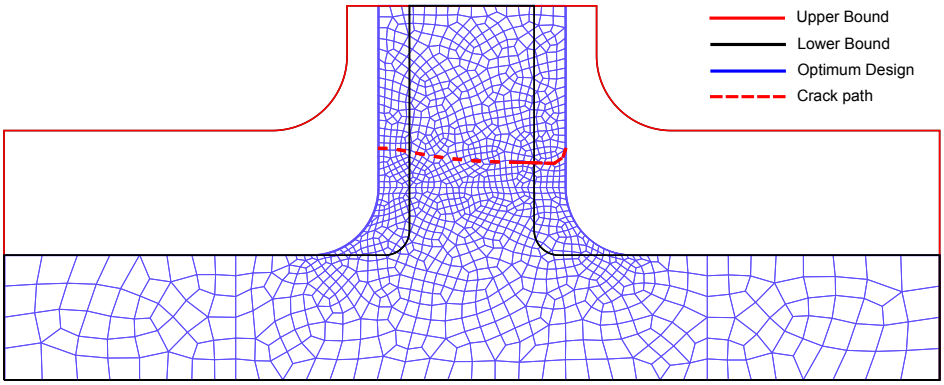

Figure 6.24: Optimum design for deterministic formulation DET100 for rigid fillet.

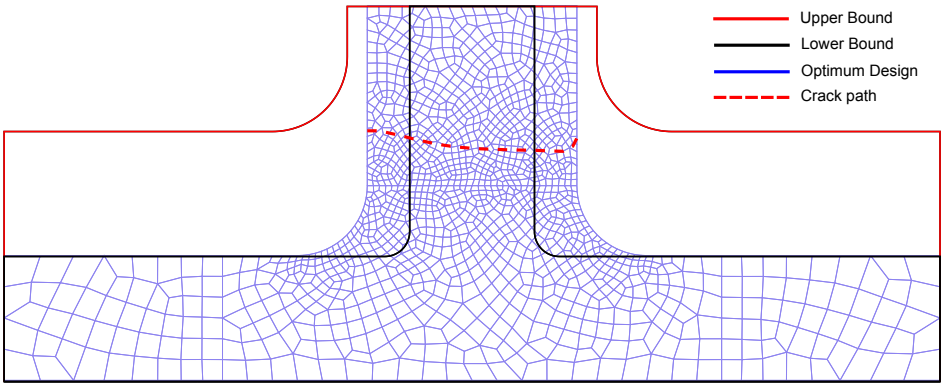

Figure 6.25: Optimum design for deterministic formulation DET200 for rigid fillet.

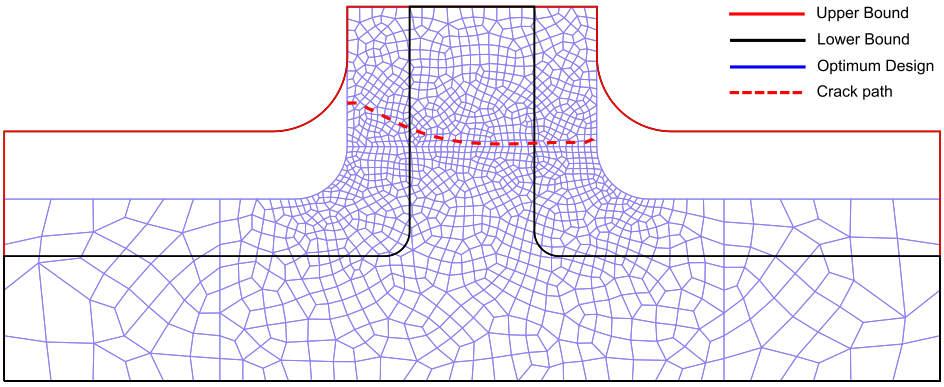

Figure 6.26: Optimum design for deterministic formulation DET500 for rigid fillet.

uncertainties, probabilistic analyses are performed for all six optimized designs obtained through the corresponding problem formulations and the statistical quantities related to the number of fatigue cycles are calculated. These quantities are provided in Table 6.4 and as it can be seen there are cases where deterministic formulation overestimates the number of fatigue cycles compared to the median value when considering uncertainty. It is clear that the mean value of the fatigue cycles is not a reliable statistical quantity since it is highly influenced by the crack behavior.

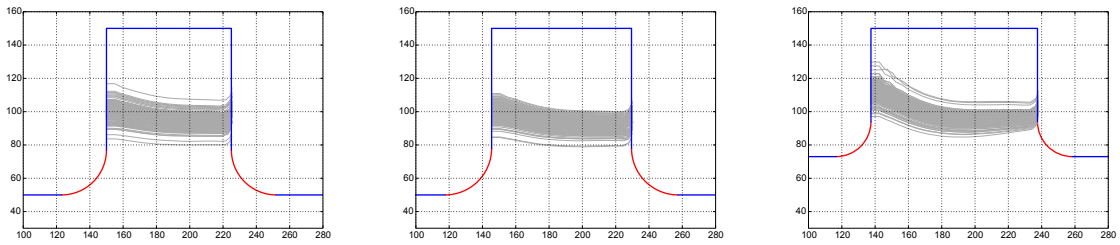

Figure 6.27: Crack patterns for DET100, DET200 and DET500 cases respectively (rigid fillet)

Design	b_1	b_2	r_3	V	$N_c^{(det)}$	$\overline{N}_c$	N_c^{med}	COV (%)
DET100K	50.0	75.0	27.0	79690	136024	99055	106573	30.43
DET200K	50.0	84.0	28.0	82461	201728	261604	198703	36.84
DET500K	73.0	100.0	21.0	105793	553038	506188	505190	33.02
PROB100K	66.0	100.0	27.0	100390	118124	107584	100894	45.14
PROB200K	88.0	100.0	19.0	118065	83143	353434	200288	23.55
PROB500K	100.0	93.0	18.0	169157	498856	269721	554890	47.19

Table 6.4: Optimum design for each problem formulation and corresponding statistical parameters for fillet rigid (MCS = 200).

6.2.4 Fillet flexible

The second test example considered is the fillet flexible test case, where as explained in Section 6.2 the two end nodes of the lower edge of the component are fixed. Similar to the previous test example two groups of optimization problems are formulated in the same way as for the rigid fillet case (see Eqs. (6.2) - (6.3)). In this case, N_{min} was taken equal to 30, 70 and 150 thousands of fatigue cycles and the material volume was considered as the objective function to be minimized in the problem formulation. Again, DE managed to solve the optimization problem and the optimization history is presented in Fig. 6.28 for the case of deterministic formulation and in Fig. 6.29 for probabilistic one, while the optimized designs achieved are presented in Table 6.5 along with the material volume which is the objective function to be minimized.

Design	b_1	b_2	r_3	V	$N_c^{(det)}$	$\overline{N}_c$	N_c^{med}	COV (%)
DET30K	50.0	60.0	26.0	75122	30500	25139	26326	19.81
DET70K	50.0	72.0	25.0	78656	89170	58294	55947	2.44
DET150K	50.0	82.0	25.0	81656	183863	168572	166816	37.95
PROB30K	51.0	63.0	29.0	77170	30694	31383	30250	25.28
PROB70K	50.0	73.0	25.0	78956	70453	70695	70907	21.28
PROB150K	50.0	100.0	19.0	86715	288050	179850	153669	121.66

Table 6.5: Optimum design for each problem formulation and corresponding statistical parameters for fillet flexible (MCS = 200).

In contrast to the rigid fillet case, the increase on the required material volume is much less. In particular, comparing the three designs achieved (see Table 6.5)

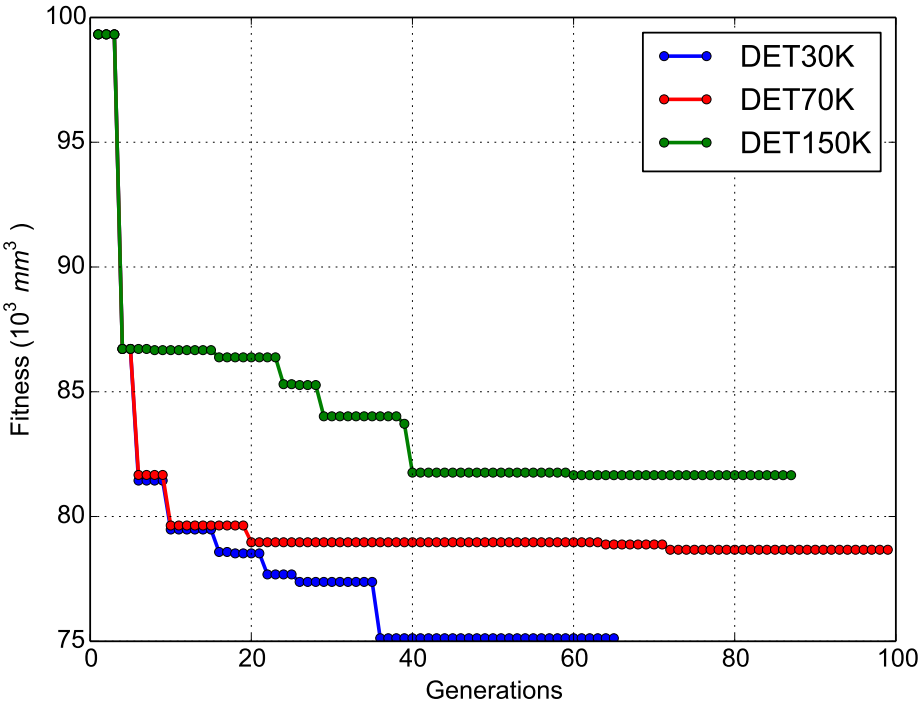

Figure 6.28: Objective function vs Generation for DET case (flexible fillet).

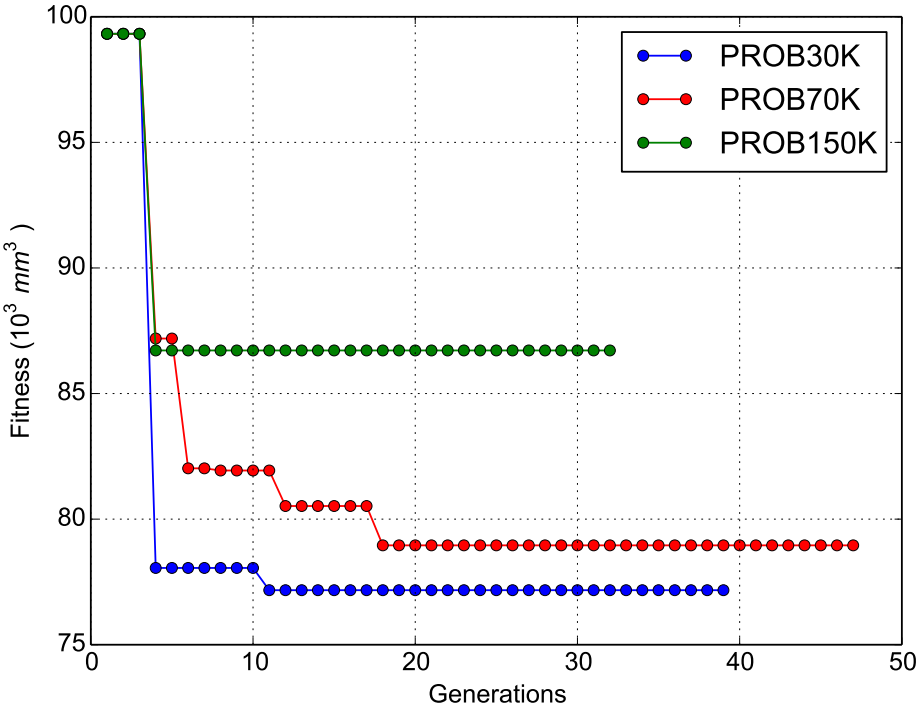

Figure 6.29: Objective function vs Generation for PROB case (flexible fillet).

by means of the deterministic formulation it can said that the material volume of DET150K is increased by 8.7% and 3.8% compared to DET30K and DET70K respectively, while that of DET70K is increased by almost 4.7% compared to DET30K. Fur-

thermore, it can be seen that there are differences to almost all design variables considered to formulate the optimization problem. On the other hand, regarding the probabilistic formulation it can said that the material volume of PROB150K is increased by 12.4% and 9.8% compared to PROB30K and PROB70K respectively, while that of PROB70K is increased by almost 2.3% compared to PROB30K. In addition, it can be seen that the material volume of designs PROB30K, PROB70K and PROB150K is increased by 2.7%, 0.4% and 6.2% compared to DET30K, DET70K and DET150K, respectively.

Again for this case, in order to justify the results obtained by the shape optimization problem considering uncertainties, probabilistic analyses are performed for all six optimized design obtained through the corresponding problem formulations and the statistical quantities related to the number of fatigue cycles are calculated. These quantities are provided in Table 6.5 and as it can be seen there are cases where deterministic formulation overestimates the number of fatigue cycles compared to the median value when considering uncertainty. Furthermore, it can be verified that the mean value of the fatigue cycles is not a reliable statistical quantity since it is highly influenced by the pattern of the crack propagation paths.

This page intentionally left blank

7

Conclusions and recommendations for further work

7.1 Summary and conclusions of the research developed

In this thesis, a unified framework for stochastic analysis and optimum design of structures subjected to fracture developed in the ambit of modern numerical techniques for crack growth simulation mainly based on enriched finite elements methods. This has been done within the context of the stochastic finite element method as well as within a modern optimization environment implementing metaheuristic search algorithms.

In the first part of this thesis, the sequentially linear analysis was implemented in the framework of a stochastic setting to investigate the influence of uncertain spatially varying material properties on the fracture behavior of structures with softening materials. The proposed approach constituted an efficient procedure avoiding the convergence problems encountered in regular nonlinear finite element analysis. The uncertain properties were described by homogeneous stochastic fields using the spectral representation method in conjunction with translation field theory. The response variability was computed by means of direct Monte Carlo simulation method and the influence of the variation of each random parameter as well as of the probability distribution, coefficient of variation and correlation length of the stochastic fields has been quantified. The analysis of two benchmark structures has shown that the load-displacement curves and the probability of failure are strongly affected by the statistical characteristics of the stochastic fields. The extension of SLA to the stochastic framework offers an efficient means to perform parametric investigations of the fracture behavior of structures in the case of variable material properties.

In the second part of this thesis, structural shape optimization problems were formulated for designing structures under fatigue. To this end, the extended finite element method which consists an appropriate framework for the simulation of the fracture process in structures was incorporated into a shape optimization environment. Based on observations of the numerical tests presented the deterministic optimized design is not always a “safe” design, since there are many random factors that affect the design during its lifetime. In order to find a realistic optimized design the designer has to take into account all important random parameters. In this thesis a reliability analysis combined with a structural shape design optimization formulation was pro-

posed where probabilistic constraints were incorporated into the formulation of the design optimization problem. In particular, structural shape optimized designs were obtained, considering the influence of various sources of uncertainty. Randomness on the crack initialization along with the uncertainty on the material properties were also considered. Shape design optimization problems were formulated for two benchmark structures, where the volume of the structural component is minimized subjected to constraint functions related to targeted service life (minimum number of fatigue cycles allowed) when material properties and crack tip initialization are considered as random variables.

Furthermore, a sensitivity analysis of four optimization algorithms based on evolution process was conducted in order to identify the best algorithm for the particular problem at hand to be used for solving the structural shape optimization problem. This sensitivity analysis was carried out in order to examine the efficiency and robustness of four metaheuristic algorithms. Comparing the four algorithms it can be said that evolutionary based algorithms can be considered as efficient tools for single-objective multi-modal constrained optimization problems. In all test cases examined, a large number of solutions need to be found and evaluated in search of the optimum one. The metaheuristics employed in this study have been found efficient in finding an optimized solution.

The applicability and potential of the formulations presented were demonstrated with two benchmark structures. The analysis has shown that with proper shape changes, the service life of structural systems subjected to fatigue loads can be enhanced significantly. Comparisons with optimized shapes found for targeted fatigue life are also performed, while the choice of the position and orientation of initial imperfection was found to have a significant effect on the optimal shapes for the structural components examined.

7.2 Main contributions

The main contributions of this thesis can be summarized in the following:

- proposed an efficient coupled approach (Georgioudakis et al., 2014c; Stefanou et al., 2014) allowing the stochastic crack propagation analysis and highlighting the necessity of it, by quantification of the stochastic behavior.
- developed and implemented a shape optimization framework based on bio-inspired evolution optimization algorithms (Georgioudakis et al., 2014a,b), capable to enhance the service life of structures subjected to fracture, with appropriate changes in the structural geometry,
- demonstrated the feasibility and utility of the developed approaches in problems of a complexity relevant to industrial applications.

7.3 Future research lines

Starting from the research carried out in this thesis, the following future developments aiming at the extension and deepening of some aspects that still remain open are proposed:

Stochastic analysis using the improved version of SLA

Investigate the influence of uncertain spatially varying material properties on the fracture behavior of structures with softening materials, using the impoved version of SLA method (Eliáš et al., 2010; Graça-e Costa et al., 2013, 2012; Slobbe et al., 2012) to solve mixed mode crack propagation problems.

Proof of RVF uniqueness in the case of SLA

An interesting theoretical aspect derived from the present thesis, is the proof of the uniqueness of the VRF described in Section 4.6.3.2. The VRF concept was used as an alternative way for the computation of the response variability in the numerical example of Section 6.1.1.

XFEM with nonlinear material behavior

The high COV values which found from the reliability analysis proposed in Section 6.2.2 emerges the necessity of a robust design formulation for the optimization problem as mentioned in Section 7.1, by minimizing these COV values and find the "real" optimum. This formulation can be also extended to topology optimization problems, in three dimensional settings, with nonlinear material description.

Stochastic failure analysis with inclusions

Use XFEM to model inclusions in the structures whose properties are spatially varying in combination with SFEM, under the same framework presented in Chapter 4 in order to investigate the influence of the inhomogeneities/discontinuities to the response variability of the structures.

This page intentionally left blank

A

Latin hypercube sampling

Latin hypercube sampling (LHS) is a form of stratified sampling (i.e. a method of sampling from a population) and can be applied to one or multiple variables in a stochastic process. The method commonly used to accurately recreate the input distribution through sampling in fewer iterations when compared with the Monte Carlo method. Monte Carlo simulations provide statistical answers to problems by performing many calculations with randomized variables, and analyzing the trends in the output data. LHS can be incorporated into an existing Monte Carlo model fairly easily, and work with variables following any analytical probability distribution.

The feature key behind LHS is that variables are sampled using a technique known as *stratified sampling without replacement* (Iman, 1980), and then randomly combined sets of those variables are used for one calculation of the target function. Stratification divides the cumulative curve into equal intervals on the cumulative probability scale, from 0 to 1.0 (see Fig. A.1a). The number of stratifications of the cumulative distribution is equal to the number of iterations performed. The sampling algorithm ensures that the distribution function is sampled evenly, but still with the same probability trend. LSH proceeds as follows:

- The probability distribution $F(x)$ is split into n intervals of equal probability, where n is the number of iterations that are to be performed on the model. In Figure A.1a, the cumulative curve of a normal distribution has been divided into 20 intervals. The bands can be seen to get progressively wider towards the tails as the probability density drops away (see Fig. A.1b).
- In the first iteration, one of these intervals is selected using a random number.
- A second random number is then generated to determine where, within that interval, $F(x)$ should lie. In practice, the second half of the first random number can be used for this purpose, reducing simulation time.
- $x = G(F(x))$ is calculated for that value of $F(x)$.
- The process is repeated for the second iteration but the interval used in the first iteration is marked as having already been used and therefore will not be selected again.
- This process is repeated for all of the iterations. Since the number of iterations n is also the number of intervals, each interval will only have been sampled once

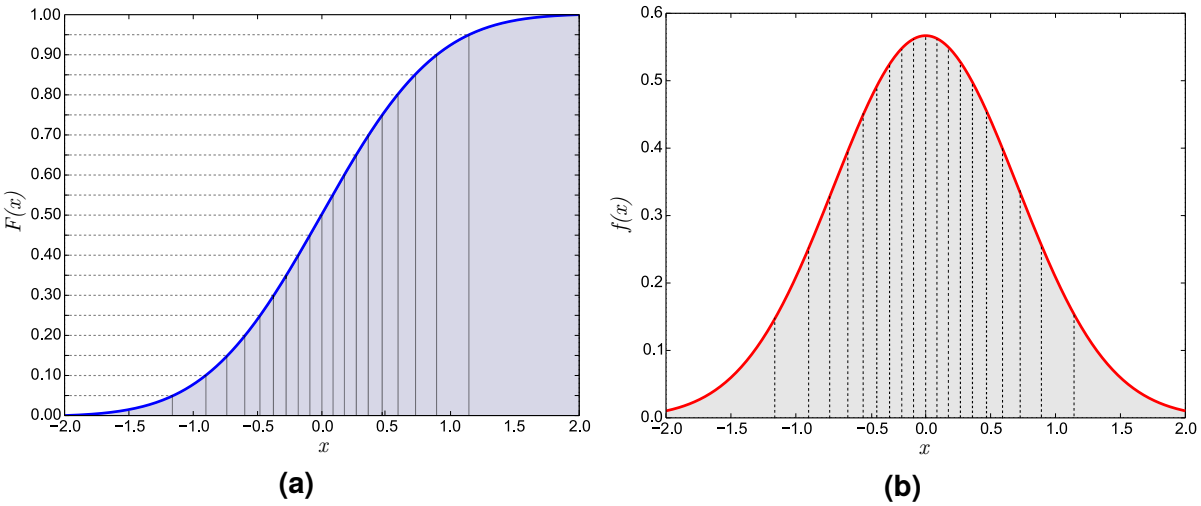

Figure A.1: a) Cumulative Distribution Function $F(x)$ split into $n = 20$ intervals of equal probability and b) corresponding Probability Density Function $f(x)$ for a normal random variable X.

and the distribution will have been reproduced with predictable uniformity over the $F(x)$ range.

The following Python snippet can generate the random picked probabilities within each segment using a uniform distribution, and then mapped to the correct representative value in of the variable's actual distribution. Hence, for a simulation with 500 iterations would split the probability into 500 segments, each representing 0.2% of the total distribution. For the first segment, a number would be chosen between 0.0% and 0.2%. For the second segment, a number would be chosen between 0.2% and 0.4%. This number would be used to calculate the actual variable value based upon its distribution, and so on.

```
from __future__ import division
import random

variableMin = 10
variableMax = 20
iterations = 10
segmentSize = 1 / iterations

for i in range(iterations):
    segmentMin = i * segmentSize
    segmentMax = (i+1) * segmentSize
    point = segmentMin + (random.random() * segmentSize)
    pointValue = (point * (variableMax - variableMin)) + variableMin
    print segmentMin, segmentMax, point, pointValue
```

When using the Latin Hypercube technique to sample from multiple variables, it is important to maintain independence between variables. The values sampled for one variable need to be independent of those sampled for another (unless, explicitly must be correlated). This independence is maintained by randomly selecting the interval to draw a sample from for each variable. This preserves randomness and independence and avoids unwanted correlation between all the variables. So, when sampling a function of N variables, the range of each variable is divided into M equally probable

intervals. Hence, the maximum number of combinations for a LHS of M divisions and N variables (i.e., dimensions) can be computed with the following formula:

$$\left(\prod_{n=0}^{M-1}(M-n)\right)^{N-1} = (M!)^{N-1} \tag{A.1}$$

To conclude, LHS is capable of reducing the number of runs necessary to stabilize a Monte Carlo simulation by a huge factor. Some simulations may take up to 30% fewer calculations to create a smooth distribution of outputs. The process is quick, simple, and easy to implement. It helps ensure that the Monte Carlo simulation is run over the entire length of the variable distributions, taking even unlikely extremities into account as one would desire.

This page intentionally left blank

B

Central Limit Theorem

Central Limit Theorem 1. *Given $X_1, X_2, \ldots$, a sequence of independent and identically distributed random variables with expected value μ_X and variance σ_X^2, the CDF of $Z_n = (\sum_{i=1}^{n} X_i - n\mu_X)/\sqrt{n\sigma_x^2}$ has the property:*

$$\lim_{n\to\infty} F_{Z_n}(z) = \Phi(z) \tag{B.1}$$

where $\Phi(z)$ is the CDF of the standard normal distribution.

This page intentionally left blank

References

Aguirre, A. H., Rionda, S. B., Coello Coello, C. A., Lizárraga, G. L., and Montes, E. M. (2004). Handling constraints using multiobjective optimization concepts. *International Journal for Numerical Methods in Engineering*, **59(15)**:1989–2017.

Allaix, D. L. and Carbone, V. I. (2009). Discretization of 2D random fields: A genetic algorithm approach. *Engineering Structures*, **31(5)**:1111–1119.

Anderson, T. L. (2004). *Fracture Mechanics: Fundamentals and Applications*. CRC Press, Boca Raton, FL, 3rd edition.

Armero, F. and Garikipati, K. (1996). An analysis of strong discontinuities in multiplicative finite strain plasticity and their relation with the numerical simulation of strain localization in solids. *International Journal of Solids and Structures*, **33(20–22)**:2863–2885.

Arwade, S. R. and Deodatis, G. (2011). Variability response functions for effective material properties. *Probabilistic Engineering Mechanics*, **26(2)**:174–181.

Bäck, T. (1996). *Evolutionary algorithms in theory and practice: evolution strategies, evolutionary programming, genetic algorithms*1volume. Oxford University Press, Oxford, UK.

Bäck, T., Fogel, D., and Michalewicz, Z. (2000a). *Evolutionary Computation 1: Basic Algorithms and Operators*1volume. Institute of Physics Publishing, Bristol.

Bäck, T., Fogel, D., and Michalewicz, Z. (2000b). *Evolutionary Computation 2: Advanced Algorithms and Operators*1volume. Institute of Physics Publishing, Bristol.

Barricelli, N. (1963). Numerical testing of evolution theories. *Acta Biotheoretica*, **16**:69–126.

Bažant, Z. and Jirásek, M. (2002). Nonlocal integral formulations of plasticity and damage: Survey of progress. *Journal of Engineering Mechanics*, **128(11)**:1119–1149.

Bazant, Z. P. and Cedolin, L. (1979). Blunt crack band propagation in finite element analysis. *Journal of the Engineering Mechanics Division*, **105(2)**:297–315.

Bažant, Z. P. and Cedolin, L. (2010). *Stability of Structures: Elastic, Inelastic, Fracture and Damage Theories*. World Scientific, Hackensack, NJ.

Bažant, Z. P. and Oh, B. H. (1983). Crack band theory for fracture of concrete. *Matériaux et Construction*, **16(3)**:155–177.

Bažant, Z. P. and Planas, J. (1997). *Fracture and Size Effect in Concrete and Other Quasibrittle Materials*. CRC Press.

Belytschko, T. and Black, T. (1999). Elastic crack growth in finite elements with minimal remeshing. *International Journal for Numerical Methods in Engineering*, **45(5)**:601–620.

Belytschko, T., Fish, J., and Engelmann, B. E. (1988). A finite element with embedded localization zones. *Computer Methods in Applied Mechanics and Engineering*, **70(1)**:59–89.

Billington, S. (2009). Nonlinear and sequentially linear analysis of tensile strain hardening cement-based composite beams in flexure. Delft, The Netherlands. Delft University of Technology.

Bletzinger, K.-U. and Ramm, E. (2001). Structural optimization and form finding of light weight structures. *Computers & Structures*, **79(22–25)**:2053–2062.

Borst, R. D., Crisfield, M. A., Remmers, J. J. C., and Verhoosel, C. V. (2012). *Nonlinear Finite Element Analysis of Solids and Structures*. John Wiley & Sons, 2nd edition.

Brenner, C. E. and Bucher, C. (1995). A contribution to the SFE-based reliability assessment of nonlinear structures under dynamic loading. *Probabilistic Engineering Mechanics*, **10(4)**:265–273.

Bureerat, S. and Limtragool, J. (2008). Structural topology optimisation using simulated annealing with multiresolution design variables. *Finite Elements in Analysis and Design*, **44(12-13)**:738–747.

Callister, W. D. and Rethwisch, D. G. (2012). *Fundamentals of materials science and engineering*. Wiley, Hoboken, N.J., 4th edition.

Cervenka, V. (1970). *Inelastic finite element analysis of reinforced concrete panels under in-plane loads*. PhD thesis, University of Colorado, Boulder (USA).

Chen, S. and Tortorelli, D. A. (1997). Three-dimensional shape optimization with variational geometry. *Structural optimization*, **13(2-3)**:81–94.

Chen, T. Y. and Chen, H. C. (2009). Mixed–discrete structural optimization using a rank-niche evolution strategy. *Engineering Optimization*, **41(1)**:39–58.

Coelho, R. F. (2004). *Multicriteria Optimization with Expert Rules for Mechanical Design*. PhD thesis, Universite Libre de Bruxelles, Faculte des Sciences Appliquees, Belgium.

de Borst, R. and Mühlhaus, H.-B. (1992). Gradient-dependent plasticity: Formulation and algorithmic aspects. *International Journal for Numerical Methods in Engineering*, **35(3)**:521–539.

Deb, K. (2000). An efficient constraint handling method for genetic algorithms. *Computer Methods in Applied Mechanics and Engineering*, **186(2–4)**:311–338.

Degertekin, S. O. (2012). Improved harmony search algorithms for sizing optimization of truss structures. *Computers & Structures*, **92–93**:229–241.

DeJong, M. J., Belletti, B., Hendriks, M. A., and Rots, J. G. (2009). Shell elements for sequentially linear analysis: Lateral failure of masonry structures. *Engineering Structures*, **31(7)**:1382–1392.

Deodatis, G. (1991). Weighted integral method. i: Stochastic stiffness matrix. *Journal of Engineering Mechanics*, **117(8)**:1851–1864.

Deodatis, G. and Micaletti, R. (2001). Simulation of highly skewed non-gaussian stochastic processes. *Journal of Engineering Mechanics*, **127(12)**:1284–1295.

Der Kiureghian, A. and Ke, J.-B. (1988). The stochastic finite element method in structural reliability. *Probabilistic Engineering Mechanics*, **3(2)**:83–91.

Dolbow, J. (1999). *An Extended Finite Element Method with Discontinuous Enrichment for Applied Mechanics*. PhD thesis, Northwestern University, Evanston, IL, US.

Dolbow, J., Moës, N., and Belytschko, T. (2000). Discontinuous enrichment in finite elements with a partition of unity method. *Finite Elements in Analysis and Design*, **36(3–4)**:235–260.

Duysinx, P., Miegroet, L. V., Jacobs, T., and Fleury, C. (2006). Generalized shape optimization using x-FEM and level set methods. In Bendsøe, M. P., Olhoff, N., and Sigmund, O., editors, *IUTAM Symposium on Topological Design Optimization of Structures, Machines and Materials*, number 137 in Solid Mechanics and Its Applications, pages 23–32. Springer Netherlands.

Edke, M. S. and Chang, K.-H. (2010). Shape sensitivity analysis for 2D mixed mode fractures using extended FEM (XFEM) and level set method (LSM). *Mechanics Based Design of Structures and Machines*, **38(3)**:328–347.

Edke, M. S. and Chang, K.-H. (2011). Shape optimization for 2-d mixed-mode fracture using extended FEM (XFEM) and level set method (LSM). *Structural and Multidisciplinary Optimization*, **44(2)**:165–181.

Eiben, A. E. and Smith, J. (2003). *Introduction to Evolutionary Computing*. Natural Computing Series. Springer-Verlag.

Eliáš, J., Frantík, P., and Vořechovský, M. (2010). Improved sequentially linear solu-

tion procedure. *Engineering Fracture Mechanics*, **77(12)**:2263–2276.

Ellingwood, B., Galambos, T., MacGregor, J., and Cornell, C. (1980). *Development of a Probability Based Load Criterion for American National Standard A58: Building Code Requirements for Minimum Design Loads in Buildings and Other Structures*. U.S. Department of Commerce, National Bureau of Standards.

Ellingwood, B. and Galambos, T. V. (1982). Probability-based criteria for structural design. *Structural Safety*, **1(1)**:15–26.

Engelbrecht, A. P. (2007). *Computational intelligence: an introduction*. John Wiley & Sons, Chichester, England; Hoboken, NJ.

Erdogan, F. and Sih, G. C. (1963). On the crack extension in plates under plane loading and transverse shear. *Journal of Fluids Engineering*, **85(4)**:519–525.

Farhat, F., Nakamura, S., and Takahashi, K. (2009). Application of genetic algorithm to optimization of buckling restrained braces for seismic upgrading of existing structures. *Computers & Structures*, **87(1–2)**:110–119.

Fleming, M., Chu, Y. A., Moran, B., and Belytschko, T. (1997). Enriched element-free galerkin methods for crack tip fields. *International Journal for Numerical Methods in Engineering*, **40(8)**:1483–1504.

Fogel, D. (1992). *Evolving artificial intelligence*. PhD thesis, University of California, San Diego.

Fogel, L. J., Owens, A. J., and Walsh, M. J. (1966). *Artificial Intelligence through Simulated Evolution*. John Wiley & Sons, Chichester, UK.

Gämperle, R., Müller, S. D., and Koumoutsakos, P. (2002). A parameter study for differential evolution. In *WSEAS Int. Conf. on Advances in Intelligent Systems, Fuzzy Systems, Evolutionary Computation*, pages 293–298. WSEAS Press.

Gandomi, A. H. and Yang, X.-S. (2011). Benchmark problems in structural optimization. In Koziel, S. and Yang, X.-S., editors, *Computational Optimization, Methods and Algorithms*, number 356 in Studies in Computational Intelligence, pages 259–281. Springer Berlin Heidelberg.

Gandomi, A. H., Yang, X.-S., and Alavi, A. H. (2013). Cuckoo search algorithm: a metaheuristic approach to solve structural optimization problems. *Engineering with Computers*, **29(1)**:17–35.

Gentle, J. E. (2003). *Random Number Generation and Monte Carlo Methods*. Springer-Verlag, 2nd edition.

Georgioudakis, M., Lagaros, N. D., and Papadrakakis, M. (2014a). Probabilistic shape design optimization of structural components under fatigue. *Structural and Multi-*

disciplinary Optimization (submitted for publication).

Georgioudakis, M., Lagaros, N. D., and Papadrakakis, M. (2014b). Shape design optimization for structural components under fatigue considering uncertainties. In *Proceedings of International Conference on Engineering and Applied Sciences Optimization*, Kos Island, Greece.

Georgioudakis, M., Stefanou, G., and Papadrakakis, M. (2014c). Stochastic failure analysis of structures with softening materials. *Engineering Structures*, **61**:13–21.

Geuzaine, C. and Remacle, J.-F. (2009). Gmsh: a three-dimensional finite element mesh generator with built-in pre- and post-processing facilities. *International Journal for Numerical Methods in Engineering*, **79(11)**:1309–1331.

Ghanem, R. and Pellissetti, M. (2002). An unified approach for generating gaussian random field simulation methods. In *Proceedings of 5th World Congress on Computational Mechanics*, Vienna, Austria, July 7-12.

Ghanem, R. and Spanos, P. D. (2003). *Stochastic finite elements: a spectral approach*. Dover Publications, Minneola, N.Y.

Gholizadeh, S. and Salajegheh, E. (2009). Optimal design of structures subjected to time history loading by swarm intelligence and an advanced metamodel. *Computer Methods in Applied Mechanics and Engineering*, **198(37–40)**:2936–2949.

Graça-e Costa, R. and Alfaiate, J. (2006). The numerical analysis of reinforced concrete beams using embedded discontinuities. *Structural Durability & Health Monitoring*, **2(1)**:11–18.

Graça-e Costa, R., Alfaiate, J., Dias-da Costa, D., Neto, P., and Sluys, L. J. (2013). Generalisation of non-iterative methods for the modelling of structures under non-proportional loading. *International Journal of Fracture*, **182(1)**:21–38.

Graça-e Costa, R., Alfaiate, J., Dias-da Costa, D., and Sluys, L. J. (2012). A non-iterative approach for the modelling of quasi-brittle materials. *International Journal of Fracture*, **178(1-2)**:281–298.

Griffith, A. (1921). The phenomena of rupture and flow in solids. *Philosophical Transactions of the Royal Society of London*, **221**:163–198.

Grigoriu, M. (1984). Crossings of Non-Gaussian translation processes. *Journal of Engineering Mechanics*, **110(4)**:610–620.

Grigoriu, M. (1993). On the spectral representation method in simulation. *Probabilistic Engineering Mechanics*, **8(2)**:75–90.

Grigoriu, M. (1998). Simulation of stationary non-gaussian translation processes. *Journal of Engineering Mechanics*, **124(2)**:121–126.

Gurley, K. R., Tognarelli, M. A., and Kareem, A. (1997). Analysis and simulation tools for wind engineering. *Probabilistic Engineering Mechanics*, **12(1)**:9–31.

Haddad, O. B., Afshar, A., and Mariño, M. A. (2006). Honey-bees mating optimization (HBMO) algorithm: A new heuristic approach for water resources optimization. *Water Resources Management*, **20(5)**:661–680.

Haftka, R. T. and Grandhi, R. V. (1986). Structural shape optimization—A survey. *Computer Methods in Applied Mechanics and Engineering*, **57(1)**:91–106.

Hansen, L. U., Häusler, S. M., and Horst, P. (2008). Evolutionary multicriteria design optimization of integrally stiffened airframe structures. *Journal of Aircraft*, **45(6)**:1881–1889.

Hansen, N. and Ostermeier, A. (2001). Completely derandomized self-adaptation in evolution strategies. *Evolutionary Computation*, **9(2)**:159–195.

Hasançebi, O. (2008). Adaptive evolution strategies in structural optimization: Enhancing their computational performance with applications to large-scale structures. *Computers & Structures*, **86(1–2)**:119–132.

Hasançebi, O., Çarbaş, S., Doğan, E., Erdal, F., and Saka, M. P. (2010). Comparison of non-deterministic search techniques in the optimum design of real size steel frames. *Computers & Structures*, **88(17–18)**:1033–1048.

Hock, W. and Schittkowski, K. (1980). Test examples for nonlinear programming codes. *Journal of Optimization Theory and Applications*, **30(1)**:127–129.

Holland, J. H. (1973). Genetic algorithms and the optimal allocation of trials. *SIAM Journal on Computing*, **2(2)**:88–105.

Hughes, T. J. R. (2000). *The finite element method linear static and dynamic finite element analysis*. Dover Publications, Mineola, NY.

Igel, C., Hansen, N., and Roth, S. (2007). Covariance matrix adaptation for multi-objective optimization. *Evolutionary Computation*, **15(1)**:1–28.

Iman, R. L. (1980). Latin hypercube sampling (program user's guide). Technical report, Dept. of Energy, Sandia Laboratories, Albuquerque, NM.

Inglis, C. E. (1913). Stresses in a plate due to the presence of cracks and sharp corners. *Trans. Institute of Naval Architecture*, **55**:219–241.

Ingraffea, A. R. and Saouma, V. (1985). Numerical modeling of discrete crack propagation in reinforced and plain concrete. In Sih, G. C. and DiTommaso, A., editors, *Fracture mechanics of concrete: Structural application and numerical calculation*, number 4 in Engineering Application of Fracture Mechanics, pages 171–225. Springer Netherlands.

Invernizzi, S., Trovato, D., Hendriks, M. A. N., and van de Graaf, A. V. (2011). Sequentially linear modelling of local snap-back in extremely brittle structures. *Engineering Structures*, **33(5)**:1617–1625.

Irwin, G. R. (1957). Analysis of stresses and strains near the end of cracking traversing a plate. *Journal of Applied Mechanics*, **24**:361–364.

Irwin, G. R. (1958). Fracture. In Flügge, S., editor, *Elasticity and Plasticity*, Encyclopedia of Physics, pages 551–590. Springer Berlin Heidelberg.

JCSS (2001). Probabilistic model code, part 3: Resistance models.

Jirásek, M. (1998). Nonlocal models for damage and fracture: Comparison of approaches. *International Journal of Solids and Structures*, **35(31-32)**:4133–4145.

Kachanov, L. (1986). *Introduction to continuum damage mechanics*. Springer Netherlands.

Kaveh, A. and Shahrouzi, M. (2008). Dynamic selective pressure using hybrid evolutionary and ant system strategies for structural optimization. *International Journal for Numerical Methods in Engineering*, **73(4)**:544–563.

Kleiber, M. and Hien, T. D. (1993). *The Stochastic Finite Element Method: Basic Perturbation Technique and Computer Implementation*. Wiley, Chichester England, New York, 1st edition.

Koza, J. R. (1992). *Genetic Programming: On the Programming of Computers by Means of Natural Selection*. MIT Press, Cambridge, MA, USA.

Koza, J. R. (1994). *Genetic Programming II: Automatic Discovery of Reusable Program*. MIT Press, Cambridge, MA, USA.

Kripakaran, P., Hall, B., and Gupta, A. (2011). A genetic algorithm for design of moment-resisting steel frames. *Structural and Multidisciplinary Optimization*, **44(4)**:559–574.

Kunakote, T. and Bureerat, S. (2011). Multi-objective topology optimization using evolutionary algorithms. *Engineering Optimization*, **43(5)**:541–557.

Lagaros, N. D., Fragiadakis, M., and Papadrakakis, M. (2004). Optimum design of shell structures with stiffening beams. *AIAA Journal*, **42(1)**:175–184.

Lagaros, N. D. and Papadrakakis, M. (2012). Applied soft computing for optimum design of structures. *Structural and Multidisciplinary Optimization*, **45(6)**:787–799.

Larsson, R., Runesson, K., and Sture, S. (1996). Embedded localization band in undrained soil based on regularized strong discontinuity—theory and FE-analysis. *International Journal of Solids and Structures*, **33(20–22)**:3081–3101.

Li, C. and Der Kiureghian, A. (1993). Optimal discretization of random fields. *Journal of Engineering Mechanics*, **119(6)**:1136–1154.

Li, L., Wang, M. Y., and Wei, P. (2012). XFEM schemes for level set based structural optimization. *Frontiers of Mechanical Engineering*, **7(4)**:335–356.

Liang, J., Huang, R., Prévost, J. H., and Suo, Z. (2003). Evolving crack patterns in thin films with the extended finite element method. *International Journal of Solids and Structures*, **40(10)**:2343–2354.

Liu, P. and Kiureghian, A. (1991). Finite element reliability of geometrically nonlinear uncertain structures. *Journal of Engineering Mechanics*, **117(8)**:1806–1825.

Liu, W. K., Belytschko, T., and Mani, A. (1986). Random field finite elements. *International Journal for Numerical Methods in Engineering*, **23(10)**:1831–1845.

Manan, A., Vio, G. A., Harmin, M. Y., and Cooper, J. E. (2010). Optimization of aeroelastic composite structures using evolutionary algorithms. *Engineering Optimization*, **42(2)**:171–184.

Mariani, S. and Perego, U. (2003). Extended finite element method for quasi-brittle fracture. *International Journal for Numerical Methods in Engineering*, **58(1)**:103–126.

Martínez, F. J., González-Vidosa, F., Hospitaler, A., and Alcalá, J. (2011). Design of tall bridge piers by ant colony optimization. *Engineering Structures*, **33(8)**:2320–2329.

McKay, M. D., Beckman, R. J., and Conover, W. J. (2000). A comparison of three methods for selecting values of input variables in the analysis of output from a computer code. *Technometrics*, **42(1)**:55–61.

Melenk, J. M. and Babuška, I. (1996). The partition of unity finite element method: Basic theory and applications. *Computer Methods in Applied Mechanics and Engineering*, **139(1–4)**:289–314.

Moës, N., Dolbow, J., and Belytschko, T. (1999). A finite element method for crack growth without remeshing. *International Journal for Numerical Methods in Engineering*, **46(1)**:131–150.

Muc, A. and Muc-Wierzgoń, M. (2012). An evolution strategy in structural optimization problems for plates and shells. *Composite Structures*, **94(4)**:1461–1470.

Ngo, D. and Scordelis, A. (1967). Finite element analysis of reinforced concrete beams. *ACI Journal*, **63(3)**:152–163.

Nguyen, G. D. (2008). A thermodynamic approach to non-local damage modelling of concrete. *International Journal of Solids and Structures*, **45(7-8)**:1918–1934.

Nuismer, R. J. (1975). An energy release rate criterion for mixed mode fracture. *International Journal of Fracture*, **11(2)**:245–250.

Oliver, J. (1996a). Modelling strong discontinuities in solid mechanics via strain softening constitutive equations. part 1: Fundamentals. *International Journal for Numerical Methods in Engineering*, **39(21)**:3575–3600.

Oliver, J. (1996b). Modelling strong discontinuities in solid mechanics via strain softening constitutive equations. part 2: Numerical simulation. *International Journal for Numerical Methods in Engineering*, **39(21)**:3601–3623.

Oliver, J. (2000). On the discrete constitutive models induced by strong discontinuity kinematics and continuum constitutive equations. *International Journal of Solids and Structures*, **37(48–50)**:7207–7229.

Oliver, J., Cervera, M., Oller, S., and Lubliner, J. (1990). Isotropic damage models and smeared crack analysis of concrete. In *Computer Aided Analysis and design of Concrete Structures: Proceedings of SCI-C 1990, 2nd International Conference*, pages 945–957, Austria.

Oliver, J. and Huespe, A. (2004). Continuum approach to material failure in strong discontinuity settings. *Computer Methods in Applied Mechanics and Engineering*, **193(30-32)**:3195–3220.

Oliver, J., Huespe, A., and Dias, I. (2012). Strain localization, strong discontinuities and material fracture: Matches and mismatches. *Computer Methods in Applied Mechanics and Engineering*, **241-244**:323–336.

Oliver, J., Huespe, A., and Sánchez, P. (2006). A comparative study on finite elements for capturing strong discontinuities: E-FEM vs x-FEM. *Computer Methods in Applied Mechanics and Engineering*, **195(37-40)**:4732–4752.

Osher, S. and Sethian, J. A. (1988). Fronts propagating with curvature dependent speed: Algorithms based on hamilton-jacobi formulations. *Journal of Computation Physics*, **79(1)**:12–49.

Papadopoulos, V., Deodatis, G., and Papadrakakis, M. (2005). Flexibility-based upper bounds on the response variability of simple beams. *Computer Methods in Applied Mechanics and Engineering*, **194(12-16)**:1385–1404.

Papadopoulos, V., Papadrakakis, M., and Deodatis, G. (2006). Analysis of mean and mean square response of general linear stochastic finite element systems. *Computer Methods in Applied Mechanics and Engineering*, **195(41)**:5454–5471.

Papadopoulos, V., Stefanou, G., and Papadrakakis, M. (2009). Buckling analysis of imperfect shells with stochastic non-gaussian material and thickness properties. *International Journal of Solids and Structures*, **46(14-15)**:2800–2808.

Paris, P., Gomez, M., and Anderson, W. (1961). A rational analytic theory of fatigue. *The Trend in Engineering*, **13**:9–14.

Pedersen, M. (2010). Good parameters for differential evolution. Technical report HL1002, Hvass Laboratories.

Perez, R. E. and Behdinan, K. (2007). Particle swarm approach for structural design optimization. *Computers & Structures*, **85(19–20)**:1579–1588.

Poirion, F. and Puig, B. (2005). An unified approach for generating gaussian random field simulation methods. In *Proceedings of Ninth International Conference on Structural Safety Reliability*27volume, pages 1621–1635, Rome, Italy, June 19–23.

Price, K., Storn, R. M., and Lampinen, J. A. (2005). *Differential Evolution - A Practical Approach to Global Optimization*. Springer.

Rabotnov, Y. N. (1971). Creep problems in structural members. *North-Holland Publishing Company*, **51(7)**:575–576.

Rechenberg, I. (1973). *Evolutionstrategie: Optimierung technischer Systeme nach Prinzipien der biologischen Evolution*. Frommann-Holzboog, Stuttgart-Bad Cannstatt.

Rice, J. R. (1968). A path independent integral and the approximate analysis of strain concentrations by notches and cracks. *Journal of Applied Mechanics*, **35**:379–386.

Riche, R. L. and Haftka, R. T. (2012). On global optimization articles in SMO. *Structural and Multidisciplinary Optimization*, **46(5)**:627–629.

Rönkkönen, J., Kukkonen, S., and Price, K. (2005). Real-parameter optimization with differential evolution. In *Proceedings of IEEE Congress on Evolutionary Computation*1volume, pages 506–513.

Rots, J. G. (2001). Sequentially linear continuum model for concrete fracture. In de Borst, R., Mazars, J., Pijaudier-Cabot, G., and van Mier, J., editors, *International Conference on Fracture Mechanics of Concrete and Concrete Structures*. Balkema, Lisse; Abingdon.

Rots, J. G., Belletti, B., and Invernizzi, S. (2008). Robust modeling of RC structures with an "event-by-event" strategy. *Engineering Fracture Mechanics*, **75(3–4)**:590–614.

Rots, J. G., Hendriks, M. A. N., Belletti, B., and DeJong, M. J. (2009). Sequentially linear analysis as a pushover analysis tool for masonry structures. In *Proceedings of the 2nd International Conference on Computational Methods in Structural Dynamics and Earthquake Engineering, COMPDYN 2009*, Rhodes, Greece.

Rots, J. G. and Invernizzi, S. (2004). Regularized sequentially linear saw-tooth softening model. *International Journal for Numerical and Analytical Methods in Geome-*

chanics, **28(7-8)**:821–856.

Rots, J. G., Nauta, P., Kuster, G. M. A., and Blaauwendraad, J. (1985). Smeared crack approach and fracture localization in concrete.

Rubinstein, R. Y. and Kroese, D. P. (2007). *Simulation and the Monte Carlo Method*. Wiley-Interscience, Hoboken, N.J, 2nd edition.

Saouma, V. (2000). Fracture mechanics (lecture notes). CVEN-6831, Univesity of Colorado, USA.

Schuëller, G. I. (2006). Developments in stochastic structural mechanics. *Archive of Applied Mechanics*, **75(10-12)**:755–773.

Schwefel, H.-P. (1995). *Evolution and Optimum Seeking*. Wiley.

Shi, C., van Dam, A. G., van Mier, J. G., and Sluys, B. (2000). Crack interaction in concrete. In Wittmann, F. H., editor, *Materials for Buildings and Structures*, pages 125–131. Wiley-VCH Verlag GmbH & Co. KGaA.

Shields, M., Deodatis, G., and Bocchini, P. (2011). A simple and efficient methodology to approximate a general non-gaussian stationary stochastic process by a translation process. *Probabilistic Engineering Mechanics*, **26(4)**:511–519.

Shinozuka, M. (1987). Structural response variability. *Journal of Engineering Mechanics*, **113(6)**:825–842.

Shinozuka, M. and Deodatis, G. (1991). Simulation of stochastic processes by spectral representation. *Applied Mechanics Reviews*, **44(4)**.

Shinozuka, M. and Deodatis, G. (1996). Simulation of multi-dimensional gaussian stochastic fields by spectral representation. *Applied Mechanics Reviews*, **49(1)**:29–53.

Shinozuka, M. and Jan, C. M. (1972). Digital simulation of random processes and its applications. *Journal of Sound and Vibration*, **25(1)**:111–128.

Sienz, J. and Hinton, E. (1997). Reliable structural optimization with error estimation, adaptivity and robust sensitivity analysis. *Computers & Structures*, **64(1–4)**:31–63.

Sih, G. C. (1974). Strain-energy-density factor applied to mixed mode crack problems. *International Journal of Fracture*, **10(3)**:305–321.

Sih, G. C., Paris, P. C., and Irwin, G. R. (1965). On cracks in rectilinearly anisotropic bodies. *International Journal of Fracture Mechanics*, **1(3)**:189–203.

Simo, J. C., Oliver, J., and Armero, F. (1993). An analysis of strong discontinuities induced by strain-softening in rate-independent inelastic solids. *Computational*

Mechanics, **12(5)**:277–296.

Simo, J. C. and Rifai, M. S. (1990). A class of mixed assumed strain methods and the method of incompatible modes. *International Journal for Numerical Methods in Engineering*, **29(8)**:1595–1638.

Slobbe, A., Hendriks, M., and Rots, J. (2012). Sequentially linear analysis of shear critical reinforced concrete beams without shear reinforcement. *Finite Elements in Analysis and Design*, **50**:108–124.

Spanos, P. D. and Zeldin, B. A. (1998). Monte carlo treatment of random fields: A broad perspective. *Applied Mechanics Reviews*, **51(3)**:219–237.

Stefanou, G. (2009). The stochastic finite element method: Past, present and future. *Computer Methods in Applied Mechanics and Engineering*, **198(9–12)**:1031–1051.

Stefanou, G., Georgioudakis, M., and Papadrakakis, M. (2014). Sequentially linear analysis of structures with stochastic material properties. In Papadrakakis, M. and Stefanou, G., editors, *Multiscale Modeling and Uncertainty Quantification of Materials and Structures*, pages 19–32. Springer International Publishing.

Stefanou, G. and Papadrakakis, M. (2004). Stochastic finite element analysis of shells with combined random material and geometric properties. *Computer Methods in Applied Mechanics and Engineering*, **193(1-2)**:139–160.

Steinmann, P. (1999). A finite element formulation for strong discontinuities in fluid-saturated porous media. *Mechanics of Cohesive-frictional Materials*, **4(2)**:133–152.

Stolarska, M. and Chopp, D. L. (2003). Modeling thermal fatigue cracking in integrated circuits by level sets and the extended finite element method. *International Journal of Engineering Science*, **(20)**:2381–2410.

Stolarska, M., Chopp, D. L., Moës, N., and Belytschko, T. (2001). Modelling crack growth by level sets in the extended finite element method. *International Journal for Numerical Methods in Engineering*, **51(8)**:943–960.

Storn, R. and Price, K. (1995). Differential evolution - a simple and efficient adaptive scheme for global optimization over continuous spaces. Technical report.

Storn, R. and Price, K. (1997). Differential evolution - a simple and efficient heuristic for global optimization over continuous spaces. *Journal of Global Optimization*, **11(4)**:341–359.

Su, R., Wang, X., Gui, L., and Fan, Z. (2011). Multi-objective topology and sizing optimization of truss structures based on adaptive multi-island search strategy. *Structural and Multidisciplinary Optimization*, **43(2)**:275–286.

Su, Y., Wang, S. N., and Du, Y. E. (2013). Optimization algorithm of crack initial

angle using the extended finite element method. *Applied Mechanics and Materials*, **444-445**:77–84.

Sukumar, N., Moës, N., Moran, B., and Belytschko, T. (2000). Extended finite element method for three-dimensional crack modelling. *International Journal for Numerical Methods in Engineering*, **48(11)**:1549–1570.

Teferra, K. and Deodatis, G. (2012). Variability response functions for beams with nonlinear constitutive laws. *Probabilistic Engineering Mechanics*, **29**:139–148.

Topa, V., Purcar, M., Munteanu, C., Grindei, L., Pacurar, C., and Garvasiuc, O. (2012). Shape optimization approach based on the extended finite element method. *COMPEL: The International Journal for Computation and Mathematics in Electrical and Electronic Engineering*, **31(2)**:477–497.

Törn, A. and Zhilinskas, A. (1989). *Global optimization*. Springer-Verlag, Berlin; New York.

van De Graaf, A. V., Hendriks, M. A., and Rots, J. G. (2009). Sequentially linear analysis of masonry structures under nonproportional loading. In *Computational Modeling Workshop on Concrete, Masonry and on Fiber-reinforced Composites*, Delft, The Netherlands.

Vanmarcke, E. (1983). *Random Fields: Analysis and Synthesis*. The MIT Press, Cambridge, Massachusetts etc.

Vořechovský, M. (2008). Simulation of simply cross correlated random fields by series expansion methods. *Structural Safety*, **30(4)**:337–363.

Wall, F. J. and Deodatis, G. (1994). Variability response functions of stochastic plane Stress/Strain problems. *Journal of Engineering Mechanics*, **120(9)**:1963–1982.

Wang, Q., Fang, H., and Zou, X.-K. (2010). Application of micro-GA for optimal cost base isolation design of bridges subject to transient earthquake loads. *Structural and Multidisciplinary Optimization*, **41(5)**:765–777.

Westergaard, H. M. (1939). Bearing pressures and cracks. *Journal of Applied Mechanics*, **6**:49–53.

Willam, K. J. (2002). Constitutive models for materials. In *Encyclopedia of physical science and technology*, Engineering. Academic Press, San Diego, 3rd edition.

Yamazaki, F. and Shinozuka, M. (1988). Digital generation of Non-Gaussian stochastic fields. *Journal of Engineering Mechanics*, **114(7)**:1183–1197.

Yang, X.-S. (2010). *Nature-Inspired Metaheuristic Algorithms*. Luniver Press, 2nd edition.

Yang, X.-S. and Koziel, S. (2011). *Computational optimization and applications in engineering and industry*. Springer, New York.

Yang, Z. and Xu, X. F. (2008). A heterogeneous cohesive model for quasi-brittle materials considering spatially varying random fracture properties. *Computer Methods in Applied Mechanics and Engineering*, **197(45-48)**:4027–4039.

Zaharie, D. (2002). Critical values for the control parameters of differential evolution algorithm. In Matouek, R. and Omera, P., editors, *Proceedings of MENDEL 2002*, Brno, Czech Republic.

Zeldin, B. A. and Spanos, P. D. (1998). On random field discretization in stochastic finite elements. *Journal of Applied Mechanics*, **65(2)**:320–327.

Zhigljavsky, A. and Zilinskas, A. (2007). *Stochastic global optimization*. Springer, [S.l.].

Zienkiewicz, O. C., Taylor, R. L., and Fox, D. D. (2014). *The finite element method for solid and structural mechanics*. Butterworth-Heinmann.

Index

This thesis was typeset with LaTeX using Bitstream Charter, Computer Modern, and TeX Gyre Heros type faces. The artwork was prepared using Inkscape (vector graphics; publishing final figures to pdf), Gmsh and Matplotlib (for 2D and 3D graphics). A copy of this thesis can be downloaded from the author's web site: www.georgioudakis.com